University of Cambridge

Department of Medicine

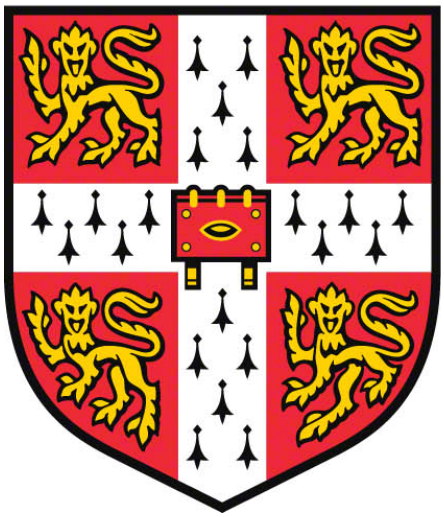

Identification and characterisation of Group 3 Innate Lymphoid Cells in the renal tract

Candidate: Dr Alexandra Mary Riding, Pembroke College

Supervisor: Dr Menna Clatworthy

May 2019

This dissertation is submitted for the degree of Doctor of Philosophy

Preface

This dissertation is the result of my own work and includes nothing which is the outcome of work done in collaboration except as declared in the Preface and specified in the text.

It is not substantially the same as any that I have submitted, or, is being concurrently submitted for a degree or diploma or other qualification at the University of Cambridge or any other University or similar institution except as declared in the Preface and specified in the text. I further state that no substantial part of my dissertation has already been submitted, or, is being concurrently submitted for any such degree, diploma or other qualification at the University of Cambridge or any other University or similar institution except as declared in the Preface and specified in the text

It does not exceed the prescribed word limit for the relevant Degree Committee.

Funding

BRC Addenbrooke's Charitable Trust/Evelyn Trust Clinical Research Fellowship

Wellcome Trust Research Training PhD Fellowship

Summary

Innate lymphoid cells (ILCs) bear similarities to T-helper (Th) cells, but lack T cell receptors. The three groups mirror the effector functions of Th1, Th2 and Th17 cells and share the same transcription factors and cytokine profiles. This project focussed on type 3 ILCs (ILC3s) found primarily at mucosal surfaces with roles in immune defence, tolerance and homeostasis. The key aims were to identify ILC3s within the renal tract (bladder, ureter and kidneys) and characterise their role in urinary tract infection (UTI).

UTI is a significant cause of morbidity and mortality, accounting for some cases of end stage renal failure. The commonest cause of uncomplicated UTI is Uropathogenic *Escherichia coli* and we used this organism in murine models to interrogate the role of ILC3s within this setting. The project focussed on three vital components of effective defence: the epithelium, mononuclear phagocytes (MNPs) and ILC3s.

Key findings and conclusions

Numbers of ILC3s and MNPs in the renal tract increased during UTI, as did their key products, interleukin 17 (IL-17a), IL-22 and granulocyte macrophage – colony stimulating factor (GM-CSF). By using Rag2 knockout mice (lacking T and B lymphocytes), we demonstrated that IL-17 was further decreased by ILC-depletion. Furthermore, we showed reciprocal loss of MNP recruitment, indicating pathways of ILC3-MNP crosstalk during UTI.

Demonstrating a mechanism for ILC3 activation by MNPs through IL-23a and IL-1β production proved challenging, indicating the complexity of the system and requirements for co-stimulation. Similarly, mechanisms of IL-22-induced epithelial repair through production of antimicrobial peptides and induction of cell cycle genes proved multifactorial in origin, but carried particular importance within the bladder.

This project also described ILC3s within the human renal tract by utilising tissues from transplant donors and genomic investigation of tissue-resident cells within the bladder was performed. This novel data will form an invaluable research resource.

Contents

List of Abbreviations

Ab	Antibody
ABU	Asymptomatic bacteriuria
ADAM17	A disintegrin and metalloproteinase 17
AhR	Aryl-hydrocarbon receptor
AKI	Acute kidney injury
AMP	Anti-microbial peptide
APC	Allophycocyanin
Areg	Amphiregulin
AWERB	Animal Welfare and Ethical Review Body
BAC	Bacterial artificial chromosome
BCR	B cell receptor
BFP	Blue fluorescent protein
BMDM	Bone marrow-derived monocyte
BV	Brilliant violet
CAMP	Cathelicidin (also *Cramp* gene mouse)
CCR/L	C-C motif chemokine receptor/ligand
CD	Cluster of differentiation
cDNA	Complementary DNA
CDP	Common dendritic cell precursor
CEACAM	Carcinoembryonic antigen cell adhesion molecule
CFP1	Cxxc finger protein 1
CFT073	Pathogenic strain of *Escherichia coli*
CFU	Colony forming unit
CHILP	Common progenitor to all helper-like innate lymphoid cells
CII	Class II (major histocompatibility complex)
CLP	Common lymphoid progenitor
CMP	Common myeloid progenitor
CNF	Cytotoxic necrotising factor
COX	Cyclo-oxygenase
CRP	C-reactive protein
cRPMI	Complete Roswell Park Memorial Institute (with FBS and P/S)
CRTH2	Chemoattractant receptor homologous receptor 2
Csf2	Colony stimulating factor 2 (gene name of GM-CSF)
CXCR/L	C-X-C motif chemokine receptor/ligand
DAMP	Damage-associated molecular pattern
DC	Dendritic cell

DNA	Deoxyribonucleic acid
DPI	Days post infection
DR3	Death receptor 3
DSS	Dextran sodium sulphate
EAE	Experimental autoimmune encephalitis
EOMES	Eomesodermin
ESRD	End stage renal disease
F	Female
FACS	Fluorescence-activated cell sorting
FBS	Fetal bovine serum
FITC	Fluorescein isothiocyanate
GFP	Green fluorescent protein
GM-CSF	Granulocyte macrophage - colony stimulating factor
GMP	Granulocyte-monocyte progenitor
GSEA	Gene set enrichment analysis
HBD	Human-β-defensin
HD5	Human-α-defensin 5
Het(s)	Heterozygote(s)
Hom(s)	Homozygote(s)
HSC	Haematopoietic stem cell
IBC	Intracellular bacterial community
Id2	Inhibitor of DNA binding 2
IEL	Intraepithelial lymphocyte
IFN	Interferon
Ig	Immunoglobulin
IL	Interleukin
ILC	Innate lymphoid cell
IP	Intraperitoneal
IQR	Interquartile range
IRF	Interferon regulatory factor
IRI	Ischaemic reperfusion injury
IκB	Inhibitory (factor of) κB
IV	Intravenous
KO	Knock out
LCN	Lipocalin
LP	Lymphoid precursor/progenitor
LPS	Lipopolysaccharide
LT-HSC	Long term – haematopoietic stem cell

M	Male
mAb	Monoclonal antibody
MAIT	Mucosal associated invariant T cell
MCP	Monocyte chemotactic protein
MCR LMB	Medical Research Council Laboratory of Molecular Biology
M-CSF	Macrophage – colony stimulating factor
MDP	Macrophage and dendritic cell precursor
MEP	Megakaryocyte erythrocyte progenitor
MHC	Major histocompatibility complex
MIP	Macrophage inflammatory protein
MMP	Matrix metalloprotease
MNP	Mononuclear phagocyte
MOG	Myelin oligodendrocyte glycoprotein
MPO	Myeloperoxidase
N (n)	Number
NA	Not applicable
NCR	Natural killer cell receptor
NFIL3	Nuclear factor interleukin-3 regulated
NFκB	Nuclear factor κB
NHSBT	National Health Service Blood and Transplant
NK	Natural Killer
NRES	National Research Ethics Service
Osm	Osmolarity
OVA	Ovalbumin
PAMP	Pathogen-associated molecular pattern
PBS	Phosphate buffered saline
PCR	Polymerase chain reaction
PE	Phycoerythrin
PLZF	Promyelocytic leukaemic zinc finger
PMN	Polymorphonuclear neutrophil
PRR	Pattern recognition receptor
P/S	Penicillin/Streptomycin
PTX	Pentraxin
QIR	Quiescent intracellular reservoir
qPCR	Quantitative polymerase chain reaction
R	Receptor
RA	Retinoic acid
RAG	Recombination activating gene

RANTES	Regulated on activation normal T cell expressed and secreted
RBC	Red blood cell
REG	Regenerating-islet-derived proteins
RNA (seq)	Ribonucleic acid (sequencing)
ROR	RAR-related orphan receptor
SAA	Serum amyloid A
SAP	Serum amyloid P
SNP	Single nucleotide polymorphism
ST-HSC	Short term – haematopoietic stem cell
TCR	T cell receptor
TG	Transgenic
TGF	Transforming growth factor
T-h/Th	T-helper
Thy	Thymocyte
TL1A	TNF-like ligand 1A
TLR	Toll-like receptors
TNF	Tumour necrosis factor
TNFSF	Tumour necrosis factor ligand superfamily
TSLP	Thymic stromal lymphopoietin
t-SNE	T-distributed stochastic neighbour embedding
UP	Uroplakin
UPEC	Uropathogenic *Escherichia coli* (also *E. coli*)
UTI	Urinary tract infection
UTI89	Pathogenic strain of *Escherichia coli*
VEGF	Vascular endothelial growth factor
WT	Wild type

List of Figures

List of Tables

Chapter 1 - Introduction

1.1 The human renal tract

The renal tract is comprised of the kidneys, ureters, bladder and urethra and together these organs are responsible for many aspects of organism homeostasis: notably maintenance of blood pressure, excretion of waste products, ion and small molecule retrieval and excretion and hormonal control of erythropoiesis and bone metabolism. The kidneys undertake most of these complex functions, but the lower urinary tract structures (ureters, bladder and urethra) form a vital conduit to transport, store and expel urine. The expulsion of waste products and fluid is critical to fulfil the functions of the kidney, but this requires proximity to the external environment, providing an important portal for infection. The specialised and robust epithelium of the renal tract, designed to protect from the chemical toxicity of urine, has been subverted by microorganisms that can ascend the urinary tract to cause pyelonephritis (kidney infection), septicaemia and even death.

Leonardo Da Vinci described the anatomical relationship of the kidneys, ureter and bladder in sketches contained at the Royal Collection (Da Vinci, 1508). His scrutiny goes further to show details of the inner lining of the bladder (Da Vinci, 1515-6) and an early appreciation of its highly specialised epithelium (figure 1.1) [1, 6].

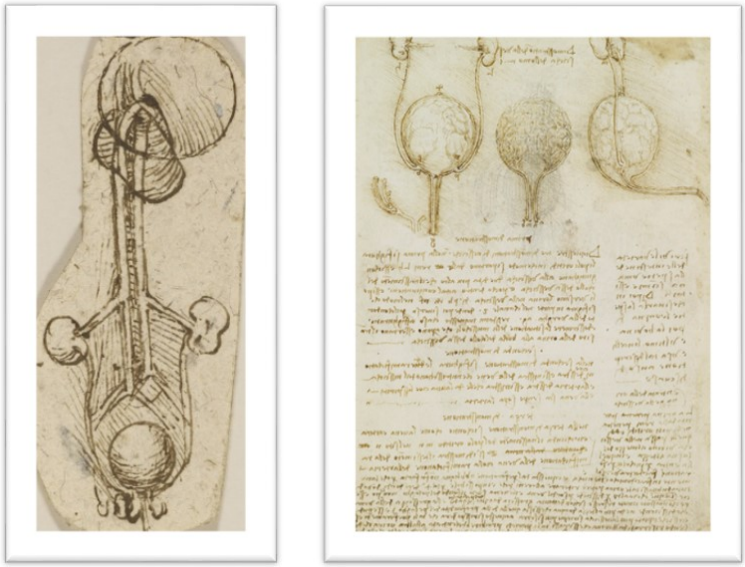

Figure 1.1: Pen and ink sketches from Leonardo Da Vinci's human dissection studies.

The renal tract (RL19126) comes from his Codex Atlanticus and the bladder (RL 19054) is contained within a later collection by Keele & Pedretti, 1979 [1].

The bladder is a hollow sphere for the storage of urine, encased by serosa, muscularis, mucosa, submucosal muscularis and lamina propria [7]. The urothelium sits inside the lamina propria, topped by a glycosaminoglycan layer [8] and lines the length of the renal tract from urethra to renal pelvis. Urothelium of the lower urinary tract (bladder and below) develops from endoderm and is stratified and hardy to withstand the constant flushing of liquid waste products within the urine and the forces exerted by repetitive stretching and emptying. The urothelium must also remain impervious to the leakage of urine and retaining this versatility of function has led to a structure of three distinct layers: a basal layer of slowly renewing cells (5-10 μm), an intermediate layer of pyriform cells (20 μm) and a surface layer of umbrella cells (50-120 μm, dependent on bladder stretching). These cells fuse as they progress towards the surface to form a large, closely-bonded impervious layer that is renewed more slowly than the epidermis, approximately every 6-20 weeks [7, 9]. Despite numerous tight junctions there is some leakage of waste products, as demonstrated by Parsons et al. (1991). They found that when the normal human bladder contains a highly concentrated urea solution, there is 4.5% absorption, rising to 25% in sufferers of recurrent cystitis who can experience epithelial dysfunction [8]. The bladder urothelium is also further specialised by molecules called uroplakins (UP) that are associated with the superficial umbrella cells. This family of four proteins (UPIb, UP1a, UPII and UPIII) form heterodimers that coalesce into a superficial plaque, providing a structure that balances the flexibility and durability required of the bladder [9]. While providing protection, UPIa is heavily mannosylated and acts as the receptor for Uropathogenic *Escherichia coli* (UPEC) and subsequent cellular invasion and urinary infection by this pathogen [10]. A cartoon representation of the bladder's layers is shown in figure 1.2.

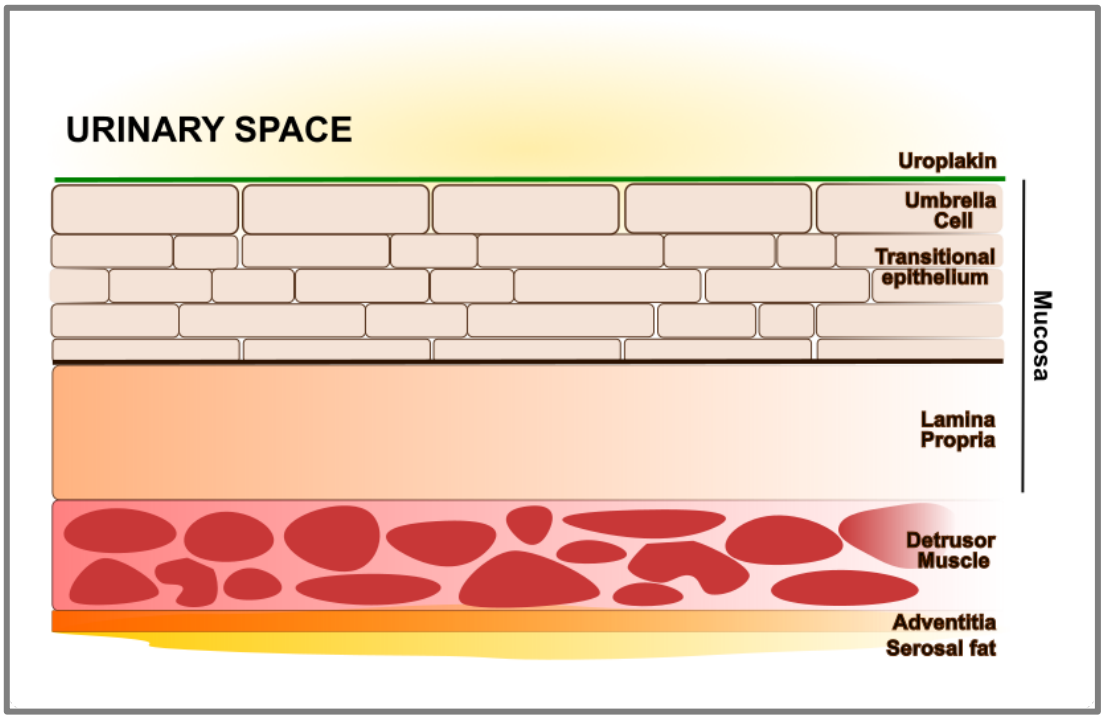

Figure 1.2: The bladder wall and its layers

The upper urinary tract (ureters and kidney) are derived from mesoderm and, while the transitional nature of the urothelium extends to the renal pelvis, the challenges for maintaining immune homeostasis within the kidney are very different to those of the bladder. Urine is made, not stored, by the kidneys and therefore the reinforced network of uroplakin plaques and umbrella cells are not required [11]. Instead, the kidneys comprise hundreds of thousands of nephrons – structures with filters and tubules. The filtering units of the nephron (glomeruli) are found with the renal cortex and the remaining nephron loops down into the renal medulla. Nephrons are highly-metabolically active and concentrate urine by regulating the passage of water, urea (and other osmolytes) and electrolytes. This produces a gradient that increases in osmolality from 300 mOsm to 1400 mOsm at the inner medulla. Flow within the nephron is reciprocal to that of the vasa recta (blood vessels), termed the counter-current system, to encourage a further increase in medullary osmolality. The kidneys therefore, can filter 25% of the body's cardiac output to remove waste products, but produce regulated and manageable urinary volumes by virtue of the osmolality gradient and variations in tubular permeability. The environment within the inner medulla is such, that the osmolality far exceeds that of blood and provides a challenging environment for immune cells. Work within our laboratory has characterised the differences in distribution of tissue-resident immune cells between the cortex and medulla and how environmental differences between these areas affect mononuclear phagocyte (MNP) function in urinary tract infection (UTI) [12].

1.2 Urinary tract infection

UTI is an important cause of morbidity and mortality and affects 150 million people worldwide per year [13]. More women are affected and nearly half will experience a UTI in their lifetime with a quarter developing recurrent infection within a year. Rates of UTI are much lower in men, owing predominantly to anatomical differences in the extent of spatial separation between the urinary and gastrointestinal systems between males and females, such that 12% of men will experience a UTI in their lifetime [14-16]. With UTI incidence peaking in young women and the elderly, it confers significant morbidity and mortality in these populations with inherent health, social and economic costs.

Gram negative bacteria are the predominate causative pathogens of UTI. UPEC is responsible for most cases (80%) of uncomplicated infection, followed by *Staphylococcus saprophyticus* at 10-15% and then *Klebsiella* and *Enterobacter* species. The *Proteus, Serratia and Enterococcus* species infrequently cause uncomplicated UTI, but are often implicated, with *Klebsiella* and *Enterobacte*r, in catheter-associated or secondary infection [17].

1.2.1 Uropathogenic *Escherichia coli*

UPEC, like other gut commensal bacteria, colonises the perineum owing to the proximity of the urethra and rectum. The bacterium has evolved strategies of invasion and immune evasion that make it particularly good at entering and ascending the urothelium to cause urethritis, cystitis and then pyelonephritis.

UPEC strains vary in their virulence factors with approximately 88% expressing at least 3 factors, though combinations are highly variable [18]. The different virulence factors expressed by UPEC can be divided into two categories that are described in table 1; structural proteins that aid motility, adhesion and invasion and secreted toxins. Many of these factors also contribute to immune evasion and are shown in figure 1.3.

Table 1.1: UPEC virulence factors

Structural proteins: Inflammation, motility and invasion	
Protein	**Function**
Type 1 pili (FimH)	FimH is a tip adhesion protein that binds to the bladder epithelium via mannosylated uroplakin 1A and $\alpha_3\beta_1$ integrin [10, 19].
Curli fimbriae	Curli fimbriae and cellulose enable adherence and formation of a biofilm for structural security and immune evasion [20].
P-pili	Adherence organelles that bind gal:gal moieties of urothelium [21].

S-pili (including F1C)	Bind to sialic acid residues of the renal tract. F1C is particularly associated with binding to the distal tubular epithelium and collecting ducts of the kidney [22].
Aggregative adherence fimbriae	Induces increase IL-8 production through an unknown mechanism [23, 24].
Afimbrial adhesins (AfaE)/ Dr fimbriae	Binds CD55/decay-accelerating factor (G-coupled receptor that protects autologous cells from complement-mediated damage) and carcinoembryonic antigen cell adhesion molecules (CEACAM) associated with the urothelium. AfaE also increases CD105 (integrin) expression to depress urothelial exfoliation and preserve colonisation [25, 26].
Cytotoxic necrotising factor 1 (CNF1)	Binds to cells using 67 KDa laminin receptor. Activates Rho GTPases to adjust the actin cytoskeleton of host cells [27, 28].
Flagellae	Extracellular structures that cause directional movement and ascension of the urinary tract [29].
Capsular antigens (0, K and H)	Hydrophilic antigens deflect phagocytosis from the hydrophobic phagocytic cell surface. Phase variation of K and H antigens protect the bacterium from antibody-mediated cell death [30].
Secreted toxins and chelating agents	
Toxin	**Function**
α-haemolysin (Hly-α)	Causes programmed cell death (via caspases 1&4) in human urothelium [21, 31].
Secreted autotransporter toxin (Sat) and Vacuolating autotransporter toxin (Vat)	Variably expressed by UPEC strains (Vat and Sat found in CFT073, but only the former in UTI89) and causing host cell vacuolation, swelling and death [32-34].
Siderophores	Iron chelation is impeded by urinary pH within the bladder and aerobactin and yersiniabactin are essential for UPEC survival [35].

Adapted from Sivick and Mobley (2010) and Flores-Mireles et al. (2015) [5, 36].

There are distinct phases of UPEC survival that allow the pathogen to establish infection and ascend the renal tract; epithelial attachment, filamentation, invasion, proliferation and exfoliation (see figure 1.2). Once within the epithelial cell, UPEC forms intracellular bacterial communities (IBCs) that promote bacterial proliferation and evasion from antibiotic therapy or expulsion during micturition [37]. These communities also form a latent or quiescent intracellular reservoir (QIR) that may be partly responsible for recurrent infections and are much harder to sterilise with antibiotic therapy [38]. Invasion of the renal epithelium is poorly understood, though it has been shown that UPEC targets the apical surface of medullary collecting α-intercalated cells and it has been postulated that these endocytically-active cells are an attractive target for pathogen renewal and spread [39-41].

UPEC has developed strategies to hijack the specialised nature of the urothelium to promote survival, but epithelial cells are not without defence mechanisms of their own. Whilst providing an

obvious structural barrier to pathogens, epithelial cells produce many factors and peptides for defence and renewal (see figure 1.4) [20, 41-49].

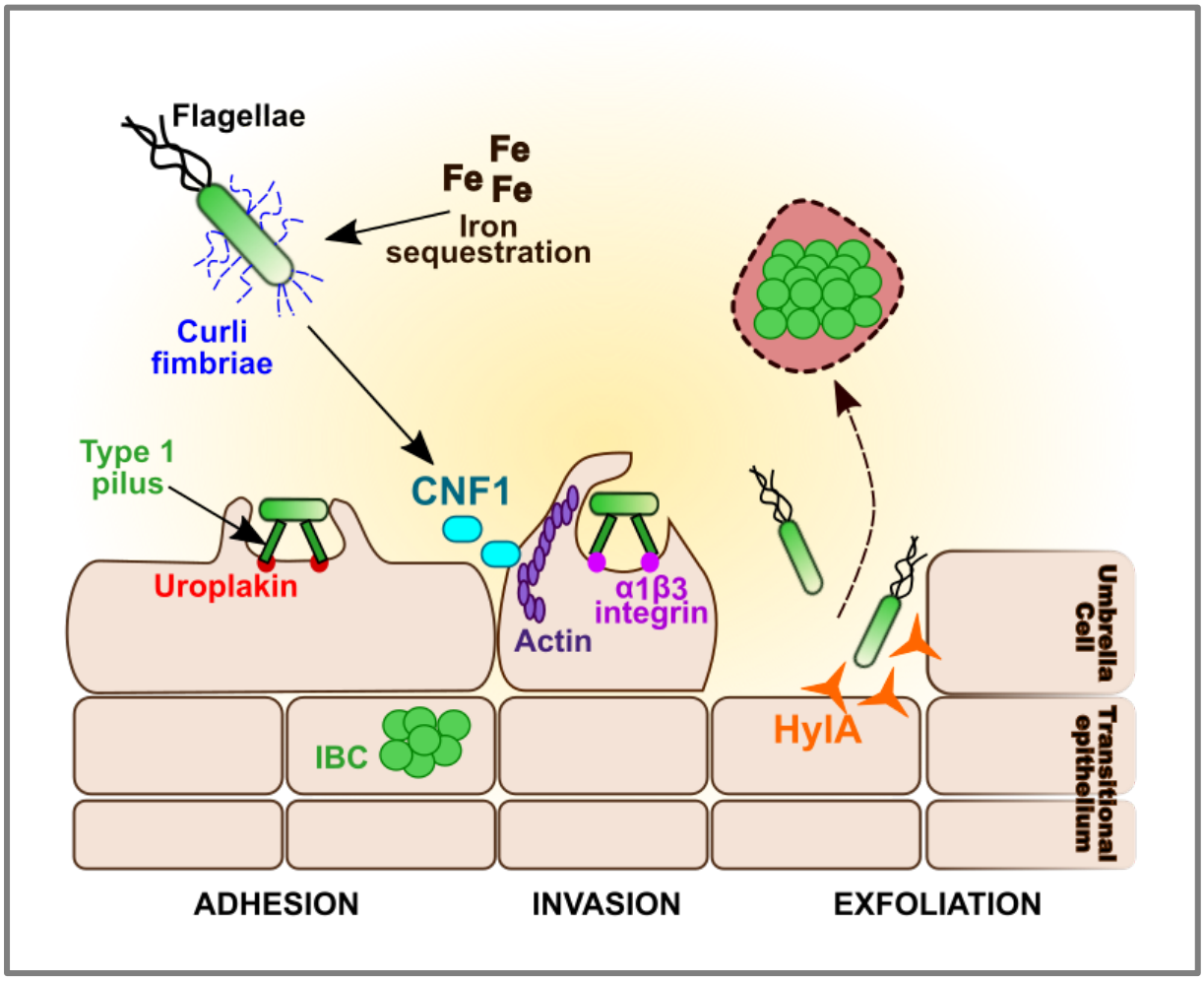

Figure 1.3: Uropathogenic E coli is adapted to invade the urothelium to form intracellular bacterial communities (IBCs).

Virulence factors include flagellae for motility, fimbria for adhesion and evasion, pili for adnhesion and cytotoxic necrotising factor 1 (CNF1) and α-haemolysin (HlyA) for invasion and apoptosis. Through epithelial shedding the pathogen causes urothelial cell lysis and spreads. Graphic adapted from Flores-Mireles et al. (2015) [5].

1.2.2 The epithelial response to urinary tract infection

To maintain integrity and function, the epithelium must be able to respond to invasion and infection. The urothelium possesses highly conserved pattern recognition receptors (PRRs), including toll-like receptors 2 and 4 (TLR2 and TLR4) which are upregulated in the medulla of inflamed kidneys after ischaemic injury [50]. TLR4 recognises lipopolysaccharide (LPS) from gram negative bacteria, such as UPEC, and represents one of the mechanisms by which pro-inflammatory pathways are initiated

within the tubular epithelium [39]. Consequently, the urothelium produces proteins called anti-microbial peptides (AMPs) and chemical mediators (cytokines and chemoattractants). Cytokines and chemoattractants are considered with the immune system, but certain AMPs and epithelial regeneration factors are described in more detail below.

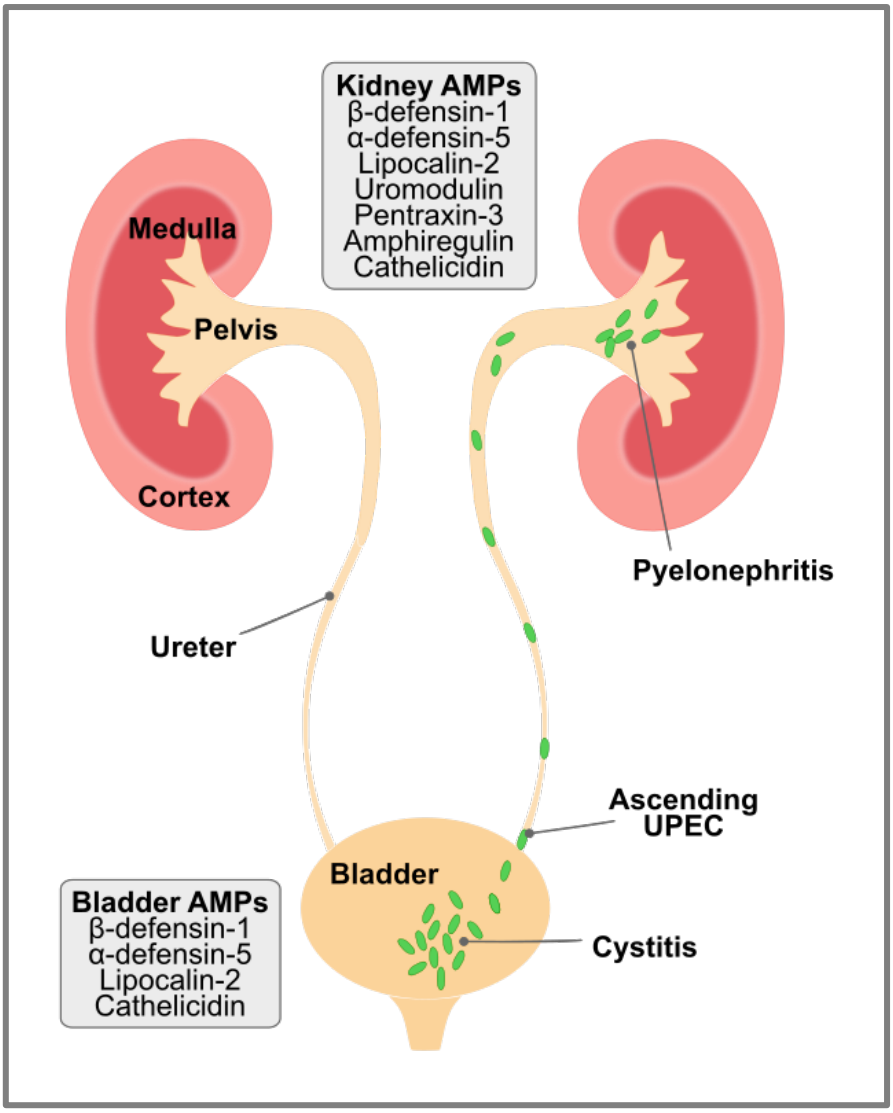

Figure 1.4: Uropathogenic E coli ascends the urinary tract to cause pyelonephritis. The urothelium responds with production of antimicrobial peptides (grey boxes).

AMPs perform multiple functions including neutralising bacteria and their products and promoting epithelial growth and survival. Some are present in health and others are produced in response to UTI and the profiles vary between the upper and lower parts of the urinary tract to provide specific defence strategies (see fig. 1.4, adapted from Becknell et al., 2015). The AMPs and epithelial regeneration factors associated with the lower urinary tract include the human β-defensins (HBD), RNase7, α-defensin-5 (HD5), lipocalin-2 (LCN2), cathelicidin (CAMP) and regenerating islet-derived

proteins (such as RegIIIγ) whereas the kidney responds with an additional number of AMPs; lactoferrin, uromodulin, amphiregulin, mucins and pentraxin-3 [51]. Further detail on these peptides and factors is given below, with reference to their function within the renal tract.

Defensins are highly conserved, cationic peptides that are rich in cysteine residues, the position of which determines further categorisation into either α-defensins or β-defensins [52-54]. Defensins are found in the renal distal tubular cells, loops of Henle and collecting ducts and whilst HD5 is typically associated with neutrophils and intestinal Paneth cells, a urothelial source has been demonstrated [43, 45]. These peptides are produced in response to pathogen associated molecular patterns (PAMPs), such as lipopolysaccharide (LPS), or inflammatory mediators, such as IL-17, TNF-α and IL-1, and can stimulate the immune system by attracting lymphocytic and monocytic cells and activating complement [45, 55-58]. Further work has demonstrated that HBD can attract dendritic cells and T cells by a CCR6-dependent mechanism *in vivo* [59]. In addition to immune stimulation, defensins neutralise bacteria and HD5 is active against *Escherichia coli* with a minimum bactericidal concentration of 2.5 μM [60]. It has been postulated that high concentrations of defensins at the epithelium may prevent bacterial adherence and it has been shown that HDB-1 promotes human neutrophil extracellular trap formation, a mechanism to kill bacteria [51, 61].

Lipocalin-2 (LCN2) is a peptide that binds iron and competes with enterobactin, a siderophore produced by *Escherichia coli* [62]. It is expressed by neutrophils, urothelial cells and the α-intercalated cells of the kidney and is elevated 10-fold in the urine of patients with UTI [41, 46]. Levels of the AMP correlated with bacterial clearance and mice deficient in *Lcn2* took longer to clear UPEC infection than wild type mice [41].

Cathelicidin (referred to as LL-37, or by the gene name *CAMP* in humans or *Camp/Cramp* in mice) causes disruption of the bacterial cell wall leading to cell lysis and inhibits formation of biofilms by UPEC by binding to their curli fimbriae [20, 51]. It is found in the urine and uroepithelium of the renal pelvis and bladder and it increases markedly in patients with urinary tract infections. *CAMP* mRNA levels rise rapidly *in vitro* UPEC stimulation of cultured renal pelvic epithelium and whilst protein production is sustained, transcript levels fall after 24 hours. Murine models have shown that cathelicidin levels are likely to be sustained by white blood cells, though the authors failed to show any difference in disease severity between neutropenic and non-neutropenic mice, despite neutrophils being the primary source [63].

The pentraxins are closely related to C-reactive protein (CRP) and serum amyloid P (SAP), indiscriminate soluble biomarkers of inflammation, and together they form a family of acute phase proteins. Pentraxin-3 (PTX3) is a related, large glycoprotein that is produced by the renal and

bladder urothelium in response to UTI. Immunohistochemistry has shown PTX3 staining within the renal tubular epithelium within 8 hours of infection, though in the bladder it took 24 hours for the epithelium to produce PTX3, with earlier sources derived from infiltrating leukocytes [42]. The same study showed that in mice deficient in *Ptx3*, there was reduced MNP bacterial phagocytosis and a higher bacterial burden (increased colony forming units). In an ischaemia-reperfusion model of acute kidney injury (AKI), *Ptx3*-deficient mice suffered worse disease. The predominant source of PTX3 was CD11c-monocytes and leukocyte recruitment via P-selectin was abrogated in *Ptx3*-deficient mice [64].

Serum amyloid A (SAA) is another major acute-phase protein and precursor to the amyloid fibrils that can cause amyloidosis. It has different isoforms, but production of SAA1/2 occurs in inflammatory states. Although the liver is the major site of SAA production, it has also been demonstrated to be produced by epithelial and endothelial cell lines in response to IL-1β, IL-6 and TNF [65]. In healthy humans, SAA deposition can be found in a range of non-hepatic tissues with a predilection for the skin and other epithelial layers. In the kidney, it was associated with tubular epithelial deposition [66]. In psoriasis, SAA1/2 levels rise in the skin in response to pro-inflammatory stimulation by IL-1α, IL-17a, IL-22, TNF-α and oncostatin-M and acts synergistically with IL-17a to promote synthesis of the AMPs; S100A7, S100A8 and defensin-β2, as well as TNF-α and CCL20. In humans, rises in SAA1/2 paralleled those of IL-17a and were associated with increased disease severity and duration [67]. The synergistic relationship of SAA and IL-17 is further demonstrated in the gastrointestinal tract. In the gut, IL-22 production by type 3 innate lymphoid cells (ILC3s) in response to segmented filamentous bacteria stimulates epithelial cells to make SAA1/2, which in turn contributes to the production of IL-17A by Th17 cells [68]. In addition to potentiating inflammatory responses through IL-17-related mechanisms, SAA has also been demonstrated to promote production of pro-inflammatory cytokines, leucocyte recruitment, synthesis of matrix metalloproteinases and angiogenesis [69-73]. Furthermore, it is an endogenous agonist of TLR4 and has been demonstrated to activate murine peritoneal macrophages [74].

RegIIIγ is produced by the Paneth cells of the gut epithelium. Previously, it has been demonstrated that RegIIIγ is directly bactericidal through its ability to bind gram positive bacterial peptidoglycan [75]. RegIIIγ is expressed in a MyD88-dependent manner and it regulates the spatial relationship between gut microbes and the epithelium [76-78]. At baseline RegIIIγ-deficient animals have increased levels of interleukin-22 (IL-22), myeloperoxidase (MPO), macrophage-inflammatory protein-2 (MIP-2), monocyte chemotactic protein-1 (MCP-1) and macrophage colony stimulating factor (GM-CSF), thus demonstrating a pro-inflammatory environment of increased mucosal activity. This effect was evident in infection with either *Salmonella enteritidis* or *Listeria monocytogenes* [79]

and during containment of commensal species, where IL-22 stimulated increased production of AMPs, including RegIIIγ [80]. Moreover, it has been identified in the lung, where it is produced after stimulation with IL-22 during allergic lung inflammation by airway epithelial cells. RegIIIγ was associated with decreased levels of inflammation and it was postulated that it might be having an anti-inflammatory effect by inhibiting production of thymic stromal lymphopoetin (TSLP) and IL-33 [81]. In 2015, RegIIIγ transcripts were identified in the renal tract using microarray analysis of bladders infected with UTI89 (a strain of UPEC) and were the most highly expressed AMP, rising to high levels 28 days after infection. They were also able to measure Hepatocarcinoma-Intestine-Pancreas/Pancreatitis-Associated-Protein (HIP-PAP), the human RegIIIγ orthologue, in the urine of patients with *E. coli*-associated UTIs. The authors demonstrated the RegIIIγ was bactericidal against *S. Saprophyticus* in a dose-dependent manner, but not UPEC *in vitro*. Owing to its known associated with activity against gram positive bacteria, the authors went on to challenge RegIIIγ-deficient mice with *S. Saprophyticus* and *E. faecalis* in vitro, but there were no observed increases in bacterial burden [44].

Amphiregulin (Areg) is not an antimicrobial peptide, but a growth factor regulator expressed as a transmembrane protein that undergoes proteolytic cleavage to bind to the epidermal growth factor receptor (EGFR) and promote regeneration. It is constitutively synthesised at high levels in ovary and placenta and to a lesser degree in the pancreas, heart, muscle, testis, colon, breast, lung, spleen and kidney [47]. After translation, Areg is found at the membrane where it is cleaved by the metalloprotease, ADAM17, to become a soluble factor capable of binding the EGFR. Its expression is upregulated by pro-inflammatory cytokines such as IL-1 and TNF and can be produced by the renal epithelium [48, 82] and by a range of different immune cells, such as macrophages [83, 84], T-helper 2 (Th2) cells [85], γδT cells [86] and group 2 ILCs (ILC2s) [87]. It has been shown to play a role in epithelial hyperplasia and fibrosis, through mechanisms of repeated damage and repair, as occurs in chronic inflammatory conditions such as asthma [88], psoriasis [89, 90] and chronic kidney disease [48].

1.2.3 Genetic susceptibility to UTI

Increased susceptibility to UTI has been linked to genetic differences in pathways of bacterial recognition and containment. It is therefore unsurprising that many of these correspond to highly conserved pro-inflammatory pathways of immune activation.

Toll-like receptors (TLRs) recognise specific PAMPs and are highly conserved to enable a rapid and stereotyped response. They are found on epithelial and immune cells and genetic differences in TLR4, TLR2, TLR5 and TLR11 have been implicated in UTI susceptibility. Certain single nucleotide

polymorphisms (SNPs) in TLR4 have been correlated to asymptomatic bacterial carriage and altered mucosal responses in paediatric and adult populations with recurrent or severe infections [91]. Furthermore, a large study of women revealed polymorphisms in TLR2 and CXCR1 (involved in immune cell recruitment) that were associated with increased chemoattractant cytokine levels, neutrophil recruitment and rates of asymptomatic bacteriuria (ABU). Other research has also highlighted the role of other pro-inflammatory cytokines and chemokines in UTI, such as IL-8, VEGF, TGF-β1, IRF3 and RANTES [92-95].

It is true that the urinary bladder has its own microbiome, including species such as Actinomycetales, Clostridiales, Lactobacilliales, Mycoplasmatales and Prevotella [96, 97]. These species were identified by polymerase chain reaction (PCR) of urinary suprapubic bladder aspirates (thereby bypassing perineal contamination) and from catheterised post-operative patients. Standard urine cultures from the post-operative patients were negative, except for the bacterial species, *Escherichia*, *Kelbsiella* and *Staphylococcus.* Eighteen percent of these women developed symptoms of infection, but only 7% could be confirmed by culture [96].

Difficulty culturing urinary bacteria using standard techniques has been established and extended culture protocols are required for species such as *Lactobacillus, Gardnerella, Streptococcus, Staphylococcus* and *Corynebacterium* [98]. Indeed, when these extended culture techniques are used and whole-genome sequencing on the isolates processed, the proportion of bacteria that were classically considered to be uropathogenic was only 7.7%. Gram positive organisms, particularly of the phyla Firmicutes and Actinobacteria, were much more abundant. By using PCR techniques, similarities between vaginal and urinary bacteria were found; an observation noted previously by Wolfe et al. (2012) confirmed by urinary and vaginal cultures taken from the same woman [97].

It is noteworthy that Nienhouse et al. (2014) also identified different AMP characteristics that correlated to particular clusters of microbiota, notably gram positive versus gram negative organisms. Differences in AMPs driven by environmental or genetic variance may therefore shape the bladder microbiome and influence symptomatic UTI [96].

Genetic susceptibility to UTI is strongly linked to the immune system, particularly the role of innate or first-responder mechanisms. The next section will outline the role of the immune system in UTI.

1.3 The immune system

The immune system can eliminate microbial infection using rapid innate mechanisms, mount augmented specific defence to previously encountered challenges using adaptive immunity, whilst remaining tolerant to self-antigen and commensal pathogens. The mechanisms employed range from basic epithelial cell barriers to the highly complex interplay of multiple cell types and chemical mediators. In the following section, I will provide an overview of mammalian immunity, with a particular focus on areas relevant to the experiments described later in the thesis. Specifically, mechanisms of bacterial defence at mucosal surfaces, the tissue-resident immune cells involved in these processes and some detail on innate lymphocytes and their associated cytokines.

Conceptually, the immune system is divided into two areas:

1. Innate immunity
    a. Mechanical and anatomical defences
    b. Cellular and chemical defence
2. Adaptive immunity

1.3.1 The innate and adaptive immune system

The innate immune system employs mechanisms that non-specifically prevent and limit the spread of infection [99]. Barrier defences consist of epithelial layers that are highly specialised to meet the demands of their environment, for example the keratinised squamous epithelium of the skin. Further detail of the uroepithelium has already been discussed in section 1.1. The adaptive immune system consists of cells that can recognise specific pathogens and mount a targeted and forceful defence.

Immune cells develop from haematopoietic stem cells (HSCs), but diverge early in development into two lineages: myeloid and lymphoid. Figure 1.5 is adapted from Wang et al. (2011) and Sonnenberg and Artis (2015) and shows a classical understanding of the development of these cells [100, 101]. Over time, our understanding of innate cell populations has increased, providing an appreciation of the diversity of tissue-resident lymphoid populations that includes innate lymphoid cells (ILCs) and invariant T cell populations.

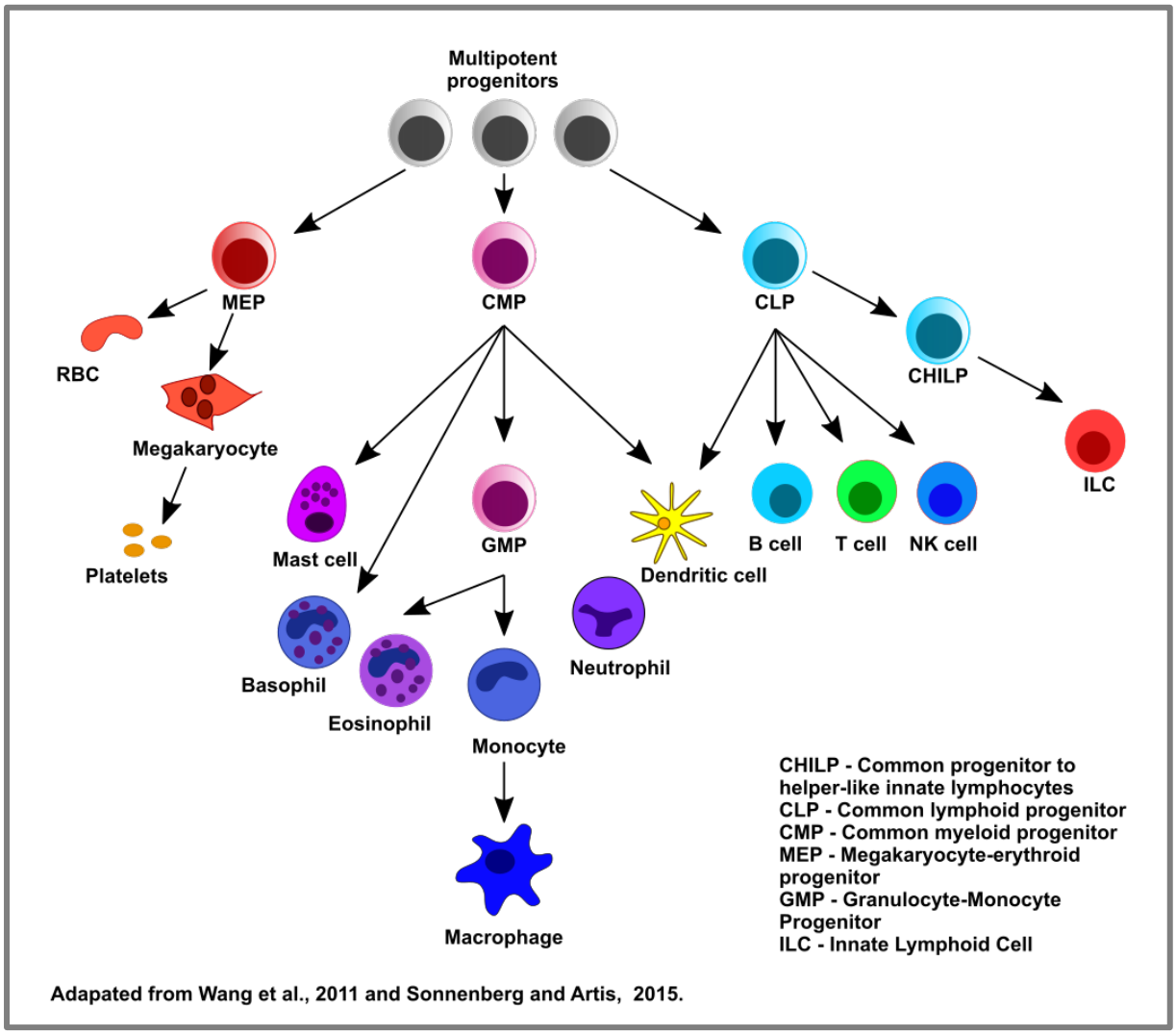

Figure 1.5: Different stem cells give rise to myeloid and lymphoid lineages, that populate the innate and adaptive immune system.

1.3.2 Myeloid cells

The myeloid cells of the innate immune system, such as neutrophils (PMNs), macrophages and dendritic cells (DCs) are thought to produce a non-specific and stereotyped response to invading pathogen. Macrophages and DCs make up mononuclear phagocytic tissue-resident populations that display tissue specificity, leading to multiple titles dependent on their location and function, such as Langherhans cells of the skin [102] or Kupffer cells of the liver [103, 104]. Their generic characteristics are given below, with more detailed reference to disease and tissue-specificity later in the chapter.

Neutrophils

Neutrophils are the major circulating phagocytes in humans that are rapidly summoned to sites of inflammation and infection. Originally termed, 'microphages' these cells are irregular in shape with a granulocytic cytoplasm of enzymes and substrate for neutralising pathogens and multi-lobed nuclei, leading to the term polymorphonuclear neutrophils (PMNs). They are recruited by chemokines released during inflammation (in humans, IL8) and leave the bloodstream by attaching to the endothelium using selectins (upregulated during the inflammatory process). By rolling along the endothelium, PMNs find gaps between cells through which they diapedese to migrate towards the inflamed tissue. Once at a site of infection, PMNs engulf pathogens into a phagolysosome which destroys the bacteria using different mechanisms; acidity, competition for iron and copper using chelating agents such as lactoferrin and degradative enzymes. Furthermore, by using a transient increase in oxygen consumption called a 'respiratory burst', through which toxic oxygen species are produced, PMNs can inactivate and destroy bacteria. Once depleted, a neutrophil is unable to restock its cytoplasmic granules and they die, leading to formation of pus [105, 106]

Macrophages

Macrophages were first described by Elie Metchnikoff in 1882, when he observed large cells engulfing a foreign object [107]. Macrophages phagocytose foreign and redundant material and produce cytokines, many of which are chemo-attractant and pro-inflammatory. This is achieved after recognition of inflammatory material (this can be a pathogen-associated molecular pattern (PAMP) in infection or damage-associated molecular pattern (DAMP) in sterile inflammation) by highly preserved cell-surface PRRs, including TLRs [108-111]. Tissue environments can have a major impact on macrophage function, for example, macrophages constantly exposed to gut microbiota downregulate pro-inflammatory pathways in favour of an anti-inflammatory phenotype, thus avoiding inappropriate or disproportionate responses in health [112, 113].

Macrophages were thought to develop from a common, bone marrow myeloid progenitor, but it is now evident that in some tissues, a proportion of the resident macrophages are self-renewing and seeded during embryogenesis [114-116]. The relative proportion of yolk sac or fetal liver-derived versus HSC/monocyte-derived macrophages differs in different tissues. Mesodermal erythroid progenitors can be found within the embryo's yolk sac as early as day 8.5 and populate the liver shortly thereafter [117]. In the intestine, macrophages are predominantly monocyte-derived [118]. In the peritoneum, embryologically-derived peritoneal macrophages are self-renewing, but become gradually replaced with age by circulating monocyte-derived cells [119]. Conversely, recent fate-mapping experiments also revealed a small population of macrophages that are yolk-sac derived and persist within the lamina propria [120]. These cells display distinct transcriptional signatures from

their monocyte-derived counterparts and can be found in close proximity to nerves, forming a macrophage neuronal-support network. This seems to have implications for gut motility in health, through preservation of the enteric plexus. In contrast, in the brain, microglia are almost wholly yolk sac derived [114].

Understanding the tissue-specificity of MNP networks is one of the current challenges in innate immune biology, both in terms of cellular origin but also the way in which these cells are adapted to respond to local cues in homeostasis and disease. The macrophage neuronal-support network in the gut referenced above is one such example, but others exist, such as description of cardiac monocytes. Through parabiosis experiments, Bajpai et al. (2018), have demonstrated the presence of CCR2+ (monocyte-derived) and CCR2- (yolk sac and embryologically-derived) macrophages. The former were associated with scar tissue and left ventricular dysfunction after cardiac ischaemia, but the latter tended to be found within the endothelium and promoted tissue regeneration and cardiac remodelling. Transcriptional analysis demonstrated differences in these subsets which further inform our understanding and identification of self-renewing, embryologically-derived and tissue-resident MNPs [121].

As murine monocytes exit the circulation to populate the gut mucosa, they undergo a process of Ly6c downregulation and upregulation of MHCII, F4/80, CD64, CD11c and CX3CR1 [112, 122]. This maturation feeds the network of tissue-resident MNPs that become macrophages (CD64 and F4/80 high) or DCs (CD11c and CD103 positive). In flow cytometry, the graphical representation of Ly6c loss and CII gain is termed the 'monocyte waterfall' [122] and this provides a useful way to interrogate monocyte-derived macrophages within tissues during infection or inflammation. The different subgroups of macrophages can become confusing, but these groups have specific transcriptional profiles and roles that we are beginning to understand in more detail. The next passages describe some of these regulatory and proinflammatory roles with reference to the gut.

The gut provides many challenges to the immune system, in terms of balancing tolerance and defence. Newly recruited macrophages assume an anti-inflammatory phenotype [113, 123]. As occurs following myocardial infarction in the description above, dextran sodium sulphate (DSS) colitis induces migration of Ly6c+ monocytes to the gut in a CCR2-dependent manner [123]. These recruited monocytes ($CX3CR1^{int}$ or $Ly6c^{hi}$) have different transcriptional signatures to resident cells ($CX3CR1^{hi}$, $F4/80^{hi}$), with the former being associated with IL-6, IL-23a, TGF-β and IL-1 transcripts and the latter being the sole producers of TNF-α and IL-10 [113, 123, 124]. IL-10-expressing macrophages within the lamina propria were shown to be regulatory by expression of an anti-inflammatory cytokine profile and by stimulating T cells to secrete IL-10 in preference to IL-2 and

IFN-γ [124]. The same authors also illustrated that macrophage-derived IL-10 in combination with TGF-β, promoted T regulatory cell differentiation. Mice with a conditional *Il10* depletion in myeloid cells (*Il10*$^{flox/flox}$*LysM-Cre)* were more susceptible to *Citrobacter rodentium* colitis and the authors went on to show that these *Il10* transcripts were associated with CD11b^{+}, CD11c^{int}, F4/80^{+}, MHCII^{+} macrophages and not granulocytes [125]. Furthermore, loss of IL-10 promoted subsequent increased production of proinflammatory cytokines from this cell type, notably IL-12 and IL-23. It is likely that IL-10 exerts its effects on macrophages using several different pathways, including: inhibition of a pro-inflammatory glycolytic switch and increased mitophagy through mTOR inhibition. Accumulation of mitochondria caused dysregulated inflammasome activation and increased IL-1β production in a murine model of colitis and was observed in patients with inflammatory bowel disease and null IL-10R mutations [126]. Complementary to the observations of MHCII expression and Ly6c downregulation during maturation, recruited cells that were CX3CR1^{int} and Ly6c^{lo} induced significant expansion of CD4+ T cells. These CCR7-expressing cells demonstrated a migratory capacity to access draining lymph nodes. The CX3CR1^{hi}, F4/80^{hi} resident macrophages were not capable of priming T cells during DSS colitis [113, 123].

Given the regulatory role of resident macrophages on T cells and pro-inflammatory effects of recruited monocytes to the gut, it is tempting to regard MNPs as master-controllers of immunity within this context. Macrophages are, however, influenced by other tissue-resident immune cells, termed cross-talk. MNPs are dependent on GM-CSF for their differentiation and survival and their functions are abrogated by its absence [127]. The same authors went on to demonstrate that GM-CSF production by intestinal ILC3s was driven by the presence of commensal bacteria and was essential for MNP function. Furthermore, in relation to the ability of ILCs to influence myeloid populations, ILC2s have been shown to perform regulatory roles in the kidney during ischaemia-reperfusion injury (IRI) and adriamycin-induced glomerulosclerosis by influencing macrophage and eosinophil function respectively [128, 129].

Dendritic Cells

DCs were first described by Steinman and Cohn in 1973 within the spleen [130]. They are classically described as professional antigen presentation cells, that act at the innate/adaptive interface by presenting foreign antigen to activate T-cells and self-antigen to tolerise them. They bear similarities to macrophages and together make up the MNP network. These similarities have led to confusion when defining macrophages and DCs, particularly within tissues where both cells perform dual roles as tissue-resident immune sentinels.

Conventional DCs (cDCs) are found in lymphoid tissues, plasmacytoid DCs (pDCs) within a range of tissues and 'migratory' DCs within peripheral tissues (such as Langerhan's cells of the skin). Conventional DCs are $CD11c^{hi}$ and can be further divided into subgroups by their CD8α and CD11b expression [131, 132], with CD8+ cDCs possessing superior levels of cross-presentation [133]. Plasmacytoid DCs lack the stellate morphology of more developed DCs, but produce type 1 interferon in large quantities and express high levels of MHC II like other DCs [134, 135]. Macrophages and DCs share some developmental similarities and differentiation factors, but only DCs require Flt3 for development [136-139]. Both cells can develop from a shared monocyte precursor, the macrophage and DC precursor (MDP) [137, 139-143], though a distinct common DC precursor does also exist (CDP) [144, 145]. DCs have also been shown to develop from the common lymphoid precursor (CLP) [138, 146].

Our understanding of DC subsets has been significantly advanced by RNA sequencing and mass cytometry techniques, that have enabled us to confirm different subtypes in more detail across a range of tissues. This section will summarise the relevant murine and human DC subtypes, though considerable heterogeneity complicates these populations. Using mass cytometry different groups of myeloid cells were found in a range of murine tissues, including the thymus, spleen, mesenteric lymph nodes, liver, brain, kidney and bone marrow [147]. In particular, pDCs (BST2+B220+) and MHCII+CD11c+ DCs were found in all tissues. The latter group could be divided into CD11b+ cDCs (with variable CD4 or CD8 expression) and CD103+ DCs (found in some peripheral tissues). Using single cell RNA sequencing, Jaitin et al. (2014) found pDCs and four further subtypes of DCs from murine spleen. DC1s predominantly expressed CD8 and DC2-4s were commonly $CD8^{int}$ and CD4+ [148]. In humans, three broad DC subtypes can be found that bear relation to the murine subsets [149-153]. These are pDCs (CD11c-HLA-DR+), cDC1s (CD11c+CD26+$XCR1^{hi}CD172a^{lo}$) and cDC2s (CD11c+CD26+$XCR1^{lo}CD172a^{hi}$). Confusion arises owing to a lack of consensus in describing cDCs, particularly in relation to tissue-specific cells types. This has led to the following groups: BDCA1+CD141+DCs (CD11c+HLA-DR+CD14+), BDCA3+ DCs (CD11c+HLA-DR+CD14-) and CD16+ (CD11c+CD11b+HLA-DR+) DCs. BDCA3+ DCs corresponded to CLEC9A+ DCs (also CD8+CD103+ in mice) and are capable of cross-presentation [149, 154]. BDCA1+ DCs and CD16+ DCs produce pro-inflammatory cytokines upon TLR stimulation, with BDCA1+ DCs producing high levels of IL-8 and CD16+ DCs producing TNF-α [151]. Much of this work has been recapitulated in detail by Villani et al. (2017) who were able to provide an unbiased analysis of single-cell RNA sequencing of blood monocytes, revealing further DC categories [155]. Suffice to say, it seems reasonable to begin by defining human DC subsets as pDC, cDC1 and cDC2, before elaborating further on tissue-specific and inflammatory designations.

The heterogeneity associated with different DC and macrophage subsets takes on a further level of complexity when considering tissue-resident subtypes. In the skin, descriptions of specialised DCs with specific humoral and cellular functions have been documented [156, 157], however detail about these groups falls outside the remit of this project. Instead, we turn our attention back to MNPs at mucosal barriers, notably the gut. DCs of the intestine serve to inform our knowledge of the role of these cells at epithelial barriers and the gating strategies used for flow cytometry by Tamoutounour et al. (2012) have informed our own experimental setup [122]. This analysis encompasses all MNPs and has been described in the descriptions of macrophages above.

In mice, DCs can perform tolerogenic functions by stimulating regulatory T cell proliferation [158, 159], but can be potently pro-inflammatory in colitis through IL-23 production [159, 160] and stimulation of T-helper-17 (Th17) cells, T-helper-1 (Th1) cells, cytotoxic T cells and ILCs [161-163]. Intestinal DCs stimulate T cells to produce IL-17 through TGF-β production and loss of TGF-β and IL-10 co-stimulation leads to a change in the balance of Th1/Th17 activation and increased levels of IFN-γ [124]. On closer examination, it was the pro-inflammatory CD11b+CX3CR1+ DC subset that precipitated IL-17 and IFN-γ production, as opposed to CD11b-CX3CR1-CD103+ DCs [113, 124]. This latter group of DCs were responsible for IL-10 production, suggesting a regulatory role. These two groups of DCs have been identified by other research groups and can be phenotyped as CD103+CD11c+CD11b+-CD14- DCs and $CD14^{int}$CD11b+CD11c+ DCs [113, 139]. (Consistent with the expression of more conventional macrophage markers (CD14 and CD11b) brings dependence on M-CSF over GM-CSF for development and expansion [139].) The same authors identified CD103+ CD11b+ DCs as the first lamina propria DCs to deliver pathogenic bacteria to the draining lymph node in *Salmonella* colitis using CCR7-dependent migration. Therefore, these cells show intrinsic motility in their patrol of the intestinal epithelium and are responsive to GM-CSF [164], potentially critical for DC-ILC cross-talk [127]. They are recruited rapidly to the epithelium by pathogenic bacteria in response to epithelial-derived chemokines and capture bacteria within the epithelium and intestinal lumen [164]. True to the more tolerogenic roles of some CD103+ DCs versus pro-inflammatory macrophages within the lamina propria, it is these cells that induce T regulatory (T-reg) cell expansion though TGF-β and retinoic acid-dependent mechanisms both locally and after migration to mesenteric lymph nodes [159, 164, 165].

Our understanding of the traditional roles of immune cells has been expanded, as further groups of innate immune cells have been described and pathways of response and memory have been defined in disease and tissue-specific contexts [166]. The following passages refer to the innate roles of lymphocytes and lymphoid cells, with particular reference to the tissue-specificity of the latter.

1.3.3 Lymphocytes and innate lymphocytes

Within the adaptive immune system, lymphocytes fall into two broad groups: T cells and B cells, that are typically found in the blood and secondary lymphoid organs. During development, auto-reactive cells are eliminated in the thymus (T cells) and bone marrow (B cells) to ensure that the immune system does not mount a significant response against self-antigen (central tolerance) [167-170]. Conversely, these lymphocytes must have receptors that recognise specific foreign antigens, and in the case of both T and B cells, these are made of two polypeptide chains anchored to the cell membrane. T cell receptors (TCRs) can be made of α,β,γ or δ chains that dimerise to produce the T cell receptor, whereas B cells express surface immunoglobulins or B cell receptors (BCRs) [171-173]. Both TCRs and BCRs have constant regions anchored to the cell membrane and variable regions for antigen binding. This variability is critical to the success of a precise, but robust adaptive immune response through recognition of specific antigens and arises through gene rearrangement of the V, D and J segments of the TCR α and β chains and the heavy and light chain loci in B cells [174-181]. When infection occurs, only a small number of lymphocytes will possess the specificity to respond, leading to clonal expansion and proliferation of those cells adapted to successfully eliminate the pathogen.

T Lymphocytes

The TCR can only recognise antigens or short peptides derived from pathogen proteins presented in the context of major histocompatibility complex (MHC), rather than the pathogen as a whole [182-184]. To achieve activation, these peptides are presented by antigen-presenting cells (typically DCs) and costimulatory signals must also be present, for example CD40-CD40L, CD80/86-CD28 [185, 186]. For pathogens of intracellular origin, for example viruses that have infected a cell, peptides are displayed by MHC I. This activates CD8 T cells (or cytotoxic T cells), which are highly effective at delivering toxic substances to any similarly infected cells to cause death by apoptosis. Conversely, extracellular pathogens are presented by MHC II molecules on the surface of DCs and activate expansion of CD4 T cells. These cells are also called T-helper cells, as they 'help' activate CD8 T cells and B cells to produce their effector protein, antibody. Many of these DC-T cell interactions occur with the lymph node distal to the site of infection, as this is where DCs travel to encounter the greatest number of lymphocytes and thus increase the likelihood of finding those with a matching TCR [187].

More recently, there has been a greater appreciation of CD4 T cell polarisation to produce specific effector cytokine profiles, such as Th1, Th2, Th17 and T follicular helper (Tfh) cells. Th17 cells are of particular relevance to defence at mucosal surfaces and develop and proliferate in response to co-stimulation with IL-6 and TGF-β. The dual combination seems to promote Th17 cells in favour of Th1

or Th2 cells, whilst also allowing development of a counter, or anti-inflammatory response in T-regs [188, 189]. Th17 cells are further dependent on stimulation by IL-23a and require the transcription factor RORγt for production of IL-17a and IL-22 during inflammation [190]. They play a role in defence against extracellular pathogens, but have also been implicated in autoimmune disease (described further below) [191].

The T cells described thus far have been associated with expression of conventional TCRs, but T cells can also bear alternative TCRs and some exhibit tissue-residency, such as those observed at mucosal surfaces. Examples of these cells, with reference to their distribution is provided below.

γδT cells

γδT cells appear in the murine fetal thymus two days ahead of αβT cells, but the latter population quickly predominate [192]. In the periphery, the γδT cell population ranges in frequency and comprises approximately 4-5% of circulating CD3+ lymphocytes in humans (though frequencies vary across different species). Whilst originally thought to be both CD4 and CD8 negative, the development of superior antibody clones to these epitopes, revealed that γδT cells can express low levels of both markers [193]. The same publication demonstrated that numbers of γδT cells numbers were variable between individuals, but the proportions in the gut, Peyer's patches, skin and lymphoid organs were consistently lower in humans than mice. These findings have been replicated at other mucosal surfaces and are summarised in a review by Chien, Meyer and Bonneville, (2014) [194]. Unlike αβTCR cells, γδT cells can recognize a wider-range of ligands without MHC restriction, such as lipids presented by CD1-molecules, MHCI-like molecules and soluble ligands [194, 195].

γδT cells increase 5 to 10-fold during some infections, as shown within the blood of paediatric and adult patients with Salmonella infection [194, 196]. They can generate effector cytokines in both an innate and adaptive context and are an important source of interleukin-17 during acute infection and disease, as will be described in more detail below. In the skin, they have been shown to clonally expand from yolk sac precursors in healthy adult mice during parabiosis experiments and accelerate their proliferation during inflammation [197]. Jensen et al. (2008) demonstrated that, unlike αβT cells, thymic γδT cells are not ligand-restricted and do not require positive or negative selection during their development within the thymus. They found that populations of antigen-naïve γδT cells were present in the periphery and could be identified as being $CD44^{lo}$ and $CD122^{lo/int}$. On examining the effector cytokine profiles of antigen-naïve and antigen-privileged γδT cells after δTCR-crosslinking *in vitro* (using the antibody, GL4), they produced IL-17 and IFN-γ respectively [198]. It is important to note, that this relates to two distinct populations of thymic or lymphoid γδT cells. Intraepithelial γδT cells behave differently and were $CD122^{lo}$ irrespective of antigen-specificity, they

did not produce IL-17 and their *in vitro* effector function was cytolytic. To test the capacity of the γδT cells to rapidly produce IL-17, mice were immunized with myelin oligodendrocyte glycoprotein (MOG) peptide and T cells harvested from the draining lymph node. γδT cells were the predominate T cell producers of IL-17 in the first 3 days and were able to produce the cytokine before and after immunisation, whereas αβT cells could only respond after immunisation and a delay of 4 days [198]. These experiments give key insight into the development of γδT cells, their differences with αβT cells and their role in early inflammatory conditions.

During collagen-induced arthritis, two of the most abundant subtypes of γδT cells, Vγ4 and Vγ1 expand rapidly. Further analysis showed that the Vγ4 subtype was responsible for IL-17a production and showed more vigorous expansion upon re-challenge with the antigen. In keeping with this preferential response to a specific antigen, there was upregulation of CD44 and downregulation of CD62L and CD45RB, as is seen on activation of memory αβT cells [199]. Within the skin, splenic Vγ1 and Vγ4 γδT cells can be found, as well as those bearing alternative TCRs, including Vγ2, Vγ5 and Vγ6. In addition, splenic and dermal γδT cells responded with slightly different cytokine profiles in an experimental model of psoriasis and the authors also demonstrated differences in expression of transcription factors and cytokine and chemokine receptors in dermal and epidermal γδT cells. Together, these data illustrated the range of function and specificity these cells can possess, not just within the body, but within the epithelium of the same organ [200].

Innate-like and intraepithelial lymphocytes

Intraepithelial lymphocytes (IELs) are a group of resident mucosal immune sentinels, best described in the gut, that comprise mainly T cells. From this position, they facilitate health and regeneration of the epithelial barrier, mediate self and microbiotic tolerance and respond to immune threats. Innate-like lymphocytes include γδT cells (described above), natural killer T (NKT) cells and mucosal associated invariant T cells (MAITs), though only the latter are restricted to mucosal epithelium. These cells share similarities in that they possess T cell receptors, but have alternative T chain homodimers of distinct but limited diversity, leading to the term invariant. These TCRs can be activated through MHC-unrestricted mechanisms.

Invariant NKT (iNKT) cells express an invariant TCRα chain (Vα14-Jα18 in mice and Vα24-Jα18 in humans), paired to a limited number of TCRβ homodimers and are activated by the MHC-like molecule, CD1 [201-203]. They share transcription factors for development with T cells, NK cells and MAIT cells, including T-bet, PLZF, RORγt and SOX4 [204]. Their conserved TCR has been shown to recognise antigens from pathogens that can cause common or important diseases, such as *Streptococcus pneumoniae*, *Sphingomonas spp* and *Borrelia burgdorferi* [205-207]. NKT cells can be

subdivided into groups of cells that differ in their tissue distribution and cytokine profiles, bearing similarity to subtypes of T-helper cells, such as IL-17, IFN-γ, IL-4, IL-10, IL-21, IL-13, IL-9, IL-6, IL-5, IL-3, IL-2, GM-CSF and TNF [208]. The position of the cells influences their cytokine production through access to stimulating antigen and they are capable of producing multiple different cytokines, as well effecting cytolytic death through perforin production [209, 210]. NKT cells in the colon can express the transcription factor required for IL-17 generation (RORγt) at levels of approximately 50%, but typically expression is much lower in other tissues (5-10% in haematopoietic tissue and liver) [211].

MAIT cells also possess an invariant TCR (Vα7.2) and were first described in 1993 by Porcelli et al., in the peripheral blood of healthy donors [212]. These cells are enriched at mucosal surfaces and recognise antigen in an MR1-restricted manner (independent of MHC or CD1) and show tissue-specific transcriptional similarity to NKT cells, that is acquired in the thymus [211]. They have been shown to respond to infection in a range of contexts meaning that cells are difficult to find in experimental mice that are typically housed in pathogen-free environments and their rapid expansion correlates to post-natal immune development [213-216]. MAIT cells respond to specific bacterial and fungal pathogens without prior exposure, such as *Mycobacterium tuberculosis, Escherichia coli, Salmonella enterica, Pseudomonas aeruginosa, Klebsiella pneumoniae, Lactobacillus acidophilus* and *Staphylococcus aureus* [217-219]. These pathogens share the ability to synthesise riboflavin and it is riboflavin metabolites that bind MR1 and result in MAIT activation. MAIT cells have been postulated to play a role in cytokine production of IFN-γ, IL-17 and IL-22 within different tissues including the lung, the female genital tract, the renal tract, the nervous system, the liver and the gut [215, 217, 218, 220-225]. A proportion of MAIT cells are RORγt-expressing at levels of 60-70% in haematopoietic tissue and up to 90-100% in the gut and skin [211].

Tissue-resident immune niches are often also home to cells that resemble T cells, but lack a TCR, described as lymphocyte-like or lymphoid. These cells are important players in innate immune responses directed towards immune defence, tolerance and homeostasis and are described in more detail in section 1.4.2.

1.3.4 Innate lymphoid cells

Innate lymphoid cells (ILCs) have only recently been categorised, but a wealth of literature now exists on their character and function. Much of their developmental biology remains elusive, but a number of recent papers have sought to obtain clarity on the complexity and heterogeneity of these cells from zebrafish to mice to humans [226-230]. ILCs possess three key features [231]:

- Absence of recombination activating gene (RAG)-dependent rearranged antigen receptors.
- Lymphoid morphology.
- Lack of lineage markers specific to myeloid or dendritic cells.

Whilst NK cells were first described in 1975 [232], other members of the ILC family have subsequently been defined, with lymphoid tissue inducer (LTi) cells identified next in 1997 [233]. Since then, the rapid increase in data pertaining to ILCs has led to a need for a uniform nomenclature. Leaders in the field divided ILC into four main groups based on their development and signature effector molecules (figure 1.4) and this approach has withstood interrogation by later genomic investigation: NK cells, group 1, group 2 and group 3 ILCs [227, 231].

Early ILC progenitors

ILCs develop from a common lymphoid progenitor (CLP) which can give rise to ILCs and lymphocytes from the foetal liver or adult haematopoietic tissue. CLP precursors to ILCs express the integrin α4β7 and are known as α-lymphoid precursors (αLP) and those that express CXCR6 can differentiate into NK cells or ILC3s, but may also contain precursors of any ILC type [234-237]. These cells are $Flt3^{-}$/c-KIT^{int}/Sca-1^{int}/$CD127^{+}$and are the earliest cells in the ILC lineage to lack B and T cell potential [228].

Downstream of CLPs are various transcription factors or repressors that facilitate ILC development and guide differentiation. The most extensively described are Id2, NFIL3, PLZF, and TCF-1 and these transcription factors are likely to form critical decision checkpoints for differentiation of early ILC precursors [228], many of which are mediated by STAT5 across all ILC lineages [238]. E proteins are helix-loop-helix transcription factors required for the development of lymphoid lineages and are regulated by Id2. Id2 is a transcription repressor that sequesters E47, thereby directing differentiation away from T and B cell development and towards ILCs and cells of this type are termed 'common progenitor to all helper-like ILCs' or CHILPs [239, 240]. The ratio of E protein activity to Id2 has been demonstrated to affect differentiation of all ILC lineages and NK cell maturation [234, 235, 241].

The transcription factor NFIL3 (also known as E4BP4) is an early, transient, pre-requisite transcription factor for ILC development of all lineages [242]. Furthermore, GATA3 has been shown to be indispensable for development of all ILC lineages that express CD127, likely influencing development at the CLP. Although high levels of GATA3 expression are associated with ILC2 populations, the transcription factor is still required for maintenance of all CD127+ ILCs and can be found at lower levels of expression within these mature populations [243].

It is clear, therefore that the transcription factors required for ILC development are complex and poorly understand, as new analyses yield larger lists of potential promotors and repressors. There is considerable heterogeneity between populations and organs and this has been confirmed using single-cell RNA sequencing from a range of different tissues and organisms [226-229, 244]. The key transcription factors required for maintenance of each ILC group are outlined below, but further detail on the developmental pathway has been reviewed by Diefenbach et al. (2014) [245]. Figure 1.6 illustrates the key steps in ILC development and has been adapted from Juekle and Romagnani (2016) [4] to fully demonstrate the development, products and relationships of different ILC subsets.

Natural killer cells and group 1 innate lymphoid cells

NK cells and group 1 ILC (ILC1) share the common cytokine product, IFN-γ. Like cytotoxic T cells, T-bet in cooperation with eomesodermin (EOMES) are key transcription factors for the development of NK and ILC1 cells. Both cell types share cell surface markers, but there are differences that have led authors to postulate that NK cells and ILC1 resemble innate versions of CD8 T cells and CD4 Th1 cells respectively [246, 247]. Table 2 demonstrates the key distinguishing cell surface markers in mice and humans.

Group 2 innate lymphoid cells

Group 2 ILC (ILC2) have been intensively investigated in disease models of allergy and hypersensitivity, in keeping with their similarity to Th2 cells. Commitment to an ILC2 precursor occurs early in ILC development and is associated with upregulation of Il1rl1, Il2ra, Ly6a, CCR9 and Klrg1 [228]. They require the transcription factors GATA3, RORα and Gfi1 for developmental maturity and respond to stimulation by IL-33 [248-250], IL-25 (also known as IL-17e) [251, 252] and thymic stromal lymphopoietin (TSLP) [253]. ILC2s respond by producing IL-4, IL-5 and IL-13 [251-254]. They play an important role in the immune response to helminth infections [252, 254], allergic asthma [253] and atopic skin conditions [255]. ILC2s have also been demonstrated to have regulatory roles in sterile models of renal inflammation, mediating their effects though macrophages and eosinophils [128, 129, 256].

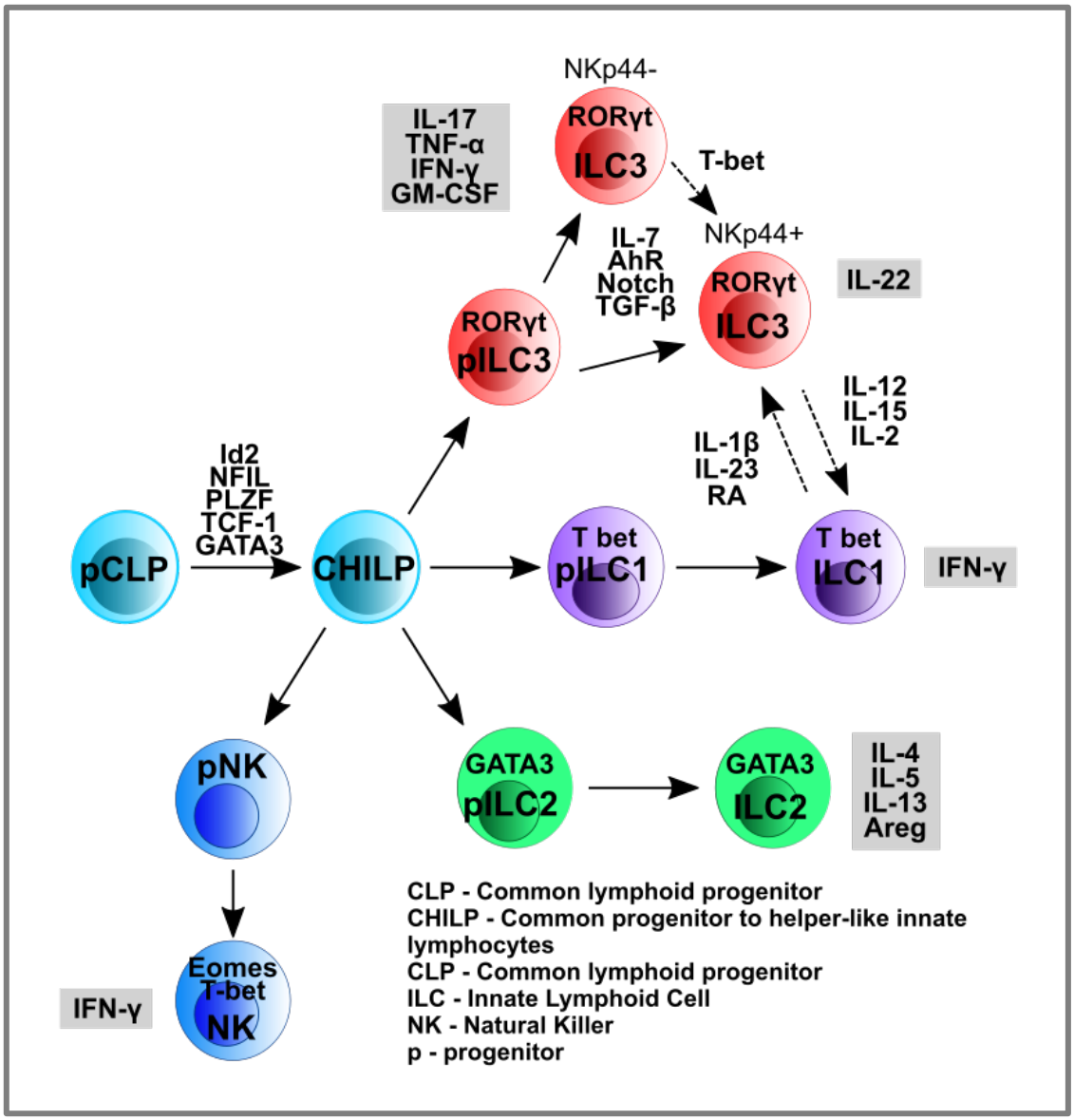

Figure 1.6: Stages of ILC development

Transcription factors are shown and cellular products (grey boxes). Plasticity between ILCs is also demonstrated (adapted from Juekle and Romagnani, 2016) [4].

Group 3 innate lymphoid cells

ILC3s display considerable heterogeneity and plasticity in their role in maintenance of immune homeostasis and defence at mucosal surfaces. The following sections will describe the different ILC3 subsets, with reference to their development and function.

ILC3 subsets and markers

ILC3s demonstrate plasticity, particularly between the ILC1 and ILC3 compartments. This leads to some difficulty in reliably categorising ILC3s, but it is widely accepted that those expressing NK

markers (such as NKp46 in mice or NKp46 and NKp44 in humans) can be termed NCR^+ and those that don't, NCR^-. The latter can be further delineated using CD4 or CCR6 expression and include LTi cells that are $CD4^-$ $CCR6^+$. Within the intestine, a T-bet gradient controls the conversion of LTi cells to IL-22 producing NCR^+ cells during *Salmonella* infection [257-259], though evidence also exists of Notch and TGF-β influence on the balance between NCR^+ and NCR^- cells [260]. Fate mapping experiments have shown that CCR6+ ILC3s emerge by gestational week 13.5 and that Ncr1 expression is transient during that period [261]. By the time the fetus reaches 18.5 weeks, distinct populations of NCR+ and NCR- cells are apparent.

Whilst several papers have outlined developmental and homeostatic heterogeneity at a transcriptional level, other studies have confirmed this using alternative methods. Mass cytometry studies of human fetal intestinal cells, tonsil, spleen, bone marrow, bowel, skin, lung and blood have confirmed the diversity of ILCs at a protein level [229, 262]. Further cell surface markers that guide segregation are shown in table 2, but it is worth remembering that all ILCs exhibit significant heterogeneity, as demonstrated by RNA sequencing of ILCs from multiple sites (mucosal and non-mucosal) [229, 230]. Despite this heterogeneity, there are a range of cell surface molecules displayed by ILCs that allow us to categorise these cells by flow cytometry. Table 2 gives a summary of the murine and human markers available for analysis.

Table 1.2: Human and murine ILC cellular surface markers.

Marker	**ILC1**		**ILC2**		**NCR+ ILC3**		**NCR- ILC3**	
	Hu	Mu	Hu	Mu	Hu	Mu	Hu	Mu
CD127	+	+	+	+	+	+	+	+
CD90	NA	+	NA	+	NA	+	NA	+
CD161	+	NA	+	NA	+	NA	+	NA
CD117	-	-	+	+	+	+	+	+
CD94*	-	NA	-	NA	-	NA	-	NA
NK1.1*	NA	-	NA	-	NA	+/-	NA	-
CRTH2	-	NA	-	NA	-	NA	-	NA
ICOS	-	-	+	+	-	-	-	-
ST2	-	-	+	+	-	-	-	-
IL23R	+/-	-	-	-	+	+	+	+
CD56	+/-	-	-	-	+	+	-	-
CCR6	+	-	+/-	-	+	-	+	+/-
NKp44	-	NA	-	NA	+	NA	-	NA
NKp46	-	-	-	-	+	+	-	-
MHC II	UD	-	+/-	-	+/-	-	+/-	-
CD4	-	-	-	-	-	-	-	+/-

*Present on NK cells.
Adapted and developed from multiple sources [101, 231, 263-265].

ILC3 development

ILC3 development is dependent on the transcription factor RORγt [240, 266-268], but differentiation is also supported by Notch signalling [236], IL-7R, c-KIT (ligand, SCF) [269] and the aryl hydrocarbon receptor (AhR) activation; AhR responds to dietary metabolites such as tryptophan [247] and retinoic acid [270, 271]. In addition, Ikaros (a zinc finger transcription factor) inhibits post-natal ILC3 development via AhR inhibition and plays a role in ILC3 regulation during health and expansion during disease [272]. These steps ensure differentiation that favours ILC3s over other ILC lineages and demonstrates further evidence for the common stages of early ILC development and the influence of environment in directing differentiation [273-275].

As well as exhibiting plasticity within their own group, ILC3 have been shown to down-regulate RORγt in favour of an ILC1 phenotype [276, 277]; this is promoted by IL-15, IL-12 and IL-2 and repression of AhR signalling and inhibited by IL-23, IL-1β and retinoic acid. There is also evidence of ILC2 differentiation into cells that express low levels of RORγt and co-produce IL-17 and IL-13 in the context of pulmonary helminth and fungal infection [278]. It is again noted, that the ILC2 signature transcription factor, GATA3, is also required for ILC3 survival, though at much lower levels of expression [243, 279, 280].

ILC3 function

NCR^+ ILC3s tend to produce IL-22 [261, 281, 282] and NCR^- cells, IL-17, lymphotoxin [258], TNF-α and IFN-γ [257], though there is overlap. ILC3s have also been shown to be the primary source of GM-CSF in the gut in inflammatory bowel disease, amongst the other cytokines mentioned above [127, 283]. NCR+ ILC3s that had been sorted from lamina propria preps showed basal IL-22 expression, that increased upon further stimulation with IL-2, IL-12 and IL-18. Addition of IL-1β, IL-2, IL-6 and IL-23 prompted IL-22, IFN-γ and GM-CSF release from NCR+ ILC3s and IL-22 and GM-CSF from NCR- ILC3s (these cells were transient NK1.1-expressors) [261]. These cells did not produce IL-17a.

The functional roles of ILC3 have been well characterised at various mucosal surfaces and most research has focussed on the gut. LTi cells are responsible for the formation of secondary lymphoid tissue *in utero* and play a role in the later development and maintenance of lymphoid tissues, such as Peyer's patches [284, 285]. As part of their role in lymphoid follicle maintenance within the gut, they are also responsible for facilitating class-switching and T cell-independent generation of IgA by B cells [286]. LTi cells play a further role in regulation within the gut, by tolerising the response of CD4+ T cells to commensal bacteria using an MHCII-dependent mechanism [287].

ILC3s are also critical in the early host response to infective colitis by producing IL-22 and IL-17 [281, 282, 288] and inflammatory bowel disease [289]. ILC3-derived IL-22 also maintained the intestinal epithelium and promoted regeneration after methotrexate-induced injury by preserving stem cells [290]. Tissue-resident MNPs provide the cytokine stimulation to promote a robust ILC3 response in the face of injury and the activating role of IL-23 from CX3CR1^{+} MNPs during *Citrobacter rodentium* colitis has been established [282]. Furthermore, ILC3s have been shown to express Death Receptor 3 (DR3) and co-stimulation with IL-1β and TL1A produced a strong IL-22 response and induced ILC3 proliferation *in vitro* [291]. TL1A is produced by MNPs in response to FcγR crosslinking and PAMPs, indicating another possible role for MNPs in ILC3 activation [292].

Human ILC3s are CD127^{+} (IL-7Rα) and were segregated using CD56 by Glatzer et al. 2013 [293]. The authors found that NKp44^{+} was enriched on CD56^{+} ILC3s and these cells were the only ILC3s capable of producing IL-22 upon stimulation with IL-1, IL-23 and IL-7. Using flow-sorted tonsillar ILC3, they performed a series of *in vitro* experiments to confirm these findings. ILC3s that produced IL-22, also produced GM-CSF, TNF and IL-2 after stimulation with IL-1, IL-23 and IL-7, or in response to virally-infected epithelial cells. The same authors attempted to recapitulate their findings in a murine model, using RORγt fate-mapping and it is interesting to note the variability in NK1.1 staining from ILC3s that were derived from the spleen and intestine. Splenic NK1.1^{+} NKp46^{+} ILC3s produced IFN-γ and TNF on IL-1/IL-23 stimulation, whereas intestinal NK1.1^{-} NKp46^{+} ILC3 produced IL-22. These experiments highlight not only the tissue-variability in ILC3 marker expression, but also the difficulty in translating *in vitro* findings and cross-referencing human and murine experiments.

In 2017, Riedel et al., described all ILC subtypes in healthy human and murine kidneys [129]. They were able to identify NKp44+ ILC3 (approx. 50% of total ILCs) and NKp44- ILC3 (approx. 20% of all ILCs) from human renal tissue that had been removed during nephrectomy for renal cell carcinoma. ILC3s were the predominant subtype in human kidneys, but ILC2s far outnumbered ILC1s and ILC3s in murine tissue. The paper went on to describe the role of ILC2s in adriamycin-induced glomerulosclerosis.

Further reference to the cytokines produced by ILC3s is made in the following section on immune cell activation.

1.3.5 Immune cell activation

Proinflammatory cytokines and mediators

Soluble chemical mediators are a critical part of shaping immunity, inflammation and repair, be it in the context of autonomous cellular immunity, local effects or activation of a systemic immune response; analogous to autocrine, paracrine and endocrine hormonal regulation, respectively.

Inflammatory mediators include neurohumoral transmitters, vasoactive peptides and eicosanoids. These mediators are typically locally-acting and contribute to mechanisms that promote vasodilation, loosening of epithelial and vascular tight junctions, activation of tissue-resident immune cells and hyperaesthesia. Together, these effects promote an immune response and produce Celsus's hallmarks of inflammation: *rubor, calor, dolor* and *tumor*.

Cytokines and chemokines are released with both local and systemic effects that can be regulatory/homeostatic, anti-inflammatory or pro-inflammatory. As is true of most processes within the body, in health these effects are often balanced and reciprocal. Pro-inflammatory cytokines include IL-1β, IL-6, IL-12, IL-18, IL-23, IL-17, TNF-α, GM-CSF and IFN-γ and anti-inflammatory cytokines include IL-10 and IL-22. It is inaccurate to describe cytokines in this way, without also recognising that cytokine action is dependent on the receptors displayed by effector cells and the presence of soluble receptors within the bloodstream. Differences in signalling can therefore lead to the same cytokine exerting balanced and nuanced pro- and anti-inflammatory effects, such as IL-6 and TGF-β [189, 294]. The specific cytokines governing ILC3 activation and those mediating their effector functions will be described in detail below in the section on Th17 cytokines.

Chemokines are chemoattractant chemical mediators that are critical in the placement and trafficking of immune cells throughout the body in both health and disease. For example, dendritic cells show greater directional migration to lymph nodes after LPS or immune-complex stimulation, by upregulating CCR7 expression and using a CCL19 gradient [295-297].

Chemokines also play a critical role in localising inflammatory monocytes and neutrophils to peripheral tissues in the context of infection or inflammation. For neutrophils, IL8 (CXCL8) in humans, and CXCL1, CXCL2, and CXCL3 in mouse and human act via their reciprocal receptors CXCR1 and CXCR2 [298-300]. In the case of inflammatory monocytes, CCL2 attracts CCR2-expressing monocytes to areas of infection, for example in gut inflammation [111, 123] or in cardiac ischaemia [121]. Other key chemokine/receptor interactions include CX3CR1-CX3CL1 that is associated with MNP placement in tissues [112, 122, 165] and CCR6-CCL20 with lymphoid cell movement [301].

In the case of ILCs, there is little data currently available on the cues governing their movement, however parabiosis experiments suggest that they do not enter the circulation [302]. Furthermore, the authors demonstrated that populations of ILCs increased within tissues and secondary lymphoid organs, but this expansion was not seeded by haematogenous precursors. Taken together, this data suggests that ILCs are tissue-resident, self-renewing cells. ILC3s do traffic to lymph nodes in a CCR7-dependent manner and they are the predominant ILC-type in mesenteric lymph nodes [303]. Just as ILC3s predominate at the gut mucosa, these cells were enriched in mesenteric versus inguinal lymph

nodes. The authors went on to demonstrate that during *Heligmosomoides polygyrus* infection (parasitic infection of the gastrointestinal tract), ILC3s expanded in the gut and mesenteric lymph nodes. Ki67 staining revealed that NKp46+ ILC3s and ILC2s proliferated, but LTi ILC3s did not. This data bears similarity to the *Ncr*-fate mapping experiments of ILC3s from the small intestine, which showed that ex-NKp46 expressing ILC3s did not proliferate, however NKp46+ ILC3s demonstrated low levels of proliferation (6-8% Ki67 positive) [261].

The following sections will focus on cytokines that promote Th 17 responses (IL-23a, IL-1β and TL1A) and can stimulate T cells and ILC3s to produce their effector cytokines (IL-17a, IL-22 and GM-CSF). Whilst these inflammatory pathways were first associated with CD4+ Th 17 cells, other cellular producers of IL-17a are now well established and will be referenced below.

Th17-inducing cytokines

Differentiation of naïve T cells into Th17 cells requires the transcription factors STAT3, RORγt, RORα and Ahr [304-307] and is driven by IL-6 and TGF-β (plus IL-1β and TNF) or IL-6, IL-23a and IL-1β stimulation [188, 189, 308-313]. These cells have been identified in a range of tissues and produce IL-17a, IL-17f, IL-22 and IL-21, the latter acting to auto-amplify the Th 17 response [309-311, 313, 314]. Early identification of a group of CD4+ T cells that produce IL-17 was made in experimental autoimmune encephalitis (EAE) in 2005 [315]. Fate-mapping of IL-17-producing cells demonstrated the differentiation of Th17 cells in EAE, though as the condition progressed, they demonstrated plasticity by switching to a Th1-effector profile in an IL-23-dependent manner and potentiating a chronic autoimmune inflammatory state [316]. It appears that Th17 cells have a greater capacity than Th1 or Th2 cells for plasticity and reciprocal activation (with Tregs), as they share an activating factor TGF-β. [124, 188, 313]. The requirement for co-stimulation and balance of pro-inflammatory and regulatory cytokines provides nuanced ways of clearing intracellular pathogens and controlling the immune response. The role of MNPs in assisting with this balance is described in section 1.3.2.

In psoriasis, IL-17a is an important pathogenic effector cytokine and originates predominately from dermal γδT cells after stimulation with IL-23a from mononuclear phagocytes. Furthermore, co-stimulation with PAMPs augments the response *in vitro* and it is known that pathogen-associated IL-17a production by peritoneal, pulmonary and splenic γδT cells requires co-stimulation with IL-23a and IL-1β. The importance of IL-23a stimulation in humans with psoriasis was also demonstrated by increased IL-17a production by γδT cells within skin lesions [200]. In a sterile model of inflammation causing glomerulonephritis, renal DCs produced IL-23a to stimulate IL-17 production from renal Vγ4 γδT cells during the early stages of nephrotoxic nephritis (independent of IL-1β). As the pathogenesis progressed, CD4+ T cells become the predominant source of the cytokine, however the

early production by the γδT cells was critical for neutrophil and macrophage recruitment and glomerular damage. Notably, the origin of the renal Vγ4 γδT cells was not fully addressed and it is unclear if these were recruited or truly resident [317].

Within the gut, the IL-23a/IL-17a axis has been demonstrated to be important in activating γδT cells and ILC3s to produce IL-22 during DSS colitis. This occurs in a retinoic acid (RA)-dependent manner and is enhanced by IL-1β [318]. This model demonstrates the interplay of diet (vitamin A is required for RA production) and IL-23a/IL-17-driven inflammation at the gut muscosa, in influencing innate lymphoid populations. During *C. rodentium* colitis, IL-10 regulated the production of IL-23. Without this anti-inflammatory effect there was increased epithelial damage and mortality, associated with reduced production of IL-22 from ILC3s [125]. Conversely, in models of T cell-driven colitis, IL-23 signalling was found to be protective through reduced levels of inflammation [319]. In this model, IL-23R deficiency reduced production of IFN-γ, IL-22, IL-17A and IL-17F, without affecting ILC expansion, however ILC3-derived-IL-22 was colitogenic though neutrophil recruitment. It is worth noting, that these models used anti-CD40 antibodies or T cell transfers to Rag KO mice to induce colitis and therefore do not truly represent wild type pathology.

TL1A is part of the TNF-family of cytokines and it acts via Death Receptor 3 (DR3) [320, 321]. It is produced upon IL-1α and TNF stimulation and PCR analysis of *Tnfsf15* (TL1A transcripts) show that it is expressed (in decreasing order of magnitude) within the kidney, prostate, stomach and intestine [320]. Early reports of TL1A activity indicated that it was capable of inducing NF-κB activation, T cell stimulation and apoptotic cell death in non-T cells [320-323]. In 2008, Meylan et al. showed that TL1A stimulated CD4+ T cells, contributing to pathology in EAE and allergic lung inflammation. They also demonstrated that DCs were the predominant source of TL1A after TLR or FcγR stimulation [324]. More recently, TL1A has also been shown to activate ILCs and NK cells, particularly ILC2s and ILC3s [282, 325-327]. In the case of ILC3 contribution to intestinal inflammation, it was TL1A co-stimulation with IL-23a and IL-1β that led to increased levels of IL-22 production [282].

Th17 effector cytokines

Interleukin-17

In the 1990s, the IL-17 family of cytokines was recognised as having unique properties, both in terms of their actions and cytokine-receptor homology. This led to IL-17-associated responses being catagorised alongside type 1 and type 2 helper-T cell responses, as Th17 immunity. Subsequently, we have come to appreciate that Th17 cells are not the only lymphoid source of IL-17, as described

earlier in the chapter; NK cells, γδT cells, MAIT cells and type 3 ILCs are rapid innate producers of IL-17 in a range of infective and sterile models of inflammation [328]. There are six IL-17 cytokines, named A-F, though IL-17A (known as IL-17) and IL-17F share receptor specificity and are the most extensively investigated. Cellular responses to IL-17A/F require signalling via the IL-17 receptor (IL-17R), made up of the ubiquitously expressed IL-17RA, paired with the inducible IL-17RC [329]. IL-17 is important at mammalian epithelial and mucosal barriers, where these cells are enriched, directed by their CCR6 expression [330]. Expression of IL17RC is enhanced in colonic epithelium and IL-17 and IL-17F are produced by different immune cells and have been shown to have defined roles in sterile arthritis, mucocutaneous *S. aureus* infection and *C. rodentium* enteritis [331].

IL-17 is typically associated with immune cell recruitment, such as neutrophils, by enhancing expression of certain pro-inflammatory chemokines and cytokines. These include the cytokines, TNF, IL-1β, IL-6, GM-CSF and G-CSF, the chemokines, CXCL1, CXCL8 and CXCL10, and metalloproteinases [332-339]. Several of these studies also demonstrate the synergistic effect that IL-17 has with other pro-inflammatory cytokines in providing positive reinforcement to the inflammatory reaction. In addition, IL-17 has further effects at the mucosa and has been shown to stimulate production of AMPs and acute phase proteins, such as defensins, serum amyloid A, S100 proteins and lipocalin-2; these effects are again synergistically mediated by IL-17 and IL-22 and alter disease severity. [58, 67, 314, 340-342].

Macrophages and interleukin-17a

Macrophages express IL-17 receptors (IL17R), though receptor specificity appears to be tissue and ligand dependent. Gut and peritoneal macrophages express IL17RA and IL17RC, whereas IL17RA predominated in lung macrophages and neither were found in splenic macrophages [343]. At baseline, $Ly6c^{+}$ monocytes expressed IL17RA at much higher levels than their 'noninflammatory' $Ly6c^{-}Gr1^{-}$ counterparts. *In vitro* stimulation of bone-marrow derived macrophages, led to increased IL17RC expression with CpG and peptidoglycan, but not IL17RA (no effect seen with LPS). *In vivo*, immunization with Freud's adjuvant led to an increase in IL17RA on hepatic macrophages, but with no corresponding increases on macrophages from the CNS, gut, spleen or lung. It is reasonable to predict, therefore, that tissue-resident macrophages may assume pro-inflammatory profiles in keeping with organ-specific threats.

Concordant with its pro-inflammatory effects, IL-17a potentiates atherosclerosis, a cause of chronic inflammation within medium to large arterial vessels that can lead to tissue ischaemia, heart attacks and strokes. In mice treated with IL-17A monoclonal antibodies (mAb), there was increased plaque stability, reduced arterial stenosis, reduced plaque necrosis and decreased plaque cellularity [344].

This is of particular interest when considering IL-17a in mediating cross-talk between immune cells within chronic inflammation, as the authors went on to show that the cytokine encourages recruitment of monocytes and bias toward a pro-inflammatory transcriptome within macrophages. Furthermore, it has been shown *in vivo*, that IL-17a induces markedly increased production of IL-12p70 (as well as the other proinflammatory cytokines CCL5, CCL4, GM-CSF, IL3 and IL9) from macrophages in the spleen, peritoneum, lung and bone marrow. By using IL-17a blockade in bone-marrow derived macrophages, the authors were able to confirm a reduction in IFN-γ production in naïve CD4 T cells after stimulation with ovalbumin (OVA) *in vitro* [343].

Interleukin-22

IL-22 is produced by Th17 cells and many of the other IL-17-producing cell types [345]. Th cells that predominantly produce IL-22 are known as T-helper-22 (Th22) cells. As such, IL-22 was originally mistaken for IL-17 and thought to be closely related, however it is a member of the IL-10 family [346]. IL-22 is considered to be mainly regulatory or protective through its actions in releasing AMPs [314, 347] and renewal of epitheliocytes [348]. The cytokine uses IL-22 receptors (IL-22Rs) that activate the Jak-STAT1/3/5 transcription pathways [314, 347-352].

Further evidence supports the protective actions of IL-22 at epithelial surfaces and many of the AMPs associated with the renal epithelium may be produced in response to IL-22 and IL-17 co-stimulation, though this association has only been demonstrated in other tissue types [314, 340-342]. In a murine model of intestinal infection with *C. rodentium*, IL-22 levels were quick to rise in response to IL-23 stimulation [347, 353]. Histological analysis indicated that mice with an IL-22 deficiency had more epithelial damage and an increased bacterial burden in peripheral tissues, indicating breaching of the epithelial layer and bacterial spread. Microarray analysis demonstrated that IL-22 treatment led to an upregulation in AMP and epithelial renewal factors such as S100A8, S100A9, RegIIIβ, RegIIIγ and SAA3. Reg fusion proteins were subsequently used to rescue the disease phenotype in *Il22*-deficient mice, supporting their role in protecting epithelial surfaces from gram negative bacterial infection [347]. In the case of RegIIIγ, γδT cells and ILC3s were demonstrated to be the predominate source of IL-22 within the murine gut during *C. rodentium* colitis [318]. *In vitro* stimulation of keratinocytes with IL-22 also leads to AMP and renewal factor production, an effect that again demonstrated synergism upon addition of IL-17 [314].

The effects of IL-22 are not all protective and excessive activation and epithelialisation is thought to underpin conditions such as psoriasis [354, 355]. IL-22 was also linked to inflammation in humans with inflammatory bowel disease, though IL-22 merely correlated with pro-inflammatory cytokines such as CXCL8, IL-1β and TNF-α and causality was not established. Instead, IL-22 was associated with

release of HBD2 and increased epithelial proliferation *in vitro* [349]. In a murine model of transferred T-cell-driven colitis, IL-22 from ILC3s was found to be colitogenic, a finding replicated in anti-CD40-induced colitis (CD40 is a T cell co-stimulatory molecule) [319].

Granulocyte macrophage colony-stimulating factor

Granulocyte macrophage-colony stimulating factor (GM-CSF) is so named for its ability to stimulate BMDMs to differentiate into myeloid cells, namely neutrophils, macrophages and DCs [356-358]. It is one of the Th17 cytokines produced by polarised CD4 T cells and by ILC3s [127, 359]. *In vitro*, GM-CSF has been routinely added to cells in culture to produce myeloid cells for decades and more recently, the dose effect of the growth factor on specific myeloid cell differentiation has been fully interrogated. Using cultured BMDMs, low doses (0.5-1 ng/ml) of GM-CSF promoted neutrophil survival, medium doses (2-4 ng/ml) promoted monocytic-DC differentiation and high doses (10 ng/ml) promoted monocyte proliferation [360]. Using the higher concentration, Hui et al. (2018), demonstrated that populations of pure $CD11b^{+}/F4\text{-}80^{+}$ macrophages are capable of potent phagocytic activity when challenged with *Listeria monocytogenes* and *Escherichia coli*. This ability was dependent on Cxxc finger protein 1 (CFP1), which promoted Csf2rα expression through histone modification [361]. Furthermore, BMDMs stimulated with GM-CSF produce proinflammatory cytokines, such as TNF-α, IL-6, IL-12p70 and IL-23 upon LPS challenge, whereas those stimulated with M-CSF produced a more anti-inflammatory profile [358].

1.4 The immune system in UTI

1.4.1 The innate immune response to urinary tract infection

The contribution of the renal tract and its epithelial products during UTI has already been discussed in section 1.2, however the cellular aspects of the innate immune system are explored below.

Macrophages orchestrate the innate immune response

Macrophages are tissue-resident immune cells that are critical for co-ordinating the host immune response to UTI. These cells recognise pro-inflammatory host DAMPs or PAMPs using PRRs. Specific recognition of these molecular patterns by the immune system was proposed by Charles Janeway at the Cold Spring Harbour Symposium of 1989 and identification of TLRs was confirmed later [362, 363]. Upon recognition, transcription pathways, such as MyD88>IκB>NFκB, are activated leading to the production of pro-inflammatory cytokines and chemoattractants (IL-1β, IL-18, TNF-α, CXCL8 and IL-12) that summon help from different arms of the immune system [363, 364]

Macrophages use TLR4 to recognise LPS and TLR5 to recognise flagellin (both present on UPEC) and this mechanism is particularly important in the bladder [365-368]. During UTI, $Ly6c^-$ macrophages release pre-formed pools of CXCL2 and CCL2 in response to tumour necrosis factor (TNF) from $Ly6c^+$ monocytes, leading to marked neutrophil recruitment via transepithelial migration and release of MMP-9 [369]. The same authors demonstrated that cytokine production was the primary function of $Ly6c^+$ macrophages in the first 24 hours of UTI (as opposed to phagocytosis) and loss of TNF led to persistent and recurrent cystitis and pyelonephritis.

CD14 is a marker also used to identify macrophages and it is a receptor for TLR4, controlling its endocytosis [368]. It is most associated with monocytes and in particular macrophages, though it is also found on DCs, PMNs and cells of non-myeloid origin [370]. CD14 expression is markedly elevated in acute UPEC UTI and mice lacking the receptor have increased bacterial burdens in their bladders after 1-2 days. By performing RNA sequencing on the bladders of WT and CD14 KO mice, Carey et al. (2016) identified CD14-dependent genes and found that the affected canonical pathways related to cell adhesion and diapedesis and the IL-17 cytokine axis. They went on to show the role of macrophage infiltration of the bladder within two hours of infection and showed a peak in F4/80 and CD14 double positive cells after 24 hours. Clodronate treatment depleted $F4/80^+$ macrophages and precipitated worse infection [3].

The innate roles of macrophages and DCs in ascending pyelonephritis has been characterised by Tittel et al. (2011). They found that neutrophils, followed by macrophages ($F4/80^+$ $CD11c^-$), were the key phagocytes of UPEC-GFP and that DCs ($F4/80^+$ $CD11c^+$) numbers declined over the first 21 hours. (It is noted that this may represent an oversimplification of MNP gating to correctly identify subsets of macrophages and DCs.) The authors go on to show that, in contrast to cystitis, $CD45^+$ $CD11c^+$ cells are the key producers of CXCL2 for neutrophil recruitment in pyelonephritis and identify these as renal DCs [371].

Our understanding of the role of MNPs in pyelonephritis was advanced by Berry et al. (2017) in defining zonal differences between medullary and cortical MNPs, by classifying their phenotypic characteristics and demonstrating heightened phagocytic capacity and cytokine production (IL-8) from medullary CD14+ MNPs in human kidneys. These differences were, in part, a consequence of the renal sodium gradient, which changes markedly from cortex to medulla to enhance the concentrating ability of the kidney by using increasing osmolality. These data provide a unique insight into the way tissue-resident MNPs have utilised their environment to create an antibacterial defence zone where it is most required in ascending pyelonephritis [12].

There remains overlap in the roles and markers of macrophages and DCs (as discussed in section 1.3.2) and the complex interplay of these cells with their environment suggests a tissue-specificity that is still poorly understood in the renal tract.

Neutrophils are rapidly recruited to the renal tract in urinary tract infection

Neutrophils are the most abundant white blood cell in the blood and they are rapidly recruited to sites of infection and inflammation, where they engulf microbes (phagocytosis) and neutralise them with cytolytic enzymes and reactive oxygen species. Neutrophils have a half-life of just hours in the blood and therefore the bone marrow devotes much of its activity to producing a large reservoir of these responsive cells [372]. They are mobilized from the bone marrow in response to a range of pro-inflammatory stimuli during UTI, that are detailed below.

After urethral catheterisation of mice with *E. coli*., neutrophil numbers rise proportionally to the bacterial burden, reaching their peak at six hours [373, 374]. Their recruitment is dependent on chemokines that allow transmigration of the cells from the blood to the interstitium of the renal tract. In humans, the epithelium and macrophages produce the pro-inflammatory factors IL-1, IL-6, CXCL12 and CXCL8, but it is CXCL8 (also known as IL-8) that is critical for recruitment of neutrophils to the urothelium [375-377]. Similarly, in murine models, CXCL2/3 is the ortholog of CXCL8 and its receptors (CXCR1 and CXCR2) are expressed by the epithelium and neutrophils in response to infection [375, 377]. Without neutrophil recruitment via CXCR1 and CXCR2, pyelonephritis and cystitis are worse in murine models of UTI, both in terms of bacterial clearance and mortality [300, 374, 378, 379]. As time passes and neutrophils give way to cells of the adaptive immune system, they die and produce DAMPs that potentiate the immune response. In addition, excessive cyclooxygenase-2 (COX2) activation by neutrophils has been associated with damage and remodelling of the bladder epithelium and predilection to recurrent UTI and chronic cystitis [380].

Natural killer cells and invariant T lymphocytes

NK cells have a recently-established role in UPEC UTI and they accumulate after infection in response to CXCL12 secretion by the urothelium [374]. Using reporter mice, NK cells were barely present within the bladder in health, but accumulated rapidly post-infection [374, 381]. Their numbers also increased within the kidney, where they were found at 2000 cells per kidney prior to UTI and 5500 cells per kidney after six days. NK cell depletion led to an increased bacterial burden in the bladders of mice treated with anti-NK1.1 depleting antibody, though interestingly anti-CD3 antibody (T cell depleting) did not lead to worse infection at the 24 hour time point [374]. Further investigation showed that NK cells produced TNF-α to attenuate UTI, but were unable to do so in UPEC strains that produced α-haemolysin (such as CFT073). Morphological changes in NK cells were observed

with α-haemolysin-producing strains of UPEC leading to increased cell death, an effect not replicated in T lymphocytes [381].

T cells with alternative T cell receptors may have an innate role in UTI. These include γδT cells and MAITs, though little has been firmly established for their role in UTI. Absence of γδT cells has been shown to increase susceptibility to UTI and their loss leads to a decrease in *IL17a* transcripts after 48 hours [382, 383]. MAITs are restricted by MHC I-related protein 1 (MR1) and recognise bacterially-infected cells. They were found in the urine of 10 out of 12 humans with leukocyturic UTI and were recruited to the bladder in UTI in mice, where they contributed significantly to bacterial clearance [223]. In humans on haemodialysis or after kidney transplantation, peripheral numbers of MAITs and iNKT were suppressed compared to healthy controls. Differences were seen in subsets of iNKT and MAITs with increased numbers of CD4+ iNKT and CD8- MAIT cells, and corresponding increases of IL-4 and IFN-γ. T cell numbers were decreased in haemodialysis patients with a decrease in IL-17 production, though this recovered in the transplanted cohort. Notably, none of these patients had developed chronic kidney failure secondary to recurrent UTI, however the differences in cell numbers may point to difference in immune profiles that promote immunodeficiency and local susceptibility to UTI in patients with CKD or after transplantation [222].

Interleukin-17 in the renal tract

IL-17 is a pro-inflammatory cytokine and has been associated with different models of AKI [339, 383-389]. IL-17A and IL-17F are the predominant pro-inflammatory cytokines and they are released in response to stimulation by IL-23 [390]. Notably, IL-17 has a central role in the pathogenesis of UTI both at the level of the bladder [3, 369] and in the kidney by promoting release of pro-inflammatory cytokines that enable neutrophil and monocyte recruitment [383]. Sivick et al. (2010), have demonstrated the role of IL-17A in *E. coli* murine cystitis with a rise in bladder *Il17a* transcripts within 8 hours of infection, reaching a peak at 48 hours, and increased bacterial burden in IL-17A KO animals (results showed a rising trend in colony forming units that reached significance after 72 hours). Subsequent analysis demonstrated the key producers of IL-17 at 48 hours were γδT cells, rather than $CD4^+$ T cells (including Th17 cells), and corresponding decreases in many key pro-inflammatory cytokine transcripts were observed (CXCL2, CXCL10, CCL5, CCL20, IL-4, IL-6, IFN-γ, TNF-α and G-CSF) [383].

Interestingly, whilst the effect of IL-17 in UTI was protective, it can be detrimental depending on the nature of the renal injury. In a cisplatin-induced model of AKI, measures of histological and biochemical severity were worse in wild type (WT) as opposed to IL-17A KO mice. The authors went on to demonstrate that they were unable to account for all the IL-17A through production by CD4 T

cells or after depletion of γδT cells, neutrophils or natural killer (NK) cells and postulated a further innate source of the cytokine. It was noted that although neutrophil recruitment was reduced in the IL-17A KO mice after 24 hours, there was no reduction in the chemoattractants; CXCL1, CXCL2, CCL2 and CCL5. [384]. It may be that the resulting AKI in this model of sterile inflammation was secondary to bystander damage caused by the inflammatory infiltrate, rather than the positive effect these cells exert in UTI.

Many different cell types are capable of producing IL-17, including Th17 cells [345, 383, 384], γδT cells [345, 383], MAIT cells [221], CD8 T cells [345, 391], NK cells [384], neutrophils [384, 392] and eosinophils [393]. Both septic (*E. coli* UTI) and sterile (cisplatin-induced) models of AKI have investigated the potential innate sources of IL-17 and found that depletion of T cells, neutrophils and NK cells does not account for all its production [383, 384]. Innate lymphoid cells are a potential source of the cytokine and have not previously associated with this role in the renal tract. These cells will be discussed in section 1.3.3.

Interleukin-22 in the renal tract

IL-22Rs can be found in the kidney with a predilection for the proximal tubular epithelium and corresponding IL-22 expression, through STAT3 signalling, is increased after ischaemia-reperfusion injury (IRI) [394-396]. In IRI, IL-22 KO mice have worse AKI than their WT counterparts and IL-22 treatment was associated with decreased levels of proinflammatory cytokines (IL-6, MCP-1, IL-1β and TNF-α), decreased neutrophil recruitment and decreased epithelial apoptosis [352]. Further work using this model confirmed the effect of IL-22 in IRI on tubular regeneration by neutralising the cytokine [350]. The same study identified tissue-resident MNPs as the main producers of IL-22 via a TLR4-mediated mechanism. In 2017, Weidenbusch et al., demonstrated that the transcriptional changes associated with IL-22 production in the kidney during IRI implicated the induction of Ahr ligands through Notch signalling [396]. They showed that IL22RA1 expression is present in the murine and human kidney in health and that gene expression of IL-22 and its receptor subunits rises with prolonged ischaemia.

In murine models of IgA nephropathy (induced by sterile and intranasal *S. aureus* methods), CD4 T cells could be found within the renal cortex, with correlated production of IL-17 and IL-22 [397]. The IL-22 producing cells were stimulated by IL-6 and recruited by the chemokines CCL20, CCL22 and CCL27. Further characterisation of the role of IL-22 within this context was not described. Systemic lupus erythematous also causes glomerular pathology, as well as nephritis and is associated with increased levels of urinary and systemic IL-22 in mice and humans [398, 399]. Treatment of MRL/lpr mice (who develop lupus nephritis) with monoclonal anti-IL-22 led to decreased proteinuria and

renal inflammation and better renal function further demonstrating its nephroprotective effects [399].

IL-22 also plays a protective role in tubular regeneration and decreased inflammation in models of chronic kidney fibrosis caused by diabetic nephropathy, unilateral ureteric obstruction and oxalate crystallopathy [396, 400, 401].

In vitro IL-22R production by human urothelial cells derived from bladder biopsies has been demonstrated, with corresponding rises in the AMPs, Lipocalin-2 and S100A9, upon stimulation with IL-22 [402]. In addition, IL-22 polymorphisms are associated with increased bladder cancer risk, which further implicates a role for this cytokine in homeostatic urothelial maintenance [403]. To the best of our knowledge, there is no published data on the role of IL-22 in the bladder during UTI.

Given the importance of both IL-22 and IL-17 in renal pathology and their demonstrated synergism, we turn out attention to another group of cells that can produce both cytokines, group 3 innate lymphoid cells. This project seeks to define their role in the urinary tract and UTI.

GM-CSF in the renal tract

In the bladder during UTI, *Csf2* transcripts rise approximately 5-fold in a manner dependent on CD14+ cells (namely, macrophages) [3] and *Csf2r* mRNA also rises [46]. Examination of urine from patients with *E. coli* UTI shows that GM-CSF is elevated, along with many other pro-inflammatory cytokines (IL-1β, IL-1, IL-12, IL-17A, IFN-γ, IL-8, MCP1 and G-CSF) [404]. *Csf2* transcripts and protein are produced both *in vitro* and *vivo* by murine bladder epithelial cells in response to LPS. The same study examined the onward effects of GM-CSF, by using a neutralising antibody, and found that *Vegf* and *Ptgs2* (COX-2) transcripts fell, but *Tnf* and *Ptgs1* (COX-1) transcripts were unaffected [405]. *In vitro* co-culture experiments of uroepithelium and monocytes leads to antagonism of GM-CSF production; infected epithelial cells produce the most GM-CSF, however addition of infection-exposed-monocytes decreased the response. This contrasted with heightened IL-10 levels in co-culture and contact [406]. These interactions help to demonstrate the interplay between immune cells and the epithelial and how this can alter cytokine profiles and the inflammatory balance during infection.

Of note, patients with end stage renal disease (ESRD) show altered peripheral MAIT cell profiles with down regulation of CD161 and increased GM-CSF and decreased IFN-γ production. The paper was primarily concerned with how MAIT cell homing might be affected in tuberculosis and ESRD, however *in vitro* stimulation of these cells with *E. coli* showed comparable *Csf2* and *Ifng* levels, but a reduction in *Tnf* transcripts. This, combined with an observed downregulation of CD161, suggests an altered response to microbial attack that might contribute to increased UTIs in CKD [407].

1.4.2 The adaptive immune response to urinary tract infection

Adaptive cellular and humoral responses to UTI

Adaptive immune responses to UTI hinge on the presentation of bacterial antigen by DCs that have travelled to the regional lymph node. This activates T lymphocytes within the lymph node to provide a robust response in the form of cytotoxic T cells, or antibody production by B cells with Th cell assistance. The roles of antibody are diverse leading a to multi-layered defence of direct pathogen neutralisation, activation of effector cells (including cytokine release, phagocytosis and direct cell toxicity) and fixation of the complement system.

Evidence for antibody production in UTI was described in 1987 by Hopkins et al., who induced *E. coli* cystitis in cynomolgus monkeys. Specific serum IgM levels rose within the first two weeks to be replaced by IgG over 7 to 21 days with peak levels at week 5-6. Non-significant rises in serum IgA were also observed. In the urine of the animals, secretory IgA levels peaked after 3-4 weeks of infection, with IgG levels peaking a week afterwards. Anti-*E. Coli* IgM was not observed in the urine [408]. Prior to this, anti-*E. coli* antibodies had been shown to impede the adhesion of UPEC in strains causing acute pyelonephritis, though the effect was strongest for antibodies specific to LPS, rather than other bacterial epitopes [409].

Subsequently, it has been demonstrated that reinfection does not lead to a significant increase in specific neutralising antibody production, but does lead to significantly increased T cell infiltration for bacterial clearance within the bladder [410]. While UPEC infection is typically cleared quickly in the kidneys (within 5 days), chronic infection can persist in the more tolerogenic environment of the bladder. In the same study, specific serum IgG levels rose in mice developing pyelonephritis and cystitis, but were impaired in mice developing cystitis alone after reinfection with UPEC. The authors went on to show that IL-10 from mast cells suppressed bladder DC activation and blunted the adaptive immune response, though full characterisation of a memory cellular response was lacking [411]. In addition, failure to engage DCs to evoke a memory response has also been linked to phagocytosis of UPEC by macrophages. In the absence of macrophages, bacterial uptake by DCs doubles and mice replete in CD4 and CD8 T cells show a trend towards fewer bacterial colony forming units (CFUs) than those treated with depleting CD4/CD8 antibodies [2].

It has been postulated therefore, that the native adaptive response in cystitis is less potent than the innate immune response, though it remains of use in clearing and preventing recurrence of pyelonephritis. This reflects the clinical importance of location in urinary tract infection, where

chronic colonisation of the bladder may cause an asymptomatic bacteriuria but pyelonephritis can cause acute kidney injury, septicaemia and death.

Vaccination in UTI

Vaccination has focused on the use of bacterial capsular or surface antigens to induce a humoral response to infection. Vaccines have been produced using heat-killed whole bacteria, bacterial proteins and purified-virulence factors. Such factors can be used to form polyvalent or fusion proteins to confer resistance to infection from multiple pathogens, such as the MrpH:FimH fusion protein with activity against *Proteus* and *Escherichia* species respectively [412]. Solco Urovac is a multivalent vaccine that provides activity against 6 strains of *E. coli* and *Proteus mirabilis, Morganella morganii, Klebsiella pneumonia* and *Enterococcus faecalis* [413]. While the vaccine passed two clinical trials showing a reduction in recurrent UTI caused by *E. coli* in sexually active women, there was no consistent increase in anti-*E. coli* antibody levels in treated recipients and it has not progressed further in trials. Subsequently, an *E. coli* tetravalent vaccine (ExPEC4V) was given to women with recurrent UTI and has produced IgG responses for all serotypes in phase 1b trials. Phase 2 studies have been initiated [414].

Hypothesis and Aims

We hypothesise that tissue-resident ILC3s contribute to local immune responses that may be beneficial for defense against UTI.

Aims:

1. Determine the anatomical location of ILC3s in kidney and bladder of mice and humans with reference to other immune sentinels.
2. Investigate the functional characteristics of ILC3s in urinary tract infection.
3. Interrogate the role of ILC3s in murine models of uropathogenic *Escherichia coli* UTI.

The aims will address the role of ILC3 in the renal tract by finding them and performing experiments to interrogate their interactions with MNPs and epithelial cells during UTI. Figure 1.5 summarises the potential pathways that we hypothesise may be involved in this process.

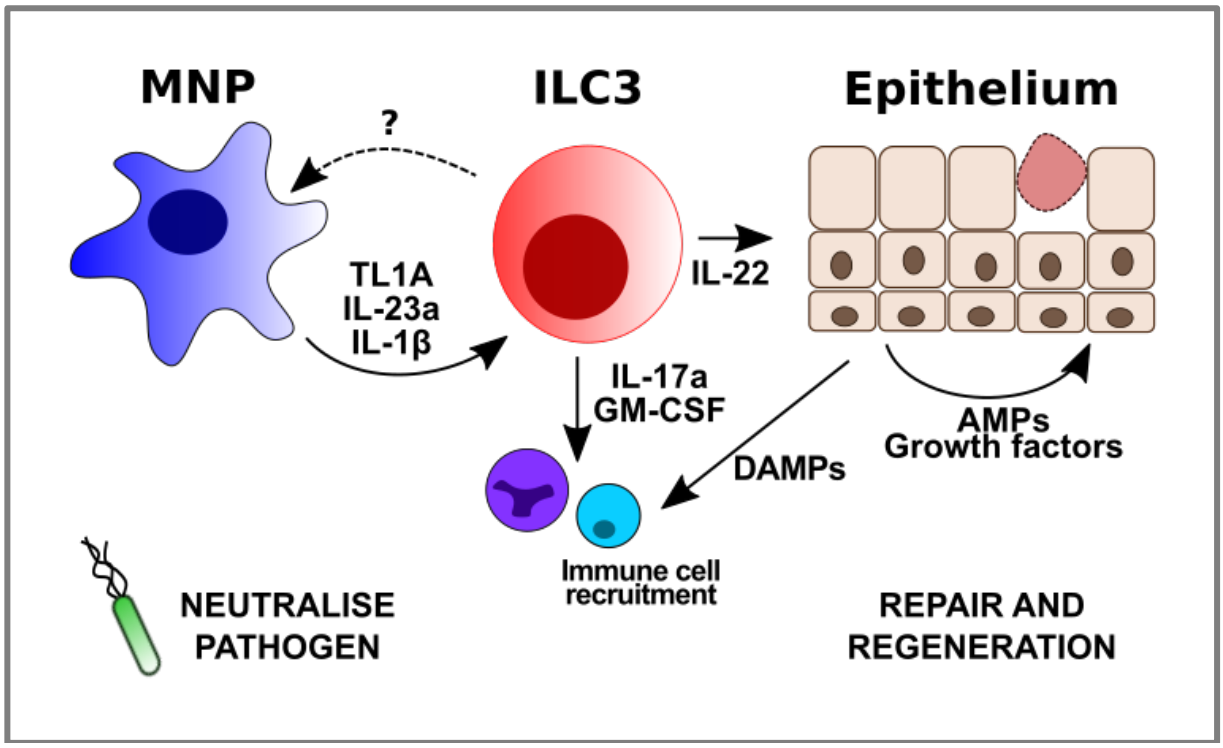

Figure 1.7: Products and relationships of ILC3s, MNPs and epitheliocytes of the renal tract during UTI.

Chapter 2 - Materials and Methods

2.1 Materials

2.1.1 Mice

All mice were housed at Cambridge Biomedical Services according to usual standards of animal husbandry and under specific-pathogen-free conditions. C57Bl6/J mice were bought via University suppliers and were co-housed when possible with experimental mice prior to experimentation. *Rorc(γt)-Gfp*^{TG} (transgenic) mice were a gift from Dr G. Eberl, Institut Pasteur, Paris, France; Id2-BFP from Dr A. McKenzie, MRC Laboratory of Biology, Cambridge, UK; *IL22ra1* and *IL23r* knockout mice via a collaboration with Prof G. Dougan, Wellcome Sanger Institute, UK and *Il1r* and *Il1b* knockout mice from Dr M. Clarke, University of Cambridge, UK. The C57Bl6/N, Rag2 (B6(Cg)-Rag2$^{tm1.1cgn}$/J) and RORγt knockout (*Rorc(γt)-Gfp/Gfp,* reference B6.129P2-Rorct^{m1litt}/J*)* strains were available in-house, having been previously supplied by The Jackson Laboratory.

2.1.2 Antibodies

Murine and human conjugated antibodies for flow cytometry are detailed in tables 2.1 and 2.2. A common live dead marker was used at a dilution of 1:300 (Invitrogen by ThermoFisher: Live/Dead Fixable Aqua Dead Cell Stain Kit; 234966). Antibodies used in microscopy are detailed in table 2.3.

Antibodies for depletion of ILC were from BioXCell: InVivoMab (BE0090) IgG2b isotype and InVivoMab (BE0066) Anti-Thy-1.2.

Table 2.1: Murine Flow Cytometry Antibodies.

Antibody	Clone	Fluorophore	Reference number	Dilution
Monocyte panel				
1/A:1/E (CII)	M5/114.15.2	Alexa-700	eBioscience 56-5321	1:200
CD103	2E7	PE-Dazzle	Biolegend 121430	1:200
CD11b	M1/70	PerCP-Cy5.5	eBioscience 45-0112	1:200
CD11c	N418	PECy7	eBioscience 25-0114	1:200
CD19	eBio1D3	PE	eBioscience 12-0193	1:200
CD19	6D5	BV785	Biolegend 115543	1:200
CD3	17A2	BV785	Biolegend 100231	1:200
CD3	17A2	Alexa-700	eBioscience 56-0032	1:200
CD45	30-F11	FITC	eBioscience 11-0451	1:200
CD64	X54-5/7.1	BV421	Biolegend 123133	1:200
CII	AF6-120.1	eFluor450	eBioscience 48-5320	1:200
CX3CR1	5A011511	BV650	Biolegend 149033	1:200
F4/80	BM8	BV605	Biolegend 123133	1:200
Gr1	RB6-8C5	APC-eFluor780	eBioscience 47-5931	1:200
Ly6c	HK1.4	APC	eBioscience 17-5932	1:200

Splenocyte anti-Thy-1.2 depletion panel				
CD11b	M1/70	Pacific Blue	Biolegend 101224	1:200
CD11c	N418	eFluor450	eBioscience 48-0114	1:200
CD19	6D5	BV785	Biolegend 115543	1:200
CD3e	145-2C11	BV605	Biolegend 100351	1:200
CD45.2	104	APC-eFluor780	eBioscience 47-0454	1:200
c-KIT	ACK2	PE	eBioscience 12-1172	1:200
Gr1	RB6-8C5	eFluor450	eBioscience 48-5931	1:200
NK1.1	PK136	Pacific Blue	Biolegend 108722	1:200
CD127	A7R34	PECy7	Biolegend 135014	1:200
ILC3 identification panel				
CD11b	M1/70	Pacific Blue	Biolegend 101224	1:200
CD11c	N418	eF450	eBioscience 48-0114	1:200
CD19	eBio1D3	APC	eBioscience 17-0193	1:200
CD3e	145-2C11	BV605	Biolegend 100351	1:200
CD45.2	104	APC-eFluor780	eBioscience 47-0454	1:200
c-KIT	ACK2	PE	eBioscience 12-1172	1:200
Gr1	RB6-8C5	eFluor450	eBioscience 48-5931	1:200
NK1.1	PK136	Pacific Blue	Biolegend 108722	1:200
Thy1.2	30-H12	PerCP-Cy5.5	Biolegend 105327	1:200
CD127	A7R34	PE	Biolegend 135010	1:50
CD127	A7R34	APC-eF780	eBioscience 47-1271	1:100
c-KIT	ACK2	PE	eBioscience 12-1172	1:100-200
c-KIT	2B8	PECy7	eBioscience 25-1171	1:100-200
NKp46	29A1.4	BV605	BD Horizon 564069	1:50
NKp46	29A1.4	PE	eBioscience 12-3351	1:50
NKp46	29A1.4	PerCPCy5.5	Biolegend 137609	Ineffective
CCR6	29-2L17	BV605	Biolegend 129819	1:100
CCR6	29-2L17	APC	Biolegend 129814	1:100
CD4	RM4-5	PE-Dazzle	Biolegend 100566	1:200
CD45	30-F11	BUV395	BD Horizon 564279	1:100
T-bet	4B10	FITC	Biolegend 644812	1:200
T-bet	4B10	A488	Biolegend 644830	1:200
T-bet	eBio4B10	PE	eBioscience 12-5825	1:200
GATA3	TWAJ	PE	eBioscience 12-9966	1:200
GATA3	TWAJ	eFluor660	eBioscience 50-9966	1:200
RORγt	AFKJS-9	APC	eBioscience 17-6988	1:200
RORγt	B2D	APC	eBioscience 17-6981	1:200
Isotypes				
Rat IgG1κ	R3-34	APC	BD Pharmingen 554686	
Mouse IgG1κ	MOPC-31C	FITC	BD Pharmingen 550616	
Mouse IgG2a	20102	APC	R&D IC003A	
Donkey anti-rabbit IgG	Polyclonal	A488	Life technologies A21206	
Mouse IgG1κ	P3.6.2.8.1	PE	eBioscience 12-4714	
Rat IgG2bκ	RTK4530	PE	Biolegend 400607	
Rat IgG2bκ	A95-1	PECy7	BD Pharmingen 552849	

Table 2.2: Human Flow Cytometry Antibodies.

Antibody	Clone	Fluorophore	Reference number	Dilution
ILC panel				
BDCA2	145-2C11	FITC	Miltenyi Biotec 130-097-927	1:100
CCR6	G034E3	BV785	Biolegend 353422	1:50-100
CD11b	ICRF4	FITC	eBioscience 11-0118	1:100
CD11c	3.9	FITC	Biolegend 301604	1:100
CD123	6H6	FITC	eBioscience 11-1239	1:100
CD127	eBioRDR5	APC-eFluor780	eBioscience 47-1278	1:100
CD14	61D3	eFluor450	eBioscience 48-0149	1:100
CD15	H198	eFluor450	eBioscience 48-0148	1:100
CD161	HP-3G10	PECy7	eBioscience 25-1619	1:100
CD19	HIB19	Alexa-700	eBioscience 56-0199	1:100
CD1a	HI149	FITC	eBioscience 11-0019	1:100
CD3	SK7	PerCP-Cy5.5	eBioscience 45-0036	1:100
CD34	561	FITC	Biolegend 343604	1:100
CD45	H130	BV650	Biolegend 304044	1:100
CD94	DX22	APC	Biolegend 305508	1:100
c-KIT	104D2	BV605	Biolegend 313218	1:50-100
CRTH2	BM16	PE-Dazzle	Biolegend 350125	1:50-100
FcεR1A	AER-37	FITC	eBioscience 11-5899	1:100
NKp44	P44-8	PE	Biolegend 350125	1:50-100
αβTCR	IP26	FITC	eBioscience 11-9986	1:100
γδTCR	B1.1	FITC	eBioscience 11-9959	1:100
CCR6	G034E3	BV785	Biolegend 353422	1:100

Table 2.3: Antibodies and stains for microscopy

Antibody/Stain	Clone	Fluorophore	Reference number	Dilution
Microscopy				
1/A:1/E (CII)	M5/114.15.2	eFluor450	Biolegend 107620	1:100
CD3	145-2C11	PE	eBioscience 12-0031	1:200
CD11b	M1/70	eFluor450	eBioscience 48-0117	1:50-100
F4/80	Rat mAb	A647	Abcam ab204467	1:100
GFP	Polyclonal IgG	FITC	Life technologies A21311	1:100
E coli	Polyclonal IgG	FITC	Abcam ab30522	1:100
Phalloidin	-	A647	Life technologies A22287	1:100
Phalloidin	-	A568	Life technologies A12380	1:100
Phalloidin	-	CF405M	Biotium 00034	1:100

2.1.3 Reagents and consumables

Table 2.4: Miscellaneous reagents and equipment

Chemicals, Peptides, Enzymes, Recombinant Proteins and Miscellaneous Reagents		
Reagent	**Supplier**	**Catalogue number**
123count eBeads, Counting Beads	Thermo Fisher Scientific	01-1234-42

Liberase TM	Sigma-Aldrich	5401119001
DNase I	Roche	10104159001
HEPES buffer	Sigma-Aldrich	H0887-100ML
Cell strainers (70µm)	Corning Falcon	352350
Cell strainers (100µm)	Corning Falcon	352360
Recombinant Murine M-CSF	PeproTech	315-02-250UG
Recombinant Mouse IL-17a	R&D Systems	421-ML-025
RPMI 1640	Sigma	R8758-500
Penicillin/Streptomycin	Thermo Fisher Scientific	15140122
PBS	MRC LMB Media Kitchen	
Distilled water	MRC LMB Media Kitchen	
Percoll	GE Healthcare	17-0891-01
Nuclease-free water	Ambion	AM9937
Fetal Bovine Serum	Sigma-Aldrich	G9665-500ML
Normal rat serum	Avivasysbio	OOMA00001
Normal mouse serum control	Invitrogen	10410
FcR blocking reagent, human	Miltenyi-Biotec	130-059-901
Ammonium chloride	Sigma-Aldrich	A9434-500G
Sodium bicarbonate	Sigma-Aldrich	S5761-500G
EdU	Glentham Life Sciences	GN5170
EDTA	Invitrogen	AM9260G
Paraformaldehyde 16% solution, EM grade	Electron Microscopy Services	15710
L-Lysine	Sigma-Aldrich	L5501-25G
Monosodium phosphate	MP	194740
Disodium phosphate	MP	194739
Sodium periodate	Acros Organics	419610050
Sucrose	VWR International	102744B
Triton X	Sigma-Aldrich	X100-100ML
Sodium azide	Sigma-Aldrich	71289-55G
Formaldehyde	Sigma-Aldrich	F8775-500ML
Ethanol, >99.9% purity	Honeywell	32221-2.5L
D-Glucose-Anhydrous	Fisher-Scientific	G/0500/53
Reagent diluent	R&D Systems	DY995
LB broth	MRC LMB Media Kitchen	
RNALater solution	Invitrogen, Thermo Fisher Scientific	AM7024
Borosilicate Glass Spheres, diameter: 3mm	Fisher Scientific, Thermo Fisher Scientific	12848353
Precellys Lysing Kit: Hard tissue grinding MK28-R	Precellys	KT03961-1-008.2
Qiashredder	Qiagen	79656
TaqMan Fast Advanced Master Mix	Thermo Fisher Scientific	4444557
High Capacity RNA-to-cDNA Kit	Applied Biosystems	4387406
MicroAmp Optical 384-Well reaction plate with barcode	Applied Biosystems	4309849
GentleMACS C tubes	Miltenyi Biotec	130-096-334
GentleMACS Dissociator	Miltenyi Biotec	130-093-235
WellTech Rapid Core (8mm)	World Precision Instruments	504535
ImmEdge™ Pen	Vector	H-4000

Fluoromount-G with DAPI	Invitrogen	00-4959-52
Fluoromount-G	Southern Biotech	0100-01
Critical Commercial Assays		
RNeasy Plus Micro Kit	Qiagen	74034
PureLink RNA Mini Kit	Ambion	12183025
Chromium Chip B Single Cell Kit	10X Genomics	1000073
Chromium i7 Multiplex Kit	10x Genomics	120262
Chromium Single Cell 3' Library & Gel Bead Kit v3	10X Genomics	1000075
FoxP3/Transcription Factor Staining Buffer Set	eBioscience	00-5523-00
Click-IT Plus EdU Alexa Fluor 647 Flow Cytometry Assay Kit	Invitrogen	C10635

2.1.4 Quantitative PCR primers (TaqMan® gene expression assays)

Table 2.5: qPCR primers

Primer name	ThermoFisher reference number
Areg	Mm01354339_m1
Camp	Mm00438285_m1
Ccl2	Mm00441242_m1
Ccl5	Mm01302427_m1
Colec11	Mm01289834_m1
Csf2	Mm01290062_m1
Cxcl1	Mm04207460_m1
Cxcl2	Mm00436450_m1
Cxcl12	Mm00445553_m1
Defb1	Mm00432803_m1
Hprt	Mm03024075_m1
Il17a	Mm00439618_m1
Il1β	Mm00434228_m1
Il22	Mm01226722_g1
Il23a	Mm00518984_m1
Lcn2	Mm01324470_m1
Ptx3	Mm00477268_m1
Reg3γ	Mm00441127_m1
Saa1/2	Mm00656927_g1
Sftpa1	Mm00499170_m1
Tnfsf15	Mm00770031_m1

2.1.5 Generic laboratory reagents and buffers

Table 2.6: Digest mix for murine kidney and bladder

Reagent	Concentration
RPMI	

HEPES*	0.1M
DNase 1	0.1 mg/ml
Liberase TM	32.5 µg/ml kidney 65 µg/ml bladder

*Added to mixes for ureter and bladder only, not essential for kidney

Table 2.7: Digest mix for human kidney, ureter and bladder

Reagent	Concentration
RPMI	
DNase 1	0.05 mg/ml
Liberase TM	32.5 µg/ml kidney 65 µg/ml ureter and bladder

Table 2.8: FacsFix

Reagent	Quantity
40% Formaldehyde w/v	12.5ml
Glucose	10g
2% sodium azide w/v	5ml
PBS	500ml

Table 2.9: Red cell lysis buffer

Reagent	Quantity
Ammonium chloride	16.6g
Sodium bicarbonate	2g
0.5M EDTA, pH 8.0	400µl
Distilled water	2L

Table 2.10: P-buffer

Reagent	Quantity
0.2M Disodium phosphate	81ml
0.2M Monosodium phosphate	19ml
Distilled water	100ml

Adjust to pH 7.4 for tissue dehydration, add 30% sucrose.

Table 2.11: PLP buffer

Reagent	Quantity
4% Paraformaldehyde w/v	12.5ml
Sodium periodate	0.106g
P-buffer	18.75ml
L-Lysine	18.75ml

Add the L-lysine to the P-buffer, followed by sodium periodate and then paraformaldehyde. Adjust to pH 7.4 with sodium hydroxide.

Table 2.12: Microscopy blocking buffer

Reagent	Quantity
0.1M TRIS	5ml
Bovine serum albumin *	1%
Normal mouse serum	50µl
Normal rat serum	50µl

* BSA powder can be substituted with 500µl of reagent diluent to make a less frothy solution.

2.2 Methods

Protocol 1: Homogenisation of murine bladders and kidneys

1. [Optional – Mice can be given an intravenous injection of anti-CD45-antibody to label circulating immune cells. The mice were euthanized 3-5 minutes after administration and organs were not subsequently perfused with PBS.]
2. Bladders, kidneys and spleen were harvested after perfusion with 20ml of PBS into the left ventricle and were placed in PBS or directly into digest mix on ice for transportation.
3. Tissue was minced finely in digest mix (table 2.6) or PBS.
    a. Bladders were shaken at 37^{o}C for 25 mins then passed through a 70µm cell strainer.
    b. Kidneys were mashed immediately through a 70µm cell strainer and left at room temperature for 20 mins.
    c. Spleen was mashed through a 70 µm cell strainer with PBS-alone (no digest mix) and kept on ice.
4. Cells were resuspended in 3ml PBS, spun at 350xg for 5 mins and the supernatant discarded.
5. Red blood cell (RBC) lysis was performed when necessary by resuspending the cells in 1ml of RBC lysis buffer for 1 minute with gentle agitation and then cells were washed in PBS (see step 4) and were ready for staining. Counting beads (25000 beads/sample) were added prior to staining, if required.
6. [Optional – immune cells can be enriched within kidney homogenates, prior to the addition of beads, using a 44% Percoll gradient (v/v), spun at 800xg for 20 mins without acceleration or break.]

Tip: Homogenisation of bladders using the GentleMacs 'Intestine' programme will increase cell yield and viability. Incubating the cells in digest mix at 37°C for longer than 25 minutes was avoided to minimise cell death.

Protocol 2: Homogenisation of human kidney, ureter and bladder

1. Ice boxes were prepared in advance to keep solutions and tissues cool where possible.
2. Capsule and surrounding fat were separated from the kidney using manual dissection. Bladder samples required the epithelium/mucosa to be detached from the muscle and serosal layers with scissors. Discarded fat, capsule, muscle or serosal tissue went into waste containers for incineration.
3. Dissected pieces of cortex, medulla, ureter and bladder were minced finely into tubes containing digest mix (table 2.7).
4. The tissue was transferred to a 37^{o}C rocking chamber for 30 mins for kidney and 1-2 hours for ureter and bladder.
5. Tissue was taken for histology or RNA in PLP (table 2.11) or RNAlater buffers, respectively.
6. The digested tissue was homogenised using the GentleMacs machine, firstly on programme 'spleen 04' then 'lung 02'.
7. The tissue slurry was mashed through a 100 µm cell strainer, diluted with PBS with 2% FBS (v/v). The filtered suspension was collected in 50ml Falcon tubes and placed on ice.
8. The cellular suspension was spun at 800xg at 4^{o}C for 10 minutes.
9. RBC lysis (table 2.9) when required was performed by resuspending the cells in 5ml of RBC lysis buffer for 1 minute with gentle agitation and cells washed 45ml PBS (as per step 8).
10. Samples could be purified using several methods if required and then washed in PBS prior to staining or 10X analysis:
    a. Percoll 44% gradient (v/v) centrifuged at 800xg for 30mins without break or acceleration at room temperature.
    b. Debris removal kit (according to manufacturer's instructions).
    c. Where there are concerns about cell viability a Live-Dead MACS separation was used (according to manufacturer's instructions). Dead cells were identified by trypan blue staining and examination by light microscopy.

Protocol 3: Flow cytometry

1. Single cell suspension was obtained using protocol 1 or 2 and resuspended in FACS tubes.
2. Fc receptors were blocked with 1:100 of normal mouse and normal rat serum in PBS for 20 mins on ice.
3. Antibody cocktail was added to cells for surface staining and incubated on ice for 45 mins. (Human ILC primary antibody cocktail was applied at room temperature for 30 mins, as CRTH2 internalises in cold conditions.)

4. Cells were resuspended in 3ml PBS, spun for 5 mins at 350xg and the supernatant discarded.
5. Live/dead marker was added to cells and incubated for 15 mins at room temperature.
6. Cells were washed in PBS, as per step 4.
7. Intracellular staining was performed according to the manufacturer's instructions using the FoxP3 intracellular staining kit and EdU-tagging according to the Click-IT kit.
8. Cells were resuspended in PBS (for GFP+ cells or cell sorting) or FACSFix.
9. Data collection was performed using LSR Fortessa flow cytometer and analysed with BD FACSDiva software.

Protocol 4: Murine urinary tract infection

1. Mice were co-housed for 6 weeks prior to infection (for equilibration of microbiomes).
2. Uropathogenic *Escherichia coli* (strain UTI89) stocks were maintained at -80^{o}C, frozen during log phase growth in 10% glycerol (v/v) with LB broth.
3. UPEC were thawed and incubated at 37^{o}C in 200 ml LB broth and passaged once they were in a log phase of growth.
4. [Optional: Mice requiring treatment with depleting antibody were given isotype or anti-Thy-1.2 at 0.25mg per mouse (1.25mg/ml in sterile PBS), IP one day prior to catheterisation. The injection can be repeated every 72 hours if required for longer experiments.]
5. [Optional: To measure proliferation, 2mg EdU was given IP (repeated daily) and/or in the drinking water (0.5mg/ml EdU with 1% sucrose (w/v)).]
6. Immediately prior to catheterisation, UPEC were spun at 3220xg for 5 mins at 4^{o}C and re-suspended in sterile PBS to an optical density of 0.4 (infective dose optimised by Hung et al. (2009) [415] and equates to 1-4 x 10^{7} colony forming units (CFUs) per mouse).
7. Mice were anaesthetised and residual urine volumes were expelled using gentle external pressure to the bladder.
8. Using an aseptic technique, 100 µl of UPEC was introduced to the bladder via a polyethelene sheath, supported by a 1ml disposable insulin syringe. Lubrication was applied using Instillagel (sterile anaesthetic jelly). The procedure took 3-5 minutes and could be repeated after 1 hour.
9. Mice are euthanized 24-72 hours thereafter and organs taken for analysis. [Optional: An intravenous (IV) labelling antibody was administered 5 mins prior to schedule 1, as per protocol 1.]

10. Cell suspensions obtained using protocol 1, were processed in sterile conditions and plated on LB agar plates in 10-fold serial dilutions (up to 4 dilutions). Sterile plating beads were used to evenly disperse the homogenate across the plate.
11. Agar plates were placed overnight in a 37^{o}C incubator and CFUs read the following morning.

Protocol 5: Quantitative PCR

1. RNA was obtained from tissue or cells:
    a. Cell suspension (see protocols 1 and 2) was lysed by snap freezing cells on dry ice or using Qiashredders in RNA lysis buffer prior to RNA extraction. To avoid contamination all the supernatant was removed prior to resuspension in RNA lysis buffer by spinning cells at 17000xg and fully removing the fluid with a pipette.
    b. Blocks of tissue (0.5 x 0.5cm) were lysed using the Precellys®24 system in RNA lysis buffer prior to RNA extraction. After lysis the solution was spun at 900xg for 2 mins and the supernatant transferred to RNase-free tubes.
2. RNA was extracted using Ambion PureLink kit for high RNA concentrations or the Qiagen Micro kit for low RNA concentrations (according to manufacturer instructions).
3. RNA was quantified using a nanodrop for concentration and purity.
4. cDNA was produced using normalised RNA concentrations (High Capacity RNA-to-cDNA Kit) to a maximum value of 2 µg RNA.
5. Quantitative PCR (qPCR) data was acquired in triplicate using the TaqMan Advanced Master Mix, RNase free water, cDNA and primer in the following ratio 5:2.5:2:0.5, to a total volume of 10 µl.
6. Data acquisition performed using AB Applied Biosystems ViiA7, Life Technologies 384-well PCR machine and QuantStudio Real-Time PCR Software v1.3.

Protocol 6: 10X Genomic Analysis

1. Single cell suspensions were prepared according to protocol 2.
2. Cells were loaded into the 10X Genomics Chromium Single Cell Controller with a recovery aim of 20 000 cells. Samples were run and libraries produced according to the manufacturer's instructions using the 3' protocol.
3. Sequencing was carried out at the Wellcome Trust Sanger Institute, as per manufacturers instructions.

Protocol 7: *In vitro* bone marrow derived macrophage stimulation with UPEC

1. Bone marrow was extracted from the femurs and tibias of C57BL6/J mice using a sterile technique. Briefly, murine legs were collected in sterile PBS, stripped of their sinew, washed in 70% ethanol and PBS and clipped at either end of the long bones. The bone marrow was expunged using sterile PBS with a needle and syringe.
2. Cells were washed and then cultured in cRPMI (RPMI 1640 supplemented with 10% FBS (v/v) and P/S) with 1 µg/ml M-CSF (top-up with fresh medium every 2-3 days) until well-established and adherent in 90mm petri dishes.
3. Cells were scraped and washed in cRPMI and redistributed at 250 000 cells/well in 24-well plates.
4. Once adherent, the macrophages were pre-stimulated for 24-48 hours with murine IL-17A (100ng/ml).
5. Cells were stimulated in triplicate, with UPEC-A647 for 1 hour at either 37°C or 4°C.
6. Cells were washed 3 times in ice-cold PBS before being scraped from the plate using the soft end of a 1ml syringe butt.
7. Cells were stained with antibody and analysed (as per protocol 3). Data was obtained immediately and cells were resuspended in PBS (not FACSFix).

Protocol 8: Confocal microscopy

1. Harvested tissues were placed directly into PLP (see table 2.11) for 24 hours
    a. When harvesting bladder, mice were catheterised post-mortem and the bladder inflated with PLP. This was essential for whole mount preparations and improved images for tissue sectioning.
    b. For kidney harvest, mice were perfused post-mortem with PBS to flush the kidneys of excess blood.
2. Tissues transferred to P-buffer with 30% sucrose (w/v) for at least 6 hours.
3. Tissues mounted in OCT or bladders for whole mount preparations were stained directly.
4. Samples were blocked in blocking buffer (table 2.12) for one hour at room temperature.
    a. Sections were circumscribed using a hydrophobic barrier pen, so that blocking and staining solutions could be directly applied to the slide.
    b. When preparing whole mounts, the tissue was bisected, so that the stain could reach the bladder lumen effectively. Tissues were blocked and stained in 1.5ml Eppendorf tubes and gently rocked during the blocking and staining steps.

5. The antibody staining cocktail was made in blocking buffer and sections/tissues stained at 4°C overnight.
6. The stain was washed three times in PBS. Bladder sections were not washed using Coplin jars to avoid displacement of the section and instead PBS was pipetted on and off carefully.
7. Sections were mounted under a coverslip with Fluoromount-G and allowed to dry.
    a. For whole mount preparations, the bladder was stretched over the slide with mounting solution and the coverslip weighted with a pound coin to apply direct pressure to the flattened tissue during drying.

Protocol 9: IL22R KO Ki67 image analysis in Imaris

1. Images were acquired using identical image settings within the microscope Leica software
2. Using Imaris software a mask was applied to the images by selecting areas of increased DAPI intensity (these correlated to the urothelium, where nuclei were in greater abundance)
    a. Manual correction of the mask edges was performed by tracking the basement membrane, delineated by phalloidin staining.
3. Background staining was subtracted using the automated option.
4. Within the area of interest (mask), nuclei could be identified using DAPI and the corresponding Ki67 staining intensity measured.
5. The same Imaris settings were then applied to all images.

2.3 Miscellaneous

2.3.1 Data protection and research ethics approval

All murine research was regulated under the Animals (Scientific Procedures) Act 1986 Amendment Regulations 2012 following ethical review by the University of Cambridge Animal Welfare and Ethical Review Body (AWERB).

The collection of human samples occurred under strict guidance from local surgical teams and NHSBT. Approval for this work had been agreed by our local ethics committee (NRES East of England committee – Reference number: 12/EE/0446). Risk assessments for the handling of human tissue and UPEC were fulfilled according to local guidelines.

Baseline demographic data was recorded on all human donors and fully anonymized. Storage of all human samples were reported to NHSBT and local MRC LMB and Addenbrooke's committees, in accordance with the respective reporting guidelines for each organisation.

2.3.2 RNA sequencing

Library preparations were carried out at the Wellcome Trust Sanger Institute. Raw data was received as demultiplexed Fastq files and quality assessed with FastQC. Files were aligned to the mouse mm10 genome with Hisat2, assigned to features and a counts table produced using Feature counts from the RSubread package. Downstream quality control and analysis was carried out using DESEQ2 with a liner model appropriate to the biological question of interest. Graphs were produced with R, using the packages GGplot2 and pheatmap.

10X Genomic libraries were prepared using the 3' kit v2 from 10x and sequencing carried out as per manufactures instructions at the Wellcome Trust Sanger Institute. Following sequencing, files were demultiplexed and a sparse matrix of counts produced using Cellranger v2.2.0. Downstream analysis and cluster identification was carried out in R, using Seurat.

2.3.3 Microarray analysis

Microarray (MA) images from a single colour Agilent array were downloaded from GEO. Files were processed with limma in R and were background corrected and quantiles normalised. Probes which did not show an expression level above the 95th quantile of expression from the negative control probes were removed from the dataset (considered as not expressed). Replicate probes were averaged. Differential expression was calculated after applying an appropriate liner model for the question of interest

2.3.4 Software and statistical analysis

Statistical analysis and presentation of data was generated using GraphPad Prism v7 and Microsoft Excel 2016. Flow cytometry data was analysed using FlowJo v10. Imaging was interpreted using Imaris v9. Generation of figures and reports used Inkscape v0.91, EndNote v7.7.1 and Microsoft Word 2016. Use of any other software packages has been described within the protocols and text above.

Chapter 3 - Characterising Innate Lymphoid Cells in the Renal Tract

3.1 Introduction

ILC populations as a proportion of all lymphocytes are typically small (0.5-5%) [226, 229, 416]. Their strategic position within tissues and contribution to homeostasis and epithelial maintenance makes them important immune regulators. ILCs within the gut, lung and skin are well documented, as are descriptions of peripheral, haematopoietic and fetal cells that have enabled us to better understand their development and character (see section 1.3.4 for more detail). Conversely, the presence of ILCs within the renal tract has only been loosely described, often as part of work relating to other innate lymphocytes or tissue resident populations [129]. In a murine study examining ILC2 control of eosinophils during immune homeostasis, the authors used their IL-5-reporter mouse to identify ILC2s in a range of tissues, including the kidney [417].

Analysing small cell populations is often facilitated by the use of reporter-animals and this strategy has been frequently used to assist ILC identification. Furthermore, human ILC populations in non-mucosal compartments (peripheral blood, cord blood, bone marrow and spleen) comprise ≤2% of the total innate lymphocyte and NK populations, although this rises to 65-75% in the skin, adenoids and mucosal tissues such as the colon and lung [229]. Interestingly, some populations of ILCs could not be found in uninflamed tissues during this study, adding a further layer of complexity to the correct identification of ILC subsets and highlighting the heterogeneity that can exist between different tissues and disease states. Owing to their similarity to other lymphocyte populations, no specific cells surface markers exist to identify ILCs, thus the presence of combinations of extracellular markers or intracellular cytokine and transcription factors are used. Without employing transcriptomic analysis, multi-colour follow panels incorporating all these markers are therefore the only way to reliably find ILC populations, an observation made by Halim and Takei, 2014 [416].

Defining a multi-colour flow panel to correctly identify ILC3s was a key requirement for this work and the panel was based on the ILC markers detailed in chapter 1, table 2. Human antibodies were typically harder to obtain and inspiration for this flow panel was taken from Mjösberg et al., 2011 [418] and has been used to verify human ILC populations in different contexts [230, 277, 419]. The flow panel uses positive selection of CD45 cells and then negative selection of lineage markers (including myeloid, lymphoid and stem cell populations). An ILC population can then be identified using CD127 or CD161 and ILC3s by c-KIT+/CRTH2- selection. To further catagorise human ILC populations, the markers CCR6 and NKp44 worked best in my experiments. Ensuring that NK cells

and T cells were excluded from ILC gating was critical, given their similarity to ILC3s in terms of both morphology and expression of surface expression markers. Multiple exclusion markers were used and included anti-δγTCR and anti-αβTCR antibodies within the lineage channel, as well as anti-CD3 (T cells) and anti-CD94 (NK cells) on separate fluorophores. Coincidentally, this panel was also used by Riedel et al. (2017) in their paper about the role of ILC2s in adriamycin-induced glomerulosclerosis [129]. The paper includes a figure on human ILC subtypes, including ILC3s and corroborates earlier findings of enriched murine renal ILC2 populations in healthy kidney tissue [417]. To the best of our knowledge, ILCs have not been identified or phenotyped in human bladder.

This chapter is concerned with my efforts to identify ILC3s within the renal tract using multi-colour flow cytometry and microscopy. The data presented comes from the kidney and proximal ureter (upper renal tract and derived embryologically from mesoderm) and the bladder (lower renal tract, derived in parts from mesoderm and endoderm). Comparable to the differences seen in development, we have sought to discover if different populations and proportions of immune cells exist within corresponding regions of the renal tract.

3.2 ILC3 selection and optimisation of flow cytometry protocols

ILCs make a very small proportion of the immune cell compartment, though this tends to increase when considering tissue resident populations compared with those in secondary lymphoid organs, an observation that we found in the renal tract, and was increasingly evident in the lower parts of the renal tract (bladder) compared with the kidneys (see figures 3.5&6). Markers that have proved useful for identifying ILCs within haematopoietic tissue have proved less useful in a tissue-resident context, as cells down-regulate or express different marker sets relative to their context. Despite this, it has been necessary to continue to use markers common to all compartments to validate findings and allow comparisons across tissues. In addition, the use of a reporter mice to identify ILC3 proved essential in our studies, owing to the challenges of employing large multi-colour flow cytometry panels with variable marker expression and the small sample size.

The murine and human cell antibody markers that proved most effective to identify ILC3 populations by flow cytometry have been summarised in table 3.1 and 3.2.

Table 3.1: Murine markers for identification of ILC3 by flow cytometry.

Marker	Clone	Fluorophore	ILC subset	Notes
CD127	A7R34	eFluor-780	Pan-ILC	
Thy1.2	30-H12	PerCPCy5.5	Pan-ILC	
c-KIT	ACK2	PE, PECy7	ILC2, ILC3	
NKp46	29A1.4	PE, BV605	ILC3	PE better conjugate, BV605 has limited efficacy. PerCPCy5.5 ineffective.
CCR6	29-2L17	BV785, APC	ILC3	

Table 3.2: Human markers for identification of ILC3 by flow cytometry.

Marker	Clone	Fluorophore	ILC subset	Notes
CD127	eBioRDR5	FITC, eFluor-780	Pan-ILC	Less effective in eFluor-450 conjugate. Typically more effective at Pan-ILC identification than CD161.
CRTH2	BM16	PE, PE-dazzle	ILC2	Present on basophils. Stain at room temperature
c-KIT	104D2	BV605	ILC2, ILC3	
NKp44	P44-8	PE, APC	ILC3	Present on NK cells. NKp46 less effective at identifying NCR+ ILC3.
CCR6	GO34E3	BV785	ILC3	
CD94	DX22	APC	-	To exclude NK and NKT cells. Also present on some CD8 T cells.

My early attempts to identify ILC3s through intracellular RORγt staining and reporter mice proved challenging, as demonstrated in figure 3.1. The bladders and kidneys from WT mice were harvested and stained for flow cytometry, using the FoxP3 intracellular staining kit for the transcription factors T-bet (ILC1) and RORγt (ILC3).

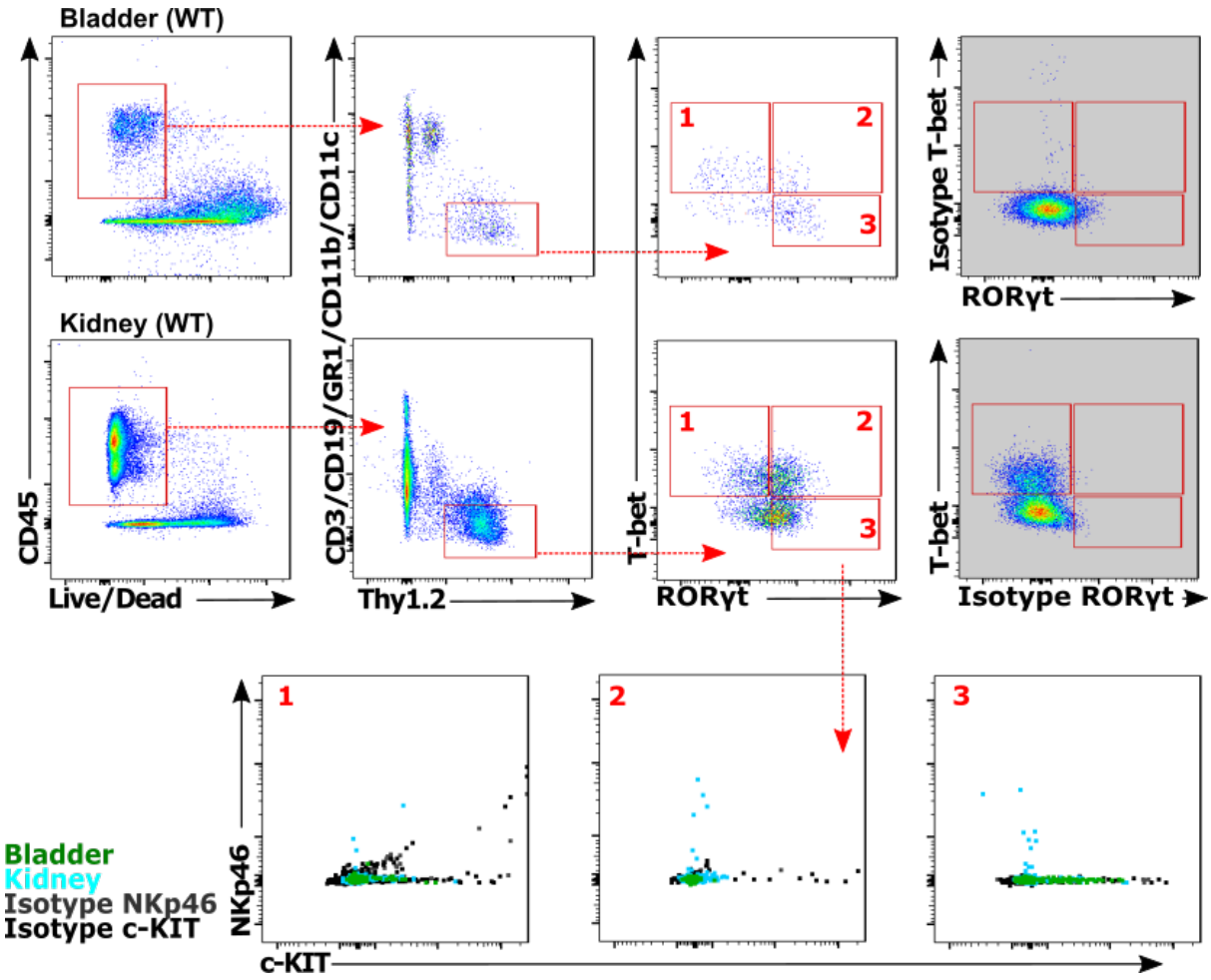

Figure 3.1: ILC3 identification using intracellular transcription factor staining.

Bladder and kidney representative of two C57BL6/J WT mice, stained with intracellular antibodies for the transcription factors, anti-T-bet-FITC and anti-RORγt-PE. Cells were preselected for singlets and ILCs identified as negative for lymphocyte and myeloid markers (CD3/CD19/GR1/CD11c/CD11b). Populations of ILC1 (1 – T-bet+), 'ex-ILC3' (2 – RORγt+/T-bet+) and ILC3 (3 - RORγt+) can be found, with the corresponding isotypes shown in the greyed flow plots. These populations have been overlaid the isotypes for NKp46 and c-KIT with cells coloured according to their tissue of origin (green - bladder, aqua - kidney). Isotypes: Tbet - Mouse IgG1κ, RORgt - Rat IgG1κ, NKp46 - Rat IgG2aκ. cKIT - Rat IgG2bκ. Repeated six times.

The flow cytometry plots showed that identifying a lineage negative population that was Thy-1.2 positive (total ILCs) was relatively straightforward in both bladder and kidney and the subsequent isotypes for both transcription factors were clean. A significant proportion of cells co-stained for T-bet and RORγt, potentially representing ex-ILC1 or NCR+ ILC3 populations. Insufficient numbers of

cells, however, rendered further ILC identification impossible owing to the small numbers that were NKp46 and c-KIT positive. It should also be noted, that anti-NKp46 conjugated to BV605, was a poorer label for the receptor than anti-NKp46-PE and other fluorophores did not work at all (figure 3.7). Despite the clones being inconsistent, adequate antibody markers were identified through trial and error.

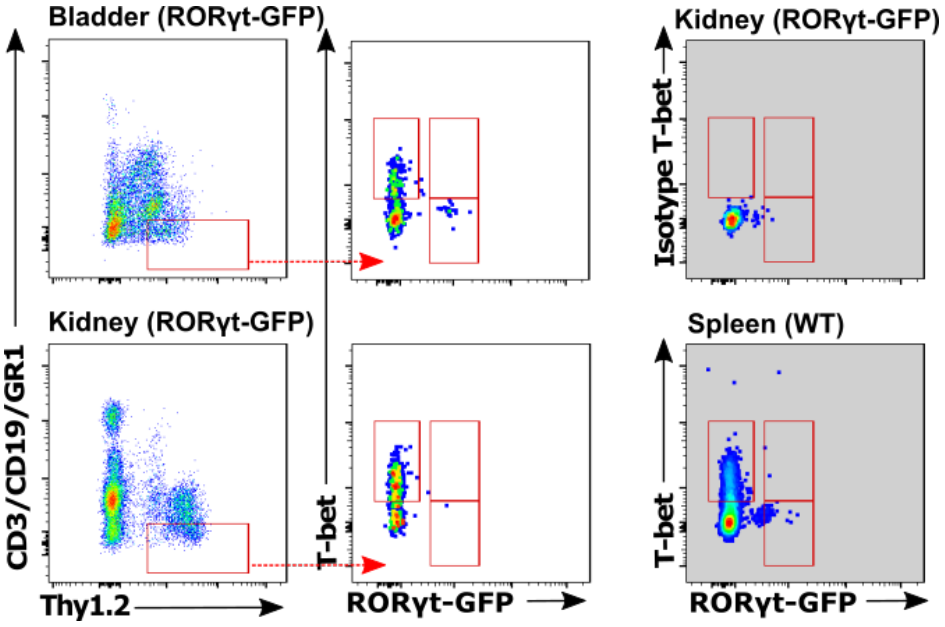

Figure 3.2: Bladder and kidney from WT and RORγt reporter mice, stained with intracellular transcription factors

Bladder and kidney representative of four C57BL6/J or RORγt-GFP mice, stained with intracellular anti-T-bet-PE. Isotypes: T-bet - Mouse IgG1κ. Spleen WT shown in bottom right panel (no GFP). Although c-KIT, NKp46 and CD4 staining was included, there were too few ILC3 post-fixation to be able to gate further. Cells pre-selected for alive, CD45+ singlets and results representative of five repeats.

Intracellular staining requires cell permeabilisation which is associated with a number of problems including loss of cell numbers, limitations on fluorophore choice to prioritise the brighter colours to the intracellular markers and an inability to sort unfixed cells for further applications and analysis. As such, it was important to find a way of identifying ILCs using a limited number of intracellular antibodies or preferably by eliminating the process entirely. We therefore tested the utility of transgenic fluorescent reporter mice that avoided some of the above issues. Figure 3.2 shows flow cytometry plots from RORγt-GFP knock-in mice (B6.129P2-Rorc^{m1litt}/J), such that homozygotes (hom) are RORγt knock-outs, but the heterozygotes (het) are RORγt-GFP positive and retain a copy of the transcription factor. The plots show animals that were heterozygotes with a splenic WT control (GFP negative).

As can be seen, T-bet intracellular staining remained convincing, but the heterozygote GFP+ cells were difficult to identify in both bladder and kidney after fixation (figure 3.2). Autofluorescence in the GFP detection channel further reduced our ability to correctly gate ILC3s, as can be seen within the isotypes and the WT tissue (greyed plots in figure 3.2).

To investigate this further, the experiment was repeated using an intracellular anti-GFP antibody, as cellular fixation methods may reduce the fluorescent signal generated following GFP excitation. Representative flow plots from RORγt-GFP bladders and kidneys (heterozygote RORγt-GFP knock-in reporters) were stained alongside WT controls, demonstrating that the populations generated using the anti-GFP-antibody were indistinguishable from both its isotype and the wild type controls. Even at lower concentrations, the staining appeared to grossly over-estimated the number of cells that were expressing RORγt and could represent ILC3s. Figure 3.3 shows that more 'ILC3s' could be identified in the WT bladder than the reporter, despite the animal being negative for GFP and it was evident that this method of ILC3 identification was not reliable. We were also concerned that the anti-GFP positive cells might be contaminated by Fcγ receptor-expressing myeloid populations that had bound or phagocytosed the antibody in a nonspecific manner, particularly as some were high in side and forward scatter (increased granularity and size) in flow cytometric analysis.

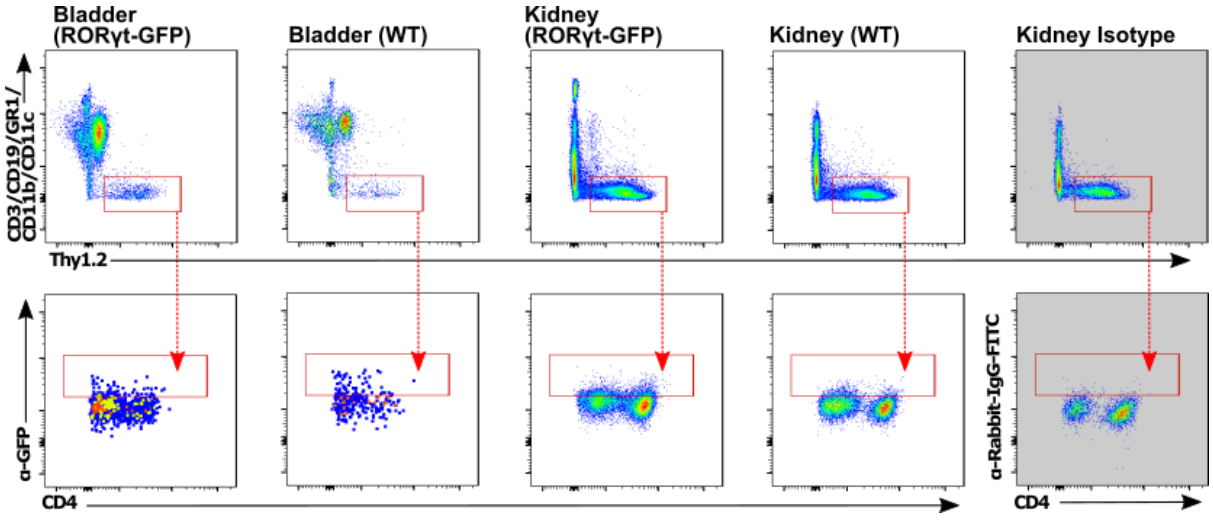

Figure 3.3: ILC3 identification using intracellular anti-GFP antibodies in RORγt-GFP reporters.

One WT and one RORγt-GFP mouse stained according to FoxP3 intracellular staining kit with intracellular anti-GFP-FITC (polyclonal IgG), isotype Donkey-anti-rabbit-FITC. Lineage negative and Thy1.2 positive cells (all ILCs) are further catagorised by GFP and CD4 staining. Isotypes are shown in the greyed plots. Cells pre-selected as CD45, alive singlets

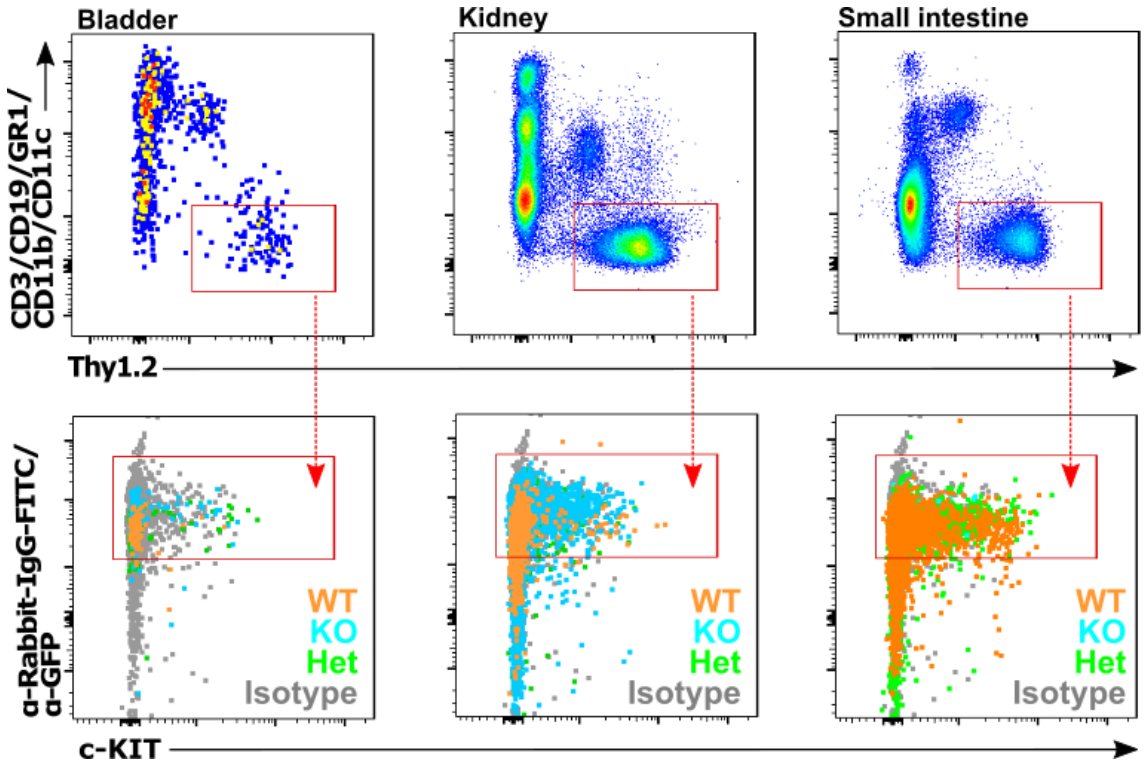

Figure 3.4: Intracellular anti-GFP staining in RORγt reporter mice using different tissues

Bladder, kidney and small intestine representative of four C57BL6J/RORγt mice, stained with intracellular anti-GFP-FITC. Cells pre-selected for alive, CD45+ singlets and negatively gated on lineage markers (eFluor-450), but positive for anti-Thy1.2-PerCPCy5.5. ILC3s should be GFP positive and may also exhibit c-KIT positivity. Cells from each tissue are overlying their isotype, showing little difference between either the mouse (presence of GFP) or its isotype.

We confirmed the difficulty in achieving accurate staining with an anti-GFP label in the small intestine (an organ known to contain a substantial population of ILC3s) alongside bladder and kidney (figure 3.4). Populations of anti-GFP positive cells are clearly overlapping in WT, KO and Het populations and the isotype control, thus indicating that this method of ILC3 identification was inaccurate in all three tissues.

To improve the specificity of intracellular anti-GFP during intracellular fixation staining methods, an alternative protocol using a second blocking step prior to intracellular staining and an alternative polyclonal IgG isotype was utilised and appeared more useful. (NB: Fixation of the RORγt-GFP reporter mice led to loss of the GFP signal, data not shown, necessitating the need to use an intracellular GFP label in this context.) Figure 3.5A shows that whilst background staining with anti-GFP-antibody persisted, the flow cytometry plots were much cleaner. In addition, anti-GATA3-antibody staining allows identification of ILC2 populations within the renal tract and spleen.

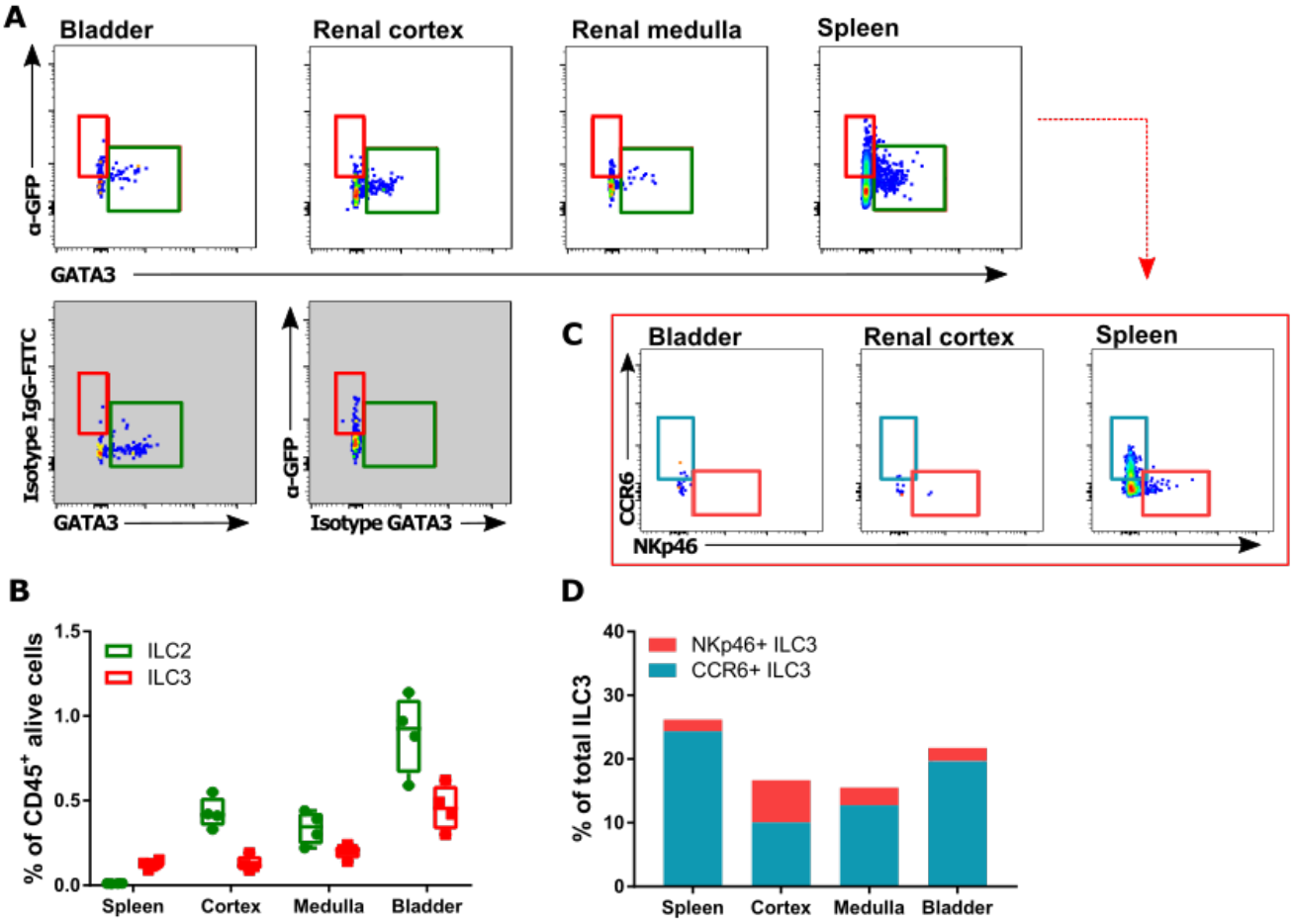

Figure 3.5: Combined transcription factor staining for ILC2 and ILC3 using RORγt-GFP reporters and anti-GATA3

A: Bladder, renal cortex and medulla and spleen representative of four RORγt-GFP - transgenic/C57BL6J mice, stained with intracellular antibodies for the transcription factors, GATA3-eF660 and GFP-FITC (RORγt). Isotypes: GATA3 – Rat-IgG2bκ, GFP - Goat-anti-rabbit-IgG. **B**: ILC2 and ILC3 proportions per tissue, relative to all CD45+ immune cells as a box plot with min/max values. **C**: ILC3s from bladder, renal cortex and spleen for characteristic ILC3 subsets, CCR6-BV605 and NKp46-PE, with their proportions in each tissue relative to the total ILC3 count (**D**). Plot representative of mean summary data from four mice.

Furthermore, the ILC3 population at baseline could be examined in more detail, showing baseline staining of CCR6 (LTi cells) and NKp46 (NCR+ ILC3), specific to each tissue (Fig 3.5C). The data is limited by the low cell numbers that can remain after processing, particularly when dividing the kidney into its two major zones, the renal cortex and medulla. Fig 3.5D shows that LTi cells are present in greater proportions in the spleen, but within the kidney and bladder, larger populations of NCR+ ILC3 can be found. This is in keeping with the known functions of secondary lymphoid organs,

specifically the role of the spleen in initiating adaptive immunity and was replicated in five experimental repeats.

In order to more reliably identify ILC3s using the transcription factor, RORγt, we sought an alternative transgenic *Rorc(γt)-Gfp*^{TG} reporter that was brighter (EGFP-tagged, expressed under control of the *Rorc(γt)* locus on a bacterial artificial chromosome (BAC) [420]) and attempted to gate ILC3s without using fixation staining protocols. In addition, the avoidance of cell permeabilisation produced improved signals from surface marker antibodies leading to a better identification and characterisation of the ILC3 population. These experiments coincided with the substitution of Liberase™ for collagenase A in the digestion protocol, leading to increased yields of alive cells within the single cell bladder homogenate.

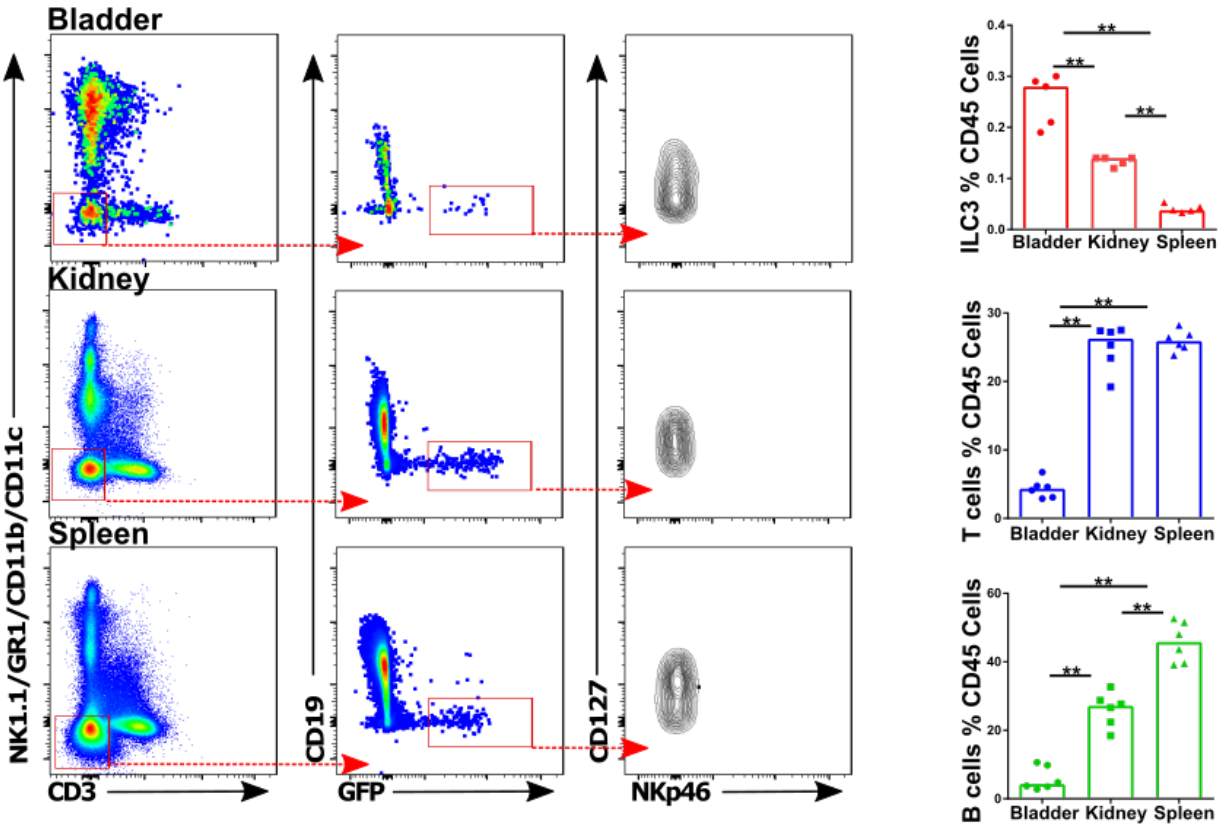

Figure 3.6: Numbers of ILC3s and lymphocytes by tissue using RORγt-GFP reporter mice

Representative of seven RORγt-GFP mice. Cells selected as CD45, alive singlets and cell proportions expressed relative to alive/CD45+ cells. Populations gated as T cells (CD3+), B cells (CD19+), ILC3 (lineage-, GFP+). Significance calculated using Mann-Whitney test: ILC3 ** p=0.0079, T and B cells ** p=0.0022.

Figure 3.6 shows flow cytometry plots and graphs demonstrating ILC3 populations in bladder, kidney and spleen (cell counts expressed as a proportion of all CD45+ immune cells) at baseline. ILC3s were

found within each tissue type and the reporter was bright. CD127 (a pan-ILC marker) was expressed by the majority of ILC3, though the NKp46 staining was low (in part due to its position within the flow panel at anti-NKp46-BV605, which gives very poor results). Interestingly, although cell numbers were universally low within the bladder, the proportion of ILC3s was greater in the distal renal tract (replicated in figure 3.5B). This is consistent with the bladder's inner mucosal surface being in greater proximity to the external environment and its inherent infectious threats.

The data presented thus far illustrates the difficulties associated with ILC identification and reinforces the utility of a transgenic fluorescent reporter. This eliminates reliance on intracellular staining protocols and the inherent problems associated with this protocol including non-specific staining and the loss of cells from an already small compartment.

3.3 Characterising ILC3 cell surface expression within the renal tract by multi-parametric flow cytometry

Identifying populations of ILC3 within the renal tract of mice using *Rorc(γt)-Gfp*^{TG} reporter animals (referred to as RORγt-GFP transgenic and used in all ILC3 identification experiments) allowed us to examine the cell surface expression of relevant ILC3 markers and gain insight into different ILC3 subtypes. Earlier attempts at applying widely-accepted ILC3 markers to our flow panels revealed that surface expression of CD127 and c-KIT in particular, were less highly expressed on ILC3s in the renal tract compared to splenic ILC3s. Figure 3.7B demonstrates this variability, but also highlights attempts to use alternative NKp46 antibodies as part of the ILC flow panel. Even when gating on NK1.1+ populations within the spleen, the anti-NKp46-PerCPCy5.5 antibody did not work and this antibody was subsequently abandoned (figure 3.7C).

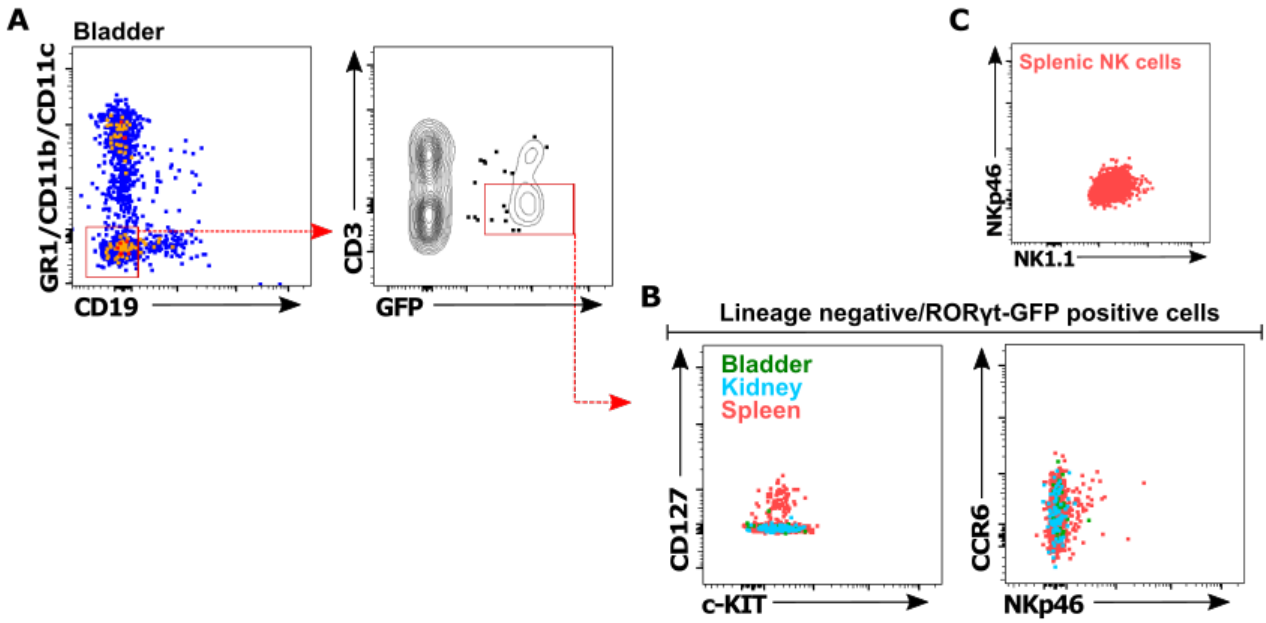

Figure 3.7: Cell surface marker expression of murine ILC3s in the renal tract and spleen

RORγt-GFP (GFP transgenic) without intracellular anti-GFP staining: **A**: Gating strategy demonstrated in bladder tissue to identify lineage negative (GR1/CD11b/CD11c-eF450, CD19-BV785 and CD3-BV605), RORγt-GFP positive cells (ILC3). **B**: ILC3 examined for cell surface expression of CD127-A780, c-KIT-PECy7, CCR6-APC and NKp46-PerCPCy5.5. **C**: Demonstration of anti-NKp46-PerCPCy5.5 staining of splenic NK cells (pre-selected as lineage negative, NK1.1 positive).

Having defined a set of markers that allowed for gating of ILC3 and optimised the concentrations of antibody required (see methods table 2.1) it was also important to demonstrate that these

populations were tissue-resident (particularly pertinent within the kidney, which is a highly vascular organ). All organs harvested to generate the flow cytometry plots thus far, came from mice that had been perfused with PBS after schedule 1. Whilst this might successfully eliminate some circulating cells from the analysis, the sheering forces can affect cells adjacent to vessel walls and expunge those relevant to analysis. Furthermore, perfusion can give variable results, dependant on the method of schedule 1, rupture of vessels and technique. To circumvent these problems, we used intravenous (IV) anti-CD45-antibody labelling prior to sacrifice [421] allowing the identification and exclusion of circulating immune cells from the analysis.

Figure 3.8 demonstrates the typical gating strategy used with IV CD45 labelling within bladder, kidney and spleen and clearly demonstrates an ILC3 group (lineage negative, RORγt+), that can be further subdivided based on CCR6 and NKp46 labelling (cells pre-selected for alive singlets). These groups are marked on the bladder flow plots, but the equivalent populations in kidney and spleen are evident. Notably, the anti-NKp46-PE antibody showed strong staining for NKp46, as demonstrated in the NK1.1+/NKp46+ NK cell population in the third column.

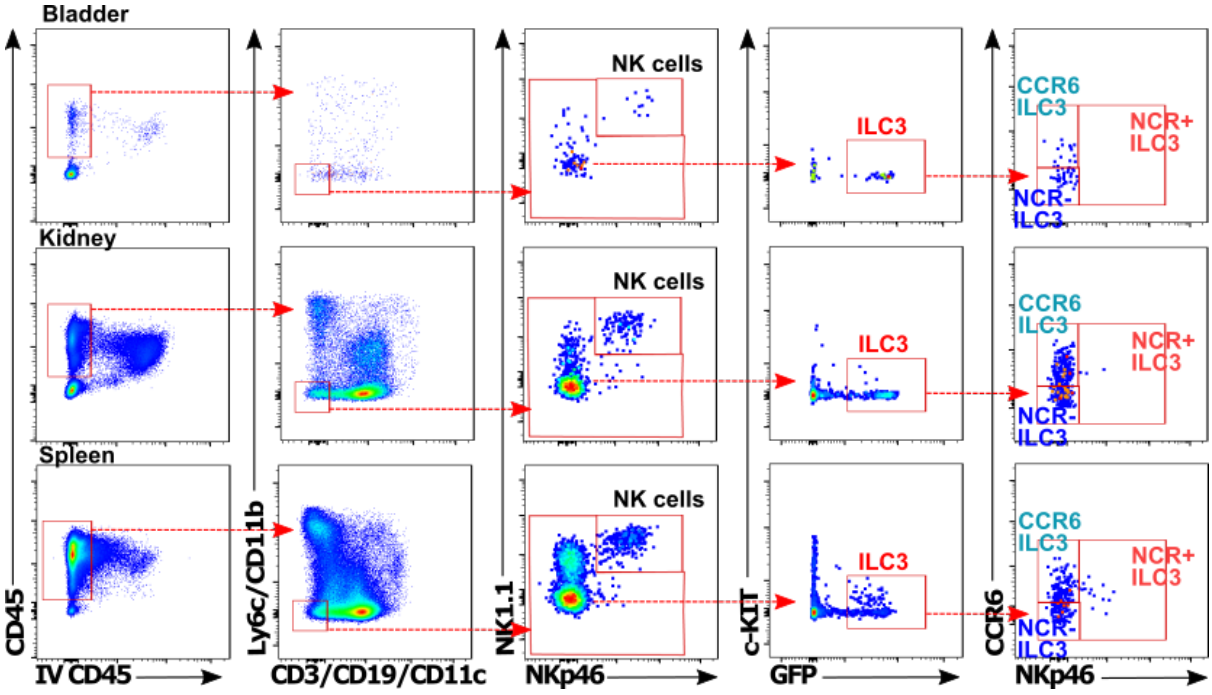

Figure 3.8: Using CCR6 and NKp46 to characterise ILC3s in the renal tract (with IV CD45 labelling)

Cells from RORγt-GFP transgenic mice pre-selected for alive, singlets and are subsequently IV CD45-BV650 negative, CD45-BUV395 positive. ILC3s defined as lineage (CD19/CD11c/CD3-eF450 and Ly6c/CD11b-PerCPCy5.5) and NK1.1-BV605 negative, and RORγt-GFP positive. Further ILC3 markers are c-KIT-PECy7, NKp46-PE and CCR6-APC cells. Flow panels in bladder representative of the gating strategy for all tissues, n=4 and repeated in three separate experiments.

To ensure exclusion of auto-fluorescent cells that might contaminate the ILC3 group, a WT mouse was sacrificed and stained alongside (figure 3.9A&B). These results are shown in tissue-specific panels with further demonstration of ILC3 subset staining with isotype controls (grey plots). Each sample is shown in combination to demonstrate the NKp46 and CCR6 positive populations of ILC3s (fig 3.9A&B). The data supports the subsets identified in figure 3.5D, as the same labelling antibodies were used. The IV labelling and use of beads in each sample permitted the calculation of absolute ILC3 counts per organ, as shown in figure 3.9C. The proportions of LTi and NCR+ ILC3s are shown in the bar graph with increased numbers of CCR6+ ILC3 (LTi) in the kidney, though not at the proportions demonstrated in the spleen (fig 3.9D). This follows the pattern we had observed previously, though the identification of NCR+ ILC3s was better.

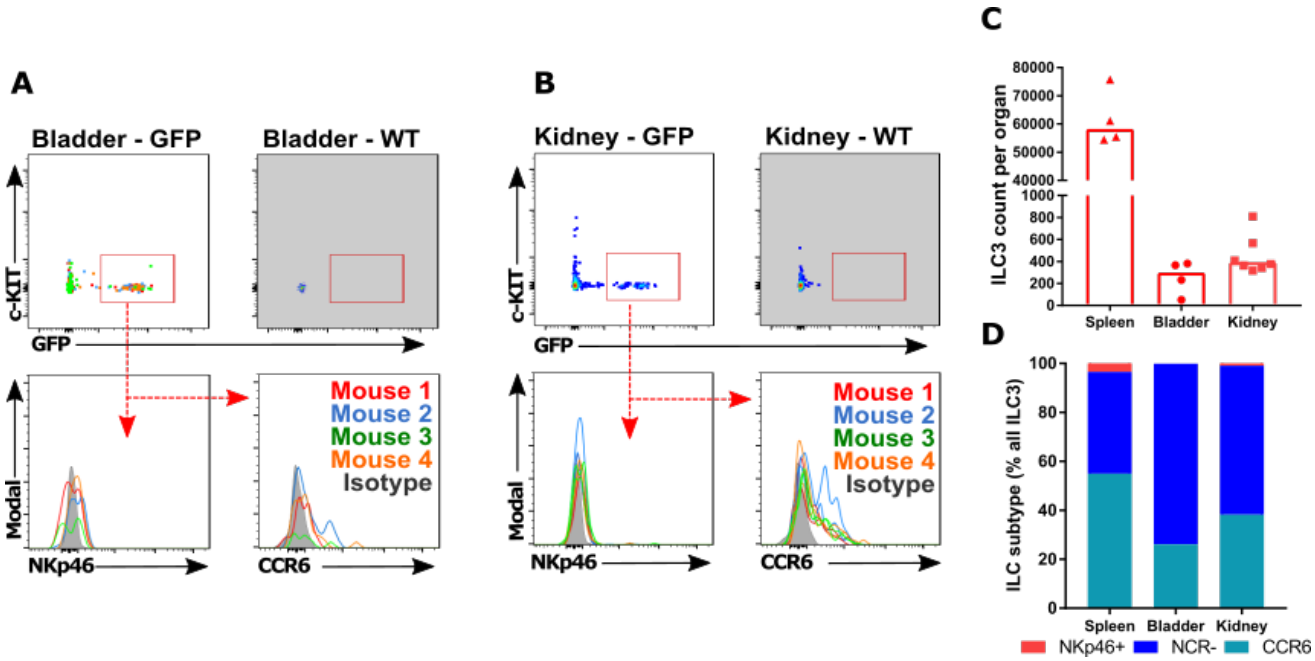

Figure 3.9: ILC3 subtypes of the murine renal tract and spleen

ILC3 identified from RORγt-GFP transgenic mice as per gating strategy in figure 3.8. Bladder (**A**) and kidney (**B**) shown with a WT animals (no GFP) to verify the identification of ILC3, n=4 (left and right kidneys homogenised separately). ILCs subdivided by NKp46 and CCR6 staining (shown with isotypes; NKp46 isotype - Rat IgG2aκ and CCR6 isotype - Armenian Hamster IgG. **C**: ILC3 counts per organ. **D**: ILC subsets expressed within a bar graph showing ILC3 proportions (median summary data).

3.4 Identifying ILC3 by confocal microscopy

Identifying ILC3s by microscopy followed a similar approach to that of flow cytometry, locating cells that expressed the transcription factor, RORγt, but were lineage negative. Staining pieces of tissue for microscopy does not allow use of the 12 colour panels required to identify and characterise ILCs by flow and so we took a more practical approach in identifying cells that were RORγt+/CD3-. In addition, by including myeloid markers in other channels, it was also possible to use relative size and position to assist with cellular identification. As our flow cytometry data had indicated that there were more ILC3s in the distal renal tract, we focussed on the bladder as the organ most likely to contain identifiable populations of ILC3s.

We used two main methods of tissue preparation for bladder imaging, tissue sectioning and whole mounts (inflating and fixing the bladder and mounting it open and flat across the slide). The former gives information on anatomical position, such as proximity to the urethra, whereas the latter preserves the tissues full thickness and provides a view on cellular location and depth within the bladder layers. Owing to the fixation processes, antibody selection was challenging, though through optimisation we were able to identify markers that reliably labelled our cells of interest (see methods, table 2.3).

Figure 3.10 shows images from a bladder whole mount, taken from a *Rorc(γt)-Gfp*^{TG} mouse, used for all microscopy of ILC3s. The phalloidin (staining actin) provides structural detail and the blood vessels of the lamina propria can be seen coursing through the tissue in 3.10A. ILC3s were observed within the lamina propria (RORγt+/CD3-), but like T cells, were scarce within the deeper layers of the bladder wall. This is demonstrated in figure 3.10B, where the tissue has been rotated to show the Z plane and compared to a cartoon schematic for clarity. The larger vessels and muscle layer lay deep to the ILC3s and T cells that occupied the layers above.

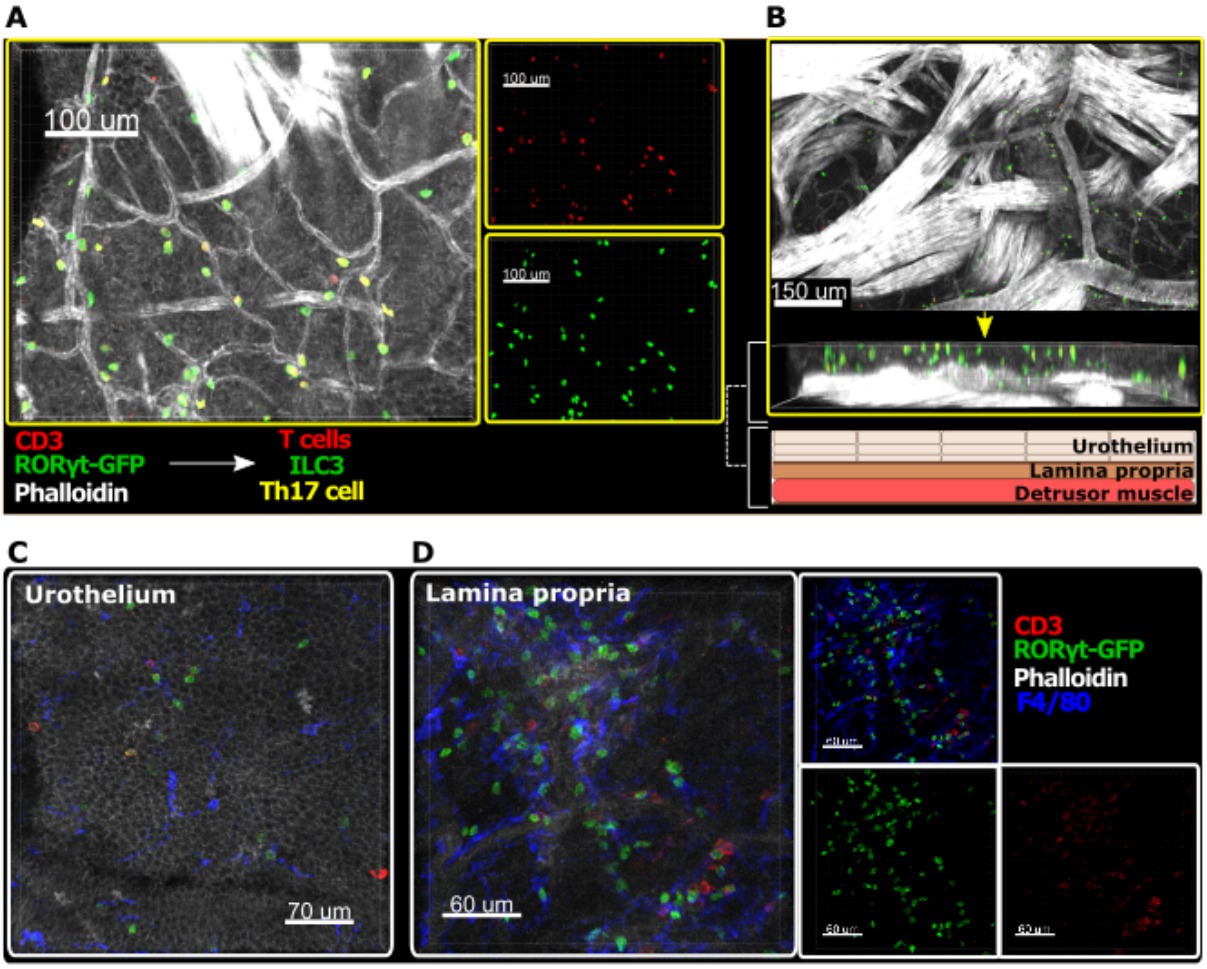

Figure 3.10: Identifying ILC3s using confocal microscopy on bladder whole mounts from RORγt-GFP transgenic mice

Bladders were inflated post-mortem with fixative and spread across the slide after staining. Staining panel: anti-CD3-PE, anti-GFP-FITC, anti-F4/80-A647 and Phalloidin-V450. Taken from control mice (RORγt-GFP transgenics). Representative of multiple repeats.

Panels C and D focus on the urothelial layer and lamina propria respectively and the tessellated appearance of the dense urothelial layer is nicely depicted. A dense network of immune cells of myeloid and lymphoid origin were identified in the lamina propria, with reduced numbers in the urothelial and muscle layers.

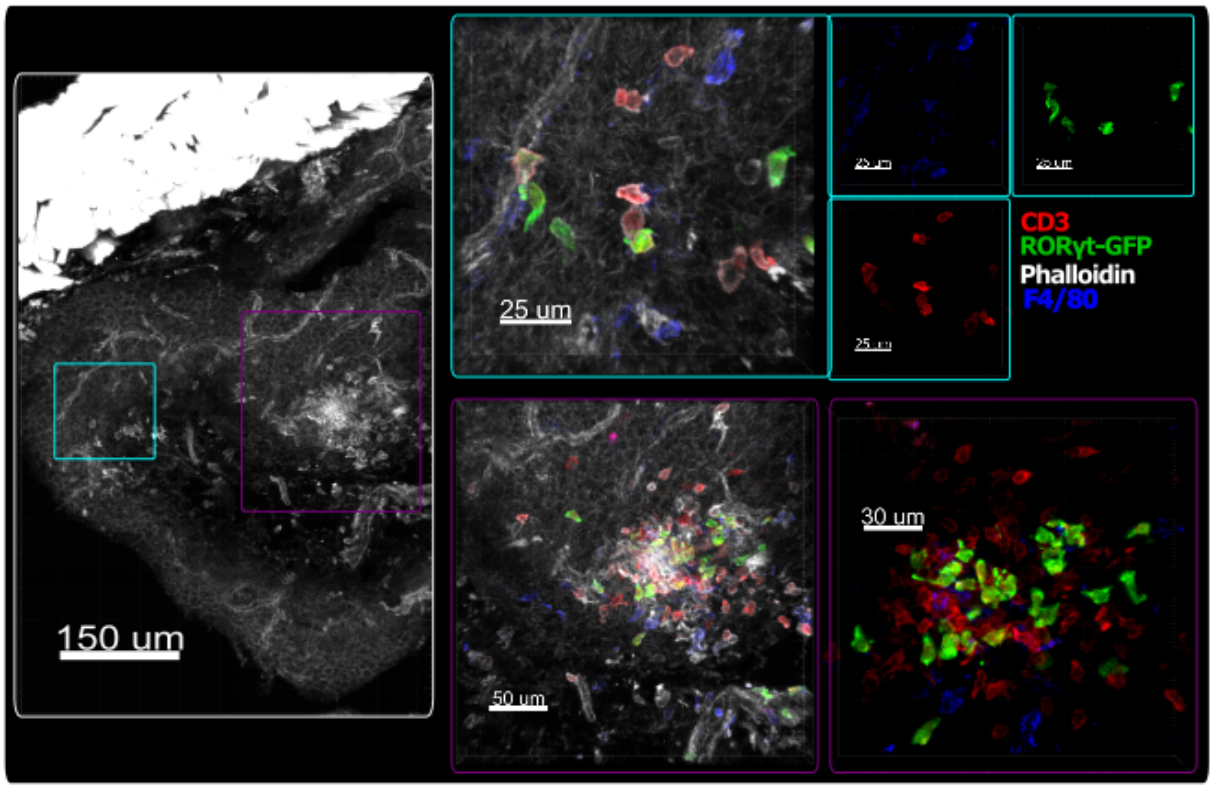

Figure 3.11: Identifying ILC3s using confocal microscopy from bladder sections of RORγt-GFP transgenic mice.

25µm sections from murine bladder of RORγt-GFP transgenic mice. Stains: anti-CD3-PE, anti-GFP-FITC, anti-F4/80-A647 and Phalloidin-V450. The images in the purple and aqua boxes demonstrate myeloid cells, T cells and ILC3s within the lamina propria. The higher power image in the purple box depicts the RORγt-GFP positive cells (green), but CD3+ positive (red) and double positive (yellow) cells can be seen within the same layer. Taken from control mice (RORgt-GFP transgenics). Representative of multiple repeats.

Figure 3.11 shows bladder sections, where the epithelium can be seen rippling over the detrusor muscle layer. Higher power images of myeloid and lymphoid immune cells are shown within the aqua box and clusters of immune cells were found within the lamina propria (purple box). Figure 3.12 also shows the layering of urothelium across the lamina propria and detrusor muscle. We observed some clusters of cells (Fig. 3.11) including RORγt-GFP T cells, ILC3s, and F4/80+ MNPs. Of note, we also saw some non-specific retention of antibody immediately adjacent to the inner aspect of the urothelial layer within the bladder lumen that persisted despite titrating the antibody concentration downwards and increasing the number of wash steps. This was reflected in the F40/80 staining in the epithelium in Fig. 3.12, which was not a true aggregation of myeloid cells. The inmost cells of the urothelium are umbrella cells coated in uroplakin and it may be this that mediated non-specific antibody binding.

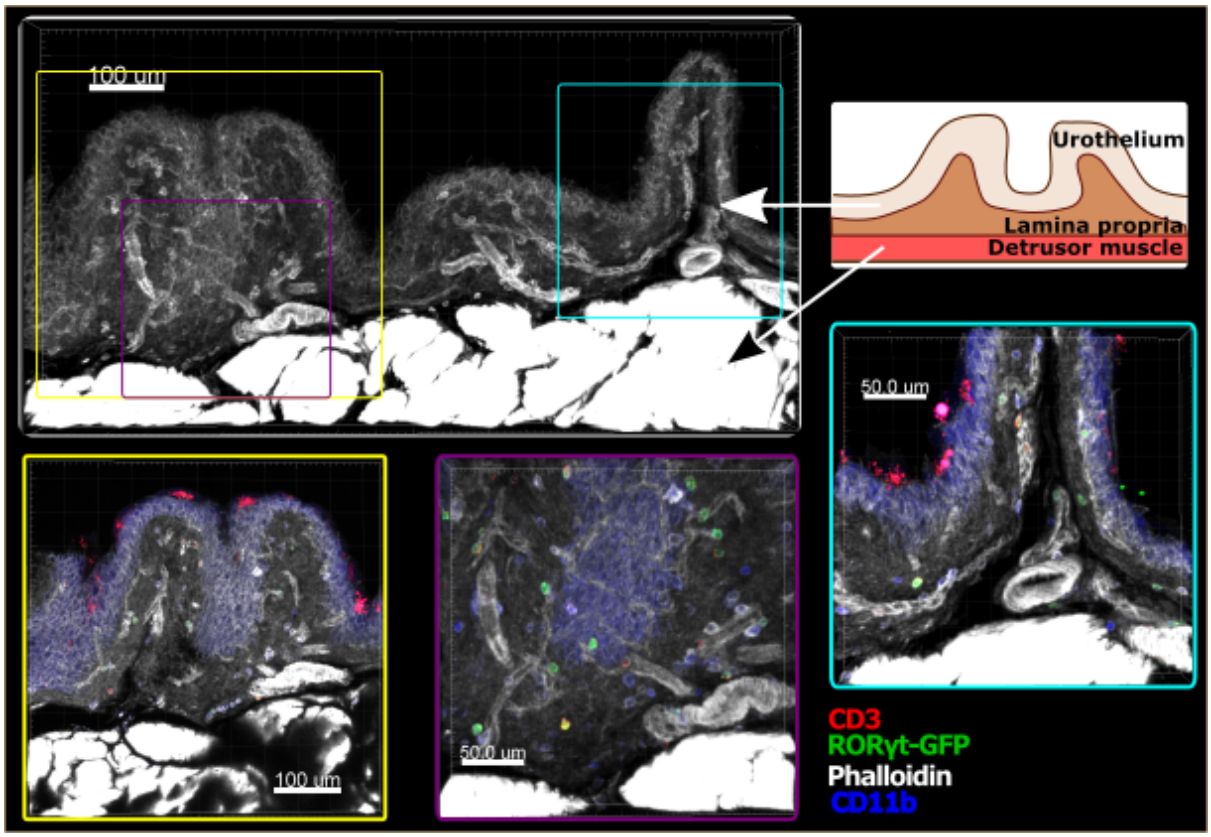

Figure 3.12: Bladder sections of the uroepithelium from RORγt-GFP transgenic mice

25µm sections from murine bladder. Stains: anti-CD3-PE, anti-GFP-FITC, anti-CD11b-eFluor450 and Phalloidin-A647. Taken from control mice (RORγt-GFP transgenics). Representative of multiple repeats.

We were able to confirm the presence of ILC3s within the bladder mucosa, as well as their spatial relationship to other immune cells. As with ILC identification by flow cytometry, the main challenge was correctly identifying ILC3s against T cells, but we were able to do this by co-staining for CD3.

3.5 Human ILCs within the renal tract

Human tissue was obtained from organ donors, whose families had consented to tissue being used for research. This occurred by two pathways: kidneys were obtained via the national allocation scheme administered by NHS Blood and Transplant, that had been declined for clinical use (see methods, section 2.3.1) and bladder tissue came from local organ donors that was obtained from the Cambridge Biorepository for Translational Medicine (https://www.cbtm.group.cam.ac.uk/). As the retrieval of bladder samples was local, these samples had a shorter cold ischaemic time compared with kidneys, and processing was possible within 30 mins to 2 hours.

The kidneys we received often required transportation from other UK centres where they had been retrieved, leading to cold ischaemic times of 6-24 hours, median 22 hours. Although cold ischaemic time had a critical impact on the viability of donor renal tissue, we found that other factors also influenced the viability of cell suspensions, including donor comorbidities, particularly conditions that affected vascular supply, such as hypertension, arterial disease and type 2 diabetes mellitus, advancing age, and tissue perfusion. However, it is worth noting that any organ harvested was deemed healthy enough to be considered for transplantation by a transplant consultant (medical or surgical). As such, all the data obtained is from 'healthy' donors. There was no reference to current UTIs in any of donors, though patients were from intensive care departments where placement of a urinary catheter is part of the standard of care. Historical reference to UTI was not recorded, nor available from the central NHSBT database, despite our efforts to trace this information.

3.5.1 Renal and ureteric ILC3 populations

The flow cytometry panel used to find ILC3s was based on work by Mjösberg et al. (2011), as described in the introduction to this chapter. To ensure that the correct lineage populations were excluded, the panel was developed to include TCR and CD3 identifying antibodies, as T cells were the population most likely to contaminate the ILC pool. The gating strategy employed to find lineage negative cells in the upper renal tract is shown in figure 3.13, using cell suspensions of renal cortex and medulla and proximal ureter.

As well as eliminating cells that might contaminate the ILC pool, care was taken to ensure cell staining was performed at room temperature, as the prostaglandin D2 receptor (CRTH2) is internalised at 4°C. Loss of this signal might have led to false inclusion of ILC2s within the ILC3 group, though in practice very few were identified using this flow cytometry panel and this was verified where possible by co-staining haematopoietic tissue (spleen or lymph node) alongside the kidney samples. We used fresh spleen/lymph node tissue obtained from the same donor and

performed simultaneous staining of the kidney/ureter staining. In a small proportion of cases, donor spleen or lymph node was not included with the donation and therefore this comparator tissue could not be included.

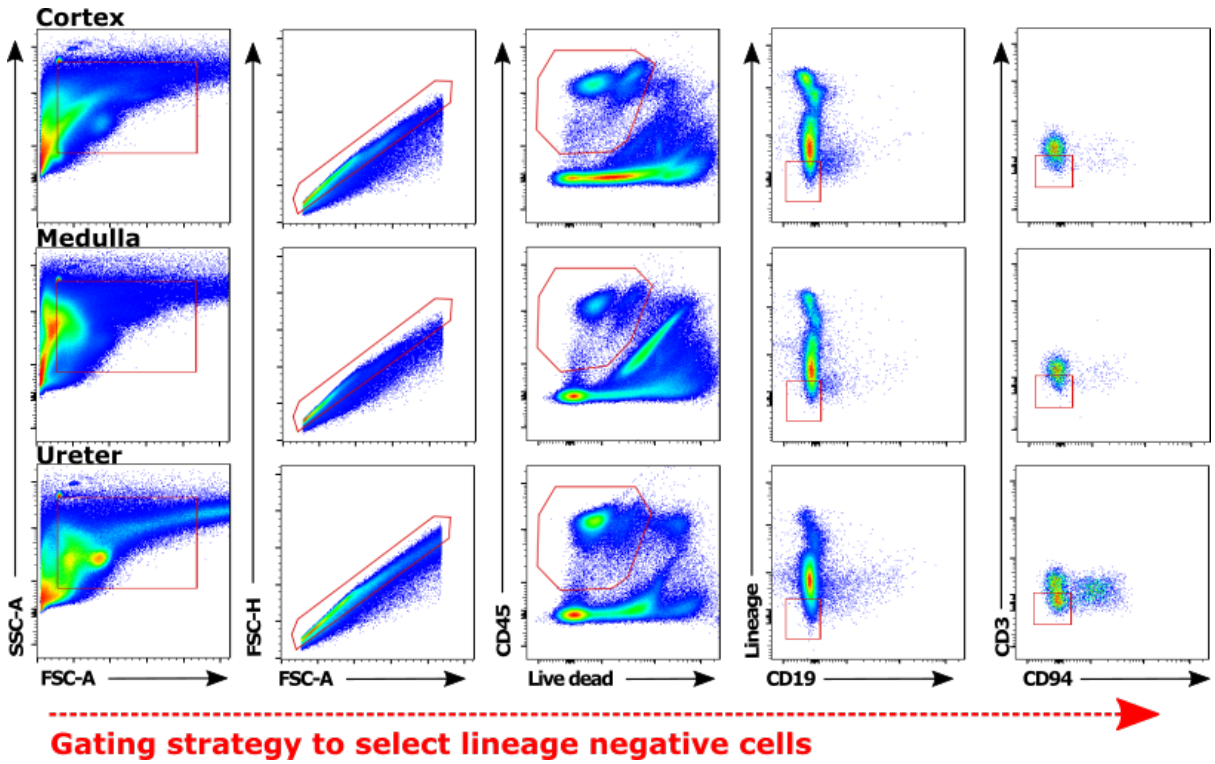

Figure 3.13: Identifying human ILCs of the kidney and ureter using flow cytometry (cell surface markers)

Flow cytometry plots from donor K175 (47-year-old female), Human kidney and ureter flow cytometry data: Flow cytometry plots representative of kidneys and proximal ureter harvested from transplant donors. Flow panel for identification of lineage negative populations includes the following antibodies: CD45-BV650, Lineage (γδTCR/αβTCR/CD34/CD11b/CD11c/FcεR1A/CD14-FITC), CD19-eFluor450, CD3-PerCPCy5.5 and CD94-APC, to ensure that a clean population of lineage negative cells can be found.

Figure 3.14A shows the continuation of flow cytometry gating for ILC3s in each of the donor tissues, with the addition of splenic plots for comparison. The plots included present the gating strategy, though many of the medullary cell suspensions were non-viable. This likely relates to the fact that the medulla has a precarious blood supply and is relatively vulnerable to ischaemia. This, combined with the cold ischaemic time, prevented the generation of cell suspensions of sufficient quality to increase the number of medullary samples analysed. Therefore, the cell counts from the renal medulla should be interpreted with caution. Despite these limitations, populations of B cell, T cell and NK cell counts were quantifiable (figure 3.14B). It is interesting to note the decreased proportion of B cells in the ureter, a finding shared with the bladder (figure 3.15C).

ILC populations from ureter and renal cortex were easier to obtain and the staining was similar to that observed in haematopoietic tissue. As observed in murine ILC populations, CCR6+ ILC3s were more prevalent than NCR+ ILC3s (figure 3.14C), though as we descended the renal tract through the proximal ureter this balance changed. The ureter represents the most distal part of the upper urinary tract and we would therefore anticipate that the ILC populations would be more akin to those in bladder and have a role in defence against ascending urinary pathogens.

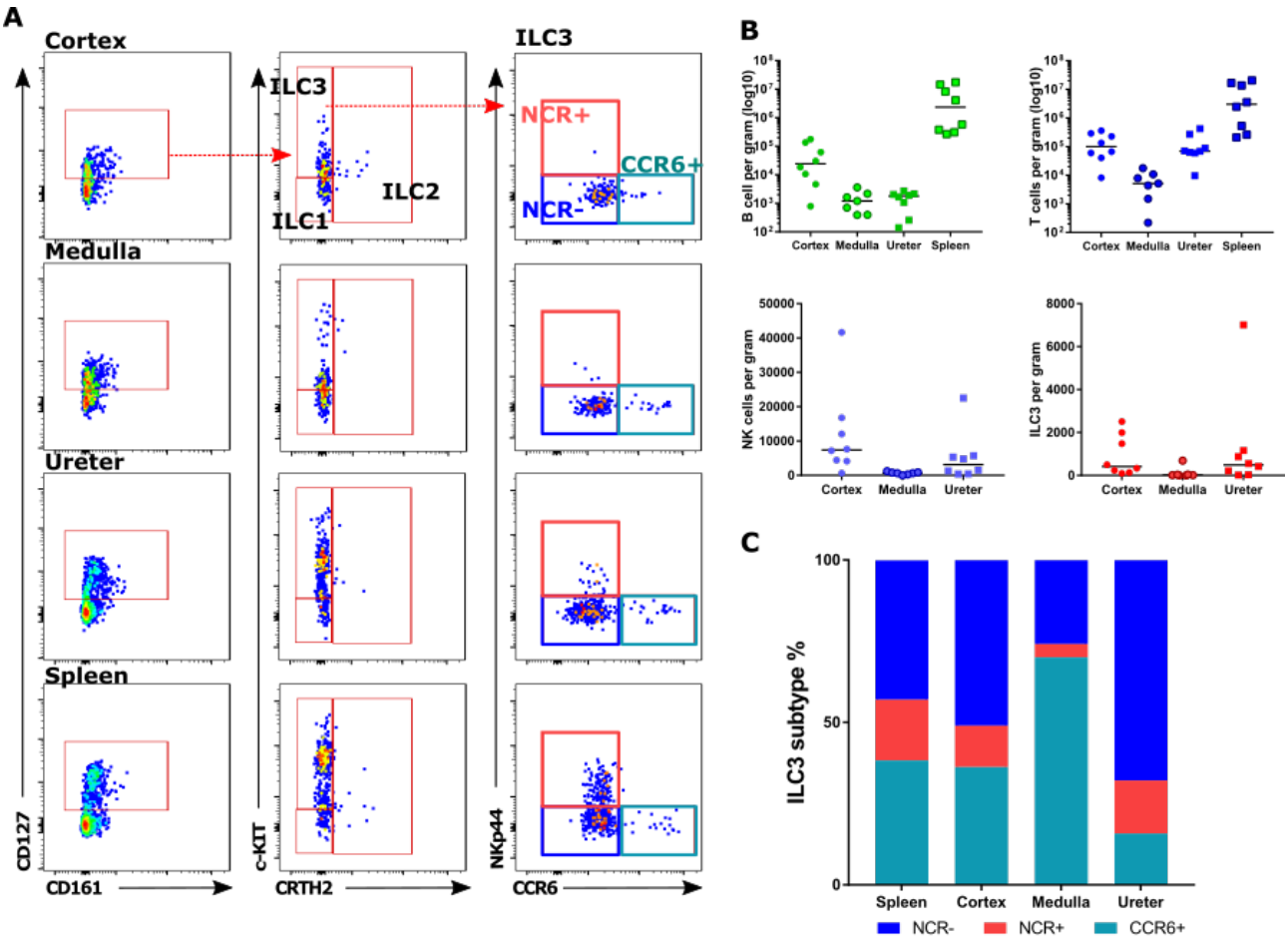

Figure 3.14: Delineating human ILC3 and lymphocyte populations in the kidney, ureter and spleen

A: Flow cytometry plots representative of tissue harvested from transplant donors, n=8. Flow panel for identification of lineage negative populations includes the following antibodies: CD45-BV650, *Lineage (γδTCR/αβTCR/CD34/CD11b/CD11c/FcεR1A/CD14-FITC), CD19-eFluor450, CD3-PerCPCy5.5* and *CD94-APC* (antibodies show in italics are negatively selected during ILC3 gating). ILCs gating strategy as CD127-A780, CD161-PECy7, c-KIT-BV605, *CRTH2-PE-Dazzle*, NKp44-PE, CCR6-APC. Data combined from 8 donors, ages in years 37M, 47F, 46M, 52F, 72F, 76M, 77F and 80M (F = female, M = male). **B**: Populations of lymphocytes, ILC3s and NK cells per gram of tissue. **C**: ILC3s by subtype.

3.5.2 Bladder ILC3 populations

The human bladder is thick walled, with adherent external fat and a tough outer serosal coat. It was obvious that digesting the serosa was unlikely to produce a cell suspension of viable immune cells, due to the intensity and duration of mechanical and enzymatic digestion required. We also reasoned that ILCs and other immune populations would likely lie closer to the bladder lumen, the region from which infectious challenges arise. Each bladder sample was dissected along the anatomical plane that was easy to see with the naked eye, to obtain a layer of mucosa. Enzymatic digestion for an hour at 37°C proved sufficient to produce a single cell suspension of viable cells, similar to the protocol used to obtain ureteric immune cells. The bladder mucosa yielded good numbers of viable immune cells and weights of 0.5-1g of tissue was sufficient to collect populations of myeloid, lymphoid and innate lymphoid cells.

Figure 3.15 shows a typical gating strategy for the identification of ILCs. To preserve cell numbers intracellular staining for transcription factors was not used and therefore we relied on cell surface markers to delineate the ILC subsets. Using this strategy, we observed CD127+ and c-KIT+/CRTH2- ILC3s (Figure 3.15B). Interestingly, the staining using the pan-ILC marker CD161 was variable, labelling a small proportion of cells. By ensuring that lineage markers were spread across the flow panel rather than employing a single 'dump' channel, we were able to identify other lymphoid populations, notably B cells, T cells, NK cells and NKT cells in the human bladder. The numbers of cells per gram of bladder mucosa is also shown in figure 3.15 and we observed that overall T cells were enriched compared with B cell and NK cell populations. This supports previous observations that the bladder houses innate intraepithelial lymphocytes, γδT cells, NKT cells, MAIT cells and other invariant T cell populations [222, 223, 374, 382, 383]. This enrichment of T cells over B cells may relate to our receiving pieces of healthy bladder tissue that lack B cell recruitment, or might correlate with the observation that an adaptive immune response plays less prominent role in the lower urinary tract during infection [2] (see section 1.4.2 for more detail).

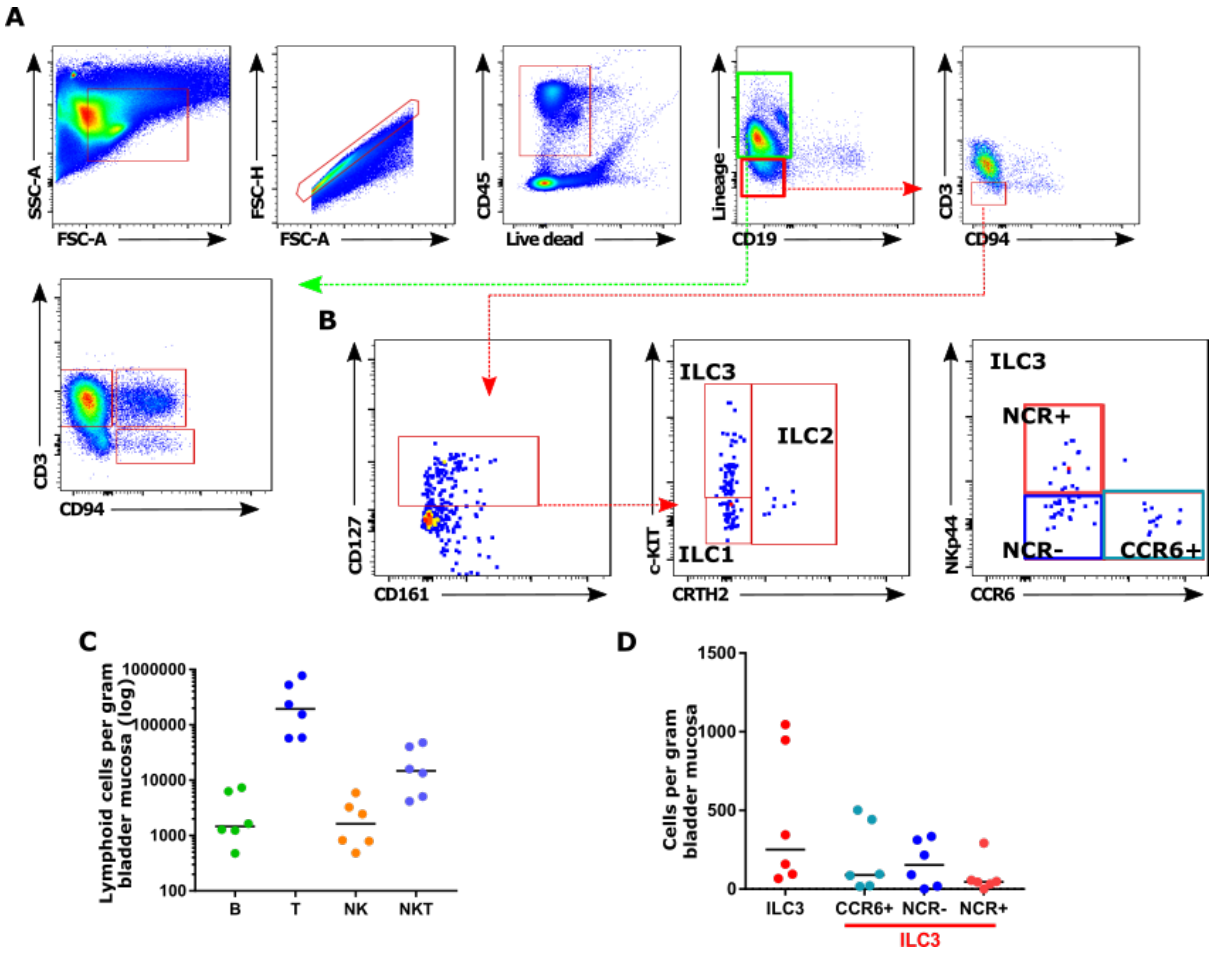

Figure 3.15: Defining human ILC populations ILC3 subtypes from bladder

Flow cytometry plots representative of bladders harvested from transplant donors; n=6; ages 58, 59, 61, 67, 70 and 75 years; male=4, female=2. Flow panel for ILC identification includes the following antibodies: CD45-BV650, *Lineage (γδTCR/αβTCR/CD34/CD11b/CD11c/FcεR1A/CD14-FITC), CD19-eFluor450, CD3-PerCPCy5.5, CD94-APC*, CD127-A780, CD161-PECy7, *CRTH2-PEDazzle*, c-KIT-BV605, NKp44-PE and CCR6-BV785. The gating strategy shown has been used to identify ILC3s in different tissues of the human renal tract (antibodies show in italics are negatively selected during ILC3 gating). **A**: Initial gating strategy for alive immune cells; lineage positive immune cells in green box and lineage negative cells in red box. **B**: Gating strategy to identify ILCs and ILC3 subsets. **C**: Lymphocyte and NK numbers per gram of bladder mucosa. **D**: ILC3 and ILC3 subsets per gram of bladder mucosa.

To further characterise bladder immune cells and their interactions with the non-immune cellular components of the bladder, we have performed single cell RNA sequencing using the 10X genomics platform. Sequencing is underway on n=5 human bladder samples, and some initial data from the first donor is shown below. As observed in our flow data, T cells dominate the immune population within the bladder mucosa (Figure 3.16B).

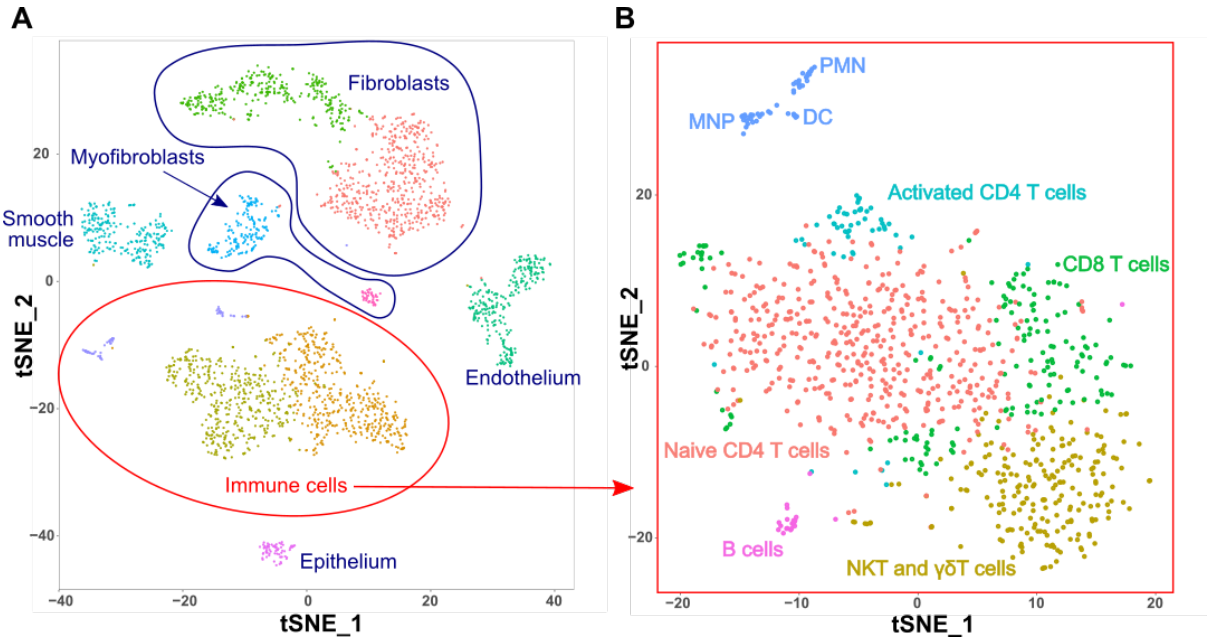

Figure 3.16: Preliminary data from single cell RNA sequencing of human bladder tissue

Single cell suspension from the bladder mucosa of a 58-year-old male transplant donor. **A:** Initial clustering based on the most highly variable genes shown in a T-distributed stochastic neighbour embedding (t-SNE) plot. The annotations are approximations based on the top marker genes for each cluster. **B:** t-SNE demonstrating re-clustering of immune cells in more detail.

3.6 Discussion

This chapter has been primarily concerned with identifying and characterising ILC3s within the renal tract of mice and humans using flow cytometry and microscopy.

3.6.1 Key findings

1. ILC3s are present in the renal tract of mice and humans in health, forming part of the tissue-resident innate immune cell network.
2. ILC3s are found in greater abundance in the lower renal tract, and in these locations, NCR-expressing ILC3s are more prominent.

The data presented in this chapter demonstrates the presence of all three subtypes of ILCs within the renal tract. Using a reporter mouse (*Rorc(γt)-Gfp*^{TG}) it has been possible to demonstrate ILC3s are tissue-resident and catagorise them more fully by their expression of CCR6 (likely to represent LTi populations) and NKp46 in mice and NKp44 in humans (NCR+ ILC3). Although the human flow cytometry panels do not include IV CD45-labelling, for obvious reasons, these organs are perfused at the time of harvest with preservation solutions. This ensures blood is flushed from the organ in preparation for transplantation, limiting intravascular cellular contaminants and facilitating the identification of tissue-resident immune cell populations.

There was anatomical variation in the number of ILC3s found in different regions of the renal tract, with decreasing numbers in the upper urinary tract. This is consistent with a role for ILC3s in immune defence, as most infections occur via bacterial spread from the bladder upwards. We have also observed differences in distribution of the subtypes of ILC3s, with increased proportions of NCR+ ILC3s in the lower urinary tract. These differences are likely to reflect the demands of each part of the renal tract; the bladder is closer to the external environment than the kidney. Urinary pathogens usually originate from gut bacteria that ascend the urinary tract via the urethra, therefore it is critical that an innate immune defence network is poised ready to respond. Our data suggest that ILC3s form part of this network. In addition, the urothelial barrier will require maintenance in health and ILC3s may also play a role in assisting with epithelial repair in health via the production of IL-22, as they do within the gut. This data expands on the descriptions of ILC3s in healthy human tissue by Riedel et al. (2017) who did not phenotype ILC3s throughout the renal tract [129]. They found variable numbers of NKp44+ ILC3s (reduced compared to NCR- ILC3s) within the kidney and it is possible that these represent populations that were pelvic in origin, as they did not delineate their samples anatomically. Furthermore in this study, ILC2s were the predominate population in murine kidneys and ILC3s in human tissue. This correlates to the populations identified in this project that

are demonstrated in figure 3.5 (murine) and figure 3.14 (human), though it must be accepted that similar human flow cytometry panels were used in both instances and may therefore reflect an inherent experimental bias.

Within the small intestine, different groups of ILCs are found in abundance and we can use this information to validate the ILCs identified in this project. In the murine gut, all groups of ILCs can be found and different subsets of ILC3s localised to cryptopatches and Peyer's patches (NKp46- ILC3 and LTi) or the lamina propria (NKp46+ ILC3s) [267]. The renal tract does not share the same diffuse network of lymphoid tissue, though this remains an avenue for investigation within the bladder, and therefore ILC3s were more heterogeneously distributed. Interestingly, populations of NCR+ ILC3s were more likely to be found in the murine and human bladder than kidney, however there was variability in these results, perhaps reflecting differences in staining protocols when using intracellular staining or GFP reporter mice. Further analysis of the NCR+ ILC3s in the renal tract is required to identify if these cells are akin to the IL-22-producing NKp46+ ILC3s found in the intestinal mucosa [267, 281]. Given the role of NCR+ ILC3s in the gut, we can predict that they should be numerous in places where there is a need for epithelial homeostasis and control of commensal and pathogenic bacteria. These functions gain importance within the more distal portions of the renal tract. It remains to be seen if ILC3 activation and plasticity in enabling IL-22 production in the small intestine and colon is replicated in the renal tract, particularly as the maintenance of these cells in the gut is driven by interactions with commensal flora and the specific balance of cytokines that direct their development [240, 267, 281-283, 291]. As has been discussed, ILCs in the gastrointestinal tract have been most extensively characterised and a good example of the different subtypes has been summarised by Robinette et al. (2015). This transcriptional analysis confirmed the range of ILCs that can be found in gut, liver and spleen and how differently these cells express ILC markers, such as c-KIT and CD127 in health [227]. A similar analysis of ILCs in the renal tract would help to validate the differences in ILC markers that have been demonstrated in this project and this is discussed in further detail below.

Work to date in the ILC field has investigated the functional importance of heterogeneous ILC populations, for example using transcriptomic and mass cytometry experiments to define the characteristics of different subtypes of ILCs [227, 229, 230, 262, 277, 419] (see chapter 1, section 1.3.4) and this introduces complexity when describing ILC populations within organs. In addition, some of the transcription factors used to define each ILC subset are shared between the groups. Notably, GATA3, an ILC2-associated transcription factor, is required for ILC development and continues to be expressed at low levels by mature ILC3s. Furthermore, T-bet (an ILC1-associated transcription factor) can be expressed by NCR+ ILC3s and 'ex-ILC3s' as they transition to ILC1s.

Therefore, the use of intracellular transcription factor staining to identify distinct ILC subsets may produce non-pure populations. Where possible, we used other cell surface markers to ensure a pure population of ILC3s, however the limitations of multicolour flow panels, co-expression of markers between cell subsets and the need to include adequate exclusion of lineage positive cells necessitated a pragmatic approach. Markers such as CD127, CD161 and c-KIT showed variability and it is not clear if this represents genuine ILC heterogeneity or artefacts generated by different staining protocols. For accuracy, ILC3 cell estimates and characterisation were produced using the RORγt-GFP transgenic mice, rather than relying on ILC3s identified by transcription factor staining. Since permeabilisation for intracellular staining reduced this signal, we were unable to use this approach to study IL-17, IL-22 and GM-CSF production.

3.6.2 Limitations

Obtaining a single cell suspension from murine kidneys was relatively easy, owing to its structure and size. The murine bladder, however, is hollow and smaller than a drawing pin head. Its tough serosal coat and dense muscular layer made dissociation challenging, particularly in preserving live immune cells. Whilst the numbers and populations of cells obtained generated convincing populations by flow cytometry, the absolute numbers were small. Typically, the number of CD45+ alive cells obtained from a murine bladder fell into the order of hundreds. The proportion of ILC3s in the bladder was double that of kidney, but at 0.2-0.4% equated to very few cells, creating difficulties for onward processing. Retrospective analysis and comparison of plots from WT and reporter animals with isotypes was straightforward but posed significant challenges when trying to sort cells in real time. This had consequences for profiling subtypes of ILC3s and made sorting for RNA analysis or cell culture impossible. Being able to identify ILC3s without intracellular staining was an important development in our experiments. Despite the bright GFP reporters circumventing problems with intracellular staining, the absolute numbers of cells that were harvested prevented collection of meaningful data for further applications.

Reference has already been made to the challenges associated with multicolour flow cytometry, but its use has been essential in defining tissue-resident, lineage negative cells. Care was taken to limit the numbers of fluorophores used and to distribute markers sensibly, so as not to introduce compensation errors that might have a critical effect during analysis of small cell populations. Accuracy in defining lineage negative populations was prioritised over subsequent ILC3 subtype characterisation, however this only became apparent as the project advanced. It is accepted that the earlier ILC phenotyping experiments using intracellular transcription factor staining did not contain sufficient labelling to fully exclude T cells (such as CD5, αβTCR or γδTCR) leading to impure and large populations of cells. By repeating these experiments with more thorough lineage

exclusion, this data may show greater accuracy for ILC analysis. Larger flow cytometry panels are unlikely to have increased our quality of depth of ILC phenotyping for the reasons mentioned, though lineage markers could have been added to the same channel. CyTOF provides another way of assessing multiple markers and would expand our panel far beyond that capable by flow cytometry. It is unlikely, however, this would be of practical use owing to the steps required to tag cells and the subsequent loss of material.

During our initial experiments, we were limited by low numbers of viable immune cells from the bladder. Protocols within the laboratory had been well-developed to process murine renal and haematopoietic tissue, but these methods were poor at releasing immune cells from within the bladder. Longer incubation times with enzymes led to increased cell death and so we sought alternative digestion strategies. Through experimentation with different enzymes and dissociation methods, an optimised protocol for bladder homogenisation is detailed in chapter 2, protocol 1.

Obtaining pictures of ILC3s from murine bladder was not straightforward, owing to its hollow nature and depth. This meant that sections were small and prone to slip from the slide, making whole mount preparations a better option. Fixation methods are associated with antigen loss, but in ILC3 identification, we were able to circumvent this by using our RORγt-GFP reporter mice with anti-GFP antibodies. Through trial and error of multiple anti-CD3 antibody clones and conjugates, we were able to identify lymphocytes and ILC3s within the bladder wall, though the urothelial layer proved an indiscriminate antibody-trap. A balance between adequate washing of the antibody stain, but not the section from the slide had to be observed. Optimal bladder sectioning required a partially inflated bladder, or technical difficulties arose as the tissue folded easily or lifted away from the slide.

Despite multiple attempts at obtaining human images of ILCs, I have been unable to do so. The reasons for this are likely to include difficulties with preserving structure and antigen availability during fixation and a paucity of human antibodies of sufficient labelling-quality.

Human tissue was retrieved and processed in accordance with strict ethical guidelines. There were challenges that were particularly associated with retrieval of human kidneys, as these organs were distributed by NHSBT to several other research groups. Tissues were prioritised for projects with direct clinical relevance (such as *ex vivo* organ perfusion), as our research was not directly related to a clinical project our supply of donor organs was reduced. Where possible, we used tissue with shorter cold ischaemic times, but accepted organs from donors with a wide range of medical conditions. As expected, our experience has taught us that cells suspensions obtained from donor organs with shorter cold ischaemic times and an uncomplicated past medical history contain an

increased proportion of viable cells. Owing to the variability and availability of donor organs, too few donors have been included in this study to draw any conclusions on past medical history, age or gender on ILC number or character. Human bladder samples were obtained from our onsite transplant team and there were fewer problems with tissue viability owing to the markedly reduced cold ischaemic times.

The laboratory has been receiving human renal tissue for over five years and during this time has refined a protocol for homogenisation and dissociation. We continued to improve this, though the difficulties with tissue viability, as already mentioned, meant that flow cytometry data was not always easy to interpret. To reduce issues with high numbers of dead, auto-fluorescent cells we observed that it was essential to homogenise smaller amounts of tissue and use a Percoll gradient to purify the sample. We have also found that the tissue does not respond well to MACS separation, which hindered our initial efforts to sort viable renal ILC3s. Despite protocol refinements, there were some instances were too few cells could be obtained and this most often pertained to the renal medulla. The medulla is the area most vulnerable to ischaemia and accruing cold ischaemic time was an unpreventable part of the retrieval process associated with research kidneys. We remain grateful to the donors and their families for their generosity in gifting us tissue for research and made great effort to use it efficiently and responsibly at all times.

3.6.3 Future work

As the field develops, advances in fate-mapping specific ILC3 subsets will provide an invaluable way of analysing these cells in the renal tract. Understanding ILC3 development, trafficking and dynamics in health and disease will help us gain a better understanding of their position and role in the renal tract. Furthermore, the microscopy presented within this chapter needs further development, both in terms of increased documentation of renal ILC3s and human imaging. We chose to focus our efforts on obtaining murine bladder imaging, as many of our UTI experiments had been optimised for investigation of lower urinary tract infection.

It was not possible for us to link historical data of urinary tract infection or current urinary microbiological results to our human donor data, as these metrics were unavailable to us. It would be useful in the future, to collect more clinical and demographic information about donors to assess the effects on tissue-resident immune cells within the renal tract. This would require greater collaboration with NHSBT to influence data collection, posing strategic challenges that could form a much larger project.

ILC3s make up a small part of the dense innate immune network of the renal tract. Experiments continue with the laboratory to better define these populations in human kidneys and bladder using single cell RNA sequencing. The use of single cell techniques, such as 10x genomics, RNAscope and RNA-expression and protein sequencing assays, within this context will provide useful insights into the cellular heterogeneity that exists. Identifying tissue resident immune cell populations and recognising intra-population diversity will enable us to hypothesise how these tissue-resident network might interact to keep us healthy. Complementary to work already underway to produce a single cells human renal atlas ([422] and Stewart et al. manuscript submitted 2019), we aim to produce a human bladder atlas to address these aims. In the renal tract, this information will have wide ranging consequences for our understanding of infection, autoimmunity, transplantation and cancer.

3.7 Graphical Summary

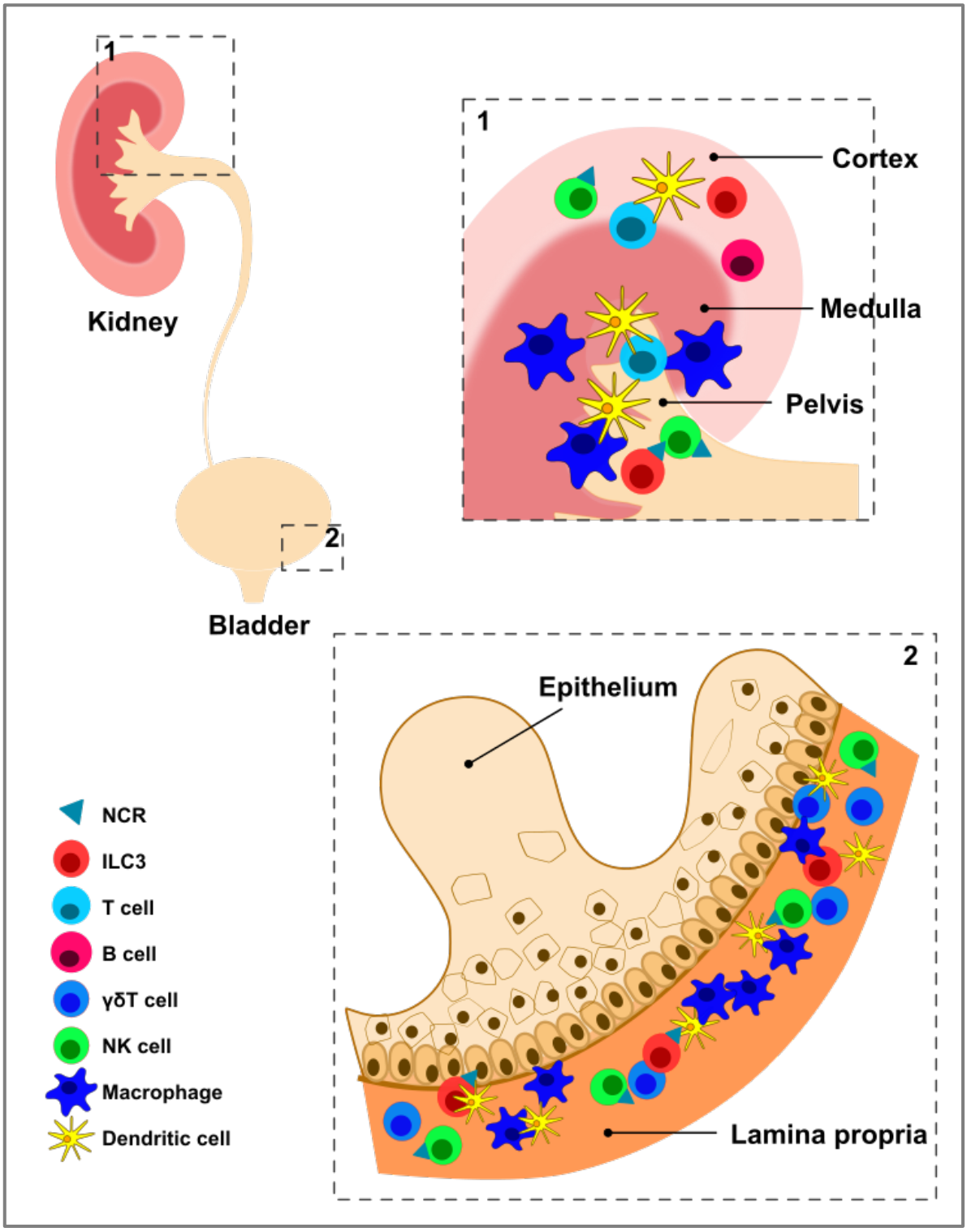

Figure 3.17: ILC3s are present throughout the renal tract

ILC3s can be found throughout the renal tract with a proportional increase in NCR+ ILC3 in the bladder and renal pelvis. ILC3s and lymphocytes colocalise with MNPs in the lamina propria of the bladder, where other innate immune cells, such as γδT cells, can be found. Adaptive immune subsets (such as B cells) are more likely to be found in the upper renal tract.

Chapter 4 - ILC3 responses during infection of the renal tract

4.1 Introduction

Exposure to Uropathogenic *E. coli* (UPEC) precipitates an immune response that is coordinated by macrophages within the bladder, however we have a limited appreciation of the relationships and interactions of these and other tissue-resident cells in health and disease within the renal tract. Urinary tract infections are a leading cause of morbidity and mortality [13] and it is key to neutralize pathogens as soon as possible, to prevent their ascension of the urinary tract to the kidney. Once in the kidney, the rich vascular supply produces a vulnerability to systemic dissemination of the bacteria and resulting septicaemia. Gram negative bacteria within the blood stream are particularly effective at producing a profound systemic effect that can cause death rapidly, called septic shock or systemic inflammatory response syndrome. As one of the commonest causes of infection in humans, it is imperative that we can respond rapidly and definitively to urinary tract infection. Bacterial UTI serves as a good model to investigate the function of immune cells within the renal tract, informing our wider knowledge of tissue-resident immune populations and their effects in health and disease.

To investigate UTI in more detail, we generated murine models of infection by instilling bacteria directly into the bladders of female mice. This technique has been used previously and is particularly good at causing pyelonephritis when a double catheterization is performed [415]. This finding was confirmed by Tittel et al. (2011), who showed that pyelonephritis rates rose from 16% to 84% with a second catheterization [371]. To interrogate the role of ILC3s within UTI we used single and double catheterization with UPEC in a variety of murine models including:

- *Rorc(γt)-Gfp*^{TG} reporter mice.
- RORγt-KO (*Rorc(γt)-Gfp/Gfp* knock-in) mice (lacking the transcription factor for development of ILC3s and Th17 cells).
- Rag2-KO mice (lacking the enzyme for VDJ recombination of BCR and TCR molecules for development of lymphocytes) treated with an anti-Thy1 antibody to deplete ILCs.
- IL22ra1-KO mice (incapable of responding to IL-22, a product of ILC3s).

Together, these murine models allowed us to examine three key areas of ILC3 biology within the renal tract:

1. The presence and expansion or recruitment of ILC3 in UTI.

2. The importance of the ILC3-derived cytokine, IL-17 in creating a pro-inflammatory immune response to UPEC.
3. The role of ILC3-derived IL-22 at the urothelial barrier for maintenance of epithelial integrity.

Recruitment and trafficking of ILC3s has been well-investigated within the gut and we have used these data to inform our own analysis. ILC1s and ILC3s express homing receptors in the presence of DCs and retinoic acid (RA); DCs are important producers of RA in the gut [159, 423]. This enables expression of CCR9 and α4β7 integrin for homing to the intestine and ILC3s primed with vitamin A (a precursor of RA) were more efficient at gut-homing than their vitamin A-deficient counterparts. Moreover, mice fed a vitamin A-deficient diet had a subsequent rapid expansion of ILC2s and ILC3s within the gut on addition of the vitamin to their diet [275]. Furthermore, in mice irradiated prior to transfer of bone marrow-derived cells, ILC3s populated the small intestine and colon, but failed to home to mesenteric lymph nodes effectively [423]. This demonstrates the predilection of ILC3s to home to the gut mucosal epithelium, from where they are capable of migrating to mesenteric lymph nodes using CCR7 [303]. Furthermore, it has also been shown that ILCs migrate to lymph nodes following skin damage, though it was ILC1s and NK cells that showed the highest levels of migration and ILC3s remaining predominantly tissue-resident [424]. The migration of these cells were tracked using local photoconversion of Kaede Green to Kaede Red after skin incision in a CD62L and CCR7-dependent manner. Despite some migration to regional lymphoid organs, ILC3s are thought to be primarily tissue-resident cells, capable of local proliferation and expansion [261, 275, 302, 303, 424]. Taken together, these data illustrated that ILC3 can both proliferate and be recruited within the gut and this is enhanced by dietary retinoic acid (vitamin A). Dietary variation is unlikely to directly impact the luminal milieu in the bladder, therefore we have not pursued this line of investigation. However, ILC3 in the gut do increase in number in the context of enteropathogenic bacteria [281, 282, 288, 353]. We therefore sought to determine how ILC3s within the renal tract respond following challenge with UPEC.

The role of IL-17 in UTI has been investigated previously, and the published literature has been considered within section 1.4. Notably, innate sources of IL-17A are key within the renal tract, as demonstrated in a sterile model of AKI by Chan et al. (2014). They used multiple murine models to elucidate the source of IL-17 in cisplatin-induced AKI, but after depleting neutrophils, γδT cells and NK cells were unable to fully account for the innate source of the cytokine [384]. It is possible that ILC3s provide this role and our models, including the use of a Rag2-KO with ILC depletion, attempt to address this question in the context of infection.

IL-22 is known to be important in inflammatory conditions within the gut, including DSS colitis and *Citrobacter rodentium* infection, in promoting epithelial repair through immune cell recruitment and production of AMPs and epithelial growth factors [80, 275, 347, 353, 423, 425]. IL-22 production from ILC3s in infective colitis was heavily dependent on factors produced by CX3CR1+ MNPs, including IL23 and TL1A, and mice lacking these cells suffered increased levels of inflammation and rates of death. IL-22 has also been shown to be important in the renal tract, as a key cytokine in enabling tubular repair after ischaemic renal injury [350, 394-396]. Its release was enhanced by TLR4 activation, a receptor for LPS, and therefore is highly relevant to the gram negative bacterium, *Escherichia coli*. Further detail on the role of IL-22 in the renal tract can be found in section 1.4.

In chapter 3, I presented data demonstrating the presence of ILC3s within the renal tract, with a predilection for a urothelial niche within the bladder mucosa. This places them in a position to respond to the threat of urinary pathogens and form part of the 'innate immune defense team', bringing complimentary actions to those of γδT cells, MAITs, intraepithelial lymphocytes and NK cells. This chapter seeks to determine if ILC3s play a role in the acute phase of bacterial defense in the kidney and bladder, via production of IL-17a and IL-22.

This chapter starts by examining the inflammatory response that occurs within the renal tract during UTI, with a focus on ILC3-stimulating factors and ILC3-mediated responses. We used published transcriptional data sets from Carey et al. (2016) who harvested whole bladders eight hours post-infection for RNA sequencing [3] and Spencer et al. (2015) [44] who harvested tissues at 2, 6 and 48 hour time points. In addition, we performed bulk RNA sequencing experiments on kidney and bladder, and confirmed key findings using qPCR on tissues taken from WT animals at various time-points following UPEC challenge. We have then related these transcriptional changes to those observed in ILC3 populations within the renal tract in UTI. Together these data contribute to a better understanding of innate immune responses to bacterial challenge within the renal tract.

4.2 ILC3 responses to UTI and early transcriptional changes within the renal tract

We sought to profile changes in ILC3 numbers and cytokines, as well as antimicrobial peptides (AMPs) during infection of the renal tract. To do this, wild type mice were given a urinary tract infection and their tissues harvested for RNA analysis and flow cytometry. Baseline immune cell counts are shown in figure 4.1 in both bladder and kidney after 24 hours of infection. Neutrophils numbers rose rapidly in bladder and kidney, though it should be noted that only two of the seven mice challenged with intra-vesical UPEC had evidence of pyelonephritis when cultured (all mice given UPEC had culture positive cystitis). The nature of pyelonephritis in this context was of ascending infection and so it may be that infection kinetics lag behind those observed in the bladder or bacteria may not have reached the kidney after only one catheterisation. This explains the increases in T cell, NK and ILC numbers that were shown in the bladder (fig. 4.1B), but not kidney at this stage (fig. 4.1C). The swift neutrophil response in the kidney may, in part, have accounted for early clearance of pathogens.

To investigate the immune response at different time points during infection, we catheterised mice with UPEC and harvested tissues after 1, 2 or 3 days. Figure 4.2 shows the profile of cytokines in the first three days following UTI in murine bladders. *Il1b* transcripts rose rapidly and were sustained, whereas *IL23a* and *Tnfsf15* (TL1A) levels rose more gradually. The rapid rise in *Il1b* was accompanied by correlated increases in *IL17a* and *IL22* transcripts, ILC3 cytokines (fig. 4.2C). The time-course of transcriptional profiles of both these transcripts and of *Csf2* over 72 hours are shown in figure 4.2B.

Figure 4.1: WT mice catheterised once with PBS or UPEC for 24 hours. **A:** Flow cytometry plots representative of cell counts from bladder and kidney (PBS=5, UPEC=7), with the gating strategy demonstrated by red dashed lines and labels for the bladder PBS sample. CD45 (anti-CD45-BV650), alive cells were divided into tissue resident and IV populations using the pre-mortem anti-CD45-FITC intravenous label. Tissue resident cells have been gated using lineage markers (NK1.1/CD11b/CD11c/γδTCR/βTCR-eFluor450), anti-GR1-PECy7, anti-CD3-PEDazzle and anti-NKp46-PE to identify neutrophils, T cells and NK cells respectively. ILCs were labelled as lineage-/CD3- and anti-CD127-eFluor780+ (gating not shown). Approximate cell counts per organ are shown in bladder (**B**) and kidney (**C**). Dot plots show median values and significance calculated using Mann-Whitney tests; bladder PMN and NK cells **p=0.0043, T cells **p=0.0087, ILCs p=0.0519; kidney PMN ***p=0.0009.

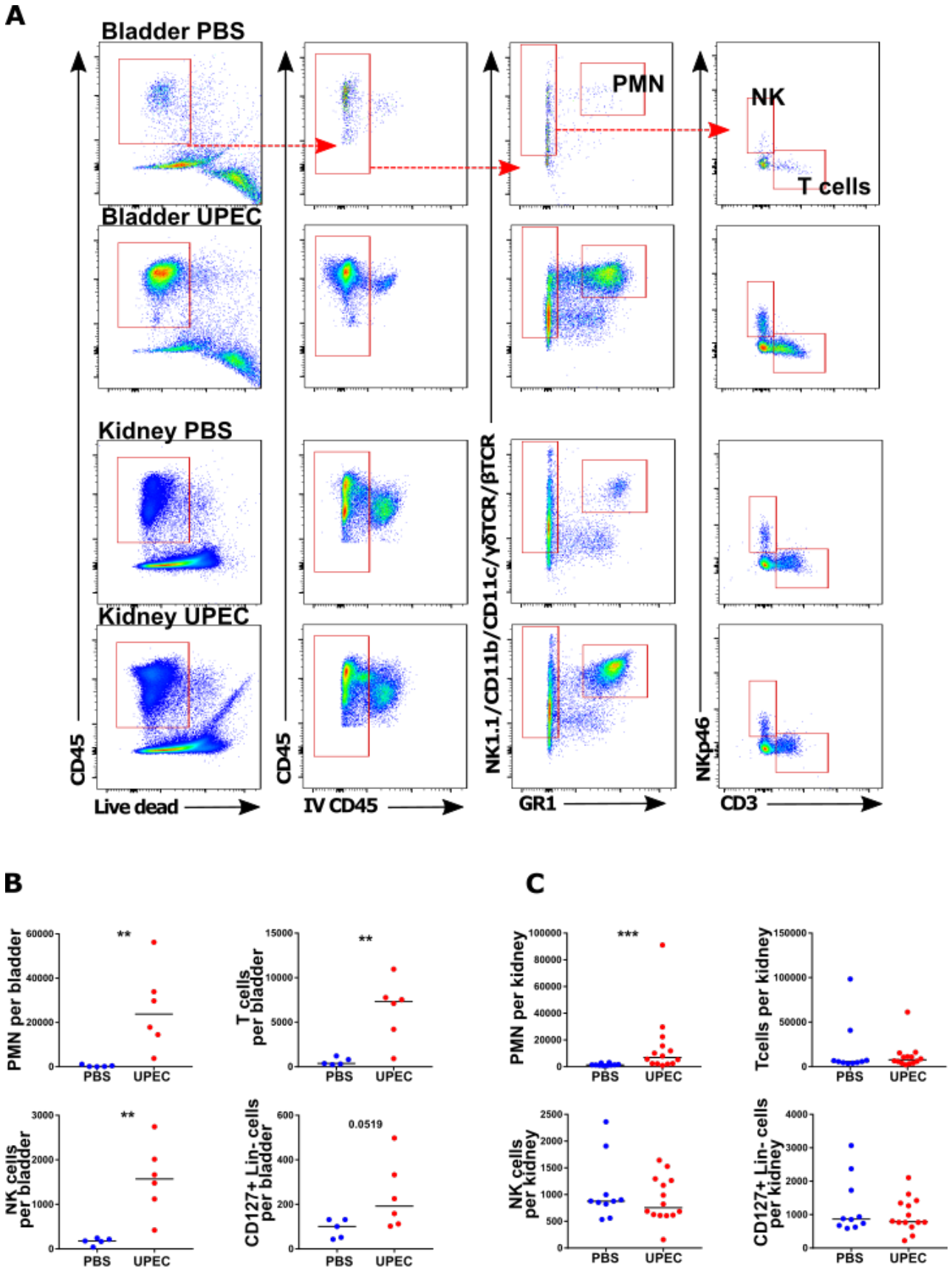

Figure 4.1: Baseline characteristics of murine lymphocytes and ILCs in UPEC UTI.

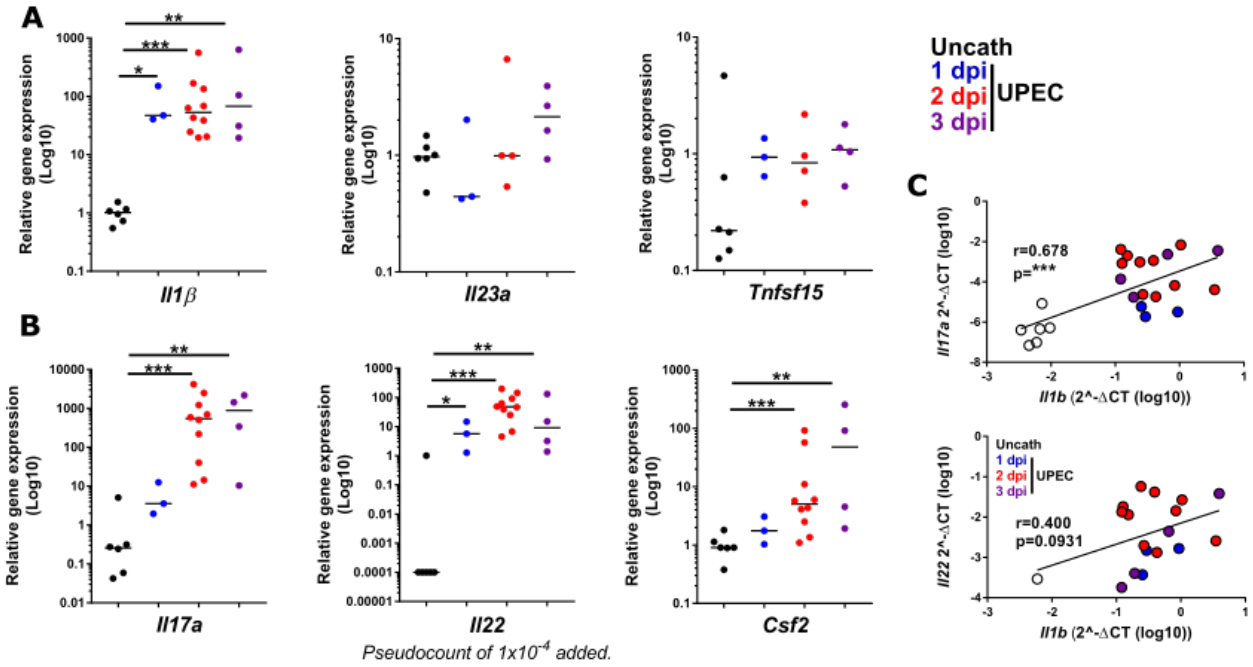

Figure 4.2: Transcript levels of ILC3 stimulatory cytokines and products during UPEC UTI.

Quantitative PCR data from time course UTI, single catheterisation of WT mice. Bladders harvested from mice at baseline (uncatheterised) or 1, 2 or 3 days post-infection (dpi) with UPEC; n=3-10 per group. Data combined from two experiments and expressed relative to *Hprt* and baseline data. **A:** Key ILC3 stimulating cytokines. **B:** ILC3 cytokine products. Significance calculated using Mann Whitney test as follows: *Il1b* *p= 0.0238, **p=0.0095, ***p=0.0002; *Csf2* **p=0.0017, ***p=0.0095; *Il17a* **p=0.0095, ***p=0.0002; *Il22* *p=0.0119, **p=0.0048, ***p=0.0002. **C:** Rises in the ILC3 transcripts, *Il17a* and *Il22* relative to *Il1b* levels. Correlation calculated by Pearson's r test, ***p= 0.0004.

We also examined the expression of other pro-inflammatory cytokines and anti-microbial peptides, and their temporal correlation with ILC3-associated cytokines (figures 4.3 & 4.4). As anticipated, chemokines that facilitated neutrophil and monocyte recruitment rose quickly *(Ccl2, Cxcl2* and *Cxcl12*). *Ccl5* (RANTES) is a T cell and myeloid cell chemoattractant and this also increased sharply within the first 24 hours of infection. Together, these transcriptional changes suggest that, following bacterial challenge, the tissue environment rapidly changes to facilitate an innate inflammatory response within tissues, enabling the recruitment of immune cells to promote pathogen clearance.

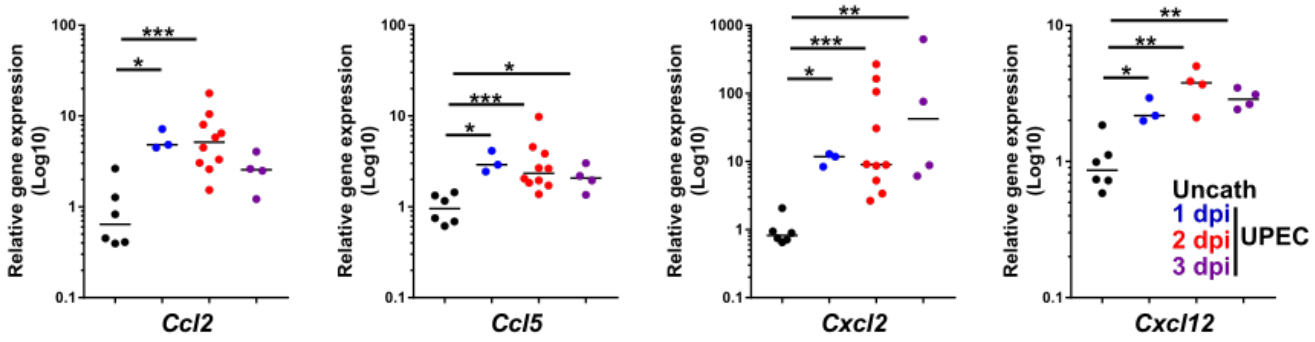

Figure 4.3: Transcript levels of pro-inflammatory and chemotactic cytokines released during UPEC UTI.

Quantitative PCR data from time course UTI, single catheterisation of WT mice. Bladders harvested from mice at baseline (uncatheterised) or after 1, 2 or 3 dpi with UPEC demonstrating critical pro-inflammatory cytokines and chemokines for monocyte and neutrophil recruitment; n=2-10 per group, where possible data combined from two experiments and expressed relative to *Hprt* and baseline data. Significance calculated using Mann Whitney test as follows: *Ccl2* *p= 0.0238, ***p=0.0001; *Ccl5* *p=0.0238 day 1, *p=0.019 day 3, ***p=0.0005; *Cxcl2* *p=0.0238, **p=0.0095, ***p=0.0002; *Cxcl12* *p=0.0238, **p=0.0095.

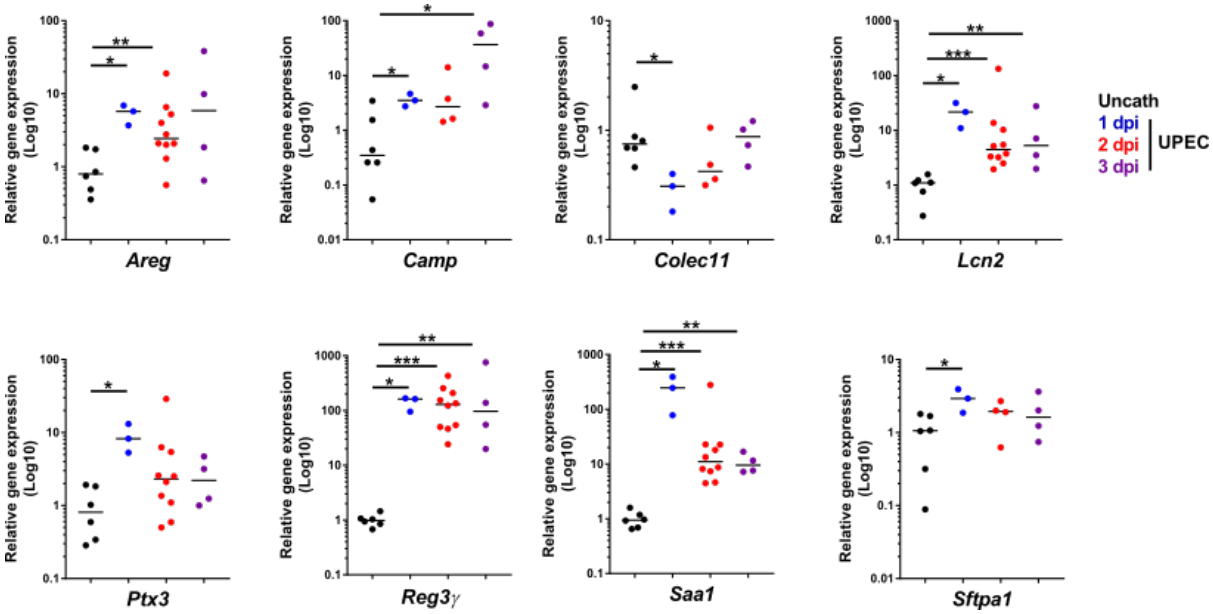

Figure 4.4: Transcript levels of AMPs and epithelial regeneration factors during UPEC UTI.

Quantitative PCR data from time course UTI, single catheterisation of WT mice. Transcripts relating to AMPs during UPEC UTI from bladder, n=3-10 per group, data combined where possible from two experiments and expressed relative to *Hprt* and baseline (uncatheterised) data. Significance calculated using Mann Whitney test: *Areg* *p=0.0238, **p=0.0075; *Camp* *p=0.0476 day 1, *p=0.019 day 3; *Colec11* *p=0.0238; *Lcn2* *p=0.0238, **p=0.0095, ***p=0.0002; *Ptx3* *p=0.0238; *Reg3g* *p=0.0238, **p=0.0095, ***p=0.0002; *Saa1/2* *p=0.0238, **p=0.0095, ***p=0.0002; *Sftpa1* *p=0.0238

There are some antimicrobial peptides that have already been associated with the renal tract (see chapter 1, figure 1.3) and these include amphiregulin (*Areg*), cathelicidin (*Camp*), pentraxin-3 (*Ptx3*), regenerating protein-3γ (*Reg3g*), and Lipocalin-2 (*Lcn2*). The profiles of these transcripts during UTI are shown, though we have sought to identify novel AMPs and epithelial factors (some associated with ILC3-derived IL22 in the gut and lungs), including surfactant protein A1 (*Sftpa1*) and collectin-11 (*Colec11*) and acute phase proteins that may contribute to defense against bacteria, such as serum amyloid A1 (*Saa1/2*).

These AMPs rose rapidly following infection, and some transcript levels were sustained for up to 3 days, including *Areg, Reg3g* and *Camp* (fig 4.4). As observed with pro-inflammatory cytokines and chemokines, AMP transcript levels also mirrored increases in *Il17a* and *Il22* levels during this early response to UTI in the bladder.

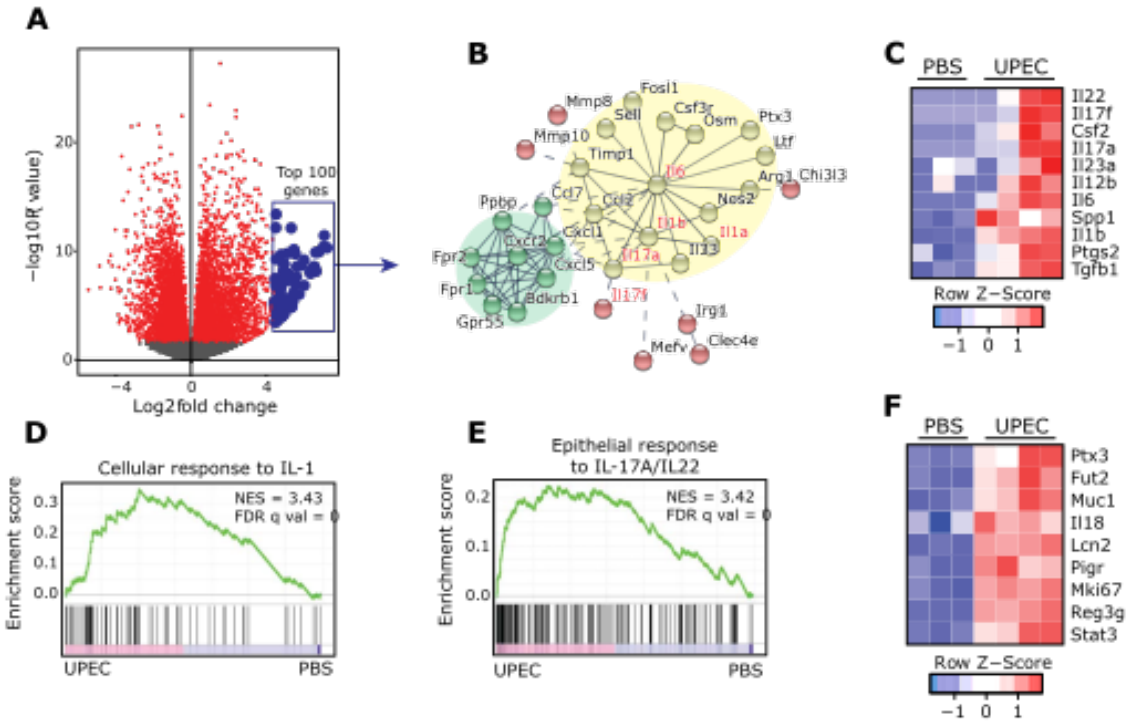

Figure 4.5: Th17 immunity genes are upregulated during UPEC UTI.

RNA sequencing data from whole bladders catheterised with UPEC for 24 hours. **A**: Volcano plot showing differential expression between PBS and UPEC treated mice, with the top 100 genes highlighted. **B**: Within the top 100 upregulated genes are nodes for Th17 immunity and Cxcl1-driven neutrophil recruitment. **C**: Heatmap of key Th17 immunity genes. **D**: Gene set enrichment analysis of IL-1 scores. **E**: Gene set enrichment analysis of epithelial responses to IL-17a and IL-22. **F**: Heatmap of genes associated with epithelial repair and regeneration, including AMPs and cell cycle genes.

To lend further support to the qPCR data shown above, we interrogated RNA sequencing data from the bladders of WT mice catheterized with UPEC for 24 hours. The bioinformatic processing was performed by Dr J. Ferdinand and Dr T. Castro and shows that genes associated with Type 17 immunity were among the 100 most upregulated genes in UTI (fig. 4.5A), forming a major gene node in STRING analysis (Search Tool for the Retrieval of Interacting Genes) (fig. 4.5B). Indeed, a number of Th17-associated genes were significantly increased post-UTI (fig. 4.5C). Gene set enrichment analysis confirmed an increase in genes associated both with Th17 immunity, but also those associated with epithelial responses to IL-17 and IL-22 (fig. 4.5D&E). These included genes associated with epithelial regeneration and repair, as well as anti-microbial peptides (figure 4.5F).

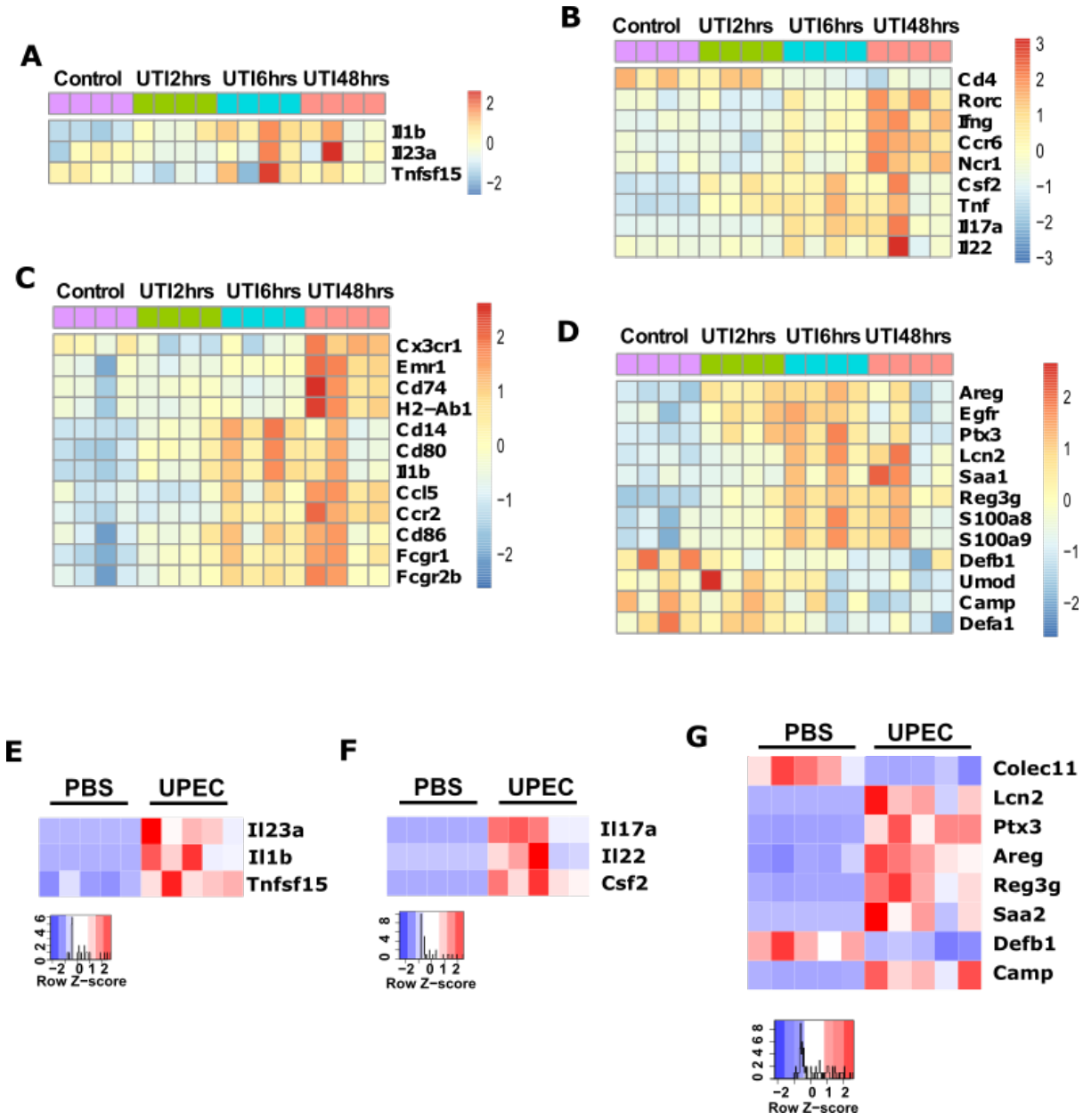

Figure 4.6: RNA sequencing data from WT murine bladders during UTI

A-D: Heatmaps showing gene transcripts during the first 48 hours of UTI. **A**: ILC3 stimulating cytokines. **B**: Genes associated with ILC3 activation. **C**: Genes associated with MNP activation. **D**: AMPs and epithelial growth factors. **E-G**: RNA sequencing data from murine bladders treated with UPEC and harvested at 8 hours. **E**: ILC3 stimulating cytokine transcripts. **F**: ILC3 product transcripts. **G**: AMP transcripts. Data re-analysed from publicly available sources - Spencer et al., 2015, accession number GSE72007 and Carey et al., 2016, accession number GSE68220.

In addition to our UTI experiments in mice, we were able to supplement our data with analysis of a publicly available data sets from Spencer et al. (2015) and Carey et al. (2016) [3, 44]. The authors catheterized mice with UPEC and harvested their bladders at a range of different time points,

however it must be noted that the strain of UPEC was slightly different in each data set. The oligonucleotide microarray data from Spencer et al., used the UPEC strain UTI89 (the same as that used by our laboratory) and the Carey et al., RNA sequencing data utilized CFT073. Figure 4.6 shows heatmaps that relate to transcriptional changes in ILC stimulating cytokines (fig. 4.6A&E), ILC3 products (fig. 4.6B&F), MNP products and activation factors (fig. 4.6C) and AMPs (fig. 4.6D&G). These data support our findings of increased Th17-related inflammatory mediators, AMPs and proinflammatory cytokines during UTI. Scripts for analysis were provided by Dr J. Ferdinand.

Due to the variable frequency and severity of pyelonephritis, Th17-associated cytokines and AMPs (as measured by qPCR) were much more variable than those observed in the bladder (fig. 4.7). Despite this, we found a trend towards increasing levels of transcripts for ILC3-derived cytokines, *IL17a* and *IL22*. At baseline, expression of *IL17a* and *Il22* were minimal/undetectable within the kidney, such that a pseudocount was required to statistically compare the subsequent increases after infection (fig. 4.7A). Expression of the ILC3-stimulating cytokines, *IL23a* and *Il1b* were also increased after UPEC challenge (figure 4.7B).

We observed variable expression of pro-inflammatory cytokines and AMPs (fig. 4.7C&D), likely relating to differences in infection rates following single catheterisation, but there were still significant increases in cathelicidin, lipocalin-2, pentraxin-3 and serum amyloid A1. The single catheterisation was optimal to interrogate bladder infection, but markedly reduces the rates of ascending pyelonephritis (approximately in the order of 20-25%, whereas a second catheterisation will produce rates of 75-80%). In addition, interpretation of these experiments was limited by the fact that I utilized the whole kidney for RNA analysis and there were no accompanying CFU counts that might allow the results to be interpreted in light of which kidneys were infected or uninfected. In order to address some of these limitations, we repeated the UTI experiments using a double catheterisation. We also assessed whether there were transcriptional differences between the renal cortex and medulla at 24 hours, providing a more detailed anatomical view across different regions of the kidney. This data has been catagorised by location and the presence of infection. Owing to the more limited amount of tissue that can be harvested using this experimental set-up, a smaller set of genes were interrogated (figure 4.8).

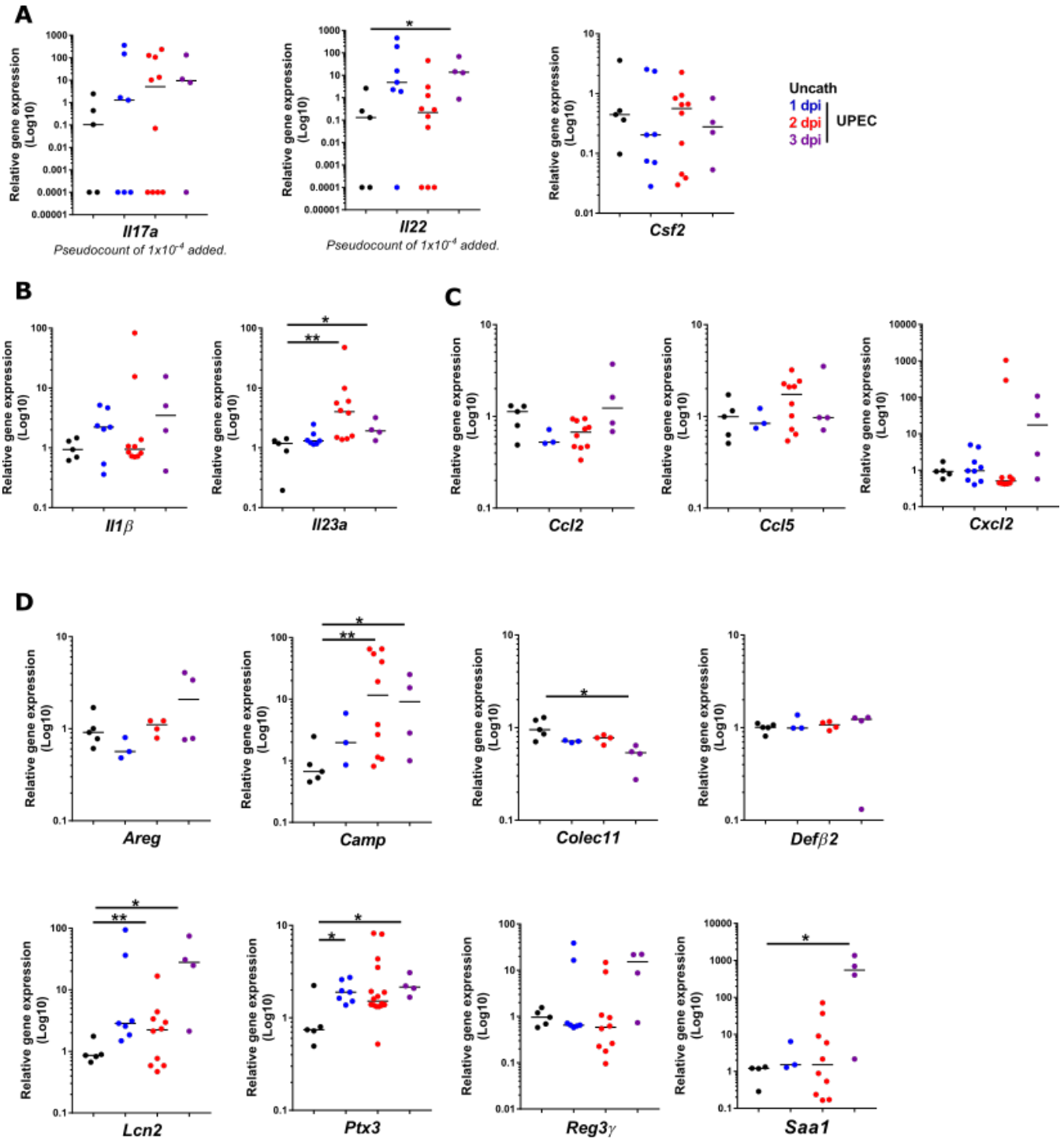

Figure 4.7: Transcripts of cytokines and AMPs over time during UPEC UTI

Quantitative PCR data from time course UTI, single catheterisation of WT mice. Kidneys harvested after catheterisation with UPEC at 1, 2, or 3 dpi; n=3-11, combined from 3 separate experiments. Dot plots showing gene of interest relative to *Hprt* and baseline (uncatheterised) with median bar. Significance calculated using Mann-Whitney test. **A**: ILC3 effector cytokines; *Il22* *p=0.0317; **B**: ILC3 stimulating cytokines; *Il23a* *p=0.0317, **p=0.0027. **C**: pro-inflammatory mediators. **D:** AMPs; *Camp* *p=0.0317, **p=0.008; *Colec11* *p=0.0159; *Lcn2* *p=0.0159, **p=0.0051; *Ptx3* *p=0.048 day 1 and *p=0.041 day 3; *Saa1/2* *p=0.0286.

We found increased *IL17a, IL22* and *Csf2* transcripts in the kidney in UTI, although there were no significant differences in *IL17a* and *Csf2* between cortex and medulla/pelvis samples (figure 4.8A), indicating uniform production across the kidney. *Il22* transcripts were more highly expressed within the cortex. This may indicate that ILC3s or other cells capable of producing Th17 cytokines are preferentially located in the cortex. This data echoes other work locating *Il22* and *Il22ra1* transcripts to the glomeruli in kidneys [394-396]. Whilst both glomeruli and tubules are required for good kidney function, we can speculate that the maintenance of the integrity of the glomerulus with its proximity to a dense network of arterioles is essential to avoid systemic spread of pathogens.

The expression of *Il1b* transcripts varied between PBS and UPEC kidneys and between the different location within the kidney with higher levels in the medulla/pelvis samples (figure 4.8B). Similar results were observed for the chemokines *Cxcl1* and *Cxcl2* and this data supports the idea that the inner regions of the kidney have a superior immune defense, as this is the area that pathogens encounter first as they ascend the urinary tract. Figure 4.8C shows increases in transcripts of AMPs previously observed in the renal tract during the time course experiments, namely amphiregulin, lipocalin-2, Reg3γ and serum amyloid A1. All these transcripts increased with infection and anatomical differences were observed in the first three.

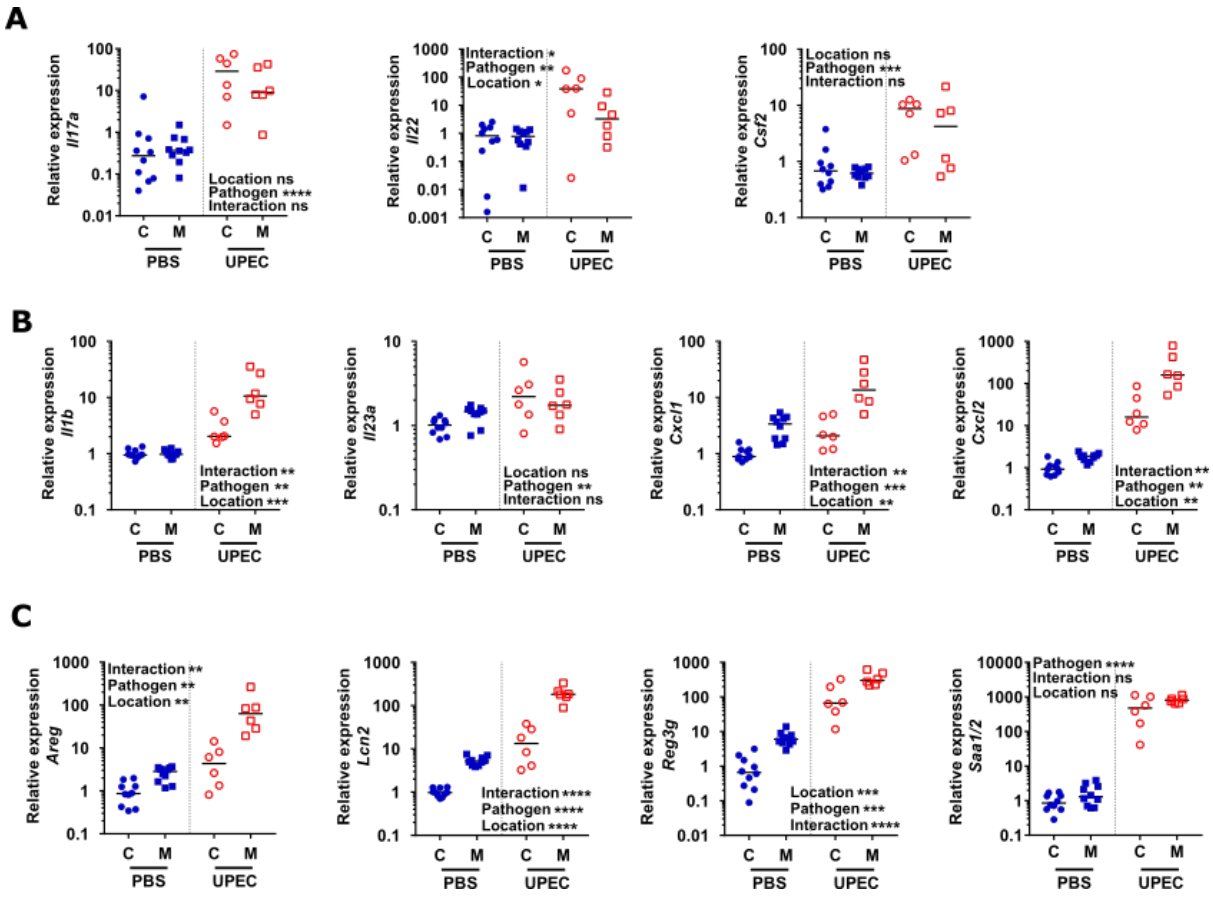

Figure 4.8: Cytokine and AMP transcripts according to renal anatomical location during UPEC UTI

Whole WT kidneys extracted for RNA analysis after 48 hours infection and dissected into cortex (C) and medulla/pelvis (M) after two catheterisations with PBS (n=5) or UPEC (n=3). qPCR data expressed as gene of interest relative to *Hprt* and PBS-treated cortex, median bar. **A**: ILC3 products, significance calculated using two-way ANOVA. P values as follows: *Il17a* pathogen ****p= <0.0001; *Il22* location *p= 0.0205, pathogen **p= 0.0044, interaction *p= 0.0215. **B**: ILC3 stimulating cytokines and chemoattractants. *Il1b* interaction **= 0.0017, pathogen **=0.0017, location ***=0.0001; *Il23a* pathogen **p= 0.0021; *Cxcl1* interaction **= 0.0071, pathogen ***= 0.0007, location **= 0.0013; *Cxcl2* interaction **= 0.0089, pathogen **= 0.0085, location **= 0.0017. **C**: AMPs. *Areg* interaction **= 0.0077, pathogen **= 0.0058, location **= 0.0034; *Lcn2* interation/pathogen/location ****= <0.0001; *Reg3g* interaction ***= 0.0007, pathogen ***= 0.0004, location ****= <0.0001; *Saa1/2* pathogen ****= <0.0001.

Having established that cytokines associated with ILC3s, both those required to stimulate them and those produced by ILC3, were increased during UTI in the bladder and kidney, we next sought to determine if ILC3 numbers increased in the context of bacterial challenge. Figure 4.9 shows the effect of UPEC UTI in the bladder at 24 hours.

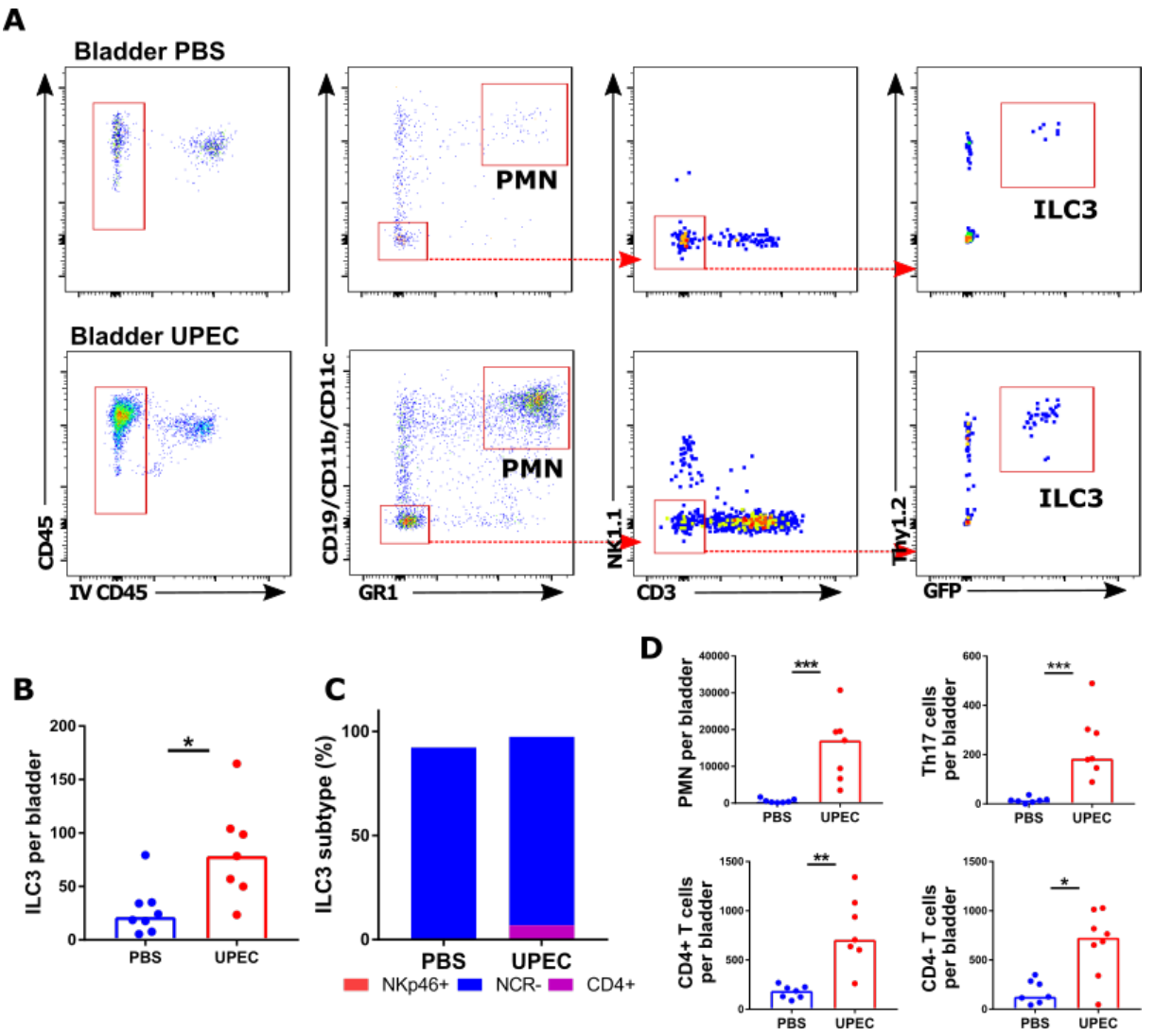

Figure 4.9: Immune cell counts in the bladder during UPEC UTI from RORγt-GFP reporter mice

RORγt-GFP (transgenic) mice catheterised twice with PBS or UPEC. Bladders harvested after 24 hours. **A**: Flow cytometry gating to show ILC3: Preselected for alive, singlets and defined as tissue-resident (CD45-BUV395 positive/IV-CD45-BV650 negative). ILC3s delineated as CD19/CD11b/CD11c-eFluor450 negative, NK1.1-BV605 negative, CD3-APC negative, Thy1.2-PerCPCy5.5 positive and GFP positive. **B**: Total ILC3 counts per organ, n=8 PBS, n=7 UPEC, *p= 0.014. **C**: ILC3 subtypes expressed as median summary data. **D**: Neutrophil count ***p= 0.0006, Th17 cell count ***p= 0.0006, CD4+ T cells **p= 0.0012 and CD4- T cells *p= 0.014. for comparison. Gating not shown for T cell subsets (CD3+, Th17 cells also CD4+/GFP+). Results combined from two experiments, significance values calculated using Mann-Whitney tests, n=7 PBS, n=7 UPEC.

Using bladders from two separate UTI experiments, we found a significant increase in ILC3s at 24 hours following UPEC challenge (fig. 4.9A, B). There was also a change in the relative frequency of the different ILC3 subsets, with an increase of CD4+ ILC3 and decrease of NCR+ ILC3 (fig. 4.9C). We also observed an increase in neutrophils and T cells at 24 hours in these experiments (fig. 4.9D), in

far greater number than ILC3s. Of note, RORγt-GFP+ T cells were also increased, confirming the induction of type 17 immunity in this context.

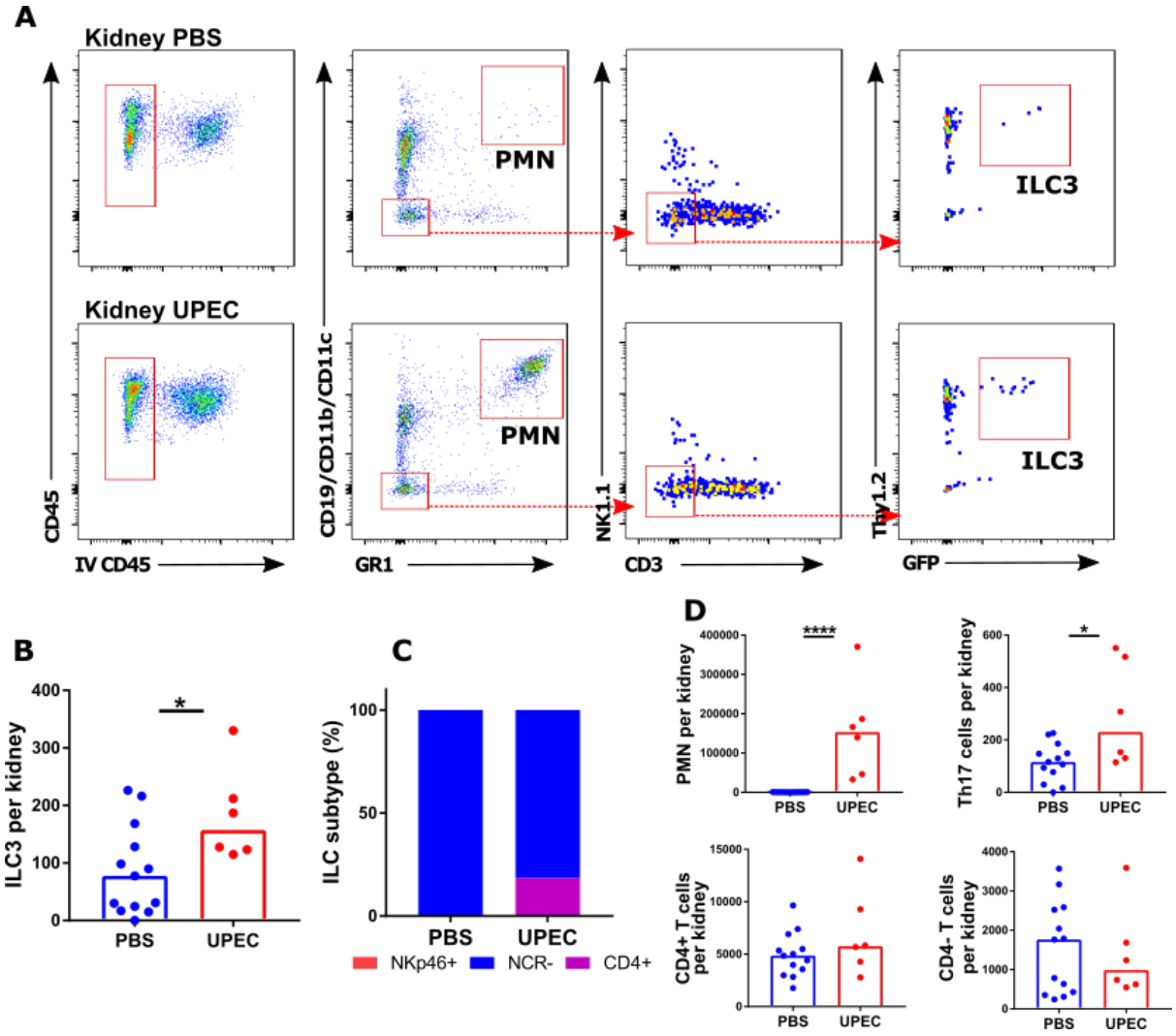

Figure 4.10: Immune cell counts in the kidney during UPEC UTI from RORγt-GFP reporter mice

RORγt-GFP (transgenic) mice catheterised twice with either PBS or UPEC. Kidneys harvested after 24 hours. **A**: Flow cytometry gating to show ILC3s: Preselected for alive, singlets and then defined as tissue-resident by gating on CD45-BUV395+/IV CD45-BV650 negative. ILC3s delineated as CD19/CD11b/CD11c-eFluor450 negative, NK1.1-BV605 negative, CD3-APC negative, Thy1.2-PerCPCy5.5 positive and GFP positive. **B**: Total ILC3 counts per organ (numbers plotted from kidneys that were culture positive for pyelonephritis), n=13 PBS, n=6 UPEC, *p= 0.0462. **C**: ILC subtypes expressed by median. **D**: Neutrophil count ****p= <0.0001, Th17 cell count (CD3+/CD4+/GFP+) *p= 0.0365, all CD4+ and CD4- T cells for comparison (PBS or confirmed pyelonephritis only). Gating not shown for T cell subsets. Results combined from two experiments, significance calculated using Mann-Whitney tests.

Within the kidney, a heightened Th17 response was evident, with increased numbers of ILC3s and Th17 cells in the kidneys with proven pyelonephritis (fig. 4.10B&D), based on positive CFU counts (data not shown). Other similarities were observed between bladder and kidney, in that the CD4+ ILC3 fraction increased (fig. 4.10C) and neutrophils were rapidly recruited to the site of infection (fig. 4.10D). In order to better understand how the ILC3 population expanded, and whether this represented recruitment of ILC3s to the bladder or proliferation of resident cells in-situ, we performed a UTI experiment with EdU supplementation.

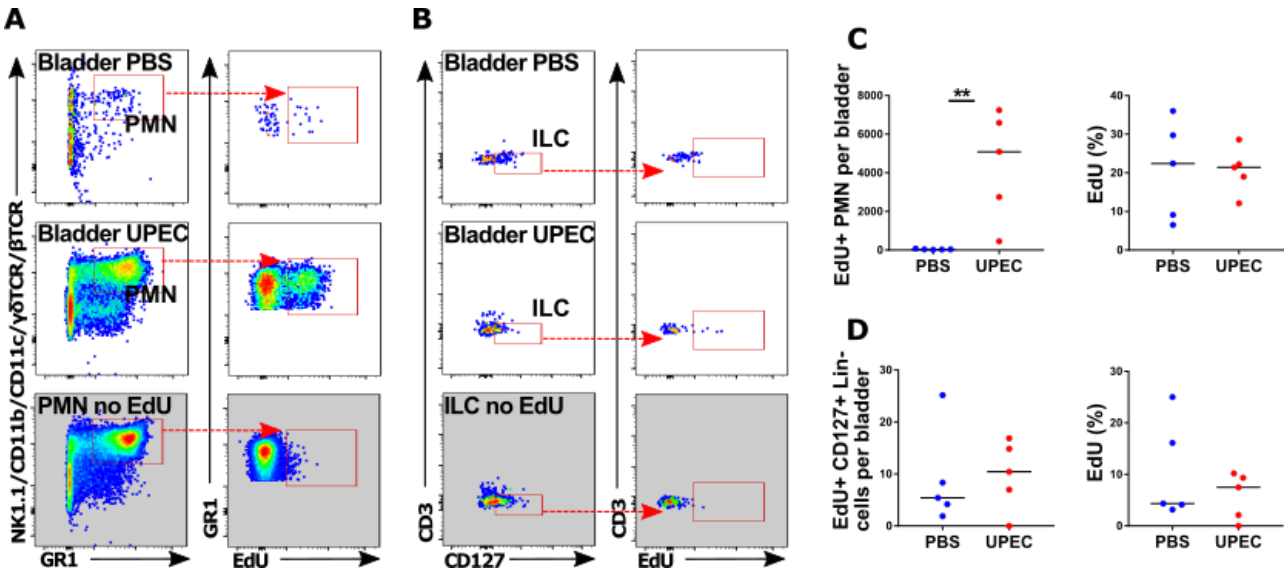

Figure 4.11: ILC3 expansion in the bladder during UTI

WT mice catheterised once with PBS or UPEC and given EdU (IP and PO) for 24 hours. **A**: Flow cytometry plots representative of cell counts from bladder for neutrophils that incorporated EdU (anti-EdU-A647) and have been preselected for alive, singlets that are IV CD45 negative. **B**: Flow cytometry gating to show ILCs (NK1.1/CD11b/CD11c/γδTCR/βTCR-eFluor450 negative, CD127-A780 positive), showing cells that incorporated EdU (PBS=5, UPEC=5). Greyed flow cytometry plots are from a mouse catheterized with UPEC but not given EdU. **C**: Neutrophils that were positive for EdU **p= 0.0043. **D**: ILC counts showing numbers and percentages that were EdU positive. Significance calculated using Mann-Whitney tests.

As demonstrated previously (fig. 4.1), neutrophil numbers rose rapidly and exhibited evidence of EdU incorporation, thus illustrating technical experimental success (fig. 4.11A). EdU inclusion was more difficult to demonstrate in ILC3s, as they were present in far smaller numbers. There was also a need to use WT mice rather than the Rorγt-GFP reporters for compatibility with the intracellular EdU staining protocol. In consequence this led to sub-optimal data, however, there is a trend towards an increase in Edu+ ILC3s post-infection, providing support for the conclusion that ILC3s in the bladder were proliferating in response to UPEC challenge (fig. 4.11D).

In the kidney, the EdU staining of ILC3s was limited, but EdU incorporation can be seen in ILCs, confirming proliferation of these cells during UTI (fig 4.12D). Figure 4.12A&C shows the equivalent effect of UTI on neutrophil recruitment for comparison.

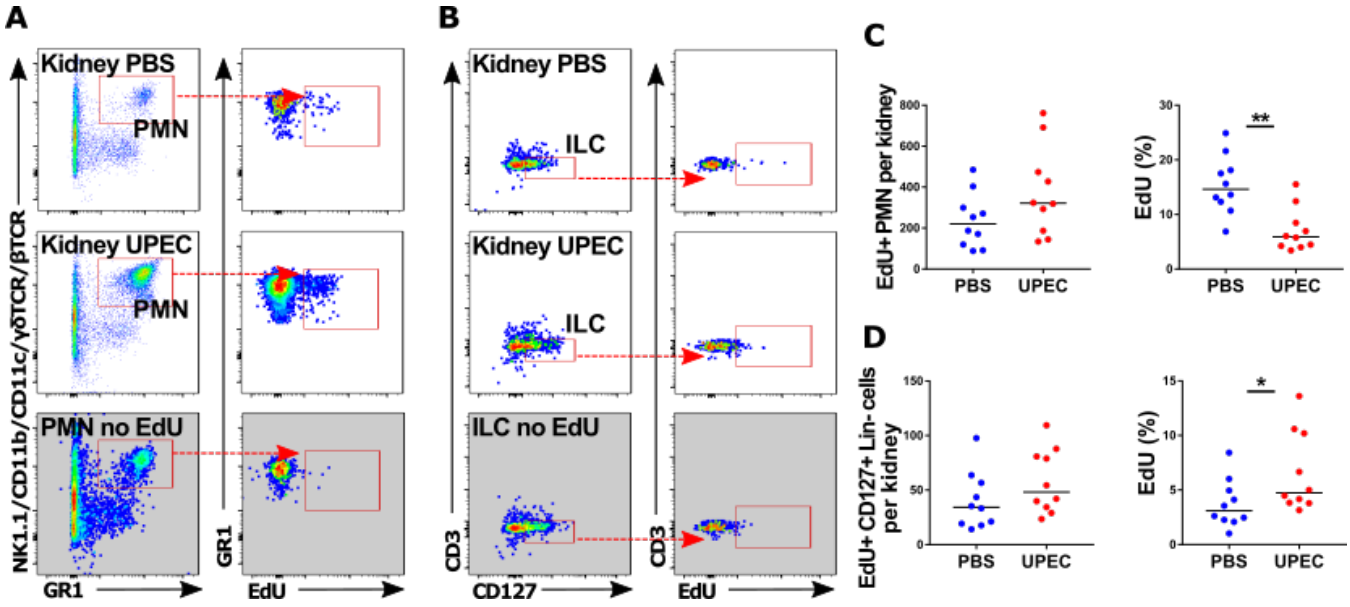

Figure 4.12: ILC3 expansion in the kidney during UTI

WT mice catheterised once with PBS or UPEC and given EdU (IP and PO) for 24 hours. **A**: Flow cytometry plots representative of cell counts from kidney for neutrophils that incorporated EdU (anti-EdU-A647) and have been preselected for alive, singlets that are IV CD45 negative. **B**: Flow cytometry gating to show ILCs (NK1.1/CD11b/CD11c/γδTCR/βTCR-eFluor450 negative, CD127-A780 positive), showing cells that incorporated EdU (PBS=5, UPEC=5). Greyed flow cytometry plots are from a mouse catheterised with UPEC but not given EdU. **C**: Neutrophils that were positive for EdU% **p= 0.0015. **D**: ILC counts showing numbers and percentages that were EdU positive, EdU% *p=0.0355. Significance calculated using Mann-Whitney tests.

Together, these data illustrated in figures 4.1-4.12 show that the IL-17 proinflammatory and IL-22 axes were activated during UTI. Furthermore, we have shown that within the renal tract, it is likely that ILC3s proliferated in response to challenge with UPEC and could therefore be responsible for production of these cytokines.

4.3 RORγt knock out mice challenged with Uropathogenic *Escherichia coli*

RORγt is a transcription factor that is critical for the development of ILC3s and Th17 cells and for the production of IL-17a. We initially carried out a series of single catheterisation UTI experiments using RORγt KO mice, harvesting organs at 24 and 48 hours.

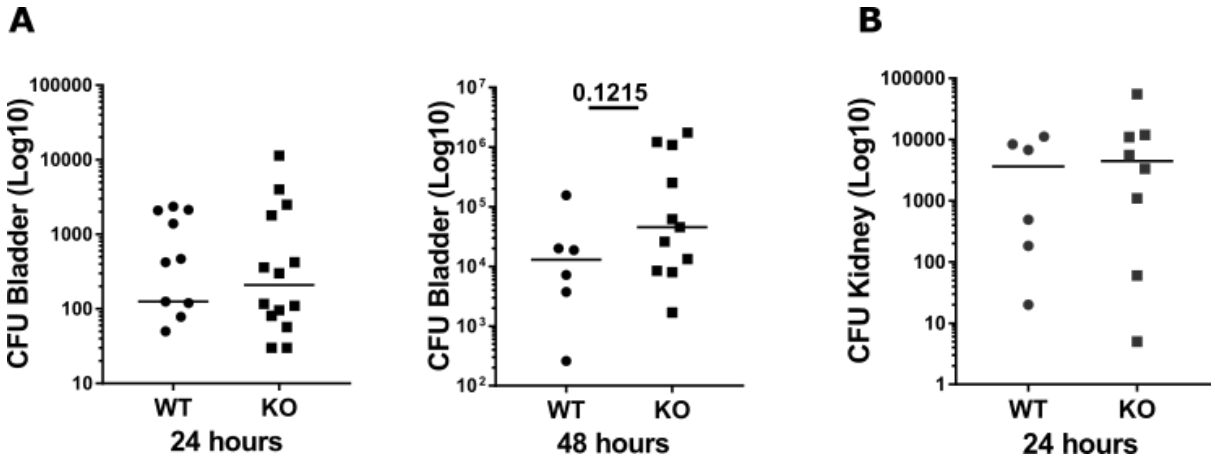

Figure 4.13: Severity of infection after single catheterisation (cystitis and pyelonephritis) in RORγt KO mice during UPEC UTI

RORγt KO mice catheterised with UPEC for 24 or 48 hours, single catheterisation, results combined from 4 experiments. **A**: Bladders harvested at 24 hours (n=10 WT, n=14 KO) or 48 hours (n=6 WT, n=11 KO) and made into a single cell suspension. This was plated on LB agar to grow CFUs. **B**: Kidneys harvested after 24 hours, results indicate CFUs from those that developed pyelonephritis (n=6 WT, n=8 KO). Kidneys harvested at 48 hours did not show levels of pyelonephritis high enough to generate data, even in combination. Significance calculated using Mann Whitney test and combined from 4 experiments

Figure 4.13 shows data collected during our initial UTI experiments, where mice were catheterised once. Initially, we had only small numbers of animals necessitating experimental repeats, but with suboptimal numbers each time. This led to substantial variability when combining the data, with no significant differences observed between WT and RORγt -deficient mice, although there was a trend towards increased infection in the KO bladders at 48 hours. As single catheterisation leads to typical pyelonephritis rates of only 0-20%, that are rapidly cleared, we were unable to generate data at 48 hours for CFU from kidneys.

To overcome the issue of the low frequency of pyelonephritis, we performed double, (two sequential) catheterisations on mice, a protocol which we had begun to optimize during the latter part of my PhD. Data from these experiments is shown in figure 4.14.

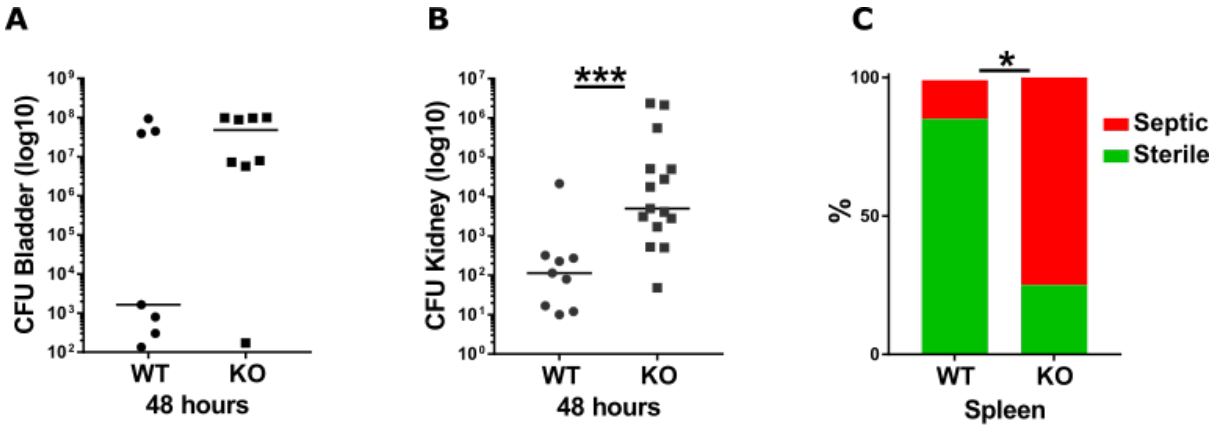

Figure 4.14: Severity of infection after double catheterisation (cystitis, pyelonephritis and septicaemia) in RORγt KO mice during UPEC UTI

RORγt KO mice catheterised with UPEC for 48 hours, double catheterisation, results combined from 2 experiments. **A**: Bladders were overwhelmed by infection during the double catherisation and colony counts became uninterpretable, leading to approximate data (n= 7 WT, n= 8 KO), individual points with median bar displayed. **B**: Kidneys that became infected (n= 9 WT, n= 15 KO). Significance calculated using Mann Whitney test, ***p= 0.0007, median bar. **C**: Bar graph showing the proportions of mice that had bacteria within their spleens and indicating bacteraemia. Significance calculated using chi-squared test, *p= 0.0187, n= 7 WT and n= 8 KO.

In the bladder, bacterial counts were so high that even with serial dilutions to 1 in 400 000, an accurate count could not be achieved (fig. 4.14A), presumably due to the repeated inoculation of bacteria directly into the bladder lumen. In the kidney, we observed a higher number of CFUs in the RORγt KO animals at 48 hours (figure 4.14B). In keeping with the increased severity of pyelonephritis, we also saw increased levels of septicaemia, as measured by splenic CFUs.

In addition to measuring CFUs, we also assessed immune cell number and frequency by flow cytometry. These data are shown below, and bladder and kidney specific data figures included separately for clarity. Where new flow cytometry gating is used, this is demonstrated but not repeated thereafter.

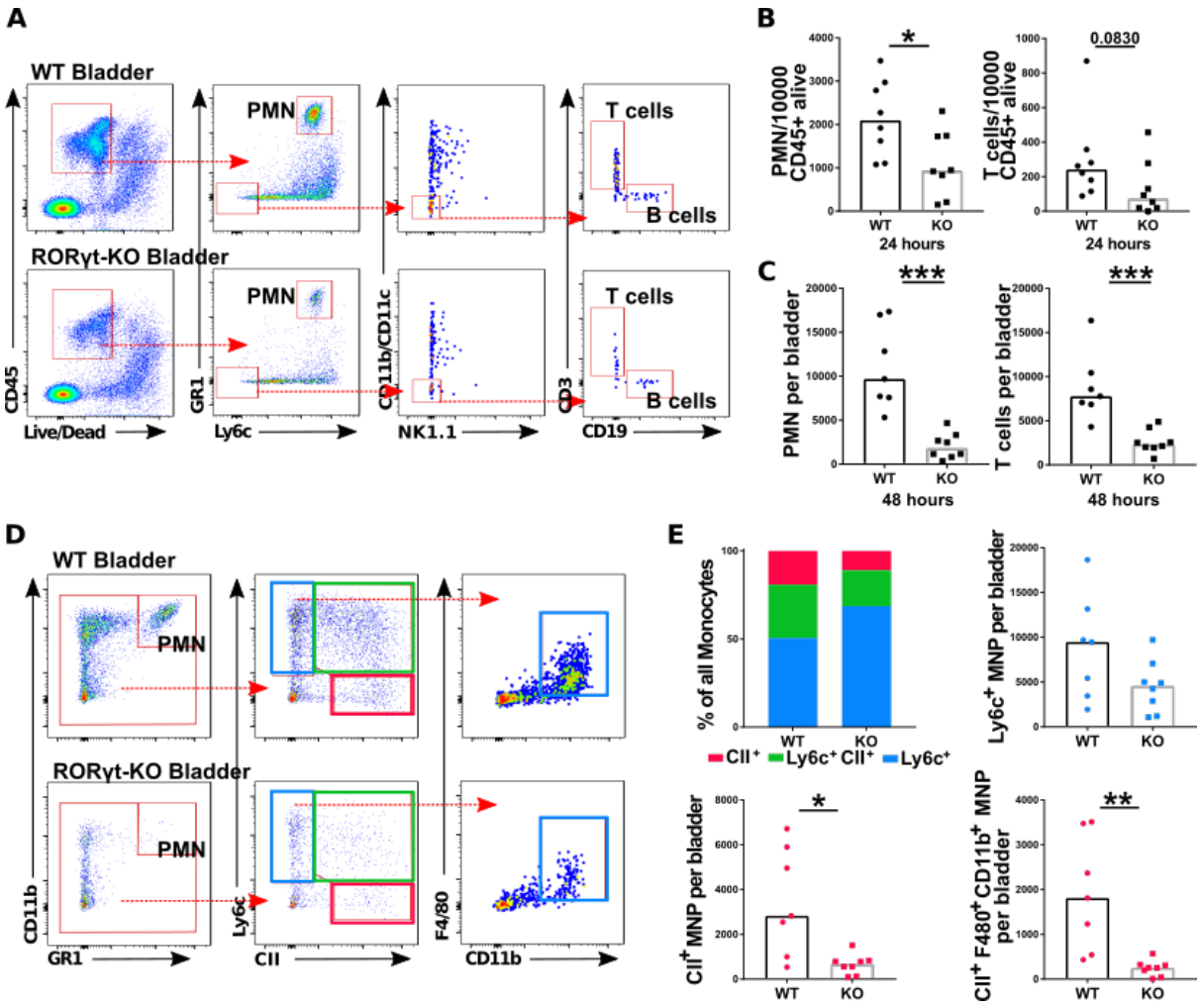

Figure 4.15: Bladder immune cell characteristics in RORγt KO mice during UPEC UTI

RORγt KO mice catheterised with UPEC for 24, single catheterisation (3 experiments) or 48 hours, double catheterisation (2 experiments). **A**: Flow cytometry plots to demonstrate the gating strategy for immune cell identification. CD45-A780, GR1-PECy7, Ly6c-APC, CD11b/CD11c-eF450, NK1.1-PE, CD3-BV605 and CD19-PerCPCy5.5. **B**: Bladders harvested at 24 hours (n=8 WT, n=8 KO) and showing T cell and neutrophil counts, *p= 0.0281. **C**: Bladders harvested at 48 hours (n=7 WT, n=8 KO) showing total neutrophil and T cell counts per bladder, ***p= 0.0003 PMN and ***p= 0.0006 T cells. Significance calculated using Mann Whitney test. Ly6c+ monocytes and B cells did not show any significant differences between groups at 24 hours (data not shown). **D**: Alternative gating strategy to identify classes of monocytes at 48 hours. Cells pre-selected as alive, singlets that are CD45.2-PECy7 positive, IV CD45-FITC negative. Neutrophils GR1-A780+/CD11b-PerCPCy5.5+, monocytes divided according to the 'monocyte waterfall' into Ly6c-APC+, CII-BV650+ or double positive. Populations of Ly6c+ macrophages are found in the bladder that are typically F4/80-BV605+/CD11b+. **E**: Monocyte proportions within the bladder. Ly6c+ mononuclear phagocytes (MNP) are shown in blue and CII+ MNP in pink, *p= 0.014, **p= 0.0012, results expressed with median bars and significance calculated with Mann Whitney tests.

During urinary tract infection in the bladder, neutrophil recruitment was reduced in the absence of RORγt-expressing cells. This is clearly demonstrated at 24 and 48 hours within the bladders of infected mice (fig. 4.15B&C). There were also decreased T cell numbers, though this may reflect inherent loss of Th17 cells, rather than a decrease in expansion *per se*. Using a gating strategy similar to Tamoutounour et al. (2012) we were able to identify populations of MNPs in the 'monocyte waterfall' within the tissue [122]. These were selected as negative for the IV CD45 label and further divided into three groups according to their expression of Ly6c and MHCII, as shown in figure 4.15D. Within the bladder we typically found larger proportions of Ly6c+ MNPs, rather than MHCII+ populations and the latter predominantly displayed an F4/80+CD11b+ phenotype. MNPs are known to upregulate MHCII on activation and maturation [112, 122] and we observed a lower number of MHCII+ MNPs and in F4/80+CII+ macrophages in RORγt KO animals compared to WT controls. This is consistent with the conclusion that RORγt-expressing cells promote the maturation of macrophages from monocytes following their entry into the bladder in the context of cystitis.

In the kidney, we observed the opposite trend in neutrophil recruitment to that found in the bladder, with increased numbers within the kidney of RORγt KO mice at 48 hours following infection (fig. 4.16B). This was not due to peripheral blood neutrophilia, as an anti-CD45 intravenous label was used to gate out circulating neutrophils. The rise in neutrophils mirrored the increased CFU counts in the knockout animals and in our UTI experiments more generally; we have noted a close positive correlation between kidney CFUs and neutrophils. Therefore, this likely reflects the more severe pyelonephritis observed in RORγt KO mice. There was also a significant rise in renal B cells, indicative of participation of both adaptive and innate immunity in response to infection (fig. 4.16B). The T cell counts were fairly similar (trending upwards, fig.4.16B), again in keeping with the increased infective burden. In the absence of RORγt, these cells must have come from non-Th17 subsets, but there was not space for more T cell markers on the flow panel to delineate this further. The increase in infiltrating Ly6c+ MNPs also correlated to the increased infective burden and was expected (fig 4.16C). In contrast to the bladder, we did not observe any differences in mature macrophages (CII+ and F4/80+) between WT and RORγt KO mice. Overall, the phenotype differed between bladder and kidney, with far more CII+ macrophages and reduced CD11b staining in the kidney (compare flow plots fig. 4.15D in bladder and fig. 4.16A in kidney). Whilst broadly similar immune populations existed throughout the renal tract, there were distinct variances in their proportions and cell surface expression, indicating organ-specificity to the differing effects of the absence of Th17 immunity in the bladder and kidney in the context of infection.

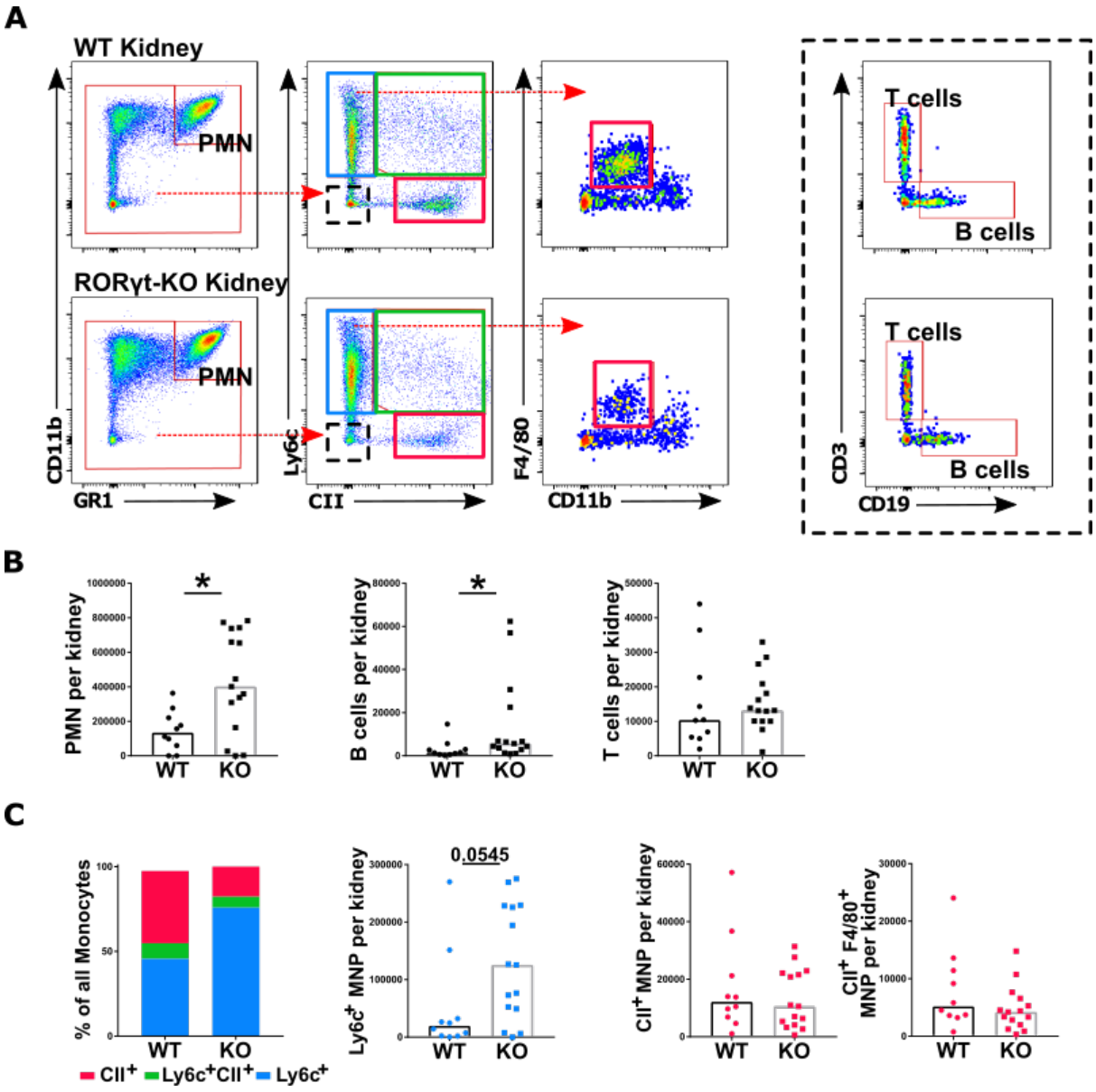

Figure 4.16: Renal immune cell characteristics in RORγt KO mice during UPEC UTI

RORγt KO mice catheterized with UPEC for 48 hours, double catheterisation (2 experiments, n=7 WT, n=8 KO). **A**: Flow cytometry plots to demonstrate the gating strategy for immune cell identification from kidneys with confirmed pyelonephritis. Gating strategy to identify classes of monocytes at 48 hours. Cells pre-selected as alive, singlets that were CD45.2-PECy7 positive, IV CD45-FITC negative. Neutrophils GR1-A780+/CD11b-PerCPCy5.5+, Monocytes divided according to the 'monocyte waterfall' into Ly6c-APC+, CII-BV650+ or double positive. Populations of CII+ MNPs are found in kidney and are F4/80-BV605 positive. Lymphocytes are negative for myeloid markers (black, dashed boxes) and were CD3-PE (T cells) and CD19-BV785 (B cells) positive. **B**: Kidneys harvested at 48 hours showing total neutrophil, T cell and B cell) counts per organ. Median data shown and significance calculated using Mann Whitney tests, *p= 0.0192. **C**: Monocyte proportions within the kidney. Ly6c+ mononuclear phagocytes (MNP) are shown in blue and CII+ MNP in pink (median data shown, significance calculated using Mann Whitney tests).

To investigate the transcriptional changes that might underpin the cellular dynamics observed during UTI, we performed qPCR on whole bladder and kidney lysates. Figure 4.17A shows the decreases in bladder *Il17a*, *Il22* and *Csf2* transcripts consistent with the decreases in neutrophil recruitment and T cell expansion seen in figure 4.15. We can also correlate the trends towards decreased *Il1b* and *IL23a* transcripts and the significant decrease in *Tnfsf15* levels (which encodes TL1A, another ILC3-sitmulating cytokine) with reduced production by the diminished MNP populations in the RORγt KO mice (fig. 4.15E). AMP levels were also affected, with significant decreases in *Lcn2* and *Reg3g* in RORγt KO mice, the latter is associated with IL-22-induced production in the gut. Trends towards decreased levels of *Saa2* were also observed. During this experiment, the CFU readings from the bladder showed no significant difference between the WT and KO groups.

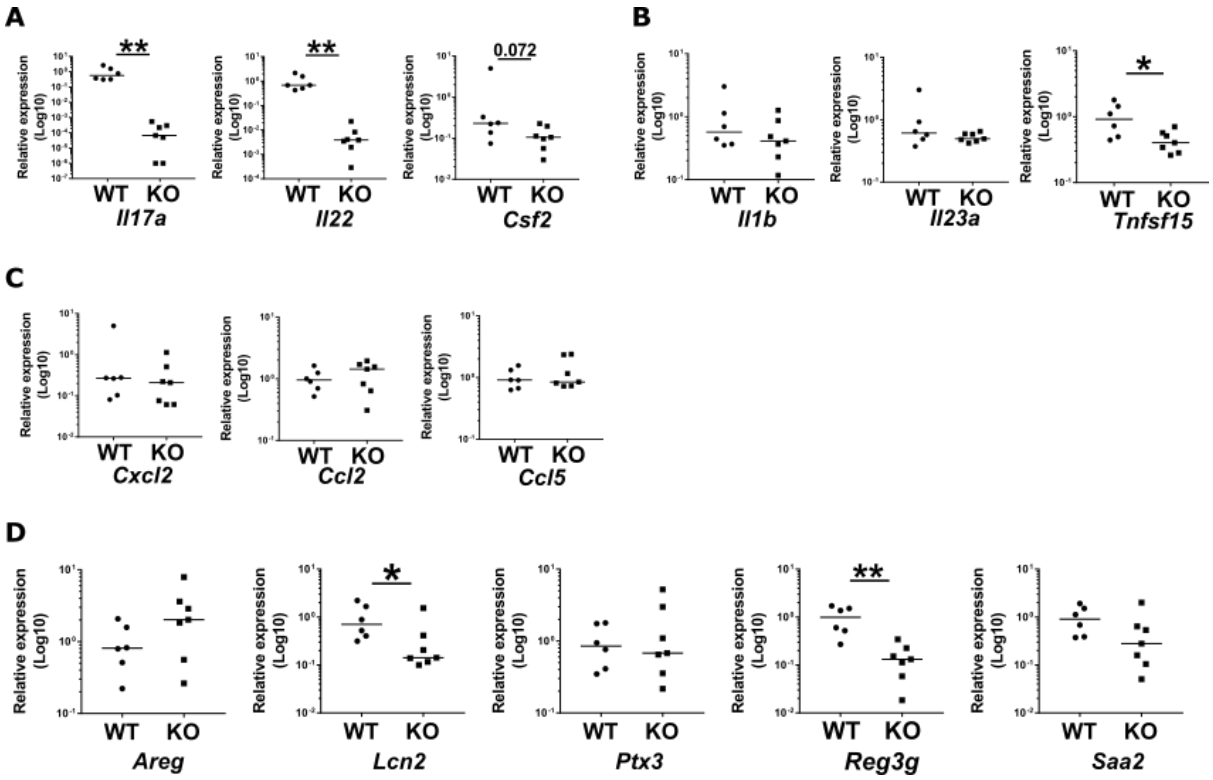

Figure 4.17: Cytokine, chemokine and AMP transcripts in the RORγt KO bladder during UPEC UTI

Quantitative PCR from RORγt KO and WT mice catheterised with UPEC for 48 hours with a single catheterisation (PBS=6, UPEC=7). CFUs were equal across groups and part of the bladder was lysed for RNA extraction. qPCR data is shown relative to *Hprt* housekeeping gene and the WT group**. A**: ILC3 cytokines **p= 0.0012 *Il17a* and *Il22*, with addition of pseudocount to *IL17a* data of 10^{-6}. **B**: ILC3 stimulating cytokines *p= 0.035 *Tnfsf15*. **C**: Myeloid and lymphoid chemoattractants. **D**: AMPs, *p= 0.035 *Lcn2*, **p= 0.0023 *Reg3g*. Median data shown, significance calculated using Mann Whitney tests.

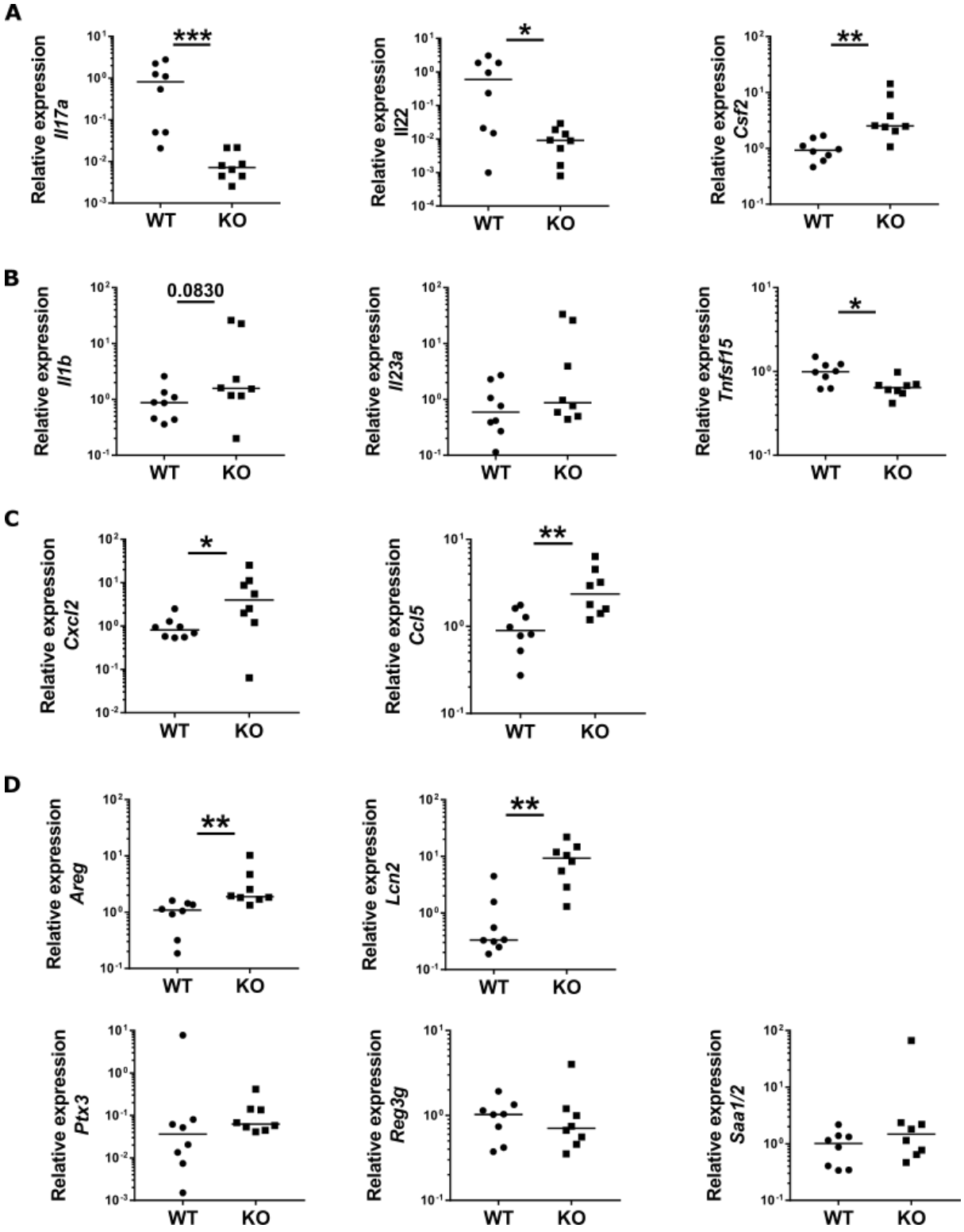

Figure 4.18: Cytokine, chemokine and AMP transcripts in the RORγt KO kidney during UPEC UTI

Quantitative PCR from RORγt KO (n=8) and WT (n=7) mice catheterised with UPEC twice for 48 hours (only kidneys with pyelonephritis plotted, KO n=4, WT n= 4). **A**: ILC3 cytokines ***p= 0.0006 *Il17a*, *p= 0.027 *Il22*, **p= 0.0011 *Csf2*. **B**: ILC3 stimulating cytokines *p= 0.0207 Tnfsf15, **C**: Myeloid and lymphoid chemoattractants; *p= 0.0281 *Cxcl2*, **p= 0.007 *Ccl5*. D: AMPs,**p= 0.001 *Areg*, **p= 0.0011 *Lcn2*. Gene expression relative to *Hprt* and wild type animals. Median data shown, significance calculated using Mann Whitney tests.

RNA was extracted from the kidneys of mice catheterised twice (48 hour time point) and the qPCR data in figure 4.18 correlates to the CFUs shown in figure 4.14B. Results were only analyzed from mice that developed pyelonephritis. Despite the increased CFU burden, striking decreases in *Il17a* and *Il22* transcripts could be seen (fig. 4.18A). The Csf2 transcripts rose, indicating that this growth factor/cytokine could be generated from cells that do not express RORγt. Modest levels of *Il1b* and *Il23a* transcripts were observed, however *Tnfsf15* transcripts fell significantly in KO group, as observed in the bladder, despite the increased infection rate (fig. 4.18B).

4.4 Rag2 knock out mice challenged with Uropathogenic *Escherichia coli*

In order to further delineate the role of ILCs in UTI, we performed experiments in Rag2 KO mice that lacked lymphocytes, thereby removing any contribution of Th17 and γδT cells to type-17 cytokines. We were able to investigate whether these T cells were the sole producers of IL-17 and IL-22 during UTI, by examining transcript levels from WT and Rag2 KO animals. Using the qPCR data from the Rag2 KO mice bladders at 24 and 48 hour time points, we compared it to the equivalent WT data from a previous experiment (fig. 4.19). Whilst these data were generated from separate experiments, they indicate that in mice lacking lymphocytes (Rag2 KO), *Il17a* and *Il22* transcripts were elevated at 24 hours. As these transcript rises persisted in the absence of T cells, we can conclude they are derived from an alternative source, in particular ILC3s.

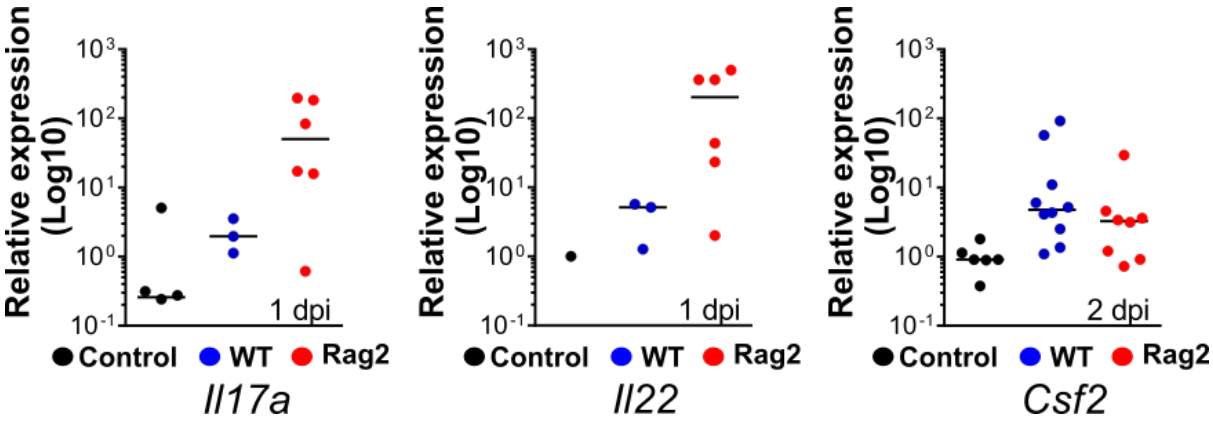

Figure 4.19: Transcripts of ILC3 products during UTI in WT and Rag2 KO mice

Quantitative PCR data combined from UPEC infections in mice at 1-2 days post infection (dpi). Transcripts are shown for key ILC3 cytokines. Data combined from different experiments, n=1-10).

To more specifically interrogate the role of ILCs we performed UTI experiments using Rag2 KO mice with and without ILC-depletion. Control animals were treated with an intraperitoneal (IP) injection of an isotype antibody and the experimental group treated with anti-Thy1.2 antibody, to deplete all ILCs. Figure 4.20 demonstrates the experimental schema. Each time the experiment was performed we confirmed successful ILC depletion, as demonstrated by a reduction in the total ILC count in splenic tissue (fig. 4.21F).

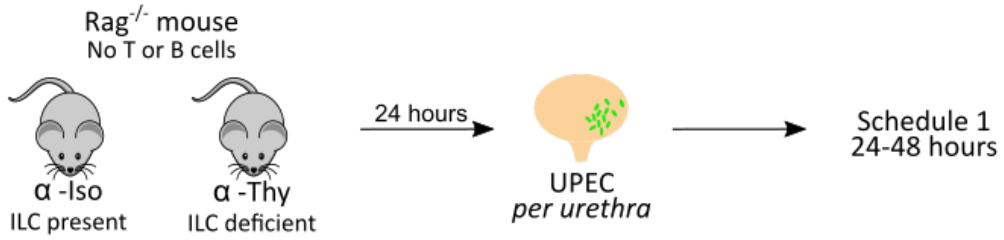

Figure 4.20: Experimental schema for ILC-depletion in Rag2 KO UTI experiments.

We performed this experiment multiple times to optimize conditions for either the bladder or the kidney and to harvest tissues for CFU, qPCR, flow cytometry and RNA sequencing. With each experiment came variability in the CFU burden consistent with differences in the batch of UPEC used, but overall, infection was more severe in the anti-Thy1.2-treated group at the 48 hour time point.

At 24 hours, bladder CFU levels were similar between groups (figure 4.21A), but there were clear differences in *Il17a* transcripts and a trend toward decreased *Il22* transcripts in the anti-Thy1 treated animals (fig. 4.21B). Bladder lysates used to generate the qPCR data demonstrated CFU values that were generally higher in the ILC-depleted group (square points, fig. 4.21A), thus giving further significance to the reduced levels of *Il17a* and *Il22* within this context.

In the bladder there was a trend towards decreased neutrophil recruitment at 24 hours (fig. 4.21C), but increased monocyte counts in the anti-Thy1.2 treated group, consistent with worse infection (fig. 4.21D). As with the RORγt KO experiments, there was impairment of MNP maturation, with reduced MHCII-expressing MNPs and macrophages (CD64+ MNPs) in ILC-depleted animals (fig. 4.21E). These experiments were limited by the fact that counting beads were not used and we did not use an IV CD45 label, so direct comparisons to the RORγt KO experiments cannot be made. Gating strategies used were similar to those demonstrated previously and so have not been replicated.

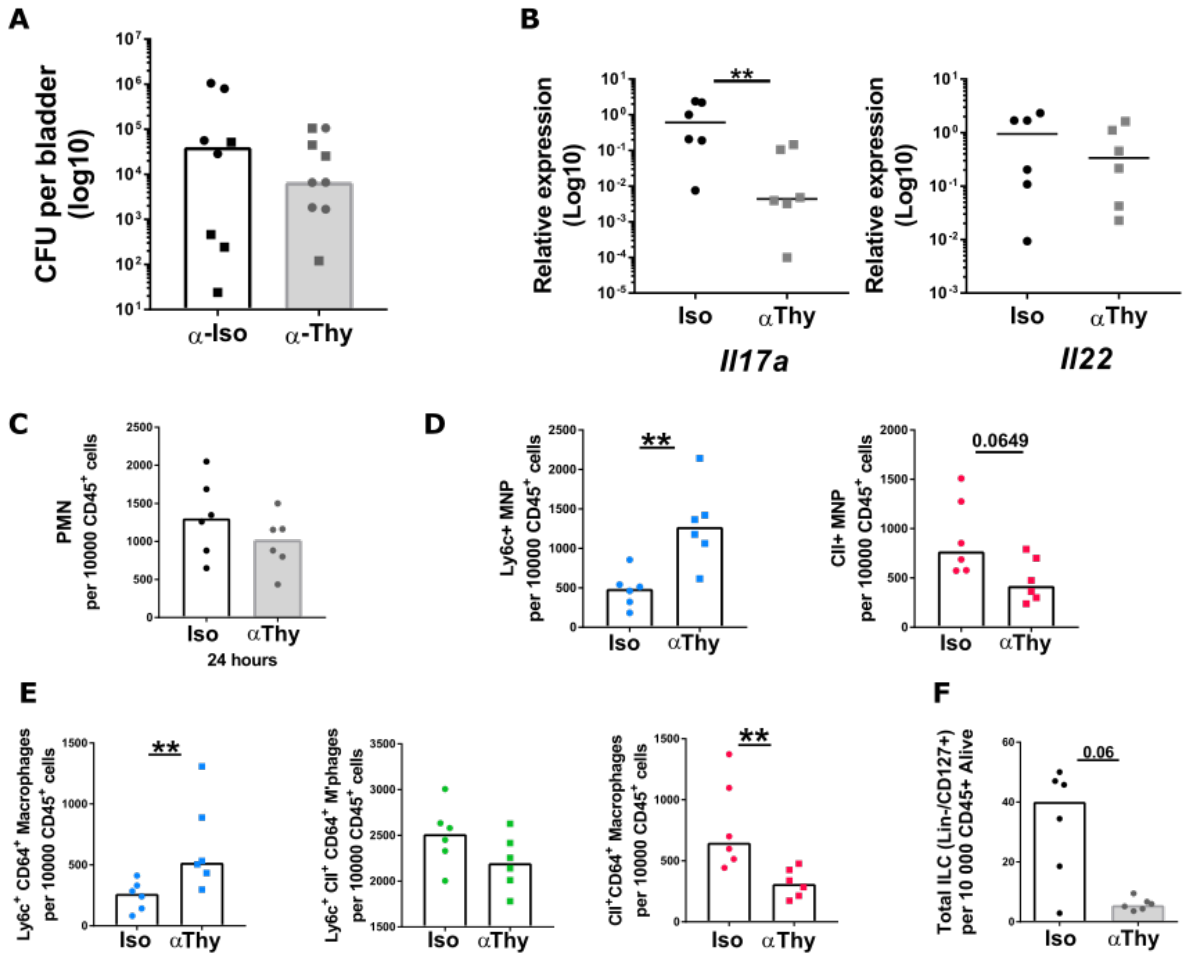

Figure 4.21: Bladder immune cell characteristics during UPEC UTI in Rag2 KO mice after ILC-depletion at 24 hours

Rag2 KO mice catheterised once with UPEC for 24 hours, after pre-treatment with intraperitoneal anti-Thy1.2 antibody (n=10) or isotype (n=9) to deplete ILCs. **A**: CFU values from bladders from two experiments (round and square points are from separate experiments and squares denote values that relate to transcriptional changes and cell counts in **B-E**; two missing values from each group relate to bladders that were too overgrown with bacteria to ascertain an accurate CFU. **B**: qPCR from whole bladders, n=6 both groups. Transcript expression relative to *Hprt* and control group, **p= 0.0087 *Il17a, Il17a* transcripts with addition of pseudocount of 10^{-4}. **C**: Neutrophil count expressed relative to all CD45+ cells. **D**: MNP counts from the monocyte waterfall; **p= 0.0043. **E**: Further gating of the MNP groups by CD64 (macrophage marker); **p= 0.0087 Ly6c+, **p= 0.0043 CII+. **F:** Total ILC counts from spleen to demonstrate effective ILC depletion. Gating strategies as previously shown. MNP flow panel demonstrated in fig. 4.15 with addition of anti-CD64-PE, but without IV CD45 labelling. ILCs were Lineage-eF450 (GR1/CD11b/CD11c/NK1.1/CD3/CD19) negative, CD127-PECy7 positive. All values expressed as median with significance calculated using Mann Whitney tests.

Figure 4.22 shows the CFU, cell counts and qPCR data at a 48 hour time point from bladders. There was a consistent increase in CFU burden in the anti-Thy1.2 treated group, replicated across four experiments (fig. 4.22A&E). The CFU counts for each experiment have been replicated, so they can

be appropriately correlated to the cell counts (fig. 4.22A-D) or PCR data (fig. 4.22E&F) respectively. As demonstrated at the 24 hour time point, there was an increased number of infiltrating Ly6c+ MNPs at 48 hours with decreased levels of monocyte maturation and a reduction in macrophages (CD64+) from each group (fig. 4.22D). Neutrophil counts were similar, to those observed in the RORγt KO data, indicating the presence of alternative sources of neutrophil-attracting cytokines/chemokines. Given the marked increase in CFU in the anti-Thy1.2 group, there was relative suppression of the neutrophil count compared to control.

Quantitative PCR data is shown in figure 4.22F, with the corresponding CFU data (fig. 4.22E). There was a trend towards decreased *IL17a* transcripts, though *IL22* transcripts remained unaffected. *Csf2* transcripts rose with infection and must therefore have originated from alternative cellular sources, such as the epithelium or myeloid cells.

Further qPCR is shown from whole bladder in figure 4.23 (CFU data from fig. 4.22E corresponds to the same bladders used for RNA analysis). Evidence for a heightened pro-inflammatory environment in the ILC-depleted bladders could be identified, with increases of *Cxcl2, Csf2* and *Ccl2* transcripts and some AMPs (figures 4.22F and 4.23).

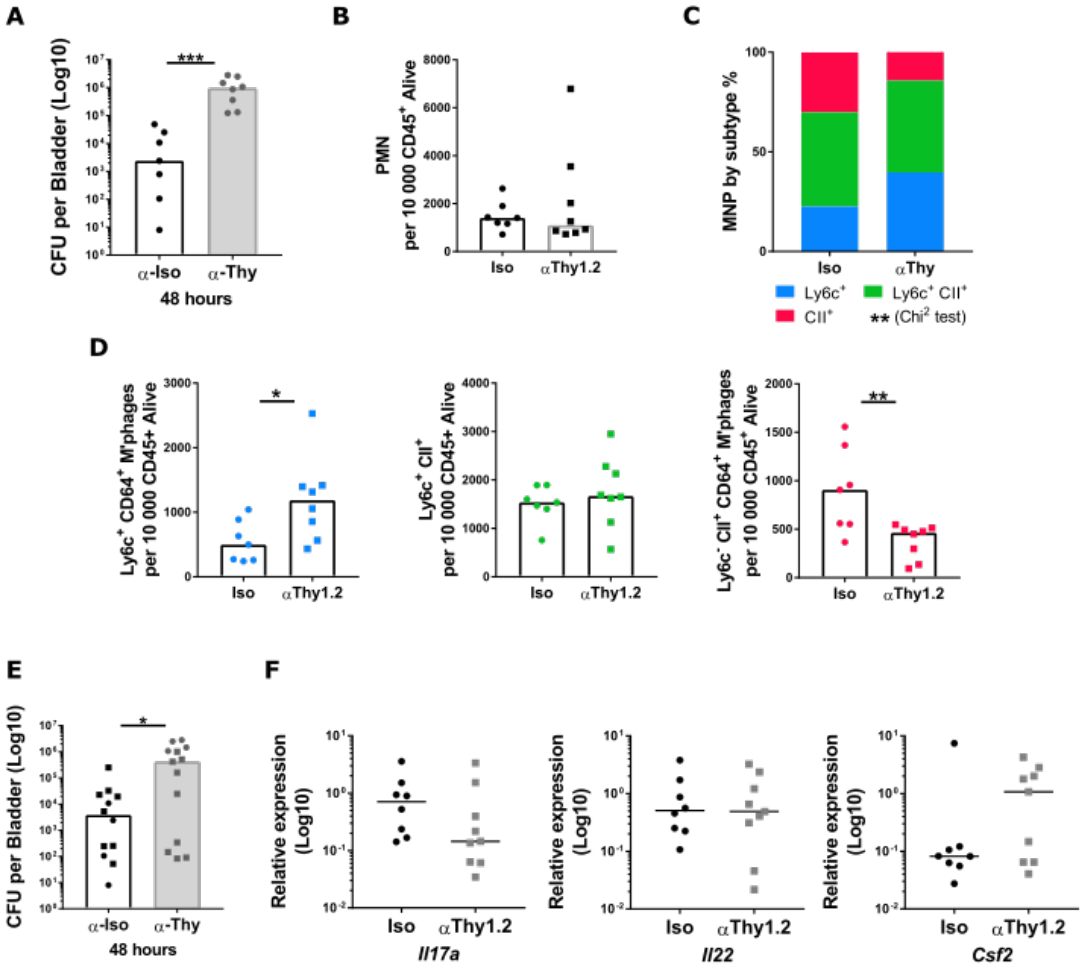

Figure 4.22: Bladder infection and immune cell characteristics during UPEC UTI in Rag2 KO mice after ILC-depletion at 48 hours

Rag2 KO mice pre-treated with an intraperitoneal injection of depleting anti-Thy1.2 antibody or isotype. **A**: CFU from bladders catheterised once with UPEC for 48 hours, n= 7 Iso, n= 8 Thy, ***p= 0.0003, 2 experiments. **B-D**: Cell counts from the same bladders as those in **A**. **B**: Neutrophil counts. **C**: Monocyte counts from the monocyte waterfall and expressed as a proportion of the total CX3CR1 MNP population, chi-squared test **p= 0.0087. **D**: Macrophage populations (CD64+) within each part of the monocyte waterfall, *p= 0.0289, **p= 0.0059. **E**: CFU values from later UTI experiments (two experiments) that correspond to the subsequent qPCR data. **F**: qPCR data from whole bladders, n=8 Iso, n=9 Thy. All data shown is with median values and significance calculated using Mann Whitney tests unless otherwise stated.

Together, this data confirms that ILCs affect the UPEC infective burden to a significant degree in the bladder by 48 hours. Decreased *Il17a* transcripts correlated to impaired monocyte maturation, thus indicating that the cytokine might have contributed to impaired recruitment and maturation of MNPs and subsequently led to reduced bacterial clearance. We hypothesize that this may also have consequences for ascension of the bacteria within the renal tract and development of pyelonephritis.

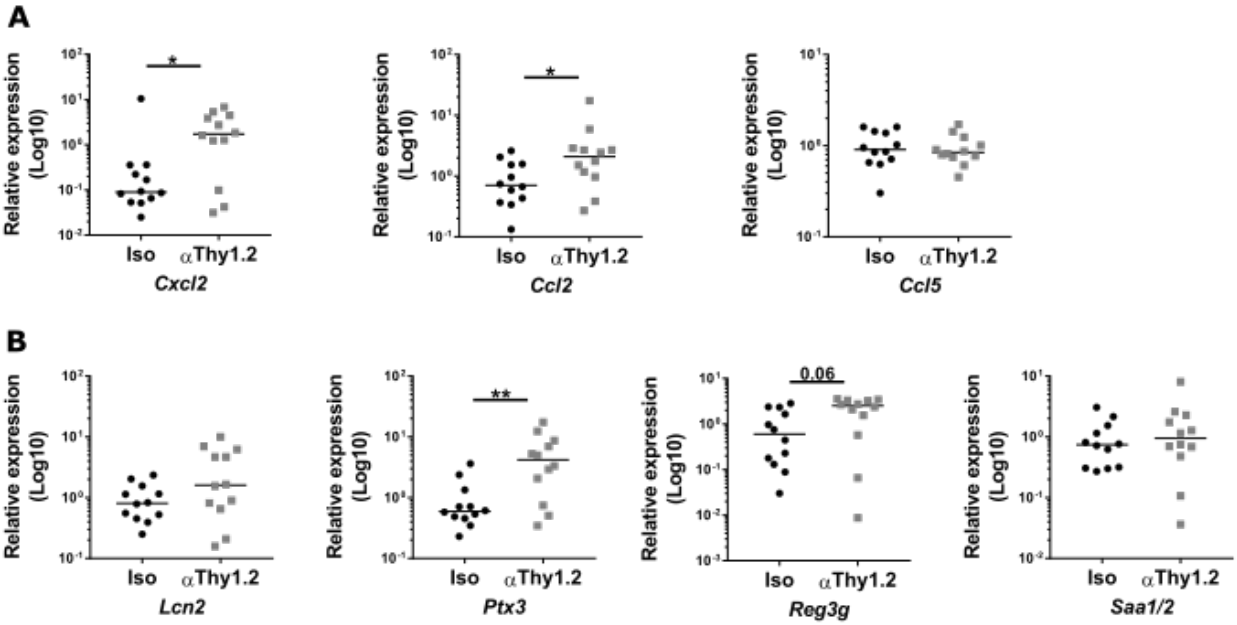

Figure 4.23: Cytokine, chemokine and AMP transcripts from bladders of Rag2 KO after ILC-depletion

Rag2 KO mice pre-treated with an intraperitoneal injection of depleting anti-Thy1.2 antibody or isotype. **A**: qPCR data from whole bladders, n=12 Iso, n=11 Thy from 3 experiments. **A**: *Cxcl2* *p= 0.0387, *Ccl2* *p= 0.0332. **B**: *Ptx3* **p= 0.0068. All data shown is with median values and significance calculated using Mann Whitney tests.

We next went on to investigate the role of ILC3s in kidney defence, using the same experimental set-up. Most of these experiments were performed using single catheterisations to focus on bladder responses and consequently yielded low numbers of infected kidneys. The figure below (4.24) shows combined data, with results pooled from 7 experiments. The CFUs were very similar between each group and are shown at 48 hours, as too few mice were affected at 24 hours to yield results. Although there was increased neutrophil recruitment in the anti-Thy1.2 group at 24 hours (fig. 4.24C), which is an indicator of severer infection, this did not manifest in increased CFU counts, which were unaffected by the ILC depletion (fig. 4.24A). The monocyte counts were similar between the two groups.

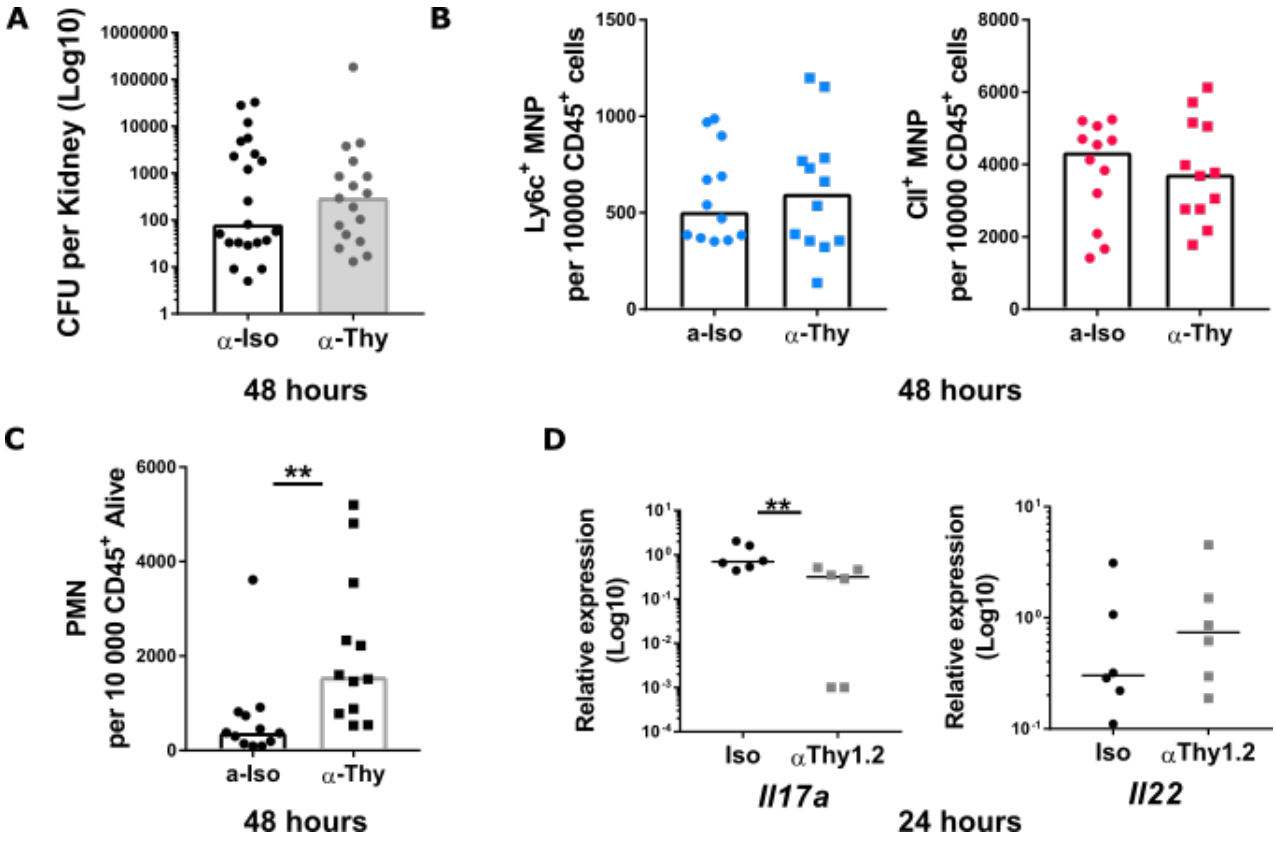

Figure 4.24: Pyelonephritis and renal immune cell characteristics during UPEC UTI in Rag2 KO mice after ILC-depletion

Rag2 KO mice pre-treated with an intraperitoneal injection of depleting anti-Thy1.2 antibody or isotype. Kidneys harvested at 48 hours from 4 experiments. **A**: CFU values (Iso = 21 pyelonephritis of 37 kidneys; Thy = 25 pyelonephritis of 50 kidneys). **B**: Monocyte counts taken from the monocyte waterfall. **C**: Neutrophil counts (no IV label), **p= 0.0014. Cell counts for **B**&**C** show kidneys that had confirmed pyelonephritis (total Iso n=18, Thy n=20). **D**: qPCR data from whole kidneys at 24 hours, **p= 0.0087 (one experiment, Iso n=6, Thy n=6), with addition of a pseudocount to the *Il17a* data of 10^{-3}. Median results plotted and significance calculated using Mann Whitney tests.

Initial qPCR data at 24 hours showed a decrease in *Il17a* transcripts in the kidney (figure 4.24D). The kidneys used to generate RNA for these experiments were contralateral to those plated for CFU therefore we cannot confirm those with or without pyelonephritis. Assuming that infection ascends bilaterally, the CFU values predicted that infection levels were equal between the groups (figure 4.24A), but this cannot be directly related to the transcriptional changes. The raised neutrophil count, however (fig. 4.24C) indicated that infection severity was worse in the ILC-depleted group. Given that *Il17a* transcripts fell, this neutrophil recruitment was secondary to alternative chemokine and cytokine expression that was not lymphocyte or ILC-dependent. Alternative sources of chemoattractants were likely to be epithelial or myeloid.

We subsequently used RNA extracted from cell suspensions, so that directly paired information on CFUs and transcript levels could be obtained. However, it is worth noting, that sterile samples may have been exposed to the pathogen, but did not exhibit demonstrable infection at the time of sampling.

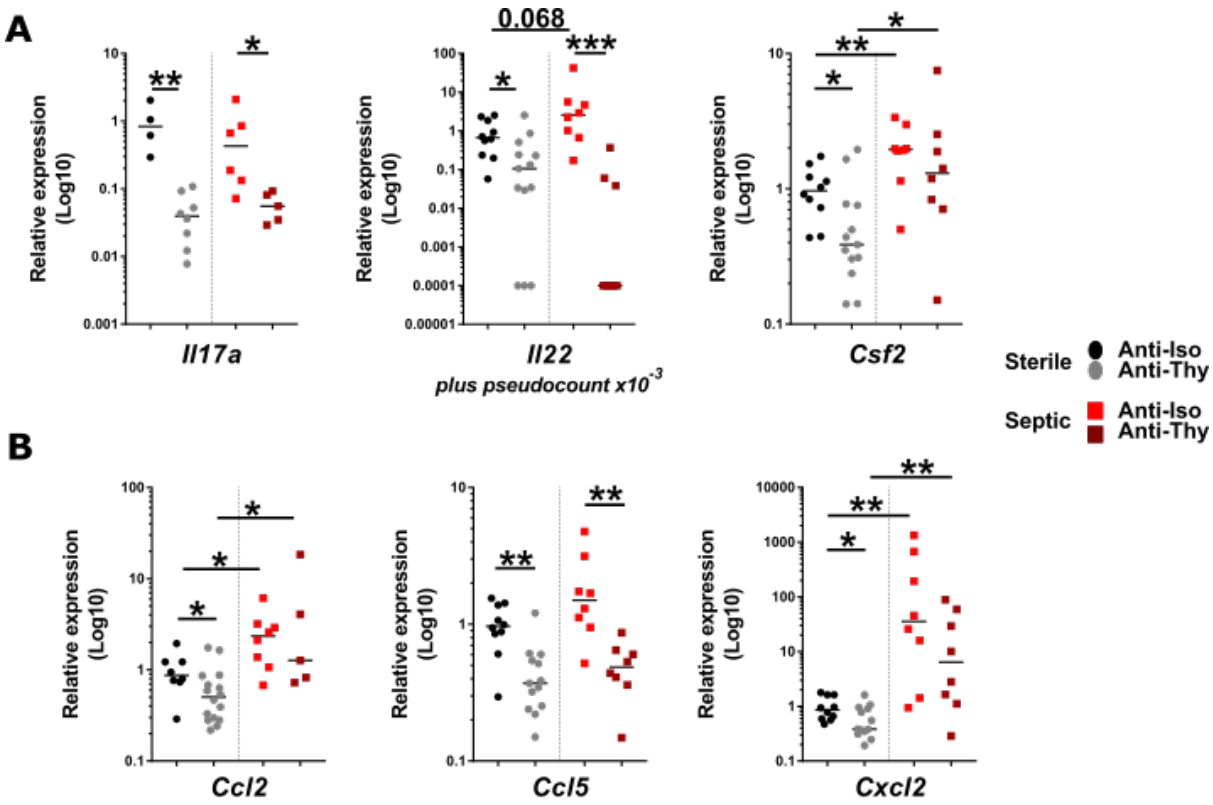

Figure 4.25: Cytokine and chemokine transcripts form kidney during UPEC UTI in Rag2 KO mice after ILC-depletion

Rag2 KO mice pretreated with anti-Thy1.2 antibody (n=11-15) or isotype (n=11-15). Kidneys harvested at 48 hours and RNA extracted from cell suspensions. **A**: ILC3 cytokines: *Il17a* *p= 0.0173, **p= 0.004; *Il22* *p= 0.0146, ***p= 0.0003; *Csf2* *p= 0.0214 Iso, **p= 0.0085 and *p= 0.0302 Thy. **B**: Proinflammatory cytokines: *Ccl2* *p= 0.0281 Iso, *p= 0.0382 Thy/Iso, *p= 0.0111 Thy; *Ccl5* **p= 0.0019 sterile, *p= 0.0015 septic; *Cxcl2* *p= 0.0358, **p= 0.0031 Iso, **p= 0.0025 Thy. Median data shown from 2-3 experiments and significance calculated using Mann Whitney tests.

The qPCR data shown in figure 4.25 clearly demonstrated that there were transcriptional differences between kidneys from Rag2 KO mice treated with anti-Thy1.2 antibody or isotype. All the kidneys may have been exposed to UPEC, but only those that had confirmed CFU counts when plated were categorized as 'septic'. These data show that *Il17a* and *Il22* transcripts decreased with ILC depletion, both at baseline and infection. The proinflammatory environment within the septic kidneys of all mice was confirmed by increased *Ccl2, Csf2* and *Cxcl2* transcripts. Interestingly, the ILC-depleted animals that developed pyelonephritis showed significantly decreased levels of *Cxcl2* and *Ccl5*

transcripts. This is consistent with the conclusion that ILC3s contribute to the immune response in UTI by influencing production of proinflammatory cytokines and chemokines. CXCL2 is a neutrophil-recruiting chemokine, while CCL5 is a chemotactic factor for cells expressing CCR5, including T cells, monocytes, macrophages, eosinophils and basophils. However, we did not observe a significant reduction in the recruitment of these cells in the context of ILC depletion, perhaps reflecting that multiple pathways can facilitate immune cell recruitment. It follows that such redundancy would exist, to increase the robustness of the immune response.

We also investigated differences in AMP expression. Almost all the tested AMP transcript levels rose with infection, but only some were affected by the ILC depletion, namely *Areg* and *Lcn2* (figure 4.26).

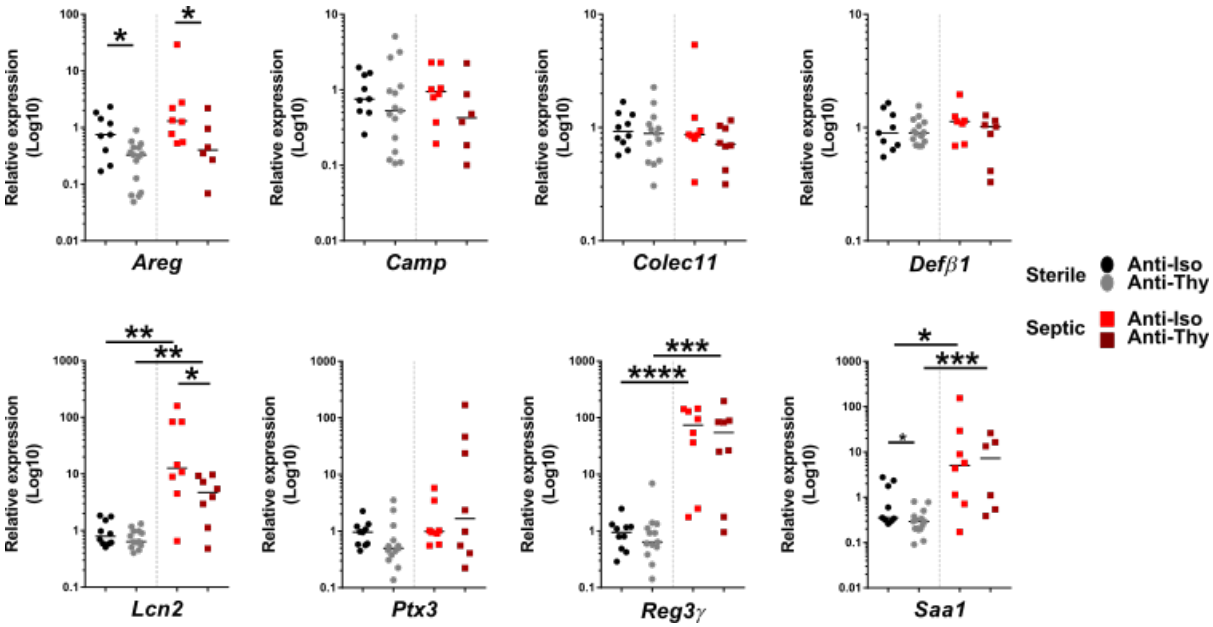

Figure 4.26: AMP transcripts from kidney during UPEC UTI in Rag2 KO mice after ILC-depletion

Rag2 KO mice pretreated with anti-Thy1.2 antibody (n=11-15) or isotype (n=11-15). Kidneys harvested and RNA extracted from cell suspensions. AMPs associated with the renal tract: *Areg* *p= 0.0148, *p= 0.0426; *Lcn2* **p= 0.0034 Thy, **p= 0.0014 Iso, *p= 0.0499 septic; *Reg3g* ****p= <0.0001, ***p= 0.0002; *Saa1* *p= 0.0464 Iso, *p= 0.0212 sterile, ***p= 0.0007 Thy. Median data shown from 2-3 experiments and significance calculated using Mann Whitney tests.

We plan to investigate the changes observed in more detail and have performed global RNA sequencing on bladders (24 hour infection) and kidneys (48 hour infection) from Rag2 KO mice treated with depleting anti-Thy1.2 antibodies. The analyses of these data are awaited.

4.5 Urinary tract infection in IL22R-deficient mice and its association with epithelial repair

In addition to IL-17a, IL-22 is produced by ILC3s and so we sought to determine if there might be a role for this cytokine in the acute phase of UTI. IL-22 is one of the IL-10 family of cytokines and associated with epithelial repair. We therefore hypothesized that it may play a role in preserving the integrity of the urothelium in the context of infection.

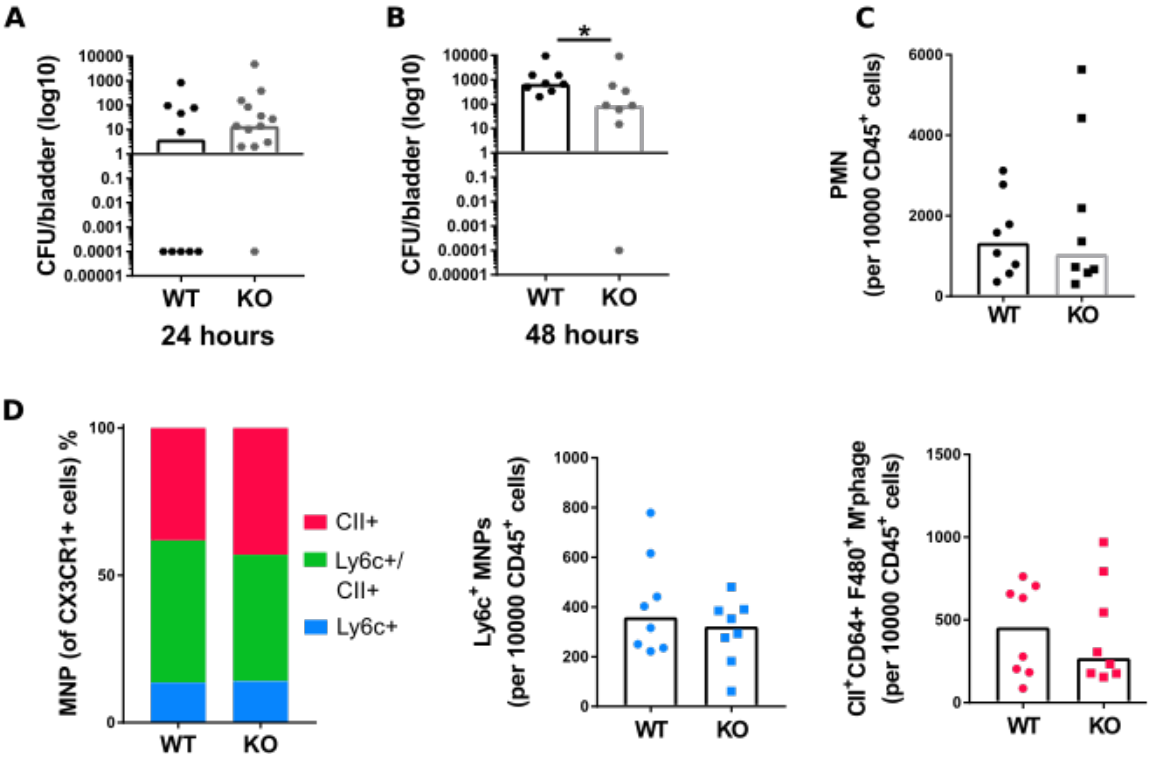

Figure 4.27: Infection severity and baseline monocyte characteristics from the bladders of IL22RA1 KO mice during UPEC UTI.

IL22RA1 KO mice treated with UPEC (single catheterisation) and bladders harvested at 24-48 hours. **A**: CFU counts at 24 hours with pseudocount of $1x10^{-4}$, (WT=12, KO=10). **B**: CFU at 48 hours with pseudocount of $1x10^{-4}$, *p= 0.0281 Mann Whitney test. **C**: Neutrophil counts. **D**: Myeloid cell proportions and counts. All cell counts produced with use of IV anti-CD45 labelling, after 48 hour infection. The gating strategy used was as demonstrated previously. Data combined from two experiments, (WT=8, KO=8).

We performed UTI in IL22RA1 KO mice and harvested samples at 24 and 48 hours. The bladder CFUs from these time points are shown in figure 4.27, as well as neutrophil numbers and myeloid cell counts from the monocyte waterfall. Interestingly, there was a decrease in CFU burden in the KO animals at 48 hours, though this data has been produced by combining two experiments and, unusually for this infection model, not all bladder tissues were positive for bacteria. Therefore these

results require repetition and could have occurred due to problems with the inoculum or tissue-processing errors leading to bacterial loss prior to plating. These were among the first UTI experiments I performed, and my technical proficiency improved during the course of the project. This result is also contrary to the trend observed in CFU quantification at 24 hours, where a greater proportion of bladders were infected in the KO group (chi-squared p=0.05, graph not shown) and therefore it is unlikely to represent a true difference between the two groups. Immune cell proportions present in the bladder were similar in both groups (figure 4.27 C&D).

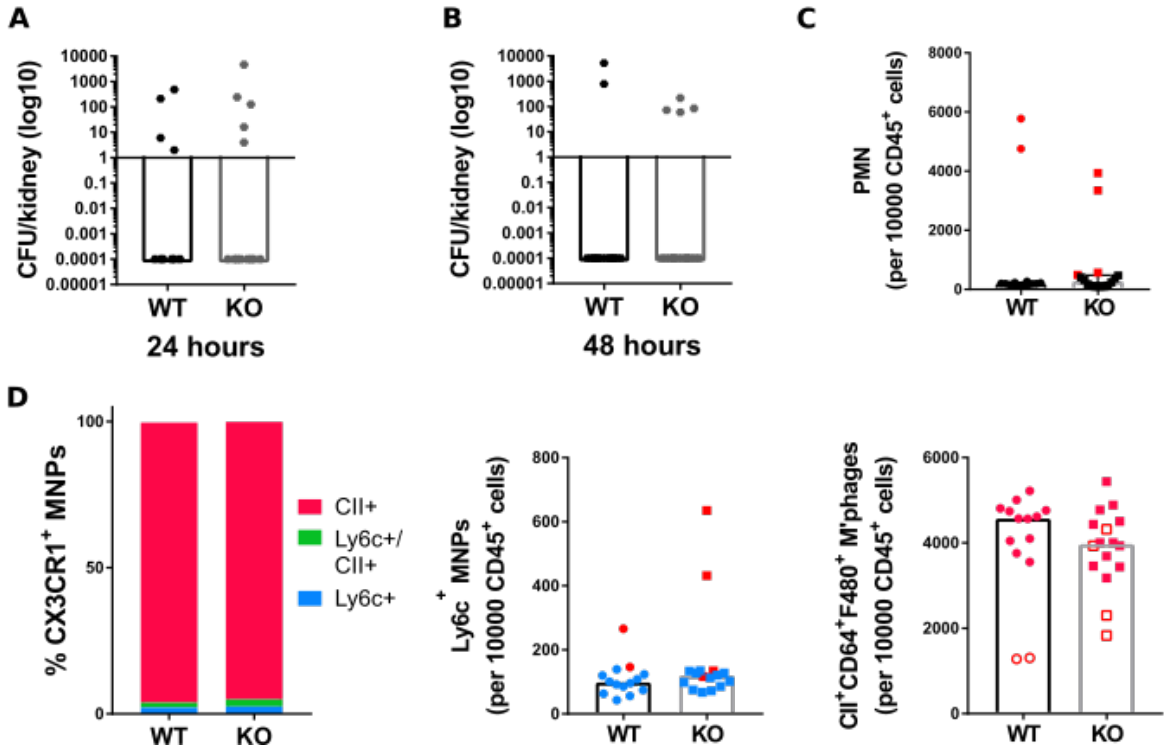

Figure 4.28: Infection severity and baseline monocyte characteristics from the kidneys of IL22RA1 KO mice during UPEC UTI.

IL22RA1 KO mice treated with UPEC (single catheterisation) and kidneys harvested at 24-48 hours. **A**: CFU counts at 24 hours with pseudocount of $1x10^{-4}$, WT=10, KO=13, data combined from 4 experiments. **B**: CFU at 48 hours with pseudocount of $1x10^{-4}$. **C**: Neutrophil counts with kidneys (infected tissue in red). **D**: Myeloid cell proportions and counts (infected tissue in red). All cell counts produced with use of IV anti-CD45 labelling. The gating strategy used was as demonstrated previously. Data combined from two experiments (WT=8, KO=8).

Kidneys harvested at the same time points (24-48 hours) showed similar results in terms of the cell counts to those from the bladder (fig. 4.28C&D), but the absence of pyelonephritis in the context of a single catheterization limited the interpretation of these results. Few tissues had demonstrable pyelonephritis, as indicated by the addition of a pseudocount to the CFU values (fig. 4.28A&B). The proportions with pyelonephritis were almost identical at 24 hours. At 48 hours a higher proportion

had pyelonephritis in the KO group (2/16 WT and 4/16 KO), but the small numbers of infected tissue did not create significant results using a chi-squared test.

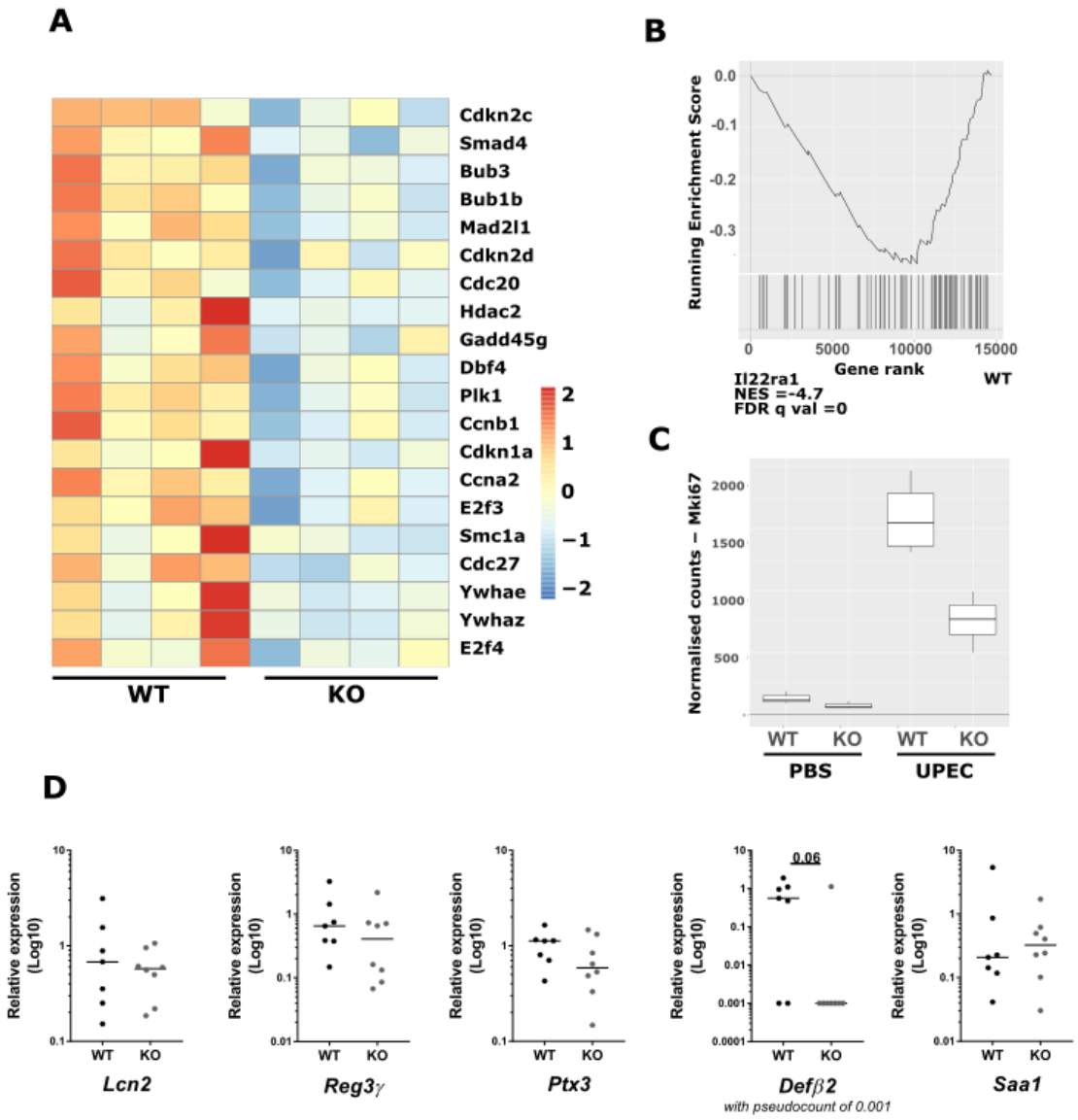

Figure 4.29: RNA sequencing of whole bladders from IL22RA1 KO mice demonstrating changes in epithelial regeneration factors and AMPs.

IL22RA1 KO mice treated with UPEC (single catheterisation) and bladders harvested at 24 hours. **A**: Heatmap of cell cycle genes. **B**: Gene set enrichment scores (Kegg) for cell cycle genes. **C**: *Ki67* transcript levels between mice catheterized with PBS or UPEC. **D**: qPCR of AMPs relevant to the renal tract, median bar shown and significance calculated using Mann Whitney test. Pseudocount added to *Defb2* transcripts of 0.001. RNA sequencing analysis performed by Dr J. Ferdinand.

To investigate IL-22 effector functions further, we performed RNA sequencing on whole tissues. Figure 4.29 shows RNA sequencing data collected from bladders harvested at 24 hours, all of which showed evidence of cystitis with positive CFUs. These data shows that there was downregulation of

cell cycle genes associated with epithelial regeneration and a significant decrease in their corresponding gene set enrichment analysis scores (GSEA) for KO compared to WT mice (fig. 4.29B). Ki67, a marker for cell proliferation, was also downregulated in the KO mice treated with UPEC (fig. 4.29C).

We also performed qPCR on AMPs and factors associated with maintaining epithelial integrity on bladders harvested at 48 hours (corresponding CFU data shown in figure 4.27B). Whilst there were trends towards decreased levels of key transcripts, none of these reached statistical significance (fig. 4.29D).

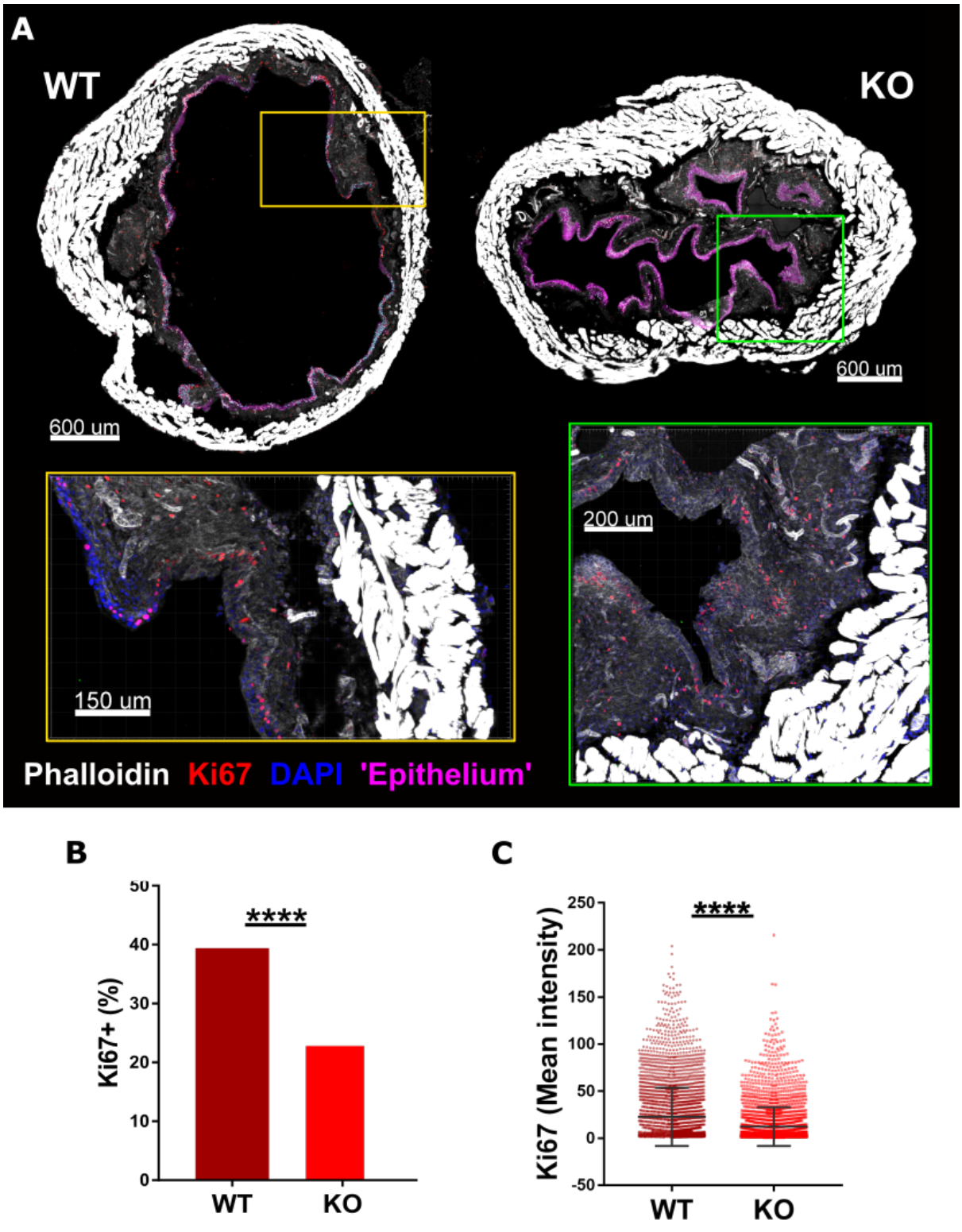

Figure 4.30: Ki67 expression during UPEC UTI in bladders from IL22RA1 KO mice

Figure 4.30: Bladder sections from IL22RA1 KO and WT mice catheterised once with UPEC for 36 hours. **A**: 25µm sections stained with phalloidin-A568, DAPI and Ki67-eFluor660. High power magnification of representative sections are shown in the yellow (WT) and green (KO) boxes. The purple layer was generated using Imaris software to identify the epithelial layer (area selected by DAPI intensity). The layer was cropped manually to align the edges with the basement membrane and background staining was subtracted electronically, as delineated by the phalloidin marker. **B**: Percentage of cells that were Ki67 positive (of total DAPI positive epithelial cells), z score = 14.9, one tailed $p < 0.001$, two tailed $p < 0.002$. C: Graph showing the mean intensity of Ki67 present in all DAPI+ cells of the epithelial layer. Plot shows mean values with standard deviation and significance ****$p<0.0001$ (paired t test).

Figure 4.30 shows microscopy sections of bladders infected with UPEC for 36 hours. The imaging parameters used for both WT and KO sections were identical, permitting subsequent computational analysis and comparison. By using a mask technique within Imaris software, we were able to delineate the epithelial layer by selecting areas of increased DAPI intensity. The phalloidin staining allowed for manual correction of the layer, so that any areas below the basement membrane could be accurately excluded. Having created the area of interest, we were then able to identify all cells that had nuclei (DAPI+) and extract their corresponding Ki67 staining intensity (background staining was subtracted automatically using the Imaris software) and the same setting applied to both WT and KO images. Nuclei that appeared purple in the high power magnification images, demonstrated DAPI and Ki67 co-staining and were observed with greatest intensity within the WT, rather than KO epithelium (fig. 4.30A). Analyzing Ki67 intensity by DAPI staining was undertaken, as expressing Ki67 staining as a proportion of the epithelial area was not feasible, given the differences in bladder inflation and epithelial depth. As demonstrated, the Ki67 staining was markedly reduced in the KO group (figure 4.30B), indicating that IL-22 signaling may promote epithelial cell proliferation. Furthermore, when we calculated the percentage of epithelial cells that were Ki67+, this was reduced in the KO bladder – 39.4% WT and 22.8% KO. Figure 4.30C shows the epithelial mask layer with epithelial Ki67 highlight by cyan dots to yield the total number. The Ki67 stain is also included in red. It is unsurprising that a proportion of cells were able to express Ki67 in the KO bladder, as this represents constitutive expression by epithelial cells.

4.6 Discussion

4.6.1 Key aims

The data within this chapter has sought to address two main aims:

1. Investigating the functional characteristics of ILC3s in urinary tract infection.
2. Interrogating the role of ILC3s in murine models of Uropathogenic *Escherichia coli* UTI.

As expected, immune cell numbers increased within 24 hours in UTI and associated proinflammatory cytokines become elevated throughout the renal tract. Key to this project were increases in cytokines pertinent to the IL-23/IL-17a inflammatory axis and the subsequent potential for ILC3 activation. The increases in the cytokines *IL1b, IL23a* and *Tnfsf15* we observed in our RNA sequencing data, would potentially provide the necessary stimulus for ILC3 activation and IL-17 secretion. IL-17a and IL-1β gene nodes were highlighted from our analysis of the top 100 upregulated genes at 24 hours from whole bladder. We were able to verify this with publicly available RNA sequencing data from WT bladders at 8 hours, where distinct rises in these cytokines could also be observed. Within the kidney, transcriptional changes were also evident and some showed anatomical differences that correlated to the passage of pathogen from bladder to kidney, but also through the kidney itself. As bacteria ascend the renal tract in the opposite direction to the flow of urine, they will encounter the renal pelvis and medulla first and this was where we observed the most profound rises in *Il1b*, *Cxcl1* and *Cxcl2* transcripts. Together, these changes help us to describe the nature of the pro-inflammatory environment in the early stages of UTI and we can begin to characterize the immune defense strategies within the renal tract and their association with ILC3 and MNP activation.

Some AMPs have been documented within the renal tract before, but we were able to demonstrate increases in some that had not been previously described in detail, such as *Reg3g* and *Saa1/2*. *Reg3g* is particularly interesting given its association with the gut and its IL-22-dependent production, though it has been noted in UTI previously [44, 353]. It has been more typically described in the context of gram positive organisms at the gut mucosal barrier, but here we saw it rising in the context of gram negative infection within the bladder and kidney. It remains to be determined if this rise is specific to UPEC and if a precise role for this AMP can be found in this context, though it has been demonstrated previously that transcripts rise in response to UPEC UTI and not *Staphylococcus saprophyticus* or *Enterococcus faecalis* UTI [44]. It may play a role in inhibiting the passage of commensal gram positive bacteria that could penetrate the damaged bladder epithelium during UPEC invasion. RegIIIγ has antimicrobial activity against *Staphylococci* and

Enterococcus (and not UPEC) and the former species contribute to the bladder's microbiome [44, 75, 98]. *Staphylococci* and *Enterococci* can cause significant infections in humans when they enter the bloodstream, such as bacterial endocarditis, septic arthritis and discitis. It is logical that the body would have prevention strategies to mitigate spread of gram positive bacteria into the blood stream from any source where these bacteria normally reside, including the bladder, skin and gut.

ILC3-specific cytokines showed upregulation throughout the renal tract during infection, though we were unable to definitively locate their cellular source in WT mice. Considering cellular sources of these cytokines with reference to T cell dynamics, places emphasis on early cytokine production by γδT cells, MAITs and ILC3s. It is likely that the tissue-resident populations of T cells observed in the bladder in figures 3.6, 3.14 and 3.16 contain γδT cells ready to provide an early innate pro-inflammatory response, as has been demonstrated in EAE [198]. We could not obtain sufficient ILC3 numbers to demonstrate intracellular staining of these cytokines by flow cytometry or flow sort and perform RNA sequencing in this subset. To help address this challenge and gain further insight into the effects of ILC-depletion in UTI, we used Rag2 KO mice treated with depleting anti-Thy1.2 antibodies which indicate that ILC3 are major producers of IL-17 in the context of cystitis, and in the kidney produce IL-17, IL-22 and GM-CSF following UPEC challenge. Our RNA sequencing data from whole tissue from bladder and kidney will enable us to further delineate the effects of ILC3s more globally.

We have demonstrated that ILC3s increase in number in both the bladder and kidney during UTI, as well as their adaptive CD4+ T cell counterparts. This indicates the possibility of IL-17a production by this population of ILC3s, potentially representing an early cellular source of the cytokine. Interestingly, CD4+ T cells, Th17 cells, CD4- T cells and ILCs increased within 24 hours of infection in the bladder (fig. 4.9) and ILC3s and Th17 cells within the kidney (fig. 4.10). This highlights the differences between the upper and lower urinary tract in terms of the resident lymphoid populations available to respond, the reliance on innate strategies in the bladder and the lag in ascension of the pathogen to the kidney and the development of an adaptive response. In terms of ILC3 dynamics, the proportion of NCR+ ILC3s decreased in favour of CD4+ ILC3s, though the absolute numbers obtained by flow cytometry were small; it is difficult to conclude that NCR+ ILC3 populations associated with IL-22 production were not also activated, or there was not T cell contamination that may influence the results. We tried to investigate the rise in ILC3s in terms of their local expansion or recruitment, to better understand their cellular dynamics in UTI. This proved challenging, again due to the small numbers of ILCs available for analysis. Our results would suggest that they do proliferate, as there was a clear indication that renal ILCs were proliferating and incorporating EdU after exposure to UPEC and a trend towards a similar finding in the bladder. The

order of magnitude of EdU incorporation in both bladder and kidney was the same or greater than the percentage of cells that were Ki67 positive in published data demonstrating proliferating ILC3s within the gut [261, 426]. Owing to the smaller absolute numbers of ILC3s in bladder, greater numbers of mice per group would be required to explore the observed trend towards ILC3 proliferation. This was technically challenging, due to the complexity of the intracellular EdU-staining protocol and the need to use reporter animals for ILC3 identification.

In our RORγt KO experiments, the infection was more severe in the KO animals, as evidenced by increased splenic infection with UPEC, indicative of systemic spread. A trend towards increased infection was observed within the bladders of mice as well as a significant rise in renal CFUs at 48 hours. We were able to demonstrate convincing cellular and transcriptional differences between RORγt KO and their WT counterparts with a reduction in *Il17a* and *IL22* transcripts and decreased neutrophil recruitment in the bladders and kidneys of KO mice. Interestingly, the decrease in neutrophil recruitment observed in the bladder did not occur in the kidney, where increased levels of pyelonephritis were associated with increased neutrophil infiltration, thereby indicating the presence of alternative recruitment mechanisms in the upper urinary tract. As indicated in the introduction, the bladder and kidney develop differently and exhibit different strategies to combat infection. The bladder relies more on an innate response, using myeloid cells to subvert the adaptive immune system and we can see the effect of decreased chemoattractant cytokines and subsequent loss of innate immune cells in the bladder that is not present in the kidney [2]. Our data supports the robust involvement of the innate and adaptive immune systems in the kidney, with neutrophil, monocyte and B cell increases, in response to pyelonephritis. This may be of an evolutionary advantage in preventing kidney failure and septicaemia, given the kidney's more vulnerable vascular contiguity to the systemic circulation.

CFUs were significantly increased in the bladders of Rag2 KO mice treated with anti-Thy1.2 antibodies at 48 hours post-catheterisation and there was a trend towards increased rates of pyelonephritis. Anti-Thy-1.2 depletion led to further loss of *Il17a* transcripts in both bladder and kidney, indicating that ILC3s were potentially responsible for some of the cytokine loss observed during the RORγt KO UTI experiments. Baseline differences were observed within the kidney in mice that had demonstrable infection or sterile kidneys after catheterisation. Interestingly, multiple cytokines and AMPs were downregulated in the anti-Thy1.2 treated animals and this raises the possibility that ILC3s facilitate or influence regulation of myeloid and epithelial cells that may produce these proteins at baseline. This data should be interpreted, with the proviso that Rag2 KO mice have baseline immunodeficiencies which may impact the phenotype observed during UTI.

Identifying ILC3-specific effects on antimicrobial peptides was more difficult, as some of these transcripts come from myeloid cells as well as the epithelium and are likely to be influenced by a wide range of inflammatory processes initiated during UTI, including the bacterial burden. Despite this, we were able to demonstrate decreased levels of *Reg3g* transcripts in the bladders of mice lacking RORγt. Quantitative PCR data from the equivalent experiment in Rag2 KO mice did not demonstrate loss of *Reg3g* transcripts, thus suggesting that ILCs are not solely required for its production. Transcriptomic (qPCR) data from the bladders and kidneys of these mice confirmed continued production of AMPs, despite ILC-depletion. The relevance of changes to RegIIIγ during UTI remain an avenue for further investigation, though its association with gram positive bacteria suggests an indirect role during UPEC UTI [44, 75]. Any infection will change the proportions of other bacteria within the bladder. We know that gram positive species are present in health and these will be affected by UPEC infection, as discussed above [96-98].

We observed changes in myeloid cell recruitment and maturation in mice lacking ILCs during infection, in both bladder and kidney. As already mentioned, the immune response between bladder and kidney differs and this was apparent in the myeloid cell proportions that we observed. The kidney had a much higher proportion of mature MNPs (CII+) and the bladder an increased proportion of Ly6c+ MNPs. When we examined these subsets in more detail, we saw populations of macrophages in the bladder that were F4/80 and CD11b positive, whereas in the kidney they tended to express less CD11b. Owing to the size of the flow panel used, we were not able to further select for DC populations and further MNP characterization falls outside the remit of this project. The gating strategy used to examine these cells was adapted from Tamoutounour et al. (2012) who described the monocyte waterfall and how to categorize MNPs throughout their maturation in the gut (see section 1.3 for more detail) [122]. When we looked at these populations in our ILC-depleted murine model in more detail, we saw changes in the proportions and maturation of MNPs, perhaps indicating potential for ILC3-macrophage cross-talk during UTI. Further investigation of myeloid-ILC3 interactions are explored in chapter 5.

Much of this chapter has focused on the proinflammatory role of ILC3s in UTI, in contributing to IL-17a production and recruitment of a robust innate immune response. We also observed loss of *Il22* transcripts in our RORγt KO murine UTI models and trends within our Rag2 KO murine model. To investigate the role of this cytokine further, we performed UTI experiments in mice lacking a component of the IL22R. IL-22 has been shown to work in synergy with IL-17 in promoting an immune response [314, 340, 341], however we did not observe proinflammatory or cellular changes in our IL22R KO model. This is not surprising, as the cytokine does not exhibit these effects alone (see section 1.4.1 for more detail on the effects of IL-22). We did observe changes in cell cycling

from tissues harvested after 24 hours of UTI, thus indicating that IL-22 is required in early UTI to promote epithelial regeneration and repair. Unfortunately, the CFU data from the bladders of IL22RA1 KO mice was not reliable and conclusions relating to the infective burden cannot be made.

Taken together, these data demonstrate the upregulation of IL-17a and IL-22 using transcriptional analysis throughout the renal tract and this correlates to increased numbers of ILC3s during UTI. Furthermore, *Il17a*, but not *Il22*, transcripts were reduced in Rag2 KO mice that received ILC-depleting antibodies and the bladder infective burden was increased. This shows that loss of ILCs leads to increased infection severity within the bladder and this will enhance the ability of the pathogen to ascend the urinary tract and cause pyelonephritis. Furthermore, we have observed that loss of ILCs is also associated with differences in immune cell recruitment and maturation. We know that ILC3s are activated by cytokine products from myeloid cells and the interactions of these cells are of vital importance. Our data supports the idea that there is ILC3-MNP cross-talk in UTI and these interactions will be examined further in chapter 5.

4.6.2 Limitations

There are two predominant limitations that have hindered collection of more robust data. Firstly, the murine bladder is so diminutive that obtaining information about small immune cell populations, such as ILC3s, is difficult. Secondly, better bladder data is typically obtained after a single catheterisation and kidney data after two catheterisations, this necessitated experimental repeats using both methods.

Due to the small volume of the bladder and resulting limited cell suspension it was difficult to generate multiple experimental readouts from the same sample (for example CFU plating, flow cytometry and qPCR). Despite this difficulty, it was imperative to know the infection severity, as this influenced interpretation of the data. In the context of UPEC UTI many immune pathways are activated and understanding the infective burden, cellular recruitment and transcriptional changes should not be attempted in isolation. In some instances, larger amounts of tissue had to be prioritised to complete intracellular staining or ILC3 counting, thus limiting the number of applications attempted per experiment. There was a natural delay in completing experimental repeats for breeding purposes, which may have implications for differences in microbiome, that have been shown to influence Th17 cell and ILC3 dynamics in the gut [427, 428].

Throughout the renal tract, we have found that the limited absolute number of ILC3s obtained has meant that we have not been able to flow sort cells for RNA analysis and culture, thus limiting these

avenues of investigation. Our EdU experiments demonstrated that total ILC numbers were sufficient to produce a significant result within the kidney, but numbers were just too small within the bladder to draw true conclusions.

Optimising the UTI experimental protocol to each organ, bladder and kidney was key to generating reproducible results. A double catheterisation brings far higher rates of pyelonephritis, but infection rates within the bladder become uninterpretable (despite dilutions of 1:1 million). There is an additional concern that an increased bacterial burden might precipitate a devastating exfoliation of the urothelium, as UPEC invades epithelial cells to form intracellular bacterial communities. Damage of this extent could impact on cell populations within the epithelium and lamina propria or the viability of the organ and affect results. It has been important therefore to consider the experimental aim carefully in terms of location and timing and adapt the protocol accordingly. In general, this means a single catheterisation for bladder (24-48 hours) and a double catheterisation for kidney (24-72 hours) and therefore increases the number of mice required and experimental repeats.

A more minor problem has been in obtaining sections for microscopy, both in terms of sufficient animal numbers and technical challenges, which were discussed in chapter 3.

Finally, for the reasons already mentioned, each UTI model has required multiple repeats. As infectivity naturally changes with each experiment, it was difficult to combine experimental replicates.

4.6.3 Future work

The data presented within this chapter has started to explore the roles of ILC3s in UTI and we have been able to use flow and PCR analysis to draw associations that correlate to published data on ILC3 and IL-17-driven inflammation. To focus further on ILC3s, we have performed RNA sequencing using our Rag/Thy UTI model and hope that this might shed further light on the role of ILC3s during UTI. In addition, we had hoped to perform intravital imaging after catheterization with UPEC to assess the dynamic capacity of ILC3s. We have not been able attempt these experiments, owing to restrictions from our local animal facility on the transfer of mouse strains. As obtaining cell numbers from bladders post-mortem is restrictive owing to small cell numbers, it is hoped that intravital imaging might prove a useful tool to assess the dynamic behavior of ILC3s.

Having suggested that there are differences in AMP levels within our RORγt KO model, further experimentation is required to fully address their role. It is likely that these peptides have a dual function in terms of antimicrobial properties and epithelial regenerative capacity. This requires much more work to answer these questions and falls outside the remit of this project.

Owing to our difficulties in performing separate experiments for bladders and kidneys, a further repeat of the RORγt KO model for bladder optimization is required. The flow cytometry and PCR data has been obtained, but the infection severity needs further characterization in the context of a single catheterization and reduced bacterial inoculum. Repetition of UTI in IL22RA1 KO and WT mice is also required to validate the Ki67 staining results within the bladder epithelium.

Finally, this project has focused on the acute phase of UTI, in order to investigate the innate arm of the immune response. As discussed within this chapter, an adaptive response is likely to be of increased significance within the kidney. It would be interesting to see how repeated UTIs over a period of weeks to months alters the tissue resident populations of the kidney in its response to recurrent infection. Further experiments using IL-17-labelled cells would help to track the cellular sources of this cytokine and the potential T cell and ILC dynamics that contribute to the innate and adaptive responses during UTI respectively. It may be that tissue-resident T cells and ILC3s may play an initial role, if they are required to direct the inflammatory response or to facilitate epithelial repair in the face of fibrosis from repeated inflammation, that is augmented by slower adaptive Th17 cell responses within this context. This would have marked consequences for the development of chronic kidney disease in patients who suffer from repeated UTI or reflux nephropathy, conditions that significantly affect the paediatric population and lead to ESRD.

4.7 Graphical Summary

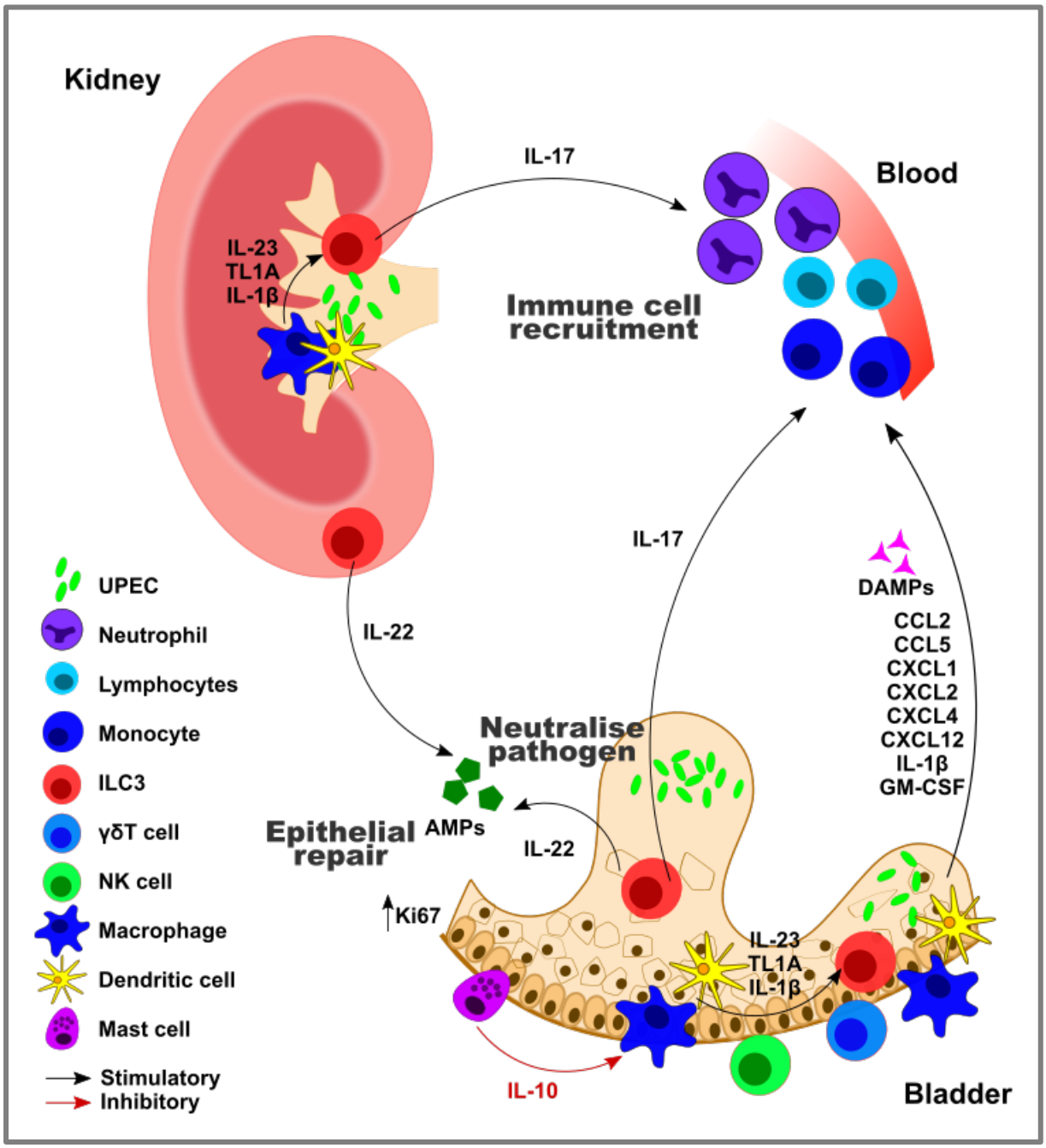

Figure 4.31: ILC3s are early producers of IL-17a in the renal tract during UTI

ILC3s are stimulated by macrophages during UTI and produce IL-17a for immune cell recruitment and IL-22 for promotion of epithelial repair and microbial neutralisation by AMPs. The epithelium and tissue-resident immune cells produce chemokines and DAMPs for peripheral immune cell recruitment. The innate immune response in the bladder is promoted by mast cells that inhibit macrophage antigen presentation by IL-10 secretion [2].

Chapter 5 – Innate lymphoid cell and mononuclear phagocyte crosstalk within the bladder

5.1 Introduction

Mononuclear phagocytes (MNPs) form a crucial part of the tissue-resident immune system throughout the renal tract. In the introduction, I reviewed their role in orchestrating the immune response to UTI (Chapter 1, section 1.4) and defined roles for these cells in both bladder and kidney are emerging. Understanding the key features and roles that MNPs exhibit during the early stages of UTI provides context for the experiments presented in this chapter and these are summarised in the following list:

1. MNPs respond rapidly to gram negative bacteria through TLRs and quickly generate pro-inflammatory and defensive cytokines [367, 368].
2. Monocytes are rapidly recruited to the renal tract during infection [369].
3. Macrophages phagocytose bacteria to neutralise the pathogen and show enhanced phagocytic activity within the bladder and renal medulla, sites encountered earliest during ascending pyelonephritis [2, 12, 371].
4. The roles of MNPs within the bladder and kidney differ. Bladder macrophages have been shown to phagocytose and hide pathogens from an adaptive immune response, whereas the kidney utilises this system for further immune defence [2, 12].

It is probable that myeloid cells of the renal tract, particularly those that are epithelial-associated, exhibit features that parallel MNPs at other mucosal surfaces. These populations of tissue-resident and recruited cells may possess distinct defensive and homeostatic functions adapted to control common urinary pathogens or commensals and maintain the environment. For example, the renal tract poses significant challenges, such as the hypersalinity of the renal medulla or variable urinary pH within the bladder [12]. These complications must be overcome to perform homeostatic and regulatory functions, including the maintenance of epithelial integrity and immune tolerance, and these processes require constant interaction between MNPs, other tissue-resident immune cells and the epithelium. These interactions need to be fully characterised within the renal tract and particularly in the bladder.

MNPs are known to stimulate ILCs and this has been well described in a range of tissues, such as the gut, lung and skin (see sections 1.3.4-5). The effect of IL-23a, IL-1β and TL1A stimulation on IL-22-

producing ILC3s has been particularly well characterised in the gut [125, 282, 318, 326, 429]. As described in chapter 3, ILC3s are resident in the renal tract and it is reasonable to predict that they are being activated by their MNP neighbours to help perform the homeostatic functions of epithelial repair and lymphoid tissue maintenance. Furthermore, their relationship to the dense network of tissue-resident cells present, including multiple lymphocyte and lymphoid cells is unclear, as is the effect of infection on this tissue-resident immune system. Little is known of these relationships in the renal tract and this chapter seeks to shed light on those that involve ILC3s and MNPs.

To assess the potential for ILC3-MNP crosstalk, we utilised murine models that allowed us to interrogate the effects of ILC depletion on MNP phenotype and function, and reciprocally the loss of ILC3-stimulating cytokines produced by MNPs on ILC3 function. To deplete ILCs, we used Rag2 KO mice treated with ILC depleting Thy-1.2 antibodies and this data was presented in chapter 4. In addition, we performed urinary tract infection experiments in mice deficient in IL-1β and those lacking the receptor for IL-23a, both of which are cytokine products from MNPs [125, 282, 318]. We sought to determine how ILC3s are affected by disrupting these cytokine axes in the renal tract during UPEC infection.

Publicly available RNA expression data was used to provide an initial outline to the potential interactions of MNPs and ILC3s in UTI. Two publications that generated whole bladder data were particularly useful, and included microarray data at three time points during the first 24 hours of UTI [44] and RNA sequencing data from mice lacking CD14+ cells [3]. By looking at the levels of MNP and ILC3-associated transcripts over time and the effect of myeloid depletion in the context of CD14-deficiency, these analyses complement the experimental results within this chapter, providing context and validation.

Data relating to the bladder and kidney is presented within this chapter, however an increased emphasis has been placed on the bladder. The reasons for this are two-fold: firstly, less is known of the immune network of the bladder, despite the presence of a higher proportion of innate immune cell populations relative to the kidney (as demonstrated in figure 4.1); secondly, the bladder epithelium and its relationship with the environment is perhaps more similar to the mucosal epithelium of the gut, where such interactions are important. Pragmatically, given these considerations, limited time and mouse numbers, and the fact that the cystitis and pyelonephritis models could not be performed simultaneously, we focused on the bladder infection model.

5.2 Confocal microscopy demonstrates the bladder's tissue-resident immune network

In health, we found that the bladder was teaming with mononuclear phagocytes. They were spatially located throughout the bladder wall but could be found in greatest numbers within the lamina propria and epithelium. Figure 5.1 shows myeloid cells from a naïve (uncatheterised) CD11c-EYFP reporter mouse, co-stained with F4/80. The larger tile is of the entire bladder, with the urethra included on the section (three o'clock position). The larger tiles were taken using only the phalloidin and CD11c-EYFP channels, to minimise the duration of image acquisition. The images shown at higher magnification included F4/80 staining (red) and clearly demonstrated macrophages and DCs (CD11c-EYFP – green) within the bladder wall. The yellow cells co-stained for both markers and thus we could detect three distinct populations.

Of particular interest, were the dense and often stellate MNPs observed within the urethra (outlined by the purple box). These predominately co-stained for CD11c-EYFP and F4/80, indicating that they were macrophages, but could be seen in a similar position to CD11c+ DCs at the bladder entrance (urethra). This supports published data and suggests that macrophages may contribute to bladder defence and surveillance at the entry portal for pathogens accessing the bladder, described in detail in section 1.4.1. The MNPs seen within the bladder had fewer dendrites, but retained features of myeloid size and morphology, as shown within the blue and orange boxes.

In summary, these images demonstrate the dense network of MNPs within the lower urinary tract, that contribute to a rich tissue-resident innate immune system. In terms of their position and morphology, they demonstrated potential for interactions with other tissue-resident immune cells and the epithelium, as well as surveillance for ascending pathogens.

To determine the relative positions of MNPs and lymphoid cells, we stained bladder sections from RORγt-GFP reporter mice (*Rorc(γt)-Gfp*^{TG}) and CD11c-EYFP mice with antibodies for Class II, CD3 (to distinguish Th17 and γδT cells from ILC3s) and smooth muscle actin. Figure 5.2A demonstrates the upper pole of the bladder (furthest from the urethra). Cells of both myeloid and lymphoid lineages could be seen and ILC3s, T cells and MNPs were visible. T cells were present in abundance, potentially representing T helper cells, cytotoxic T cells, γδT cells, NKT cells and invariant T cells, such as MAITs. More detailed staining to delineate these populations was not possible with the other markers required to identify ILCs and MNPs, but our awaited 10X genomic data (fig. 3.16) will contribute to this work. Cells that were solely RORγt-GFP positive (CD3 and CII negative) indicated ILC3s. Although ILC3s can be MHCII positive, these cells did not exhibit MHCII by confocal microscopy, though this may in part be due to the density of MHCII surface molecules and the

resulting staining intensity. Cells that were recognisably MHCII positive and lacked CD3 were larger and had a myeloid morphology, consistent with their identity as MNPs. All the cell types described were present throughout the entire lamina propria and urothelium (figure 5.2C) indicating a close spatial relationship and subsequent potential for cell to cell interactions between MNPs, lymphocytes and ILCs. There are a number of examples of close apposition (i.e. direct cell-cell contact) of both ILC3s and MHCII+ MNPs, and of ILC3s and CD3+ T cells, that can be seen throughout figures 5.1-5.5. Figure 5.2 features high magnification images taken from the same mice to indicate some of these interactions in greater detail (figure 5.2A&B).

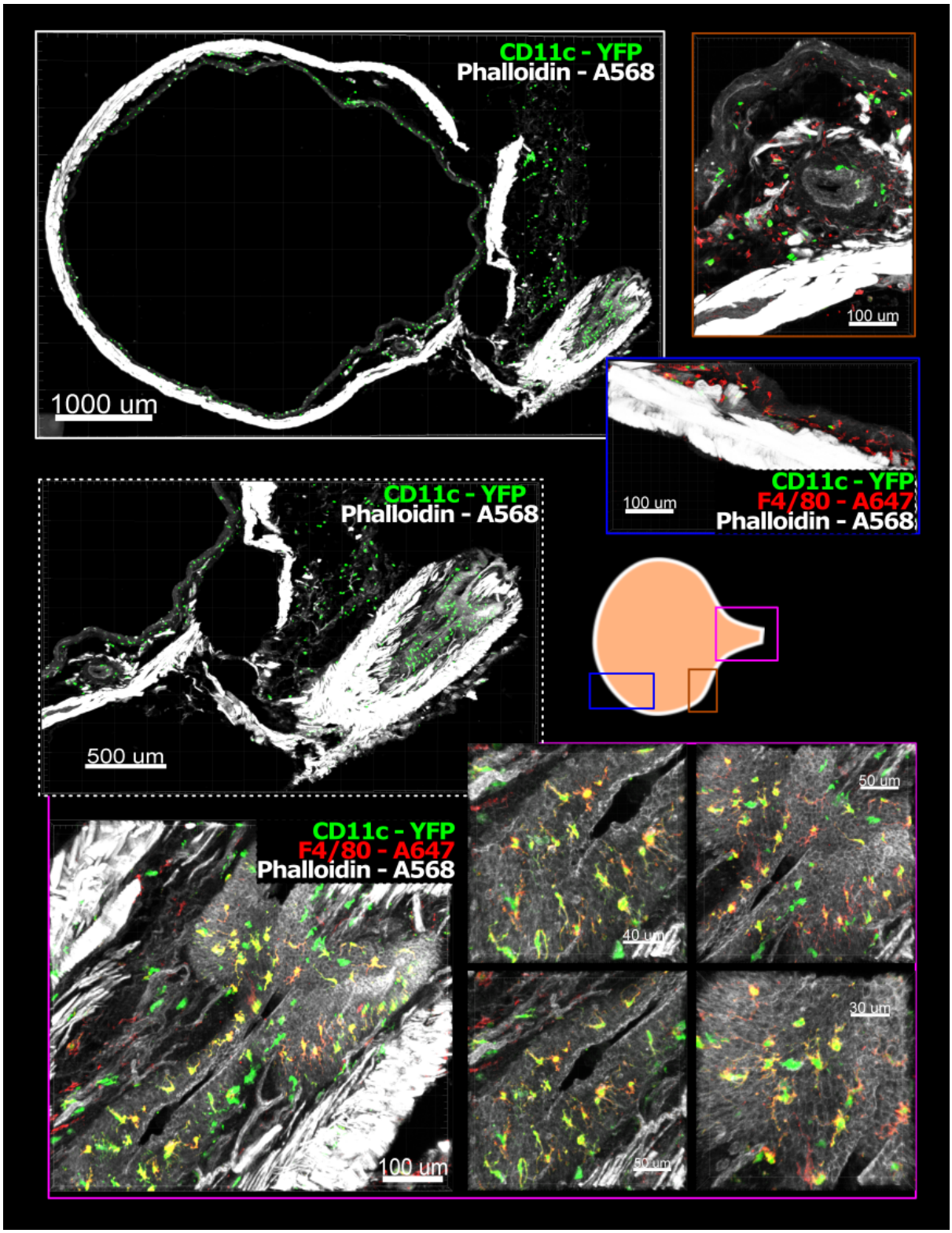

Figure 5.1: Confocal microscopy demonstrating tissue residency of bladder MNPs

Naïve CD11c-EYFP mouse. Staining for smooth muscle actin (phalloidin-A568) and anti-F4/80-A647. Larger tile shows only phalloidin and CD11c. Blue and orange boxes are from the bladder and pink box from the urethra. Positions with the bladder marked on the cartoon.

Images taken from bladder sections demonstrated a uniform presence of immune cells after UPEC infection in RORγt-GFP reporter mice. The pictures in figures 5.3-5.5 illustrate the presence of ILC3, T cells and MNPs in various positions throughout the bladder. These images were taken from the same mouse, 24 hours after inoculation with UPEC. A cartoon of the bladder indicating the precise location of image capture is provided for context.

As we have seen from flow cytometry plots of murine bladder in chapter 4, myeloid populations were typically Ly6c and F4/80, rather than class II, positive. The plots produced above used anti-class II-eFluor450, as it worked well for microscopy sections and allowed for concomitant use of GFP (augmented by anti-GFP-FITC) and anti-CD3e-PE, both of which proved essential to define RORγt ILC3 and T cell populations by microscopy. Despite the lack of F4/80 and Ly6c staining in these images, multiple MHCII positive cells could be seen and these correlated to the locations occupied by F4/80+ MNPs of figure 5.1.

Figure 5.2 **A**: Naïve RORγt-GFP mouse bladder sectioned at 30 µm. Staining for smooth muscle actin (phalloidin-V450), CD3-PE, F4/80-A647 and anti-GFP-A488. Dashed border delineates zoomed image of T cells, MNPS and ILC3s. **B**: Sections (30 µm) from naïve CD11c-EYP mouse showing the close relationship of DCs (CD11c-EYP) and T cells (CD3-PE) within the urothelium (phalloidin-V450). **C**: Bladder whole mount from a RORγt-GFP mouse with staining for GFP-A488, CD3-PE and Phalloidin-V450. Cartoon shows the dotted line on which the bladder is divided and flattened. Cells that co-stain for CD3 and GFP are likely to be Th17 cells, or other lymphocytes capable of producing IL-17 (MAIT, NKT and invariant T cells). These cells are located in the urothelial and lamina propria layers.

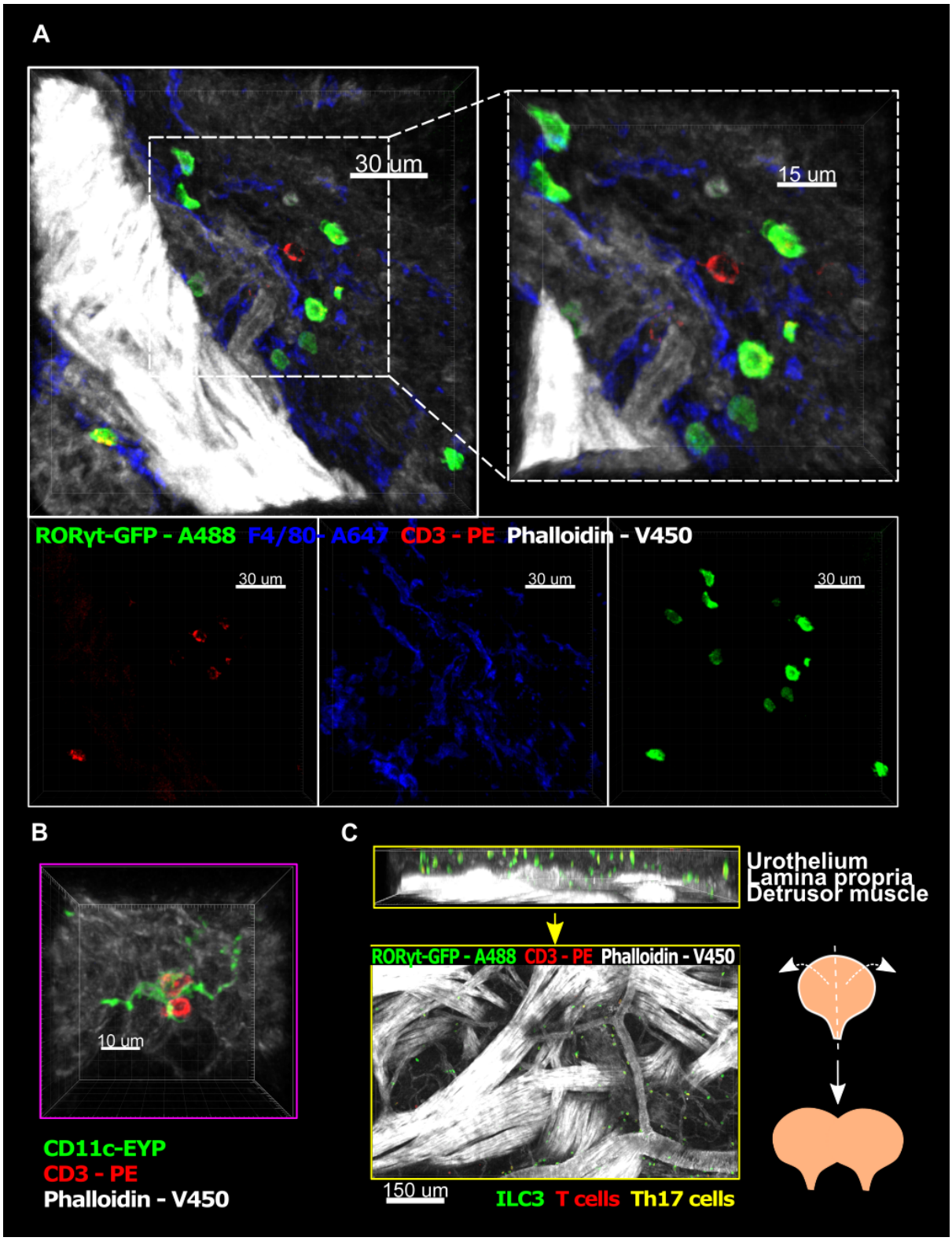

Figure 5.2: Tissue-resident ILC3 and lymphocytes of the murine bladder

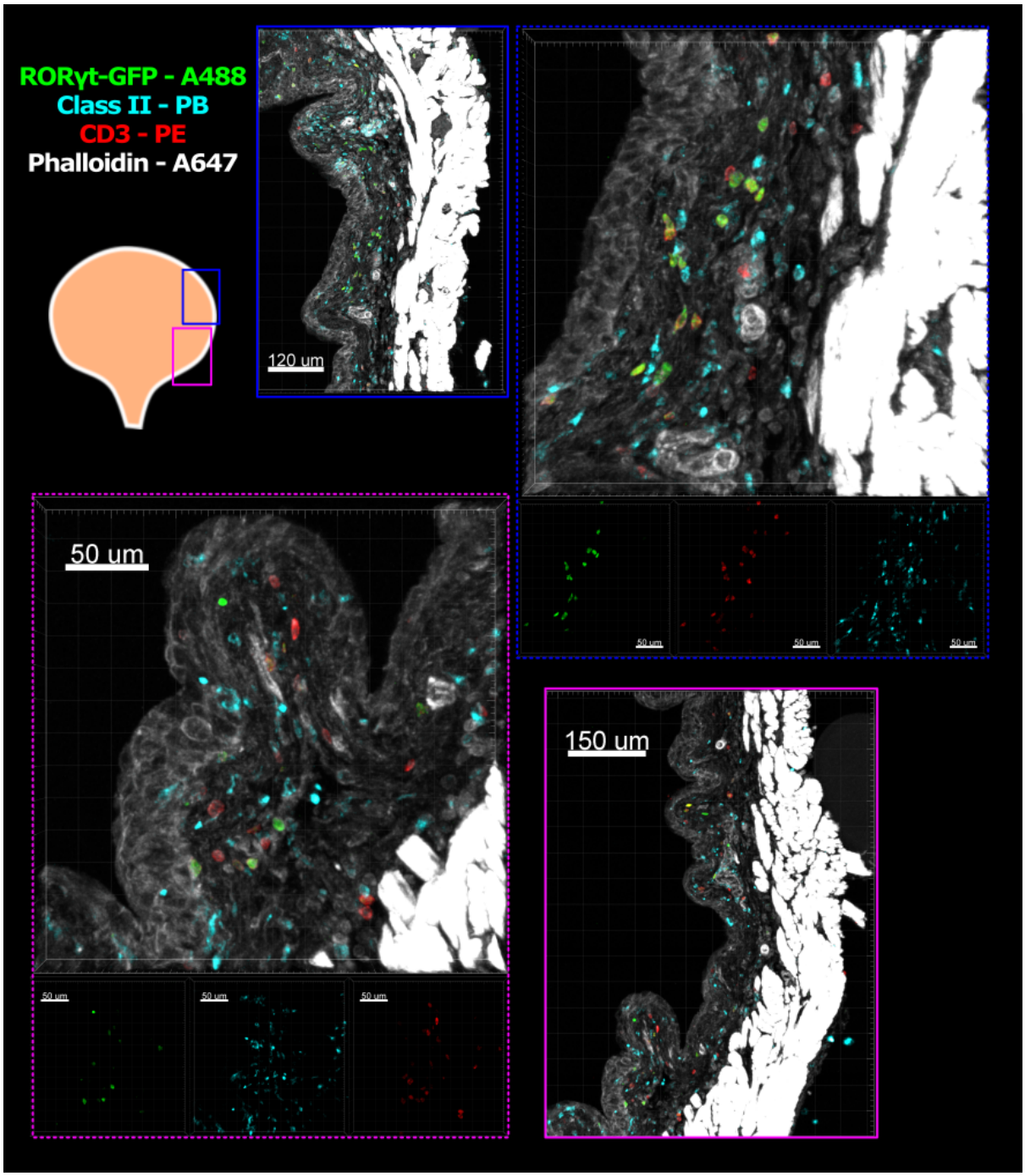

Figure 5.3: Confocal images of immune cell position in RORγt-GFP reporter mice after UPEC UTI (lateral wall, 9 o'clock)

RORγt-GFP mouse catheterised with UPEC for 24 hours. Staining for smooth muscle actin (phalloidin-A647), CD3-PE, Class II-eFluor450 and anti-GFP-A488. Position with the bladder marked by the cartoon. Dashed border colours of close-up images correspond to the larger tiles.

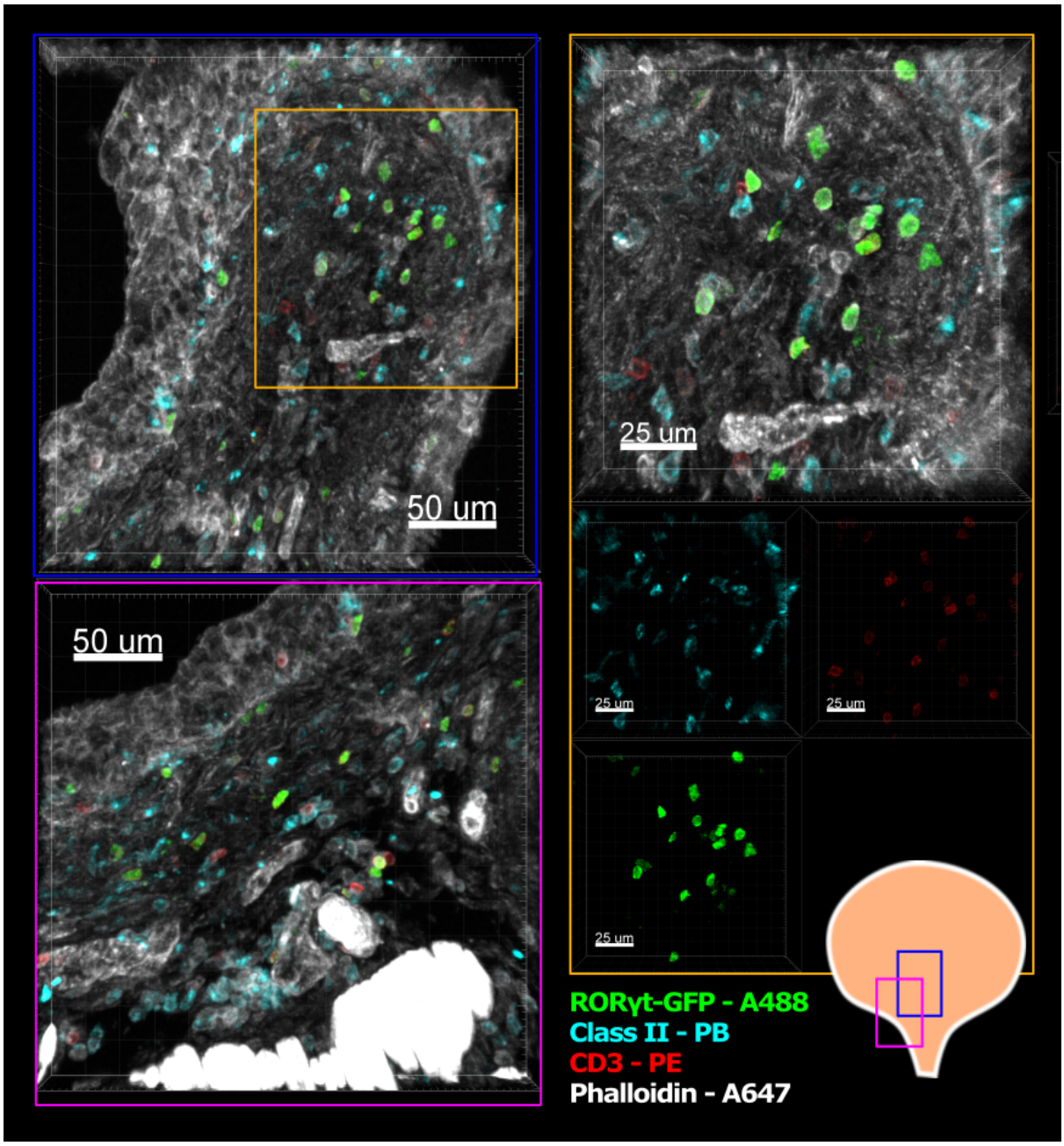

Figure 5.4: Confocal images of immune cell position in RORγt-GFP reporter mice after UPEC UTI (juxta-urethral)

RORγt-GFP mouse catheterised with UPEC for 24 hours. Staining for smooth muscle actin (phalloidin-A647), CD3-PE, Class II-eFluor450 and anti-GFP-A488. Position with the bladder marked by the cartoon. The yellow box shows a zoomed image to demonstrate cell-cell interactions.

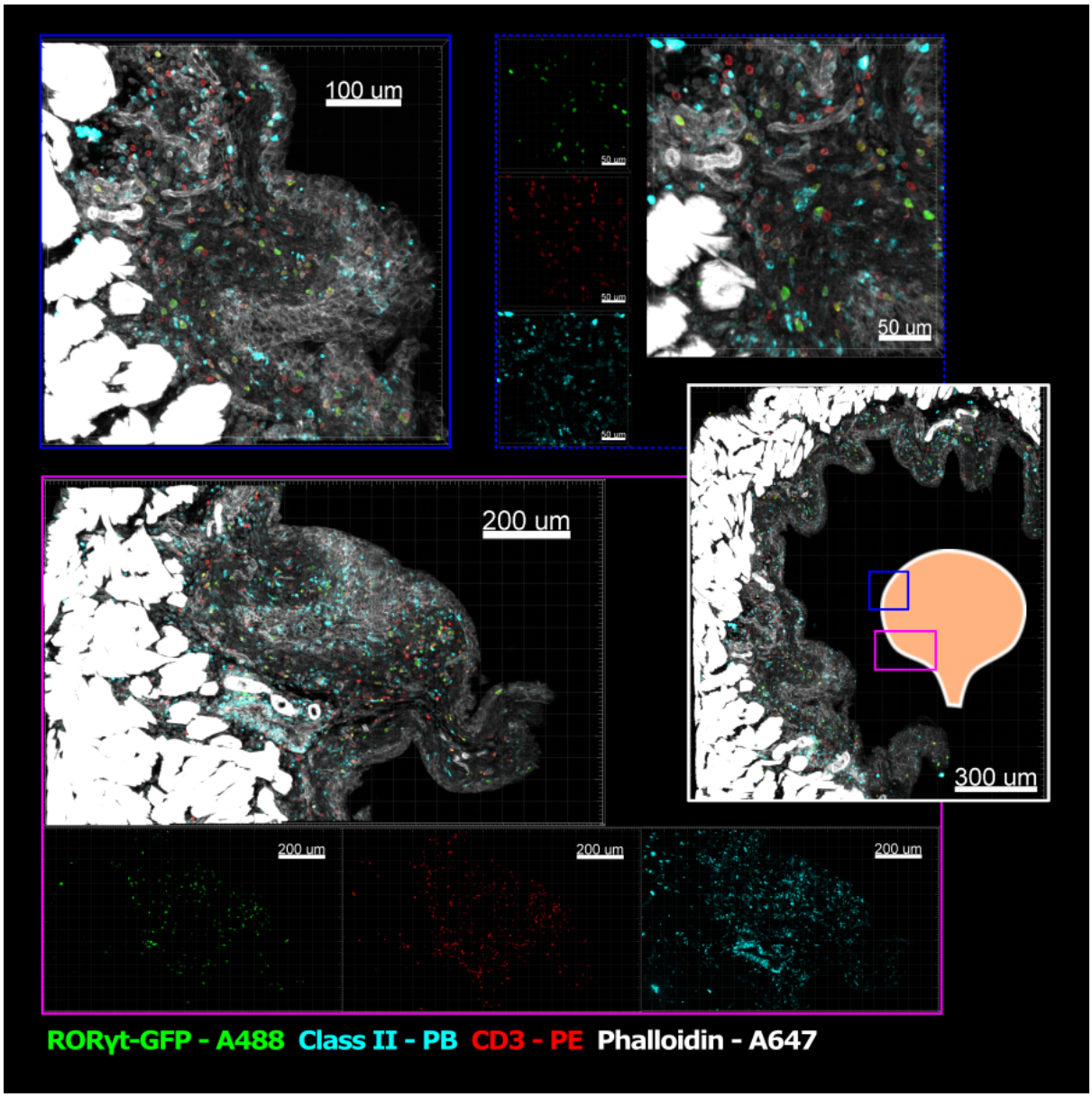

Figure 5.5: Confocal images of immune cell position in RORγt-GFP reporter mice after UPEC UTI (lateral wall, 3 o'clock)

RORγt-GFP mouse catheterised with UPEC for 24 hours. Staining for smooth muscle actin (phalloidin-A647), CD3-PE, Class II-eFluor450 and anti-GFP-A488. Position with the bladder marked by the cartoon.

5.3 ILC depletion leads to alterations in MNP populations and their function

In the previous section, we saw that myeloid and lymphoid cells were spatially co-localised within the bladder in health and after UPEC infection. In the gut, it is known that ILC3s respond to cytokines produced by MNPs [125, 282, 429]. We therefore asked if there was a similar interaction between MNPs and ILC3 within the bladder. Figure 5.6 relates to experiments first presented in chapter 4 but focuses on MNP counts from the Rag2 KO anti-Thy1 UTI experiments. Following ILC depletion and UPEC challenge, there were alterations in MNP recruitment or maturation within the bladder. At 24 hours, we observed differences in MNP maturation with an increased proportion of immature Ly6c+ MNPs, relative to CII+ MNPs (there were no corresponding differences in CFU counts during this experiment, as shown in figure 4.20). In an independent experiment, using CX3CR1 as a tissue-residency MNP marker, as described by Bain et al. (2013 and 2014) as we had not yet introduced intravenous anti-CD45 labelling, we identified similar changes in the MNP compartment following ILC depletion (fig. 4.22) [112, 118].

At a later, 48 hour time point, the changes in monocyte proportions previously observed were present and persisted despite the increase in infective burden associated with ILC depletion (fig. 4.22). MNP counts from mice catheterised with UPEC for 48 hours are shown in figure 5.7. These findings suggested that ILC-depletion was associated with an increase in Ly6C+ monocyte numbers but a reduction in mature Ly6C-MHCII+ macrophages, which may have consequences for a successful immune response. Given the reliance within the bladder of a robust myeloid response to infection [365-369], perturbations in MNP populations are likely to have a profound influence on effectively eliminating pathogens. In particular, work from Schiwon et al. (2014) has demonstrated the importance of both Ly6c+ and Ly6c- MNPs in releasing cytokines for neutrophil recruitment and data from Mora-Bau et al. (2015) details the importance of MHCII+ MNPs (primarily populated by maturation of recruited monocytes) in the development of bladder response to UTI [2, 369]. Given the dependence on a functioning myeloid response in the bladder, we can assume that any change in MNP number and maturation could have an impact on the immune response during UTI.

Within the kidney, we did not observe any differences in monocyte numbers (see fig. 4.24), even in kidneys with pyelonephritis at 48 hours. Using the Rag2 KO model of UTI, infection levels were similar in the kidneys of ILC-depleted mice and monocyte counts were unaffected. In the bladder, infection was significantly worse at 48 hours and this correlated to increased monocyte recruitment (greater numbers of Ly6c+ MNP), but decreased monocyte maturation (MHCII+ MNP) (fig. 5.7). As already suggested, changes in the MNP response in the bladder may have implications for the containment of infection and prevention of spread to the kidneys.

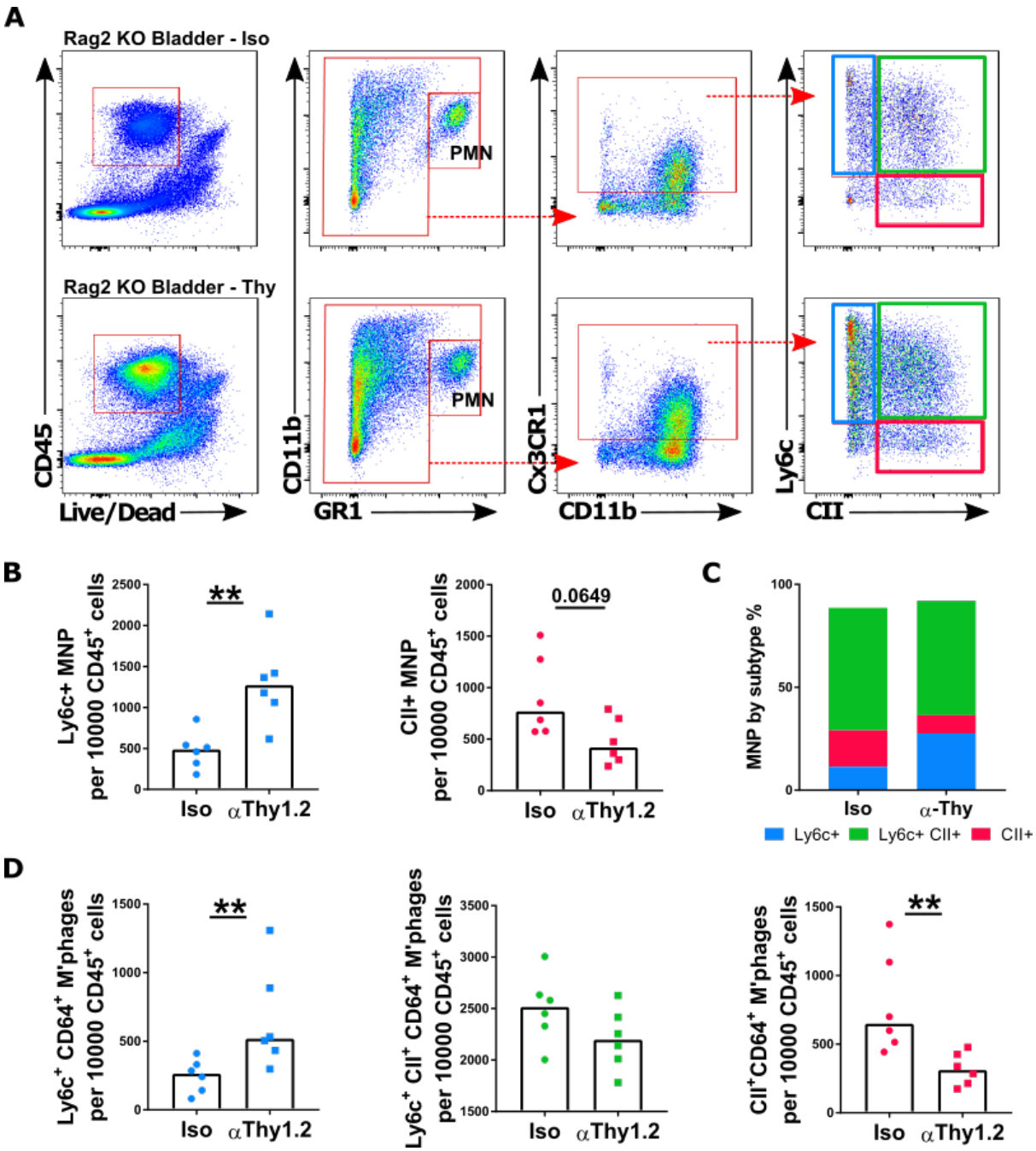

Figure 5.6: MNP proportions in bladders of Rag2 KO mice lacking ILCs in UPEC UTI at 24 hours

Rag2 KO mice treated with UPEC UTI (single catheterisation) for 24 hours, after pre-treatment with intraperitoneal anti-Thy-1.2 antibody or isotype to deplete ILCs. **A:** Gating strategy used to identify bladder MNPs. Flow panel: CD45-FITC, Live-dead-Aqua, CD11b-PerCPCy5.5, GR1-PECy7, CX3CR1-BV650, Ly6c-APC, CII-eF450 and CD64-PE (not shown). **B:** MNP counts from the monocyte waterfall; **p= 0.0043. **C**: MNP as a proportion of all CX3CR1+ MNPs (median summary data). D: Further gating of the MNP groups by CD64 (macrophage marker); **p= 0.0087 Ly6c+, **p= 0.0043 CII+. Values expressed as median with significance calculated using Mann Whitney tests, n=6 per group.

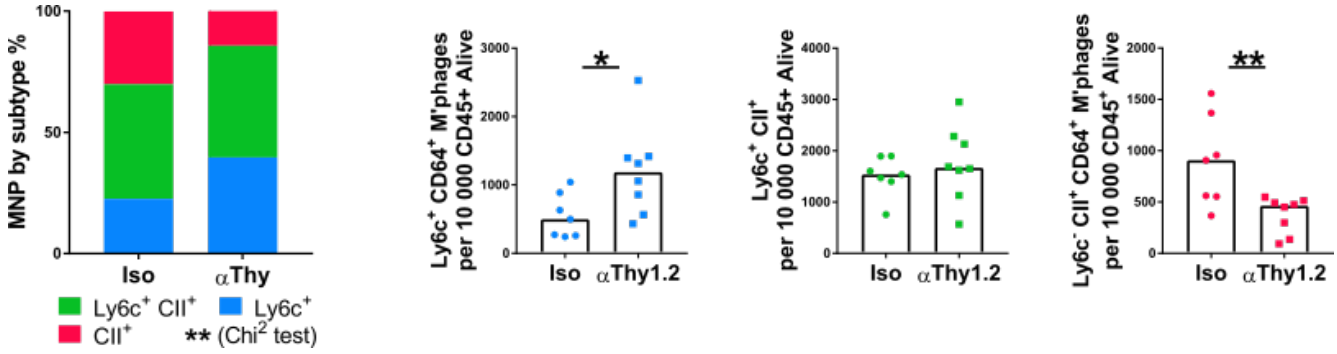

Figure 5.7: MNP proportions in bladders of Rag2 KO mice lacking ILCs in UPEC UTI at 48 hours

Rag2 KO mice treated with UPEC UTI for 48 hours (single catheterisation), after pre-treatment with intraperitoneal anti-Thy 1.2 antibody or isotype to deplete ILCs. Bladder monocyte counts from the monocyte waterfall and expressed as a proportion of the total CX3CR1 MNP population, chi-squared test **p= 0.0087. Macrophage populations (CD64+) within each part of the monocyte waterfall, *p= 0.0289, **p= 0.0059. Values expressed as median with significance calculated using Mann Whitney tests, results combined from two experiments, n= 7 Iso, n=8 Thy.

Using whole bladders from Rag2 KO mice infected with UPEC at 48 hours, we repeated qPCR experiments on the cytokines associated with ILC3 recruitment. These data points relate to the same bladders that demonstrated a significantly increased infective burden in mice treated with the ILC-depleting antibody, anti-Thy1.2 (figure 4.21A). Figure 5.8 shows changes to *Il1b*, *Il23a* and *Tnfsf15* (TL1A) transcripts between the two groups. In keeping with increased levels of infection, the cytokine transcripts *Il1b* and *Il23a* trended upwards, but *Tnfsf15* remained the same between the two groups. These changes did not reach significance.

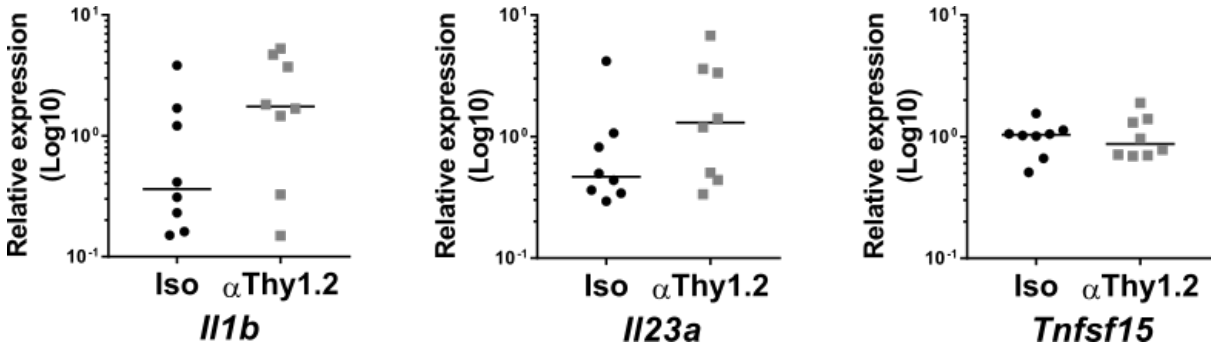

Figure 5.8: ILC3 stimulating cytokine transcripts after ILC-depletion from Rag2 KO murine bladders in UTI

Rag2 KO murine bladders treated with UPEC UTI for 48 hours, after pre-treatment with intraperitoneal anti-Thy1.2 antibody or isotype to deplete ILCs. Quantitative PCR of *Il1b, Il23a* and *Tnsfs15* transcripts expressed relative to *Hprt* and the control group (Isotype). Values expressed as median from two experiments, n= 8 Iso, n=8 Thy.

Using a publicly available RNA seq. dataset, we looked at the same cytokines from whole bladders catheterised with UPEC and harvested after eight hours [3]; the heatmap for *Il23a*, *Il1b* and *Tnfsf15* transcripts is shown in figure 5.9A. This experiment compared WT and CD14 KO animals and the heatmaps relate to ILC3 stimulating cytokines (fig. 5.9A), ILC3 products (fig. 5.9B) and AMPs (fig. 5.9C). This allowed us to interrogate the effect of MNP depletion during UTI, by comparing the CD14 KO and WT animals. The authors chose an eight hour time point, as this was when *Cd14* transcripts were at their highest (although data pertaining to infection was presented at 21-24 hours in this paper and showed a significant increase in CFU within the bladder tissue). The CD14 cells they identified showed transcriptional profiles that included *Emr1* (F4/80) and the co-stimulatory molecules, Cd80 and Cd86. This means that these cells are most likely to be equivalent to the mature or maturing populations of MNPs that we have found (MHCII+ MNPs) using the monocyte waterfall.

At the early, eight hour time point, differences could be seen in the expression of key ILC3 stimulating cytokines and products, confirming the role of MNPs in promoting IL-17 and IL-22 immune responses. It is possible therefore that the 48 hour time point used to produce the qPCR data in figure 5.8 was too late and an earlier time point might have yielded changes in these cytokine transcripts (*Il23a, Il1b* and *Tnfsf15*). Figure 5.9C shows how the impaired CD14 response also translated to decreased levels of AMPs in the KO group. The emphasis on early cytokine production and MNP/ILC stimulation reinforces the principle of a pre-positioned homeostatic immune network within tissues poised to respond rapidly to infective threats. Through appropriate local immune cell activation, development of a larger and more robust immune response can be promoted. This highlights the potential significance of ILC-depletion on impaired MNP maturation and the subsequent broader immune system dysfunction, such as impaired recruitment of neutrophils.

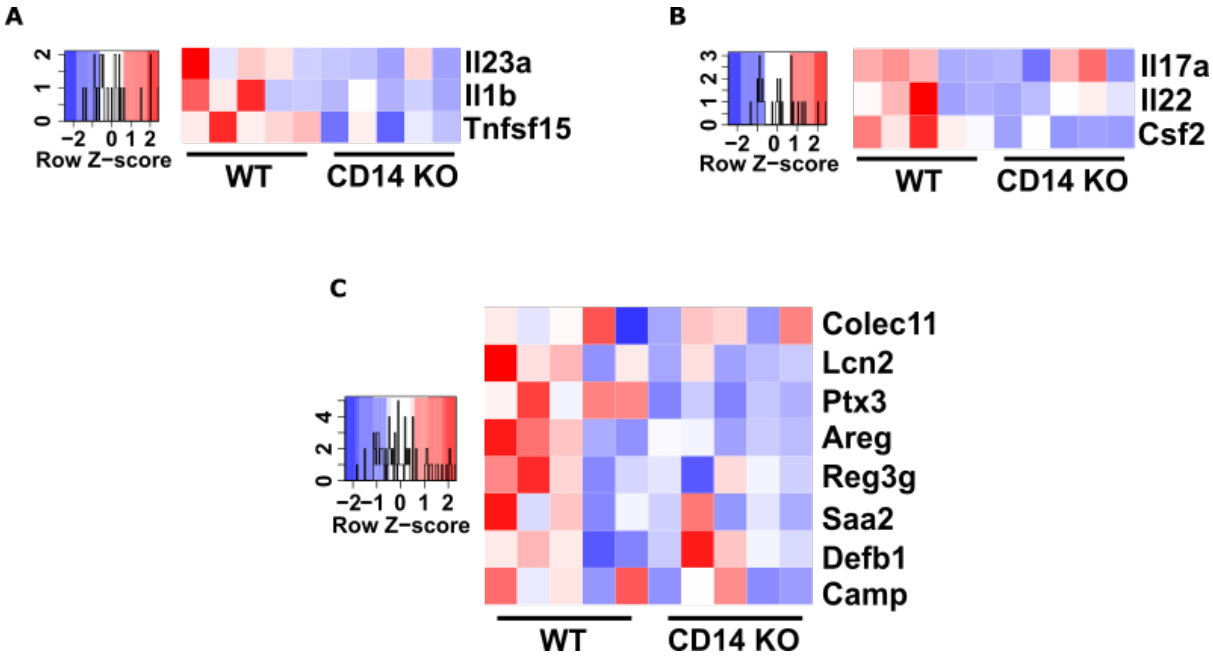

Figure 5.9: RNA sequencing from whole bladders comparing WT and CD14 KO mice in UTI

Heatmaps showing RNA sequencing data from bladders catheterized with UPEC and harvested at eight hours. WT=5, CD14 KO=5. **A**: ILC3 stimulating cytokines. **B**: ILC cytokine products. **C:** AMPs. Data interrogated from Carey et al., 2016, accession number GSE68220 [3].

Given that *Il17a* transcripts were the most reduced of the ILC3-associated cytokine transcripts within the bladders of Rag2 KO following anti-Thy treatment (figure 4.21), we assessed macrophage responses to IL-17a stimulation *in vitro*. Addition of IL-17a to macrophage cultures led to increased phagocytosis of fluorescently labelled UPEC, as demonstrated in figure 5.10B. The increase in both geometric mean and percentage ingestion suggests increased phagocytic activity by each macrophage, as well as the population as a whole. In addition, we were able to demonstrate that macrophages expressed the receptor for IL-17a, by analysing flow sorted macrophages by RNA sequencing (figure 5.10A). The *Il17ra* gene is highlighted in red and shown alongside the GM-CSF receptor gene, *Csf2ra*. We can surmise therefore that MNPs are capable of responding to IL-17a in UTI and we have demonstrated that this cytokine can augment their phagocytic activity *in vitro*.

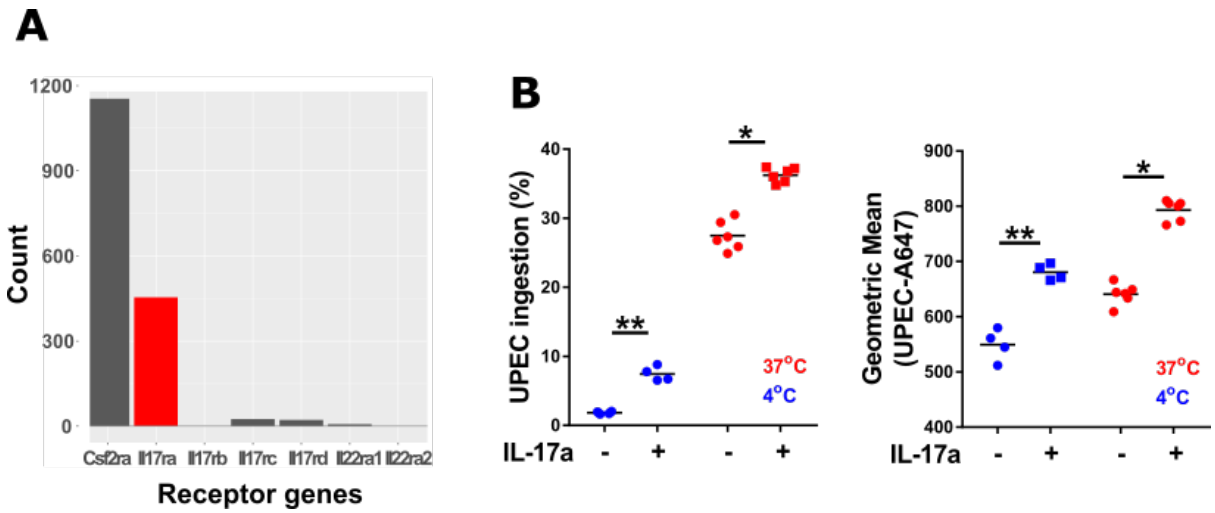

Figure 5.10: The role of IL-17a on macrophage function in UTI

A: Flow sorted macrophages from bladder after UPEC UTI (CD45+, F4/80+, CD64+). Transcript counts calculated using RNA sequencing to show relevant receptor expression, with the *Il17ra* receptor gene highlighted in red. **B**: Bone marrow derived macrophages from WT mice pre-stimulated with IL-17a (100ng/ml) for 24 hours prior to incubation with PBS or UPEC-A647 for one hour. Cells were harvested and stained with a live/dead marker and macrophage markers (CD45-BV650, CD64-PE and F4/80-FITC) to ensure purity. Significance calculated using Mann Whitney tests (**p=0.0022, *p=0.0286; n= 4-5).

As already described, we were unable to demonstrate cellular changes relating to ILC3-MNP cross-talk within the kidney, however we did observe differences in gene transcripts in our Rag2 KO UTI model that supports a role for these relationships. These data are shown in figure 5.11 and demonstrated that ILC depletion produced a significant decrease in *Il23a* and *Tnfsf15* and a trend towards decreased *Il1b* transcripts within the kidney. This was particularly striking for *Tnfsf15* transcripts, which were decreased in animals with sterile and septic kidneys (determined as culture negative and positive, respectively, though sterile kidneys may have been exposed to the pathogen).

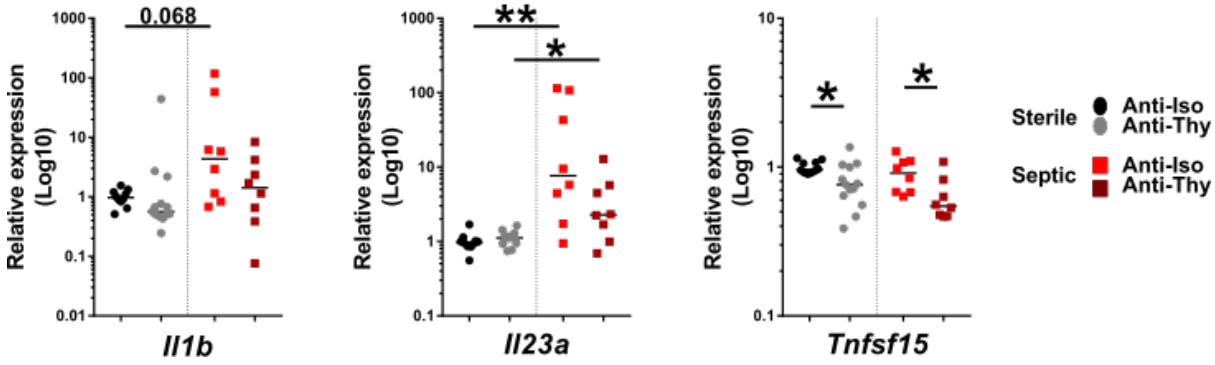

Figure 5.11: Transcripts of ILC3 stimulating cytokines from kidneys of Rag2 KO mice without ILCs exposed to UPEC

Rag2 KO mice pretreated with anti-Thy1.2 antibody or isotype at 48 hours. Kidneys were harvested and RNA extracted from cell suspensions. ILC3 stimulating cytokines. *Il23a* **p= 0.0021, *p= 0.0246; *Tnfsf15* *p= 0.0214 (sterile), *p=0.0148 (septic). Results combined from 3 experiments, median data shown and significance calculated using Mann Whitney tests.

Taken together these data support a role for ILC3-MNP cross-talk in defence against UTI and this was of particular relevance within the bladder, though key transcriptional changes were also evident after ILC-depletion in the kidney. In the following section, we performed UTI experiments on mice lacking the cytokine IL-1β or the receptors for IL-23a and IL-1β, to assess the role of these cytokines in more detail.

5.4 ILC3 activation by MNPs during UTI

We performed several UTI experiments using mice lacking the IL23R, kindly gifted by Prof Gordon Dougan and Dr Simon Clare. We did not see a significant difference in CFU counts in either the bladder or the kidney at 24 or 48 hours, even when results were combined across five experiments (data not shown, but representative CFU values from a single experiment are shown in figure 5.12B). The following figure demonstrates the gating strategy used to identify tissue-resident cells within the bladder, using an intravenous CD45 labelling antibody prior to schedule 1 (fig. 5.12A). Myeloid populations were easy to identify within the infected bladder and a macrophage population of Ly6c+, F4/80+ and CD11b+ cells predominated, consistent with data from our other murine UTI models.

The CFU burden was equal between the WT and control groups, indicating that loss of the IL-23R did not significantly impair the ability of the bladder to mount an immune defence against the pathogen at 16 hours (fig. 5.12B). We did not see any cellular differences within the bladder, despite indications from earlier experiments that T cell recruitment might be affected at 24 hours (figures 5.12C & 5.13A). In these earlier experiments we did not use IV CD45 labelling and so cell counts were expressed as a proportion of CD45+ alive cells and are therefore not directly comparable. Within the kidney, the CFUs indicated that there might be a trend towards increased pyelonephritis at 24 hours and the renal tissue demonstrated significantly decreased recruitment or proliferation of T cells (fig. 5.13B). A trend towards decreased T cell recruitment was also observed within the bladder at this time point (fig. 5.13A).

To assess T cell recruitment at a later time point, we performed five experiments at 48 hours, but this did not show any difference between the groups within either the bladder or kidney (data not shown). It is possible therefore, that T cell recruitment is at its most vulnerable at 24 hours of infection, but compensatory mechanisms exist to overcome the loss of IL-23 signalling throughout the renal tract thereafter.

The ILC count was more difficult to assess within the bladder, owing to the need to split the tissue in order to perform CFU quantification and flow cytometry. As described within chapter 3, ILC identification requires multi-colour flow cytometry panels and the proportion of lineage negative cells was heterogenous and small. It is therefore not surprising that we were unable to demonstrate any changes to ILC recruitment within the bladder (fig. 5.12C), as absolute cell numbers were very low, and this result should be interpreted with caution accordingly.

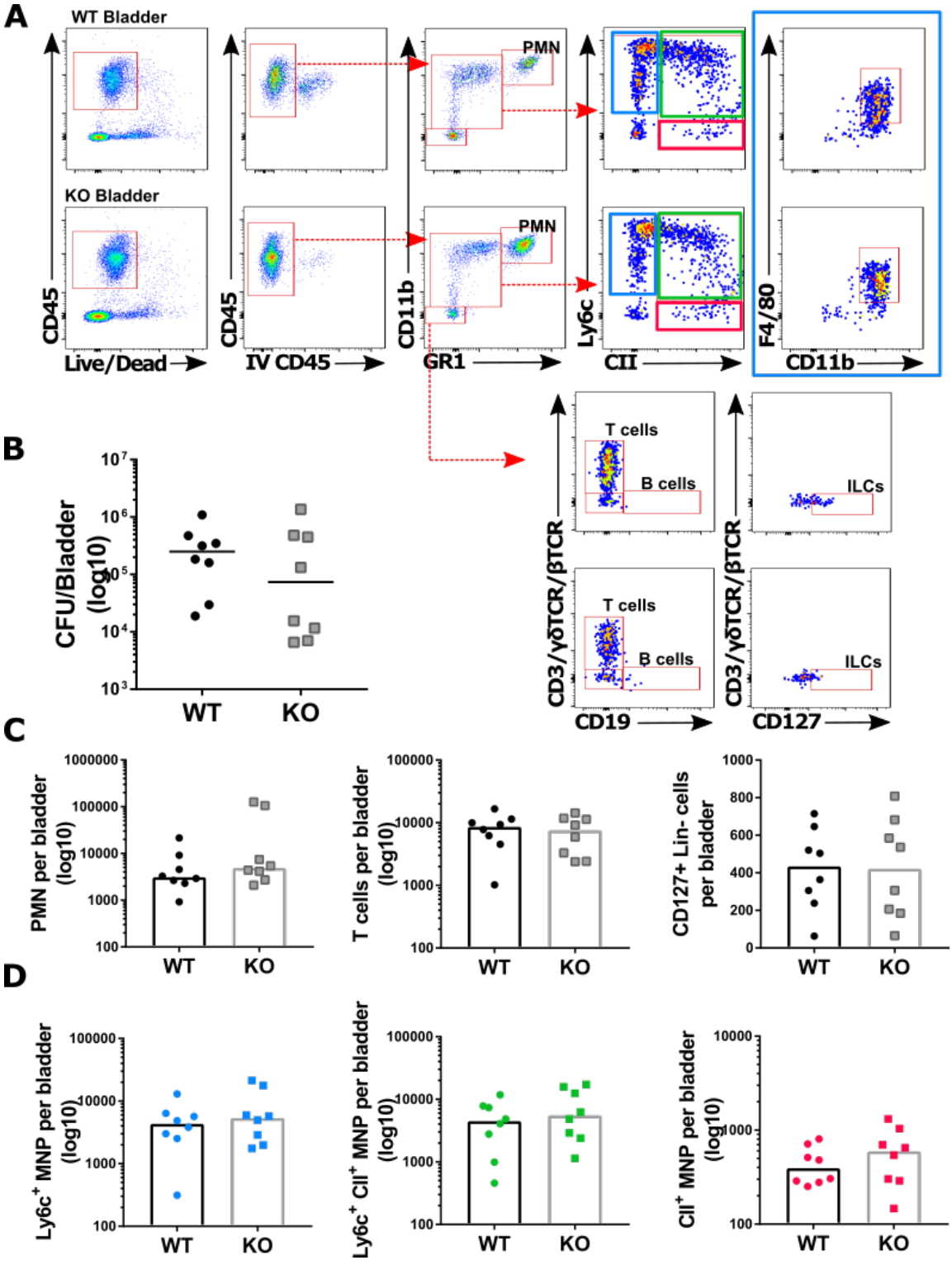

Figure 5.12: Infection severity and cell counts from bladders of IL23R KO mice after UPEC UTI

IL23R KO mice treated with UPEC for 16 hours (single catheterisation) and given an IV anti-CD45-FITC injection prior to sacrifice. **A**: Gating strategy to identify different monocyte and lymphoid populations. Flow panel included CD45.2-PECy7, Live/Dead-Aqua, CD11b-PerCPCy5.5, GR1-A780, Ly6c-APC, CII-BV650, F4/80-BV605, CD3/γδTCR/βTCR-eF450, CD18-BV785 and CD127-PE. **B**: CFU per bladder. **C**: Neutrophil, T cell and ILC counts per bladder. **D**: Monocyte counts per bladder. All data shown with median bar, n=8 both groups.

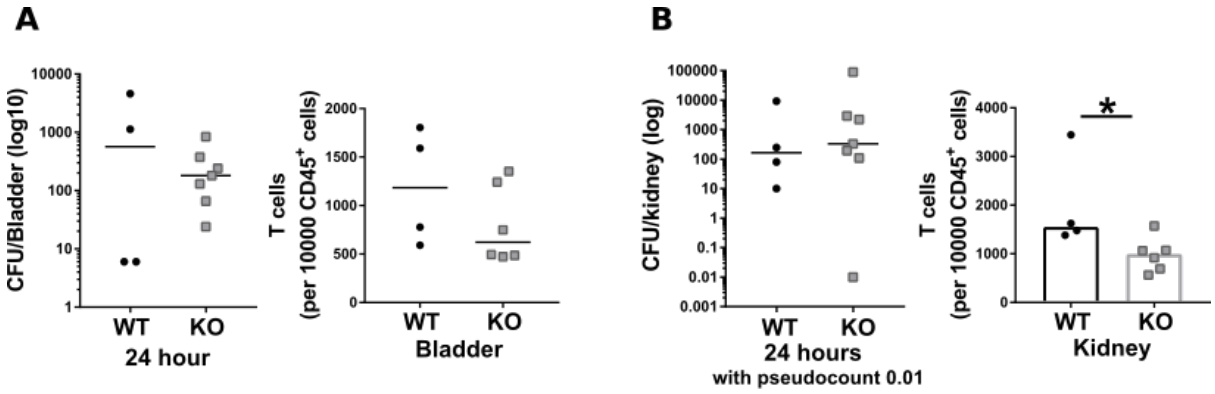

Figure 5.13: Infection severity and T cell counts from bladder and kidneys of IL23R KO mice after UPEC UTI

IL23R KO mice treated with UPEC for 24 hours (single catheterisation) CFU and T cell counts from bladder (**A**) and kidney (**B**). T cell kidney count, *p= 0.0381. Kidneys were combined and analysed together (ie: 1 data point per mouse). All data shown with median bar and a pseudocount added to the kidney CFU data, as pyelonephritis was absent in one animal; n=4 KO, n=7 WT.

The corresponding gating strategy and cell counts from kidneys infected with UPEC for 16 hours are shown in figure 5.14. In keeping with the previous observations at 24 hours, T cell numbers were decreased relative to control animals, in mice that developed pyelonephritis. We also saw a decrease in the total number of ILCs at 16 hours. This decrease is likely predominantly to represent ILC3s, owing to their association with IL-23 stimulation. Although we established that relative innate immune cell populations, such as ILCs were lower in the kidney, the absolute numbers of cells were higher than in the bladder (figure 3.6). This made gating and calculation of renal ILC counts per organ more reliable.

Whilst it has not been possible to prove the effect of IL-23 signalling on ILCs within the bladder in UTI, the effect on renal ILCs and T cells suggested that the renal tract did depend on this axis for optimal immune defence in UTI. This seemed to be particularly important in the initial 24 hours of infection, when cells were being first recruited to the relevant tissue. To investigate the IL-23/IL-17 axis in more detail, we performed qPCR on whole bladders and kidneys infected with UPEC. Whole bladder tissue showed decreased levels of *IL17a* transcripts in KO animals, in keeping with the loss of IL-23 stimulation (figure 5.15B). Interestingly, *Il17a* transcript levels rose with the CFU value in WT animals, but not in the KO group. This finding is expressed most clearly using the correlation shown in figure 5.15C, illustrating the relationship between infection and *Il17a* production during IL-23-deficiency more clearly. Csf2 transcripts rose and this most likely related to the trend towards increased levels of infection within the knock out group (figure 5.15A). Panel D shows that other

pro-inflammatory cytokines were largely unaffected, though there was an emerging trend towards decreased levels of *Tnfsf15*.

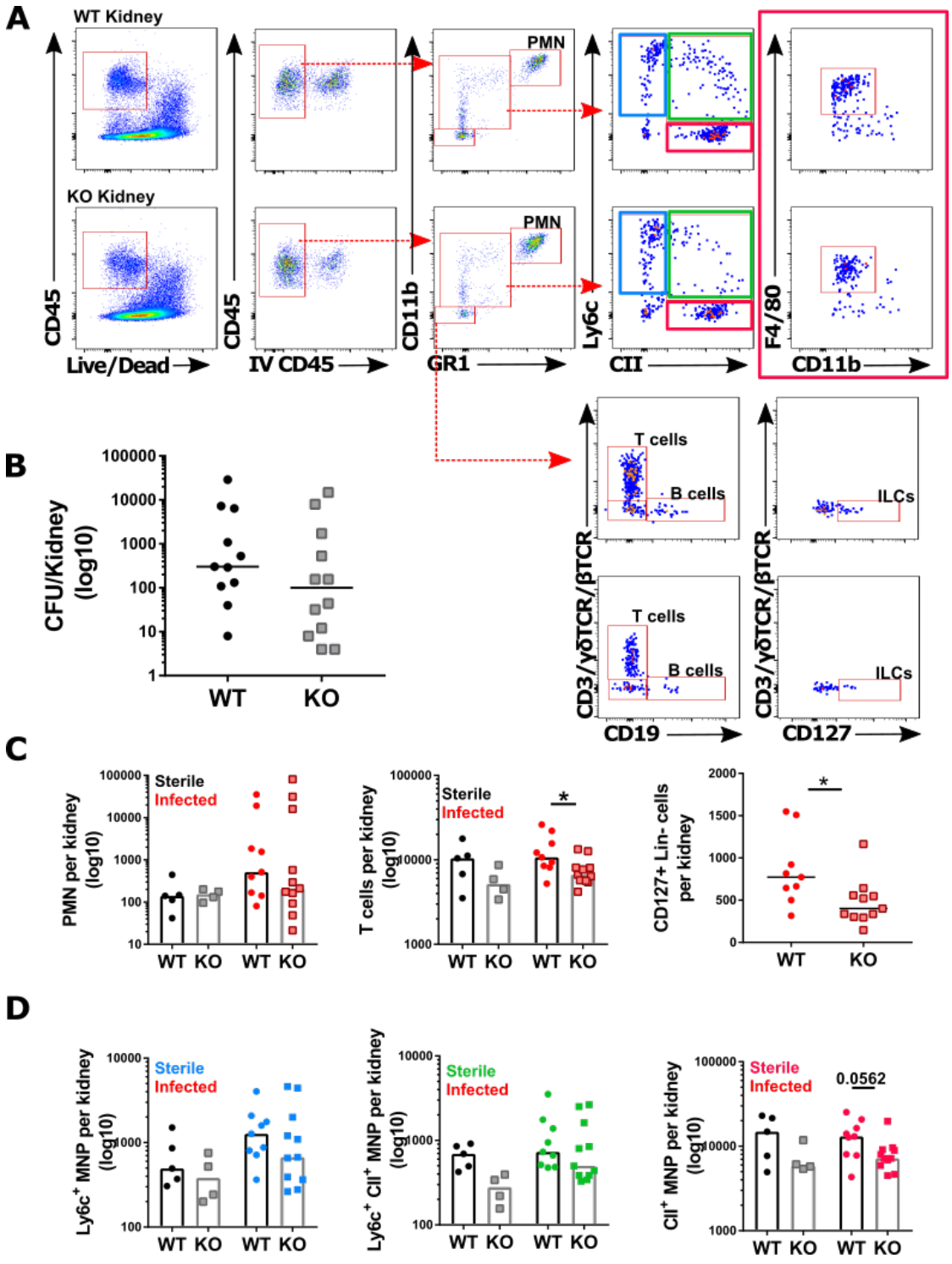

Figure 5.14: Kidney infection severity and cell counts after 16 hour UPEC infection in IL23R KO mice

IL23R KO mice treated with UPEC for 16 hours (single catheterisation) and given an IV anti-CD45-FITC injection prior to sacrifice. **A**: Gating strategy to identify different monocyte and lymphoid populations in kidney. Flow panel included CD45.2-PECy7, Live/Dead-Aqua, CD11b-PerCPCy5.5, GR1-A780, Ly6c-APC, CII-BV650, F4/80-BV605, CD3/γδTCR/βTCR-eF450, CD18-BV785 and CD127-PE. **B:** CFU per bladder. **C**: Neutrophil, T cell (*p= 0.0251) and ILC counts (*p= 0.0159) per bladder. **D**: Monocyte counts per kidney. All data shown with median bar and significance calculated using Mann Whitney tests; n=8 both groups.

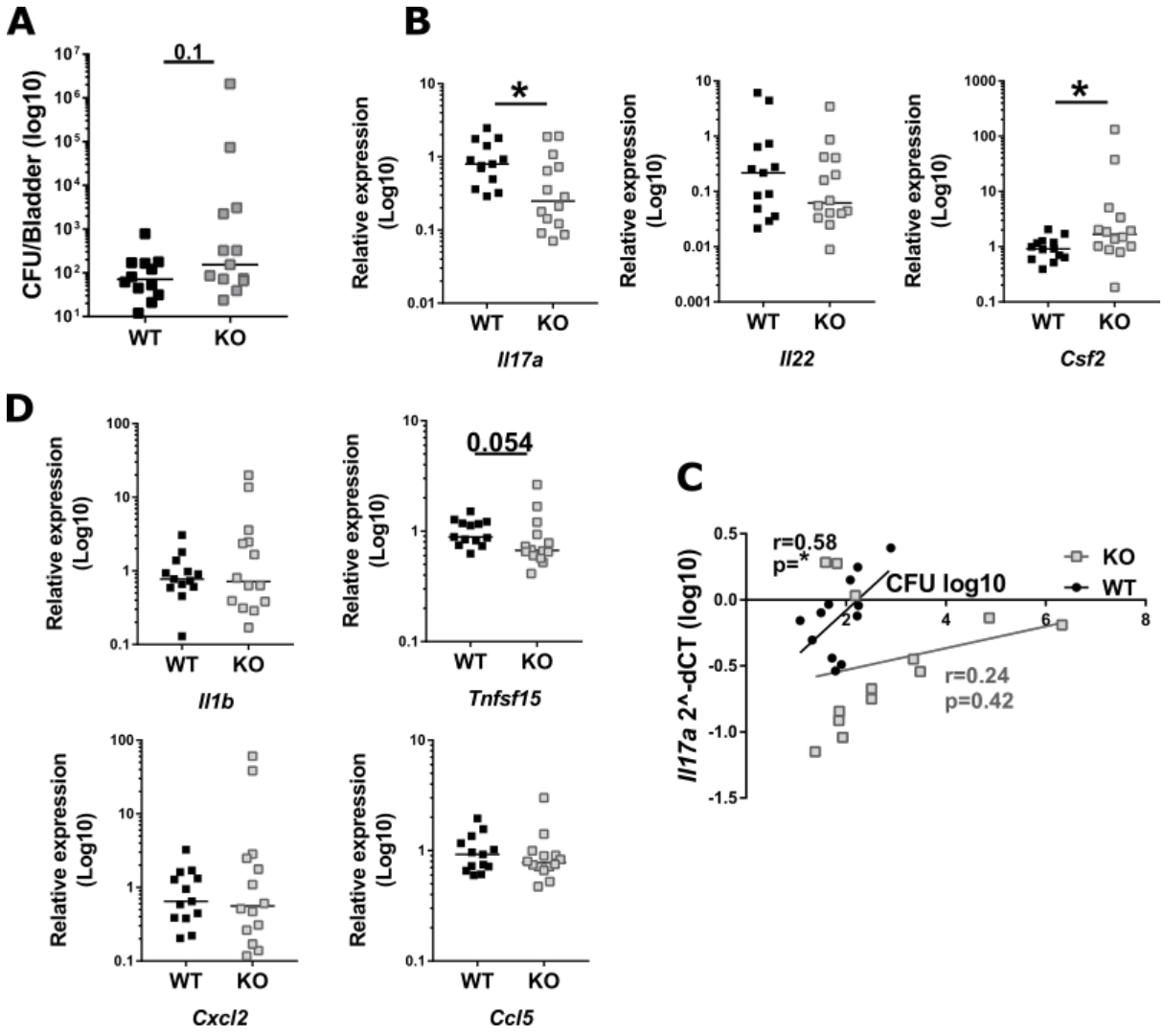

Figure 5.15: Cytokine transcripts from bladders of IL23R KO mice during UPEC UTI

IL23R KO mice treated with UPEC for 48 hours. Whole bladders extracted for qPCR. **A**: CFUs from the relevant UTI experiments in bladder. **B**: ILC3 associated cytokines; *p= 0.0222 Il17a and *p= 0.0291 Csf2. Mann Whitney tests. **C**: Il17a transcripts plotted against the corresponding CFU value; p=* 0.0463 calculated using Pearson's correlation. All results shown with median bars, 3 experiments combined; n=12-13 WT, n= 12 KO.

We went on to test for various AMPs and epithelial regeneration factors, but these did not show a difference between groups, other than increased *Camp* (cathelicidin) transcript levels in relation to increased infection levels (figure 5.16).

There was very limited qPCR data from renal tissue, as so few kidneys developed pyelonephritis during our single catheterisation experiments. As such, this data was inconclusive and so is not shown.

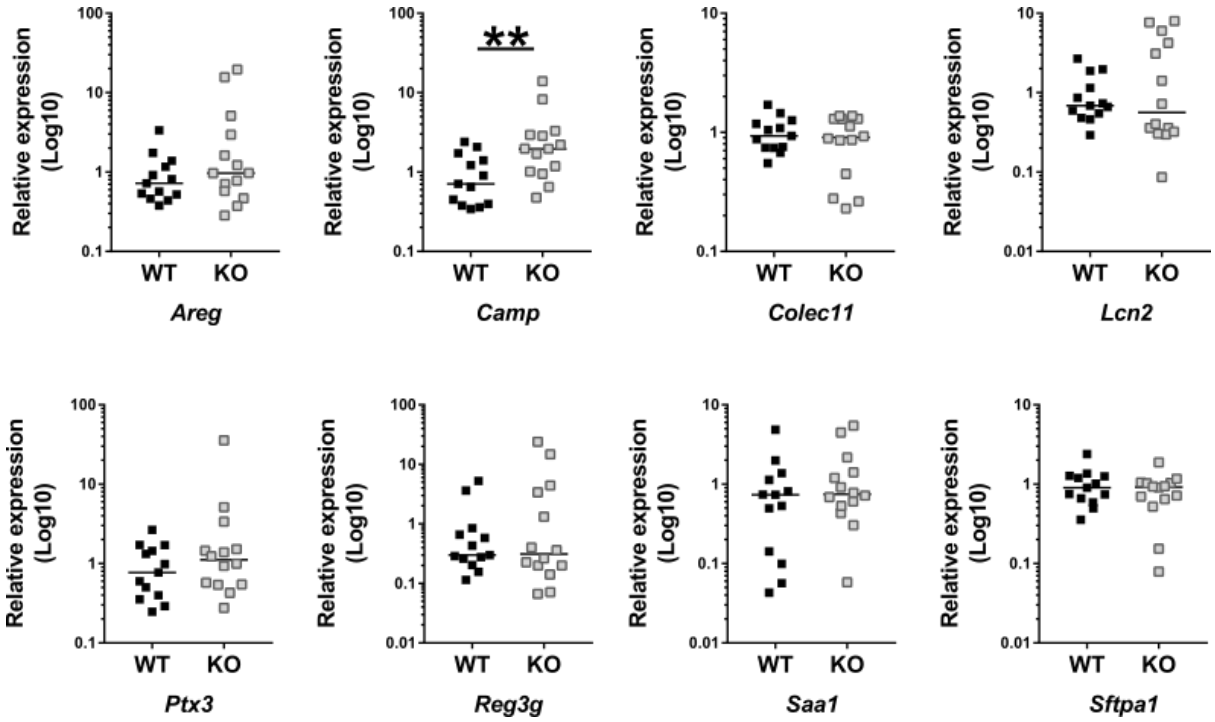

Figure 5.16: AMP transcripts from bladders of IL23R KO mice during UPEC UTI

IL23R KO mice treated with UPEC for 48 hours. Whole bladders extracted for qPCR of AMP transcripts; *p= 0.0019 Camp. Median data and Mann Whitney test. Results summarized from 3 experiments; n=12-13 WT, n= 12 KO.

The cytokine, IL-1β is associated with ILC3 activation [127, 318] and so we performed UTI experiments on IL-1β KO mice, kindly gifted by Dr Murray Clarke. This allowed us to explore the importance of this axis of communication between MNPs and ILC3s within the renal tract. The experiment was performed once with the results shown in the following figures. Figure 5.17 relates to bladder tissue collected after a single catheterization with UPEC, duration 24 hours. The same flow cytometry panel was used in this experiment, as that used in figures 5.12 and 5.14 with the omission of anti-CD127-PE. The gating strategy is illustrated in figure 5.16A. Clear populations of MNPs, T cells and lineage negative cells could be distinguished and the relevant cell counts are shown (fig. 5.17C). There was a trend towards decreased recruitment of these cells, but due to the limited number of mice available, the study was too underpowered to draw significant conclusions. MNP numbers were also reduced across all three subtypes within the bladder in the KO animals (fig. 5.17D) and this raises the possibility that these counts were diminished in response to the slightly lower levels of infection in the KO group (CFUs shown in fig. 5.17B).

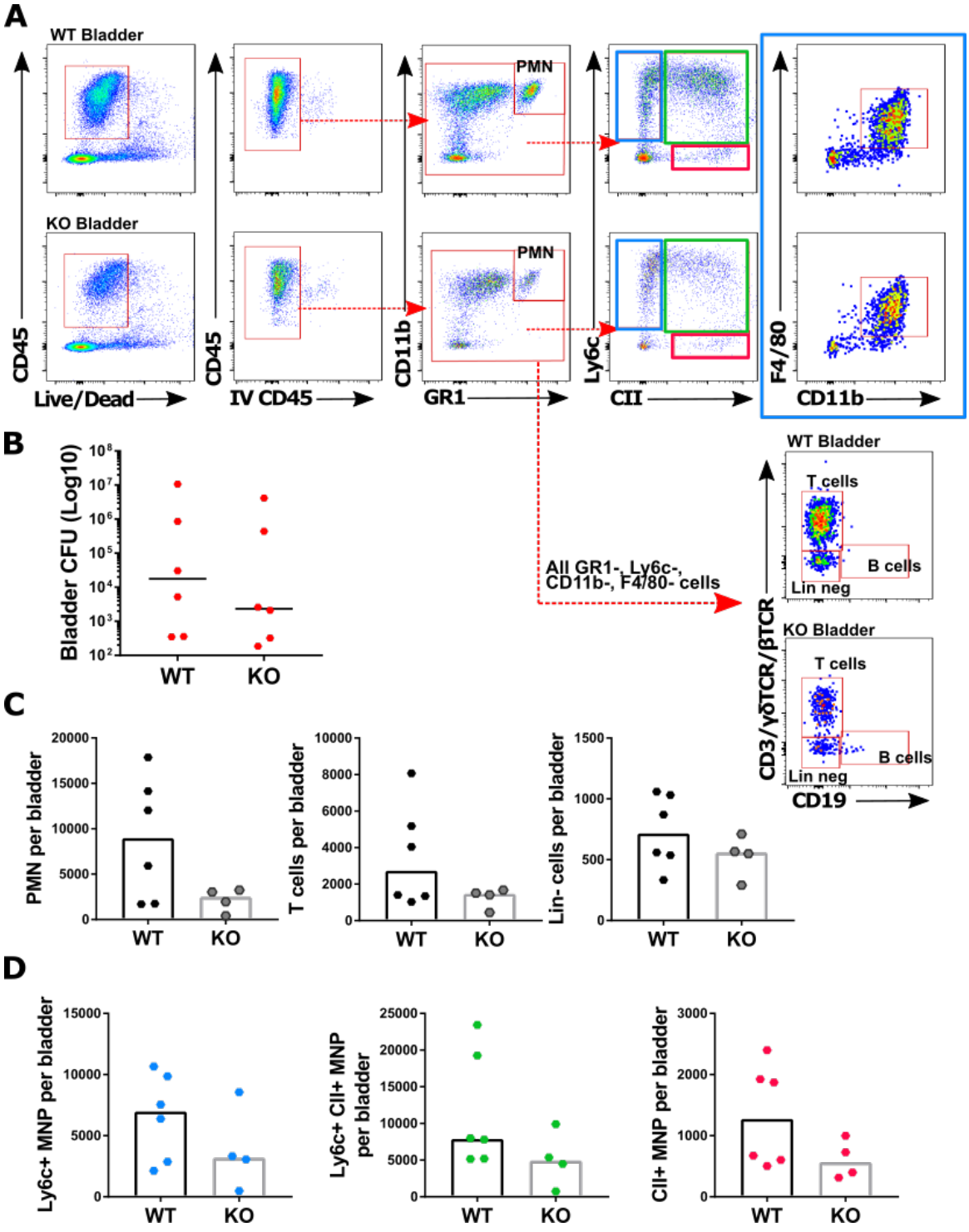

Figure 5.17: Bladder infection severity and immune cell counts from IL-1β KO mice after UPEC UTI

IL-1β KO mice treated with UPEC for 24 hours (single catheterisation) and given an IV anti-CD45-FITC injection prior to sacrifice. **A**: Gating strategy to identify different monocyte and lymphoid populations. Flow panel included CD45.2-PECy7, Live/Dead-Aqua, CD11b-PerCPCy5.5 , GR1-A780, Ly6c-APC, CII-BV650, F4/80-BV605, CD3/γδTCR/βTCR-eF450, CD18-BV785 and CD127-PE. **B**: CFU per bladder. **C**: Neutrophil, T cell and lineage negative cell counts per bladder. **D**: Monocyte counts per bladder. All data shown with median bar, n=6 per group. Some cells were lost for flow cytometry leading to 4 data points in the KO group.

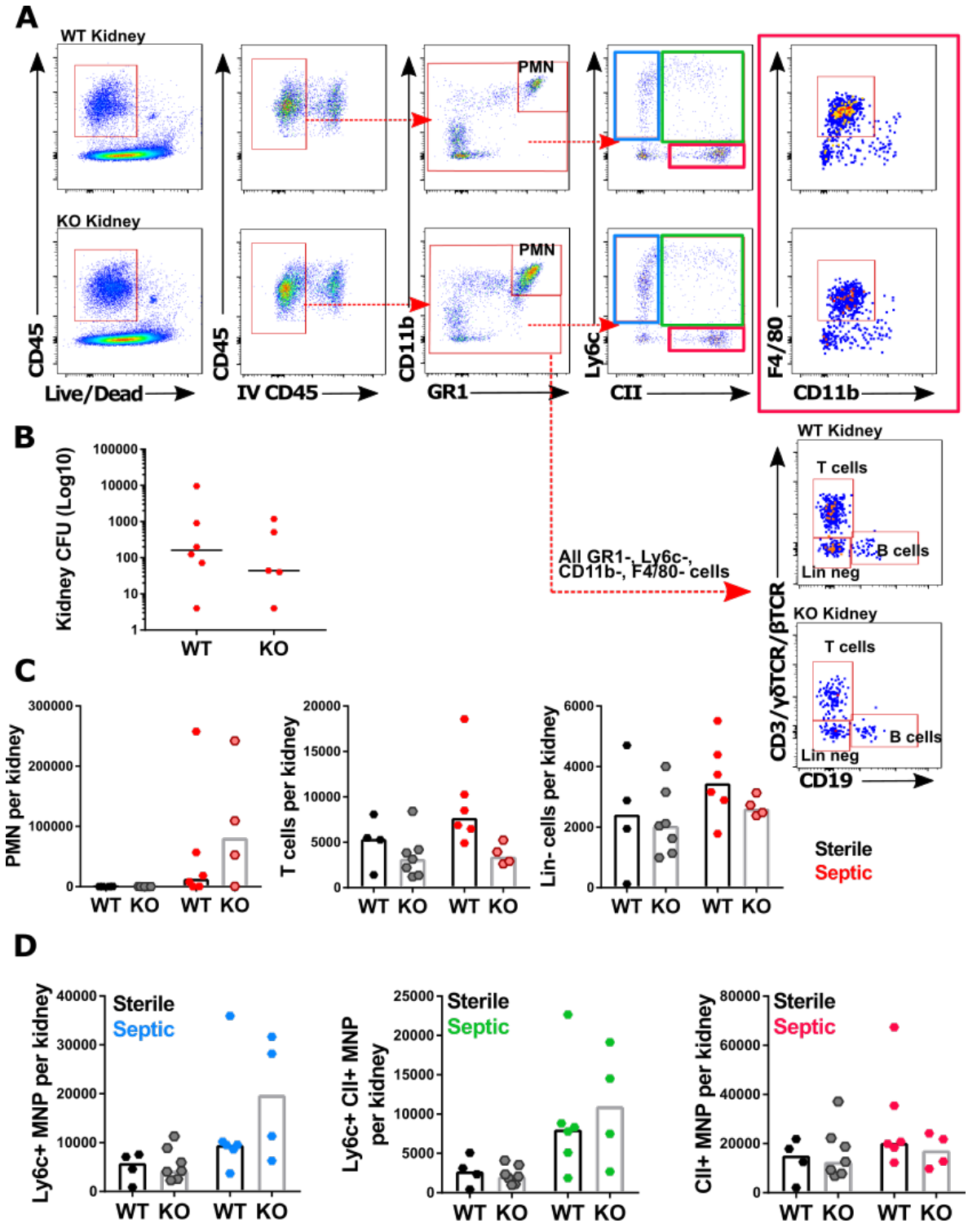

Figure 5.18: Infection severity and immune cell counts from kidneys of IL-1β KO mice after UPEC UTI

IL-1β KO mice treated with UPEC for 24 hours (single catheterisation) and given an IV anti-CD45-FITC injection prior to sacrifice. A: Gating strategy to identify different monocyte and lymphoid populations. Flow panel included CD45.2-PECy7, Live/Dead-Aqua, CD11b-PerCPCy5.5, GR1-A780, Ly6c-APC, CII-BV650, F4/80-BV605, CD3/γδTCR/βTCR-eF450, CD18-BV785 and CD127-PE. B: CFU per bladder. C: Neutrophil, T cell and lineage negative cell counts per kidney. D: Monocyte counts per bladder. All data shown with median bar, n= 6 per group.

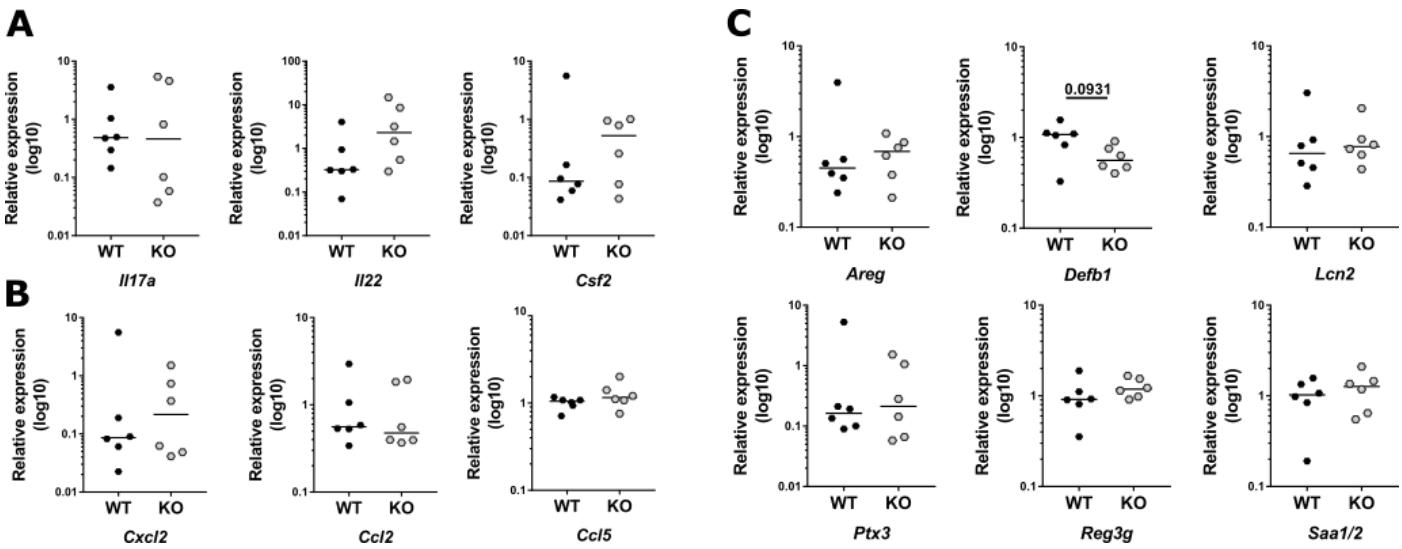

Figure 5.19: Cytokine, chemokine and AMP transcripts from bladders of IL-1β KO mice after UPEC UTI

IL-1β KO mice treated with UPEC for 24 hours (single catheterisation). Bladders harvested for CFU, flow cytometry and qPCR (see figure 5.17). A: ILC3 associated cytokines. B: Proinflammatory cytokines. C: AMPs associated with the renal tract. Median data shown with Mann Whitney tests; n=6 per group.

A similar panel is presented in relation to kidneys harvested at the same time, though the rate of pyelonephritis was lower owing to the single catheterisation. CFU values were evenly spread across WT and KO kidneys that had become infected. The trend towards decreased lymphoid cell recruitment in the bladder persisted within the kidney, which may be linked to the loss of IL-1β signalling (figure 5.12C). Neutrophil and MNP counts were unaffected in the KO group, though greater numbers of infected kidneys are required to draw conclusions.

Changes to transcript levels of cytokines associated with ILCs and increased inflammation were assessed during the same experiment but did not reveal any significant findings (figure 5.19). This finding was consistent between bladder and kidney (data not shown), even when groups were analysed according to the presence or absence of pyelonephritis.

5.5 Discussion

5.5.1 Key aims

The data presented in this chapter has focussed on two key aims:

1. To determine the anatomical relationship of tissue-resident MNPs and ILC3s within the renal tract, and the extent to which they may be co-localised to promote cross-talk.
2. To investigate MNP and ILC3 cross-talk via cytokine production during UTI and to ascertain whether this reciprocal relationship might potentiate an anti-bacterial response.

Microscopy proved a powerful tool to reveal the dense network of immune cells present within the bladder. MNPs were easily identified throughout the bladder layers and some were spatially co-localised adjacent to ILCs in health and disease. The stellate appearance of MNPs within the urethra was particularly striking, as this is the entrance to the bladder and an area where we would expect heightened pathogen-surveillance. We were also able to identify ILC3s by microscopy and observed many T cells occupying similar niches. These will likely be comprised of conventional T cells, γδ T cells, invariant T cells and other intraepithelial lymphocytes. These tissue-resident lymphocyte and lymphoid cells represent a spectrum of T cells that span the innate and adaptive system. There are functional similarities between ILC3s and some T cell subsets and the data produced within this chapter must be interpreted within this context. However, emphasis was placed on distinguishing T cells by using a robust CD3 marker, as well as experiments with Rag-deficient mice. Equally, it is important to remain mindful that these populations may form cohesive, heterogenous biological networks, that together deliver and optimal tissue-specific immune response. Together, our microscopy images show that MNPs, T cells and ILCs occupied the same urothelial niche and were poised to interact in both health and infection.

Critical to isolating the effect of ILCs in UTI, was ensuring that the effect of T cells (of whichever type) was eliminated from that of ILCs. The Rag2 KO +/- anti-Thy1.2 depletion experiments were particularly useful in achieving this, owing to the lack of lymphocytes at baseline. It is within this context that we were able to demonstrate perturbations in MNP recruitment and maturation and their associated transcriptional changes most clearly. It seems likely, given this data, that ILC3s do affect MNPs throughout the renal tract and this contributes to the increased levels of infection that we have observed within the bladder. This data compliments that published by Riedel et al. (2017) who were able to show that populations of $CD11b^{hi}F4/80^{int}$ MNPs were reduced in a sterile model of glomerulosclerosis in *Rag2*$^{-/-}$ mice, but not in the dual knockout *Rag2*$^{-/-}$ *IL2rcg*$^{-/-}$ mice [129]. These dual KO mice lack lymphocytes and ILCs and the authors attributed the effects to ILC2s, as the

adriamycin-induced renal injury was driven by type 2 immunopathology and the cytokine IL-33 (ILC2-stimulating) was used. It is likely, therefore, that myeloid cell recruitment and maturation can be influenced by all ILC subtypes and the nature of the immune insult/response will guide whether this is related to cells that produce Th1, Th2 or Th17-type cytokines. Whilst removing lymphocytes from our murine model was useful, it must be acknowledged that the control mice used (Rag2 KO) are therefore not wild type and we must accept the inherent immune system alterations at baseline.

Given that the dominant effect of ILC-depletion in the Rag2 KO experiments was a reduction in *Il17a* transcripts, we went on to interrogate macrophage responses to this cytokine. IL-17 stimulated BMDMs more effectively phagocytosed bacteria *in vitro*. It seems, therefore, that the effect of ILC-depletion and IL-17a loss on myeloid cells could be two-fold: firstly, recruitment/maturation of cells from the circulation and secondly, promoting effective bacterial clearance by phagocytes, thus defining two important outcomes of ILC3-MNP crosstalk during UTI.

Analysis of the RNA seq. data from Carey et al. (2016) allowed us to further interrogate ILC3-MNP interactions from the reverse perspective, as these experiments utilised MNP-depletion, rather than ILC-depletion. The early time point utilised suggests that any transcriptional effects were more likely to be associated with changes to tissue-resident or rapidly recruited cells of the innate immune response within the bladder. The data showed that myeloid cells were critical for the increase in IL-17, IL-22 and GM-CSF-associated inflammation, and that this impacted AMP production, with a likely net effect of reducing pathogen neutralisation and epithelial repair. It is not possible to say if the loss of AMPs were a direct result of CD14+ cell depletion, or due to indirect mechanisms, by which MNP-associated cytokines stimulated epithelial cell AMP production. It is likely to be a combination, as AMPs can be produced by both myeloid and epithelial cells, as described in section 1.2.2 [51].

Taken together, these data support a role for ILC3-MNP cross-talk in response to UTI, both for a robust pro-inflammatory immune response to clear the pathogen and an effective epithelial response to preserve barrier integrity and prevent septicaemia.

Identifying the triggers for effective ILC3 activation was more difficult and we used IL23R and IL-1β KO murine models to assess the contribution of these cytokines. In both cases, we have seen evidence to support decreased lymphocyte and ILC recruitment in both the bladder and kidney. Timing was important in these experiments, as T cell numbers at 16 hours were the same within the bladder in our IL23R KO UTI model, however at 24 hours there was a trend towards decreased recruitment. This response was more pronounced in the kidney, where organs affected by pyelonephritis showed both decreased T cell and ILC expansion. Similar trends were also observed in the IL-1β KO UTI experiment at the level of both bladder and kidney, though these results did not

reach significance. It is likely therefore, that there is some redundancy in their action and that these cytokines are working together to create an effective ILC response, as has been observed in other disease systems [282], but this will require more precise delineation with additional experiments. It also helps to explain some of the variability observed during the IL23R UTI repeats, as the effect of multiple activating factors and their associated synergy creates more complicated patterns of cell activation and immune compensation.

We also observed changes to *Tnfsf15* expression that implicate TL1A as a third co-stimulator of ILC3s in the urinary tract. A TL1A-deficient murine model was unavailable to us but performing further experiments on single gene knockouts is unlikely to provide significant results. As other work has shown, these stimulatory cytokines work together synergistically [282]. TL1A requires accompanying cytokines to activate T cells, NK cells and ILCs, though this activation demonstrates disease specificity, such as ILC2 activation in allergic versus helminthic lung disease [325, 326]. These activating pathways are further complicated by membrane-bound and soluble forms of TL1A that have been shown to activate adaptive and innate immune cells in the context of type 2 inflammation respectively [430]. Furthermore, TL1A expression has relevance within the renal tract, as DR3 was shown to be expressed by the renal epithelium and TL1A by MNPs in the context of allograft rejection and to promote renal injury [431]. This paper reported that TL1A was not found in the urine of these patients and we might infer that the soluble form was endocytosed by renal epithelial cells (as indicated by their *in vitro* experiments) and was not readily available in this context. This complements the adaptive immune pathology associated with the cases of antibody-mediated rejection presented, which rely on membrane-bound forms of TL1A [430]. It remains to be seen if, in the context of acute UTI, the soluble form of TL1A might be available within the renal tract, particularly the bladder, to contribute to innate immune cell activation.

In summary, this work contributes to our understanding of the complex relationships that exist between MNPs and ILC3s in the renal tract in both health and urinary tract infection. In relative terms, the bladder has been a neglected in terms of research, but a rich innate immune network resides within the urothelium. The data presented begins to delineate early innate immune mechanisms involving ILC3s and MNPs, and how their cross-talk promotes an effective immune response in the bladder to combat a more serious ascending infection.

5.5.2 Limitations

Although there are some parallels between gut and bladder, namely a dense and highly specialised epithelial surface, ranks of tissue-resident immune sentinels, a microbiome and close proximity to an

external surface, there are also key differences which may influence ILC maturation, maintenance and function. These factors include differences in the resident microflorae and availability of dietary nutrients that might influence transcriptional programming in resident immune cells [247, 270, 271]. Most notably, retinoic acid and its effects on ILC3 maturation (see section 1.3.4). Indeed, the urothelium is exposed to urine, which is toxic and purposefully partially-segregated from the urothelium by uroplakin. These factors alone demonstrate the differences between these organ systems, without touching on the diverse roles performed by the gut for nutrient and water absorption and immune defence and tolerance to ingested and commensal pathogens.

When planning experiments that involve the urinary bladder, we used data from the gut to inform our hypotheses, but there are likely to be significant differences in ILC3-MNP interactions in the bladder for the reasons described above. Whilst similar relationships between MNPs and ILCs may exist, the levels at which these interactions occur in the bladder are played on a smaller scale and I found that statistically significant results were difficult to elicit. The bladder is much smaller in size, with a much smaller muscosal area and volume than the gut. Hence the number of tissue-resident cells is markedly lower. This proved a significant practical challenge to experiments aimed at addressing ILC3 function and cross-talk.

Owing to the variability of the murine UTI models, we have combined results were possible. Care has been taken to include balanced and controlled groups, to eliminate systematic errors. In the case of the IL23R UTI experiments, the results were variable and it was not appropriate to combine cell counts from different experiments. There are multiple reasons that contribute to this variability, including experimental differences (minimised where possible), different UPEC strains, duration of co-housing and availability of large groups of appropriately aged female mice. In the case of the IL23R experiments, and as discussed above, activation of ILC3s is likely to require co-stimulatory pathways. For these reasons, results were not combined so as not to sacrifice accuracy.

Our murine UTI models used two different approaches to interrogate the role of stimulating cytokines; the effect of receptor loss (IL23R) and the effect of cytokine loss (IL- 1β). These were driven by pragmatic factors, namely the availability of these strains to us. They represent two different ways to approach each mechanism. Using the receptor knock out model, we can assume that the effects we observe are all receptor-mediated, but in the case of the IL-1β KO UTI we cannot differentiate between receptor-mediated and non-receptor-mediated IL-1β effects. It is unclear if this distinction is important within the context of UTI.

5.5.3 Future work

Recent publications relating to tissue-resident MNPs have flooded the field with different subtypes and divisions of macrophages and DCs (see section 1.3.1). Owing to the limitations of our flow panel, we were not able to fully describe corresponding populations in murine and human bladder. A future project to distinguish these cells types by flow cytometry and transcriptional analysis would be interesting, as would further functional investigation of these subtypes in terms of immune cell stimulation and activity in UTI. Some evaluation of the different subsets of MNPs within the bladder may be achieved through the human bladder atlas project, on going in the Clatworthy lab, using the 10X genomics platform (single cell RNA sequencing) to analyse cells harvested from the bladder mucosa. In addition to these analyses, there is a need to visualise these cells by microscopy using a greater range of cells surface makers by confocal and RNAscope methods. A project investigating the tissue-resident myeloid and lymphoid cells of the human bladder in health and infection would be worth pursuing.

The work within this chapter could form an introduction to a much wider project about MNP-ILC3 cross talk within the renal tract. The interplay of ILC3 co-stimulation needs further investigation, by using a model that interrogates the role of different cytokines simultaneously. Such an experiment could be achieved by crossing the various knockouts we have used to create single, double and triple-knockout animals by blocking the relevant receptors with antibodies, or creating bone marrow chimeras using *IL1b*, *Il23a* or *Tnfsf15* deficient bone marrow. Furthermore, conditional DC or MNP knockouts would also contribute to elucidating the precise mechanisms of crosstalk. Clearly, this would be no small undertaking, but the effects on development of sepsis and mortality following UPEC challenge would be of interest.

To supplement the *in vivo* investigation, experiments using BMDMs and DCs from mice lacking IL-1β, IL-23a or TL1A might also prove insightful, however sorted cells from the gut have been used to produce some of this data already [282]. Sufficient numbers of macrophages could be sorted from murine bladders after infection to perform co-culture experiments and this is an avenue for further research. This is limited in the context of investigating ILC3-MNP cross-talk however, owing to the insufficient numbers of bladder ILC3s available for cell sorting.

We have performed RNA sequencing from the bladders (24 hour) and kidneys (48 hour) Rag2 KO mice with and without anti-Thy1.2 depleting antibodies. The results of these experiments are undergoing analysis and we hope that this data will also identify new factors involved with ILC3-MNP interactions for future investigation. We have found that transcriptional analysis has proved particularly useful in interrogating the complex immune cell interactions of the renal tract, helping to

circumvent the problems associated with small immune cell populations and tissue size. Single cell RNA sequencing is of particular relevance within this context, as a tool to assess population heterogeneity. Observations at this level may generate data to inform our understanding of the complex tissue-resident immune cell relationships at the urothelium and prove useful in the future.

5.6 Graphical summary

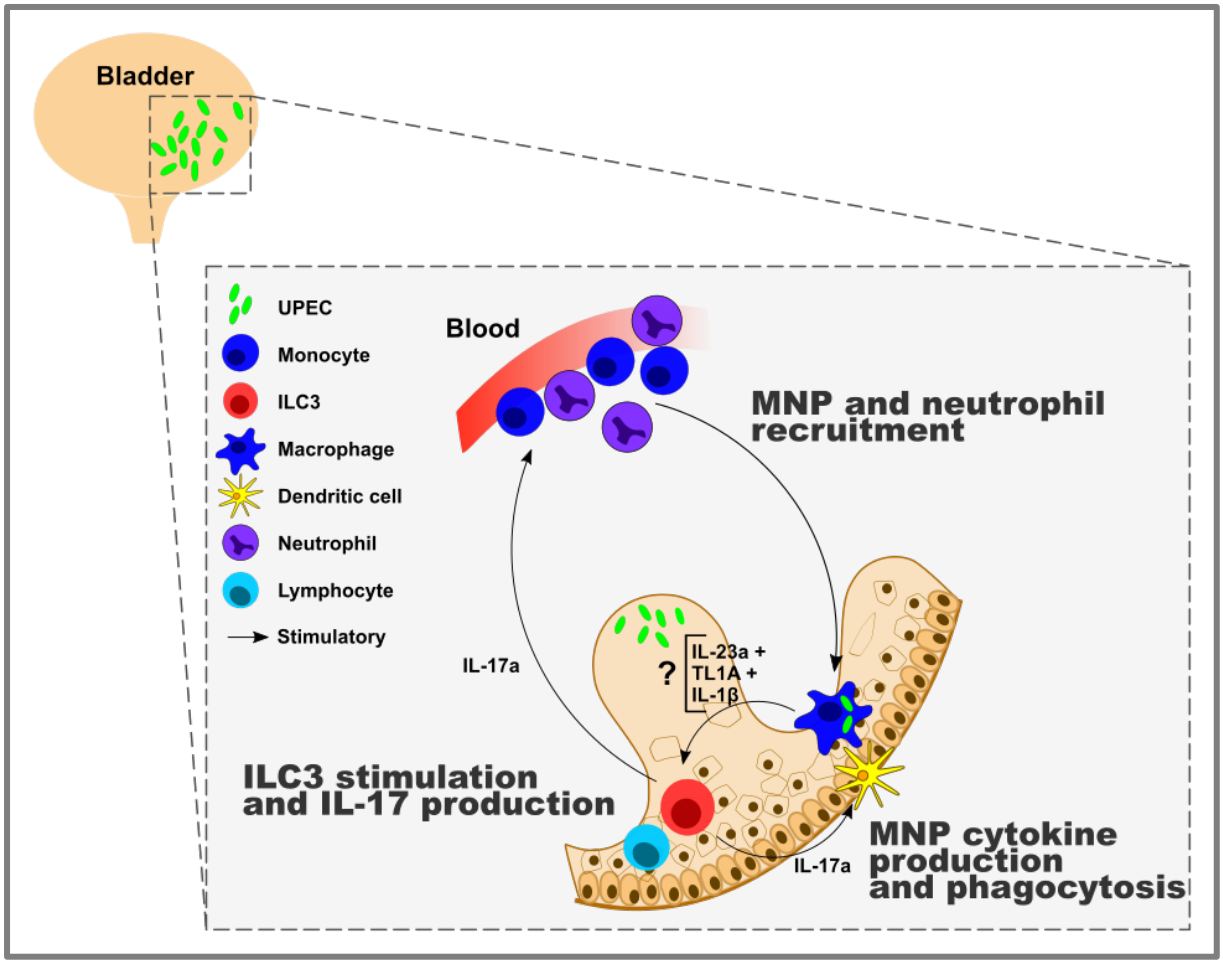

Figure 5.20: ILC3-MNP crosstalk in UTI

ILC3s are located within the urothelium, in close proximity to other tissue-resident immune cells, such as MNPs and lymphocytes. ILC3s are co-stimulated by IL-23a, IL-1β and TL1A from macrophages during UTI and produce IL-17a for immune cell recruitment. Through MNP-ILC3 cross-talk, IL-17a promotes MNP and neutrophil recruitment and promotes increased phagocytic activity of UPEC by MNPs. It is likely that T cells also respond to cytokine stimulation by MNPs using similar mechanisms.

Chapter 6 - Summary and conclusions

This chapter summarises the key data and themes presented within this thesis and progresses to consider future research avenues and clinically relevant models for conditions affecting the renal tract.

6.1 ILCs in the renal tract

There has been a rapid accumulation of data pertaining to ILCs over the last 10 years [265, 432]. The importance of these previously overlooked cell populations has been confirmed at mucosal barriers and epithelial surfaces [229, 252-255, 262, 278, 281, 282, 286-289]. Here, interactions with commensal and environmental pathogens require both regulatory and defensive immune strategies to maintain the integrity, function and safety of the mucosal barrier and a homeostatic relationship with commensals. Whilst most work relating to ILCs has come from the gut, skin and lungs, the renal tract represents another organ system with its own portal to the exterior and a urothelial mucosal barrier. The renal tract is critical to our survival and through its physiological function of waste removal and control of fluid balance, it encounters a set of diverse immunological challenges throughout its length, that require a balance of immune tolerance and inflammation. For example, the kidney is often implicated in sterile inflammatory conditions, such as antibody-mediated glomerulopathy, by virtue of filtering the blood for downstream removal of waste products and retrieval of useful ones. Conversely, pyelonephritis can cause septicaemia and death and must be dealt with swiftly [13]. Further down the urinary tract, the renal pelvis and bladder are lined by a dense layer of urothelium and have their own commensal microbiome, leading more commonly to the immunological challenges of infection and neoplasia [96-98]. The role of ILCs in renal pathology is poorly understood, although their presence in the healthy murine kidney was first noted in 2013 [417]. The bulk of data describing ILCs in the kidney has been in relation to type-2 immunity and ILC2s [128, 129, 256, 417], but descriptions of all ILC subsets at baseline have been made in both mice and humans [129].

Our descriptions of ILCs, particularly ILC3s throughout the renal tract, are the first to describe their presence in the bladder and their role in responses to bacterial infection throughout the length of the renal tract. The data presented in chapter three demonstrates that we can find ILC3s reliably by flow cytometry by using intracellular transcription factor staining and RORγt-GFP reporter mice and by utilising previously validated extracellular staining panels in human tissues [230, 239, 277, 419].

These cells are present in health and are enriched in the lower urinary tract. Furthermore, ILC3s contribute to the innate immune cell milieu of the ureter and bladder, correlating to a requirement for pathogen control and defence within these tissues.

More work is required to characterise renal tract ILCs in greater detail. Owing to their numbers, particularly diminished in healthy tissues, they are a challenging subset of cells to investigate. As transcriptomic tools develop, we anticipate that single cell RNA sequencing might prove a useful tool to delineate the heterogeneity associated with innate lymphoid populations of the renal tract. This will prove more challenging for human ILC collection, owing to the availability of tissue from healthy donors, but it is anticipated that the human cell atlas will generate additional data in this area. Analysis of these tissues is underway in the Clatworthy laboratory and will form a crucial reference dataset for researchers in this field.

6.2 ILC3 function in UTI

T helper-17 immune responses have been well described at epithelial surfaces [200, 328, 330, 331] and within the kidney [339, 384, 386-389]. Given the pro-inflammatory character of this axis, its activation also been described within the bladder and kidney during bacterial infection [3, 369, 383]. Attempts to characterise the cellular sources of IL-17 during UTI have been made and several candidate innate cells have been investigated [374, 383]. Our data demonstrates that ILC3s contribute to IL-17a production in the early phase of UTI and that ILC3s confer an improvement in bacterial clearance within the bladder. We have also demonstrated that IL-17a influences tissue-resident MNP populations by enhancing maturation (downregulation of Ly6c and upregulation of class II) in both kidney and bladder. These changes may have implications for improving the effectiveness of phagocytosis and presentation of antigen to clear the pathogen and elicit an adaptive immune response. Although we were unable to prove the precise mechanism for MNP stimulation of ILC3s, this has been well established in other tissues (see section 1.3.5). It is likely therefore, that ILC3-MNP cross-talk plays a vital part in early immune defence during UTI. Our studies using IL-1β and IL23R knockout mice showed no substantial impact on bacterial CFUs in the bladder, indicating that there may well be redundancy of these cytokine axes, where deficiency of one is compensated by the activity of another. Further investigation using combinations of *Il1br*, *Il23r* and *Tnfrsf25* knockout mice (or lacking their corresponding receptors) may prove fruitful in delineating the relative importance of combinations of factors required for ILC3 stimulation.

Investigating the role of the ILC3 product, IL-22, led us to explore the effect of this cytokine on epithelial repair in the bladder. IL-22 transcripts levels were not statistically significantly reduced by ILC depletion during UTI, but they may still contribute to its effect. Using the IL22RA1 KO mouse we have been able to show that loss of IL-22 signalling leads to decreased Ki67 expression in the urothelium during UTI, though this requires repetition and further validation. Given the pathogenesis of UPEC UTI and its invasion of the urothelium to cause infection (see figure 1.3), rapid urothelial repair is very important to protect the host. We were also able to demonstrate differences in AMP expression with ILC loss and of particular relevance were changes in *Reg3g* expression. This peptide is dependent on IL-22 for production and exhibits activity against gram positive bacteria [44, 75, 347]. It is possible that the urothelium produces AMPs, such as RegIIIγ, in a seemingly indiscriminate manner in UPEC UTI, however it seems more likely that they contribute to immune defence by preventing invasion of commensal bacteria when the urothelial barrier is compromised. The role of AMPs and factors that promote epithelial repair have been poorly characterised in the bladder and this remains an area for further research. Given the pathogenic role of excessive IL-22 in epithelial conditions, such as psoriasis, it remains to be seen if this cytokine-axis contributes to epithelial dysfunction in chronic urinary tract infection and cystitis within the bladder. Aberrant cell cycling is an important factor in neoplasia at epithelial surfaces and conditions causing chronic cystitis are known to be associated with an increased risk of bladder carcinoma (for example, schistosomiasis infection and arylamine dyes) [433, 434]. Understanding the way in which infection influences IL-22 production by ILC3s and the regulatory roles of tissue-resident MNPs in epithelial repair will be critical to understanding how conditions such as bladder cancer can develop. Whilst this falls well outside the remit of this project, our work on IL-22 signalling in the bladder highlights this pathway may be important in preserving urothelial integrity.

Assessing the contribution of ILC3s to different parts of the immune response to UTI has been made more difficult by the lack of an ILC3-specific knockout mouse. Like other research groups, we have used several strategies to interrogate the function of ILC3s, including using Rag KO mice with subsequent antibody-depletion of ILCs. To fully assess the contribution of ILC3s to IL-17-mediated inflammation and IL-22-mediated repair, we could perform urinary tract infections using bone marrow chimeras with RORγt KO/Rag2 KO reconstitution, or transfer of ILC3s to mice lacking IL-17 or IL22RA1. However, the use of bone marrow chimeras can be limited by the radio-resistance of tissue-resident cells including ILC3. One potential useful strategy using this technique is outlined in figure below and was initially proposed for this project:

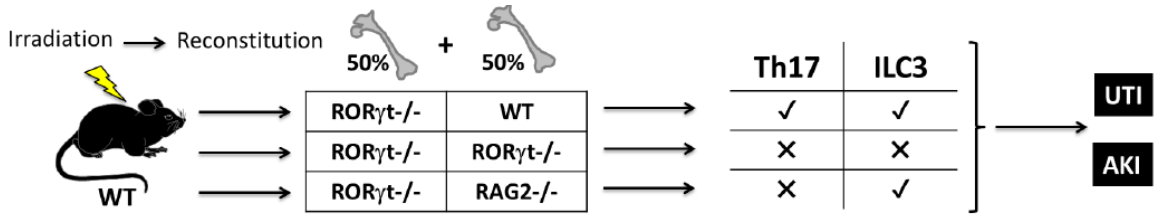

Figure 6.1: Experimental schema to investigate the role of ILC3s in UTI by creating an ILC3-deficient murine model

ILC3-deficient mouse created using radio-ablation and reconstitution with WT, Rag2 KO and/or RORγt KO bone marrow. The table indicates which IL-17-producing cells will still be present in each reconstitution.

Analysis of RNA sequencing data from UTI in murine bladders and kidneys of Rag2 KO +/- ILC depletion will provide useful data to guide future experiments within these areas and begin to identify specific molecular pathways activated during bacterial infection within the renal tract. As already mentioned, we have performed these experiments and the analysis is ongoing.

6.3 Differences in the response of the upper and lower renal tract to UTI

Although the kidneys, ureters, bladder and urethra form one functional system, immunologically they are very different. We have seen these differences born out in our data and conceptually can think of the response to infection being dominated by innate immunity in the lower urinary tract, but broadening to encompass adaptive mechanisms in the upper urinary tract. Data to support this hypothesis already exists, in terms of limited antigen presentation by DCs [2] and poor responses to vaccination in recurrent cystitis [413]. The bladder is rich in T cell populations, that include innate populations [222, 223, 381-383]. This was confirmed by our own microscopy data, where identification and exclusion of T cells was critical to ensure correct labelling of ILC3s; our initial human bladder atlas data highlighted the high proportion of T cells within the bladder (fig 3.16). Furthermore, we have been able to demonstrate differences in MNPs using flow cytometry. There is a tendency for bladder MNPs to be Ly6c+CD11b+F4/80+ and renal MNPs to be CII+CD11b^{int}F4/80+. These bladder MNPs mirror populations observed in the gut, which has parallels in terms of the fact that it is a mucosal epithelial barrier [112, 122]. We did not comprehensively phenotype DCs and macrophages in more detail, such an effort would benefit from a mass cytometric approach to incorporate the many emerging markers of DC and macrophage subsets [147-153, 155-157]. Further

delineation of these subsets in the murine and human bladder, as has been described by recent transcriptomic and mass cytometric publications from other tissues [152, 155] and will form part of our proposed efforts to generate a bladder cell atlas.

The differences in tissue-resident kidney and bladder populations needs characterisation that goes beyond transcriptional description to include a functional analysis of these subsets. Our work has focussed on UTI, but models of sterile inflammation may identify additional aspects of the differences between immune responses in the upper and lower renal tracts, for example, interrogating the role of ILC3s and MNPs in antibody-mediated glomerulonephritis or chemical cystitis.

6.4 Implications and future directions

The work produced in this thesis adds to our understanding of immune cell interactions during UTI, particularly for innate responses within the bladder. UTI remains an important cause of morbidity and mortality in the UK and gaining a better insight into the factors that influence the immune system may prove useful in predicting the risk of complicated UTI and progression to septicaemia and death. Developing strategies to augment treatment in UTI is a difficult prospect, as blocking IL-17 signalling to dampen inflammation might prevent initiation of helpful immune responses and augmentation of IL-22 pathways could lead to over-epithelialisation (such as in psoriasis) in uncomplicated UTI. Acute effective pathways in defence of the urinary tract already exist in immunocompetent individuals and for the majority of sufferers, infection is usually short-lived and easily resolved with antibiotic therapy. In the case of recurrent, catheter-associated or complicated UTI (such as resistant or unusual organisms and immunocompromised patients), there may be a role for biologic treatment to prevent formation of intracellular bacterial reservoirs, inhibit fibrosis and facilitate maintenance of epithelial integrity. As we have found with our own experiments, infections can be highly variable and altering the balance between complex and nuanced immune responses and the commensal bladder microbiome with biologic therapy could have consequences for the health and integrity of the mucosa. Only by advancing our knowledge in the field can we identify specific circumstances in which this might be therapeutically useful.

As described above, inhibiting the body's immune response in acute, self-limiting infection represents a dubious application in UTI, however when the renal tract is affected by recurrent infection or chronic conditions that can lead to renal failure, immunomodulatory therapy might prove more useful. There are certain times when we can predict that a patient will be at high risk of

acute kidney injury, for example, patients with chronic kidney disease or diabetic nephropathy undergoing a CT scan with nephrotoxic contrast agents. Such instances may be amenable to therapy to dampen sterile inflammation and the associated collateral tissue injury. Further investigation into the role of IL-17 in these contexts is required, but we hope that our work in identifying ILC3s in the kidney adds to this field.

The complex interplay of tissue-resident populations within the renal tract merits further analysis and work is underway to describe some of these interactions, as already described in the human single cell atlas projects. ILCs form an interesting subset for further examination of their dynamic behaviour and interactions with other immune cells, which could be observed using intravital imaging. Furthermore, there is much still be investigated to confirm their longevity and phenotypic stability. ILC3s are known to demonstrate plasticity and it remains to be seen if they downregulate RORγt in favour of an ILC1 phenotype in the renal tract, as has been observed in the context of Crohn's colitis [276].

Only by better understanding the immune relationships within the renal tract will we have the potential to positively affect the lives of over 2.6 million people with renal disease in the UK alone [435]. The bladder has been a neglected research organ, but infective cystitis and neoplasia are common causes of morbidity and mortality. It is worth considering the bladder as more than just the research equivalent of the gut's poor relation and focus our attention on understanding the way in which its resident immune system is formed and operates.

Acknowledgements

Dr Menna Clatworthy

For hypothesis generation, funding applications, project supervision and support and critical reading of all my data and reports. Without Menna's expertise in every facet of this project I would not have been able to complete this body of work.

Dr Rebeccah Mathews

For her support in all aspects of my PhD, but most particularly in writing funding applications, procedural and technical advice and emotional guidance.

Dr John Ferdinand

John gave invaluable advice at moments of experimental hiatus, training in murine procedures, biocomputational analysis of genomic data and assistance with producing conference data and posters.

Dr Kevin Loudon

Kevin helped me devise a UTI experimental protocol of maximum efficiency and contributed hugely to the procedural elements of the UTI experiments presented in this thesis. Without his enthusiasm, humour and fighting spirit this PhD would have been difficult and the number of UTI experiments performed greatly reduced.

Team Kidney

Multiple people contributed to the swift handling of human tissue from transplant donors. Particular thanks to Dr Miriam Berry and Dr Rebeccah Mathews for their input in devising the early protocols for tissue processing. To the several people who worked thereafter as a team to complete these experiments, I thank them for sharing the load and for their company and humour no matter the hour or experimental length: Dr Kevin Loudon, Dr Ben Stewart, Dr Ondrej Suchaneck, Mr Nathan Richoz, Dr Elizabeth Wlodek, Dr Joy Staniforth and Dr John Ferdinand.

The Clatworthy Lab

My thanks to all those in the Clatworthy Lab for creating a constructive and fun research environment and for their varied experimental tips and assistance. Several people assisted with particular expertise, including Dr Gordon Frazer (Imaris software and confocal microscopy) and Dr Tom Castro Dopico (computational analysis and advice on ILC identification). Lastly, I thank Dr Mary-

Ellen Lynall who was the best desk buddy a PhD Fellow could ask for and who picked me up in times of scientific woe!

Where appropriate, scientific collaborations have been acknowledged at the relevant experimental juncture throughout this thesis and include Prof Gordon Dougan, Dr Simon Clare, Dr Murray Clarke, Dr Kourosh Saeb-Parsey and his laboratory and Dr Sarah Teichmann and her Sanger team.

References

1. Da Vinci, L. *Collection of Anatomical drawings*. [Pen and ink drawing] 1452-1519 [cited 2017 20/03/2017]; Available from: https://www.royalcollection.org.uk/.
2. Mora-Bau, G., et al., *Macrophages Subvert Adaptive Immunity to Urinary Tract Infection.* PLoS pathogens, 2015. **11**(7): p. e1005044-e1005044.
3. Carey, A.J., et al., *Uropathogenic Escherichia coli Engages CD14-Dependent Signaling to Enable Bladder-Macrophage-Dependent Control of Acute Urinary Tract Infection.* Journal of Infectious Diseases, 2016. **213**(4): p. 659-668.
4. Juelke, K. and C. Romagnani, *Differentiation of human innate lymphoid cells (ILCs).* Curr Opin Immunol, 2016. **38**: p. 75-85.
5. Flores-Mireles, A.L., et al., *Urinary tract infections: epidemiology, mechanisms of infection and treatment options.* Nat Rev Microbiol, 2015. **13**(5): p. 269-84.
6. Keele, K. and C. Pedretti, *Leonardo da Vinci: corpus of the anatomical drawings*. 1979: Royal Collection of Her Majesty the Queen at Windsor Castle. London.
7. Lewis, S.A., *Everything you wanted to know about the bladder epithelium but were afraid to ask.* Am J Physiol Renal Physiol, 2000. **278**(6): p. F867-74.
8. Parsons, C.L., J.D. Lilly, and P. Stein, *Epithelial dysfunction in nonbacterial cystitis (interstitial cystitis).* J Urol, 1991. **145**(4): p. 732-5.
9. Wu, X.R., et al., *Uroplakins in urothelial biology, function, and disease.* Kidney Int, 2009. **75**(11): p. 1153-65.
10. Zhou, G., et al., *Uroplakin Ia is the urothelial receptor for uropathogenic Escherichia coli: evidence from in vitro FimH binding.* J Cell Sci, 2001. **114**(Pt 22): p. 4095-103.
11. Riedel, I., et al., *Urothelial umbrella cells of human ureter are heterogeneous with respect to their uroplakin composition: different degrees of urothelial maturity in ureter and bladder?* Eur J Cell Biol, 2005. **84**(2-3): p. 393-405.
12. Berry, M.R., et al., *Renal Sodium Gradient Orchestrates a Dynamic Antibacterial Defense Zone.* Cell, 2017. **170**(5): p. 860-874 e19.
13. McLellan, L.K. and D.A. Hunstad, *Urinary Tract Infection: Pathogenesis and Outlook.* Trends Mol Med, 2016. **22**(11): p. 946-957.
14. Nielubowicz, G.R. and H.L.T. Mobley, *Host-pathogen interactions in urinary tract infection.* Nature reviews. Urology, 2010. **7**(8): p. 430-441.
15. Barber, A.E., et al., *Urinary tract infections: Current and emerging management strategies.* Clinical Infectious Diseases, 2013. **57**(5): p. 719-724.
16. Foxman, B., *Recurring Urinary Tract Infection: Incidence and Risk Factors.* AJPH, 1990. **80**(3): p. 331-333.
17. Ronald, A., *The etiology of urinary tract infection: traditional and emerging pathogens.* Am J Med, 2002. **113 Suppl 1A**: p. 14S-19S.
18. Paniagua-Contreras, G.L., et al., *Comprehensive expression analysis of pathogenicity genes in uropathogenic Escherichia coli strains.* Microb Pathog, 2017. **103**: p. 1-7.
19. Eto, D.S., et al., *Integrin-mediated host cell invasion by type 1-piliated uropathogenic Escherichia coli.* PLoS Pathog, 2007. **3**(7): p. e100.
20. Kai-Larsen, Y., et al., *Uropathogenic Escherichia coli modulates immune responses and its curli fimbriae interact with the antimicrobial peptide LL-37.* PLoS Pathog, 2010. **6**(7): p. e1001010.
21. O'Hanley, P., G. Lalonde, and G. Ji, *Alpha-hemolysin contributes to the pathogenicity of piliated digalactoside-binding Escherichia coli in the kidney: efficacy of an alpha-hemolysin vaccine in preventing renal injury in the BALB/c mouse model of pyelonephritis.* Infect Immun, 1991. **59**(3): p. 1153-61.
22. Khan, A.S., et al., *Receptor structure for F1C fimbriae of uropathogenic Escherichia coli.* Infect Immun, 2000. **68**(6): p. 3541-7.

23. Boisen, N., et al., *New adhesin of enteroaggregative Escherichia coli related to the Afa/Dr/AAF family.* Infect Immun, 2008. **76**(7): p. 3281-92.
24. Harrington, S.M., et al., *Aggregative adherence fimbriae contribute to the inflammatory response of epithelial cells infected with enteroaggregative Escherichia coli.* Cell Microbiol, 2005. **7**(11): p. 1565-78.
25. Muenzner, P., et al., *Uropathogenic E. coli Exploit CEA to Promote Colonization of the Urogenital Tract Mucosa.* PLoS Pathog, 2016. **12**(5): p. e1005608.
26. Nowicki, B., et al., *Short consensus repeat-3 domain of recombinant decay-accelerating factor is recognized by Escherichia coli recombinant Dr adhesin in a model of a cell-cell interaction.* J Exp Med, 1993. **178**(6): p. 2115-21.
27. Kim, K.J., J.W. Chung, and K.S. Kim, *67-kDa laminin receptor promotes internalization of cytotoxic necrotizing factor 1-expressing Escherichia coli K1 into human brain microvascular endothelial cells.* J Biol Chem, 2005. **280**(2): p. 1360-8.
28. Croxen, M.A. and B.B. Finlay, *Molecular mechanisms of Escherichia coli pathogenicity.* Nat Rev Microbiol, 2010. **8**(1): p. 26-38.
29. Schwan, W.R., *Flagella allow uropathogenic Escherichia coli ascension into murine kidneys.* Int J Med Microbiol, 2008. **298**(5-6): p. 441-7.
30. Murray, P.R., et al., *Medical Microbiology*. 4th ed. 2002, USA: Mosby, Inc.
31. Nagamatsu, K., et al., *Dysregulation of Escherichia coli alpha-hemolysin expression alters the course of acute and persistent urinary tract infection.* Proc Natl Acad Sci U S A, 2015. **112**(8): p. E871-80.
32. Welch, R.A., *Uropathogenic Escherichia coli-Associated Exotoxins.* Microbiol Spectr, 2016. **4**(3).
33. Wiles, T.J., R.R. Kulesus, and M.A. Mulvey, *Origins and virulence mechanisms of uropathogenic Escherichia coli.* Exp Mol Pathol, 2008. **85**(1): p. 11-9.
34. Guyer, D.M., et al., *Sat, the secreted autotransporter toxin of uropathogenic Escherichia coli, is a vacuolating cytotoxin for bladder and kidney epithelial cells.* Infect Immun, 2002. **70**(8): p. 4539-46.
35. Garcia, E.C., A.R. Brumbaugh, and H.L. Mobley, *Redundancy and specificity of Escherichia coli iron acquisition systems during urinary tract infection.* Infect Immun, 2011. **79**(3): p. 1225-35.
36. Sivick, K.E. and H.L.T. Mobley, *Waging war against uropathogenic Escherichia coli: Winning back the urinary tract.* Infection and Immunity, 2010. **78**(2): p. 568-585.
37. Mulvey, M.A., J.D. Schilling, and S.J. Hultgren, *Establishment of a persistent Escherichia coli reservoir during the acute phase of a bladder infection.* Infect Immun, 2001. **69**(7): p. 4572-9.
38. Rosen, D.A., et al., *Detection of intracellular bacterial communities in human urinary tract infection.* PLoS Med, 2007. **4**(12): p. e329.
39. Chassin, C., et al., *Renal collecting duct epithelial cells react to pyelonephritis-associated Escherichia coli by activating distinct TLR4-dependent and -independent inflammatory pathways.* J Immunol, 2006. **177**(7): p. 4773-84.
40. Chassin, C., et al., *A role for collecting duct epithelial cells in renal antibacterial defences.* Cell Microbiol, 2011. **13**(8): p. 1107-13.
41. Paragas, N., et al., *alpha-Intercalated cells defend the urinary system from bacterial infection.* J Clin Invest, 2014. **124**(7): p. 2963-76.
42. Jaillon, S., et al., *The humoral pattern recognition molecule PTX3 is a key component of innate immunity against urinary tract infection.* Immunity, 2014. **40**(4): p. 621-32.
43. Spencer, J.D., et al., *Human alpha defensin 5 expression in the human kidney and urinary tract.* PLoS One, 2012. **7**(2): p. e31712.
44. Spencer, J.D., et al., *Expression and Significance of the HIP/PAP and RegIIIgamma Antimicrobial Peptides during Mammalian Urinary Tract Infection.* PLoS One, 2015. **10**(12): p. e0144024.

45. Lehmann, J., et al., *Expression of human beta-defensins 1 and 2 in kidneys with chronic bacterial infection.* BMC Infect Dis, 2002. **2**: p. 20.
46. Duell, B.L., et al., *Innate Transcriptional Networks Activated in Bladder in Response to Uropathogenic Escherichia coli Drive Diverse Biological Pathways and Rapid Synthesis of IL-10 for Defense against Bacterial Urinary Tract Infection.* The Journal of Immunology, 2012. **188**: p. 781-792.
47. Plowman, G.D., et al., *The amphiregulin gene encodes a novel epidermal growth factor-related protein with tumor-inhibitory activity.* Mol Cell Biol, 1990. **10**(5): p. 1969-81.
48. Kefaloyianni, E., et al., *ADAM17 substrate release in proximal tubule drives kidney fibrosis.* JCI Insight, 2016. **1**(13).
49. Chen, F., et al., *Neutrophils Promote Amphiregulin Production in Intestinal Epithelial Cells through TGF-beta and Contribute to Intestinal Homeostasis.* J Immunol, 2018.
50. Wolfs, T.G., et al., *In vivo expression of Toll-like receptor 2 and 4 by renal epithelial cells: IFN-gamma and TNF-alpha mediated up-regulation during inflammation.* J Immunol, 2002. **168**(3): p. 1286-93.
51. Becknell, B., et al., *Amplifying renal immunity: the role of antimicrobial peptides in pyelonephritis.* Nature Reviews Nephrology, 2015. **11**(11): p. 642-655.
52. Fehlbaum, P., et al., *Insect immunity. Septic injury of Drosophila induces the synthesis of a potent antifungal peptide with sequence homology to plant antifungal peptides.* J Biol Chem, 1994. **269**(52): p. 33159-63.
53. Harder, J., et al., *A peptide antibiotic from human skin.* Nature, 1997. **387**(6636): p. 861.
54. Stolzenberg, E.D., et al., *Epithelial antibiotic induced in states of disease.* Proc Natl Acad Sci U S A, 1997. **94**(16): p. 8686-90.
55. Chertov, O., et al., *Identification of defensin-1, defensin-2, and CAP37/azurocidin as T-cell chemoattractant proteins released from interleukin-8-stimulated neutrophils.* J Biol Chem, 1996. **271**(6): p. 2935-40.
56. Lillard, J.W., Jr., et al., *Mechanisms for induction of acquired host immunity by neutrophil peptide defensins.* Proc Natl Acad Sci U S A, 1999. **96**(2): p. 651-6.
57. Prohaszka, Z., et al., *Defensins purified from human granulocytes bind C1q and activate the classical complement pathway like the transmembrane glycoprotein gp41 of HIV-1.* Mol Immunol, 1997. **34**(11): p. 809-16.
58. Kao, C.Y., et al., *IL-17 markedly up-regulates beta-defensin-2 expression in human airway epithelium via JAK and NF-kappaB signaling pathways.* J Immunol, 2004. **173**(5): p. 3482-91.
59. Yang, D., et al., *Beta-defensins: linking innate and adaptive immunity through dendritic and T cell CCR6.* Science, 1999. **286**(5439): p. 525-8.
60. Mathew, B. and R. Nagaraj, *Antimicrobial activity of human alpha-defensin 5 and its linear analogs: N-terminal fatty acylation results in enhanced antimicrobial activity of the linear analogs.* Peptides, 2015. **71**: p. 128-40.
61. Kraemer, B.F., et al., *Novel anti-bacterial activities of beta-defensin 1 in human platelets: suppression of pathogen growth and signaling of neutrophil extracellular trap formation.* PLoS Pathog, 2011. **7**(11): p. e1002355.
62. Goetz, D.H., et al., *The neutrophil lipocalin NGAL is a bacteriostatic agent that interferes with siderophore-mediated iron acquisition.* Mol Cell, 2002. **10**(5): p. 1033-43.
63. Chromek, M., et al., *The antimicrobial peptide cathelicidin protects the urinary tract against invasive bacterial infection.* Nat Med, 2006. **12**(6): p. 636-41.
64. Lech, M., et al., *Endogenous and exogenous pentraxin-3 limits postischemic acute and chronic kidney injury.* Kidney Int, 2013. **83**(4): p. 647-61.
65. Steel, D.M., et al., *Expression and regulation of constitutive and acute phase serum amyloid A mRNAs in hepatic and non-hepatic cell lines.* Scand J Immunol, 1996. **44**(5): p. 493-500.

66. Urieli-Shoval, S., et al., *Widespread expression of serum amyloid A in histologically normal human tissues. Predominant localization to the epithelium.* J Histochem Cytochem, 1998. **46**(12): p. 1377-84.
67. Couderc, E., et al., *Interleukin-17A-induced production of acute serum amyloid A by keratinocytes contributes to psoriasis pathogenesis.* PLoS One, 2017. **12**(7): p. e0181486.
68. Sano, T., et al., *An IL-23R/IL-22 Circuit Regulates Epithelial Serum Amyloid A to Promote Local Effector Th17 Responses.* Cell, 2015. **163**(2): p. 381-393.
69. Su, S.B., et al., *A seven-transmembrane, G protein-coupled receptor, FPRL1, mediates the chemotactic activity of serum amyloid A for human phagocytic cells.* J Exp Med, 1999. **189**(2): p. 395-402.
70. He, R., H. Sang, and R.D. Ye, *Serum amyloid A induces IL-8 secretion through a G protein-coupled receptor, FPRL1/LXA4R.* Blood, 2003. **101**(4): p. 1572-81.
71. Mullan, R.H., et al., *Acute-phase serum amyloid A stimulation of angiogenesis, leukocyte recruitment, and matrix degradation in rheumatoid arthritis through an NF-kappaB-dependent signal transduction pathway.* Arthritis Rheum, 2006. **54**(1): p. 105-14.
72. O'Hara, R., et al., *Local expression of the serum amyloid A and formyl peptide receptor-like 1 genes in synovial tissue is associated with matrix metalloproteinase production in patients with inflammatory arthritis.* Arthritis Rheum, 2004. **50**(6): p. 1788-99.
73. Cheng, N., et al., *Cutting edge: TLR2 is a functional receptor for acute-phase serum amyloid A.* J Immunol, 2008. **181**(1): p. 22-6.
74. Sandri, S., et al., *Is serum amyloid A an endogenous TLR4 agonist?* J Leukoc Biol, 2008. **83**(5): p. 1174-80.
75. Cash, H.L., et al., *Symbiotic bacteria direct expression of an intestinal bactericidal lectin.* Science, 2006. **313**(5790): p. 1126-30.
76. Vaishnava, S., et al., *The antibacterial lectin RegIIIgamma promotes the spatial segregation of microbiota and host in the intestine.* Science, 2011. **334**(6053): p. 255-8.
77. Vaishnava, S., et al., *Paneth cells directly sense gut commensals and maintain homeostasis at the intestinal host-microbial interface.* Proc Natl Acad Sci U S A, 2008. **105**(52): p. 20858-63.
78. Abt, M.C., et al., *TLR-7 activation enhances IL-22-mediated colonization resistance against vancomycin-resistant enterococcus.* Sci Transl Med, 2016. **8**(327): p. 327ra25.
79. Loonen, L.M., et al., *REG3gamma-deficient mice have altered mucus distribution and increased mucosal inflammatory responses to the microbiota and enteric pathogens in the ileum.* Mucosal Immunol, 2014. **7**(4): p. 939-47.
80. Sonnenberg, G.F., et al., *Innate Lymphoid Cells Promote Anatomical Containment of Lymphoid-Resident Commensal Bacteria.* Science, 2012. **336**: p. 1321-1325.
81. Ito, T., et al., *IL-22 induces Reg3gamma and inhibits allergic inflammation in house dust mite-induced asthma models.* J Exp Med, 2017.
82. Cao, Q., et al., *Potentiating Tissue-Resident Type 2 Innate Lymphoid Cells by IL-33 to Prevent Renal Ischemia-Reperfusion Injury.* J Am Soc Nephrol, 2018. **29**(3): p. 961-976.
83. Mograbi, B., et al., *Human monocytes express amphiregulin and heregulin growth factors upon activation.* Eur Cytokine Netw, 1997. **8**(1): p. 73-81.
84. Koeppen, M., et al., *Hypoxia-inducible factor 2-alpha-dependent induction of amphiregulin dampens myocardial ischemia-reperfusion injury.* Nat Commun, 2018. **9**(1): p. 816.
85. Morimoto, Y., et al., *Amphiregulin-Producing Pathogenic Memory T Helper 2 Cells Instruct Eosinophils to Secrete Osteopontin and Facilitate Airway Fibrosis.* Immunity, 2018. **49**(1): p. 134-150 e6.
86. Krishnan, S., et al., *Amphiregulin-producing gammadelta T cells are vital for safeguarding oral barrier immune homeostasis.* Proc Natl Acad Sci U S A, 2018.
87. Monticelli, L.a., et al., *IL-33 promotes an innate immune pathway of intestinal tissue protection dependent on amphiregulin–EGFR interactions.* Proceedings of the National Academy of Sciences, 2015: p. 201509070-201509070.

88. Hirota, N., et al., *Histamine may induce airway remodeling through release of epidermal growth factor receptor ligands from bronchial epithelial cells.* FASEB J, 2012. **26**(4): p. 1704-16.
89. Yoshida, A., et al., *The role of heparin-binding EGF-like growth factor and amphiregulin in the epidermal proliferation of psoriasis in cooperation with TNFalpha.* Arch Dermatol Res, 2008. **300**(1): p. 37-45.
90. Cook, P.W., et al., *Suprabasal expression of human amphiregulin in the epidermis of transgenic mice induces a severe, early-onset, psoriasis-like skin pathology: expression of amphiregulin in the basal epidermis is also associated with synovitis.* Exp Dermatol, 2004. **13**(6): p. 347-56.
91. Ragnarsdottir, B., et al., *Toll-like receptor 4 promoter polymorphisms: common TLR4 variants may protect against severe urinary tract infection.* PLoS One, 2010. **5**(5): p. e10734.
92. Yim, H.E., et al., *Genetic control of VEGF and TGF-beta1 gene polymorphisms in childhood urinary tract infection and vesicoureteral reflux.* Pediatr Res, 2007. **62**(2): p. 183-7.
93. Artifoni, L., et al., *Interleukin-8 and CXCR1 receptor functional polymorphisms and susceptibility to acute pyelonephritis.* J Urol, 2007. **177**(3): p. 1102-6.
94. Centi, S., et al., *Upper urinary tract infections are associated with RANTES promoter polymorphism.* J Pediatr, 2010. **157**(6): p. 1038-1040 e1.
95. Fischer, H., et al., *Pathogen specific, IRF3-dependent signaling and innate resistance to human kidney infection.* PLoS Pathog, 2010. **6**(9): p. e1001109.
96. Nienhouse, V., et al., *Interplay between bladder microbiota and urinary antimicrobial peptides: Mechanisms for human urinary tract infection risk and symptom severity.* PLoS ONE, 2014. **9**(12): p. 1-26.
97. Wolfe, A.J., et al., *Evidence of uncultivated bacteria in the adult female bladder.* J Clin Microbiol, 2012. **50**(4): p. 1376-83.
98. Thomas-White, K., et al., *Culturing of female bladder bacteria reveals an interconnected urogenital microbiota.* Nat Commun, 2018. **9**(1): p. 1557.
99. Paul, W.E., *Fundamental Immunology*. 7th ed, ed. W.E. Paul. 2013, Philadelphia, USA: Lippincott Williams and Wilkins. 1283.
100. Wang, L.D. and A.J. Wagers, *Dynamic niches in the origination and differentiation of haematopoietic stem cells.* Nat Rev Mol Cell Biol, 2011. **12**(10): p. 643-55.
101. Sonnenberg, G.F. and D. Artis, *Innate lymphoid cells in the initiation, regulation and resolution of inflammation.* Nature Medicine, 2015. **21**(7): p. 1-11.
102. Langerhans, P., *Uber die Nerven der menschlichen Haut.* Archives of Pathological Anatomy, 1868. **44**: p. 325-337.
103. Kupffer, C.V., *Über Sternzellen in der Leber. Briefliche Mitteilung an Prof. Waldyer. .* Arch Mikr Anat, 1876. **12**: p. 352-358.
104. Kupffer, C.V., *Über die sogennanten Sternzellen der Säugethierleber.* Arch Mikr Anat, 1899. **54**: p. 254-288.
105. Parham, P., *The Immune System*. 3rd ed. 2009, USA: Garland Science, Taylor & Francis Group, LLC.
106. Kolaczkowska, E. and P. Kubes, *Neutrophil recruitment and function in health and inflammation.* Nat Rev Immunol, 2013. **13**(3): p. 159-75.
107. Metchnikoff, E., *Phagocytosis "Untersuchung uber die mesodermalen Phagocyten einiger Wirbel tiere.".* Biologicial Centralblatt, 1883. **18**: p. 560.
108. Underhill, D.M., et al., *The Toll-like receptor 2 is recruited to macrophage phagosomes and discriminates between pathogens.* Nature, 1999. **401**(6755): p. 811-5.
109. Rock, F.L., et al., *A family of human receptors structurally related to Drosophila Toll.* Proc Natl Acad Sci U S A, 1998. **95**(2): p. 588-93.

110. Chaudhary, P.M., et al., *Cloning and characterization of two Toll/Interleukin-1 receptor-like genes TIL3 and TIL4: evidence for a multi-gene receptor family in humans.* Blood, 1998. **91**(11): p. 4020-7.
111. Platt, A.M., et al., *An independent subset of TLR expressing CCR2-dependent macrophages promotes colonic inflammation.* J Immunol, 2010. **184**(12): p. 6843-54.
112. Bain, C.C., et al., *Resident and pro-inflammatory macrophages in the colon represent alternative context-dependent fates of the same Ly6Chi monocyte precursors.* Mucosal Immunol, 2013. **6**(3): p. 498-510.
113. Rivollier, A., et al., *Inflammation switches the differentiation program of Ly6Chi monocytes from antiinflammatory macrophages to inflammatory dendritic cells in the colon.* J Exp Med, 2012. **209**(1): p. 139-55.
114. Ginhoux, F., et al., *Fate mapping analysis reveals that adult microglia derive from primitive macrophages.* Science, 2010. **330**(6005): p. 841-5.
115. Schulz, C., et al., *A lineage of myeloid cells independent of Myb and hematopoietic stem cells.* Science, 2012. **336**(6077): p. 86-90.
116. Mass, E., et al., *Specification of tissue-resident macrophages during organogenesis.* Science, 2016.
117. Gomez Perdiguero, E., et al., *Tissue-resident macrophages originate from yolk-sac-derived erythro-myeloid progenitors.* Nature, 2015. **518**(7540): p. 547-51.
118. Bain, C.C., et al., *Constant replenishment from circulating monocytes maintains the macrophage pool in the intestine of adult mice.* Nat Immunol, 2014. **15**(10): p. 929-37.
119. Bain, C.C., et al., *Long-lived self-renewing bone marrow-derived macrophages displace embryo-derived cells to inhabit adult serous cavities.* Nat Commun, 2016. **7**: p. ncomms11852.
120. De Schepper, S., et al., *Self-Maintaining Gut Macrophages Are Essential for Intestinal Homeostasis.* Cell, 2018.
121. Bajpai, G., et al., *The human heart contains distinct macrophage subsets with divergent origins and functions.* Nat Med, 2018.
122. Tamoutounour, S., et al., *CD64 distinguishes macrophages from dendritic cells in the gut and reveals the Th1-inducing role of mesenteric lymph node macrophages during colitis.* Eur J Immunol, 2012. **42**(12): p. 3150-66.
123. Zigmond, E., et al., *Ly6C hi monocytes in the inflamed colon give rise to proinflammatory effector cells and migratory antigen-presenting cells.* Immunity, 2012. **37**(6): p. 1076-90.
124. Denning, T.L., et al., *Lamina propria macrophages and dendritic cells differentially induce regulatory and interleukin 17-producing T cell responses.* Nat Immunol, 2007. **8**(10): p. 1086-94.
125. Krause, P., et al., *IL-10-producing intestinal macrophages prevent excessive antibacterial innate immunity by limiting IL-23 synthesis.* Nat Commun, 2015. **6**: p. 7055.
126. Ip, W.K.E., et al., *Anti-inflammatory effect of IL-10 mediated by metabolic reprogramming of macrophages.* Science, 2017. **356**(6337): p. 513-519.
127. Mortha, A., et al., *Microbiota-Dependent Crosstalk Between Macrophages and ILC3 Promotes Intestinal Homeostasis.* Science, 2014. **343**(6178): p. 1439-1440.
128. Huang, Q., et al., *IL-25 Elicits Innate Lymphoid Cells and Multipotent Progenitor Type 2 Cells That Reduce Renal Ischemic/Reperfusion Injury.* Journal of the American Society of Nephrology, 2015: p. 1-13.
129. Riedel, J.H., et al., *IL-33-Mediated Expansion of Type 2 Innate Lymphoid Cells Protects from Progressive Glomerulosclerosis.* J Am Soc Nephrol, 2017. **28**(7): p. 2068-2080.
130. Steinman, R.M. and Z.A. Cohn, *Identification of a novel cell type in peripheral lymphoid organs of mice. I. Morphology, quantitation, tissue distribution.* J Exp Med, 1973. **137**(5): p. 1142-62.

131. Vremec, D., et al., *The surface phenotype of dendritic cells purified from mouse thymus and spleen: investigation of the CD8 expression by a subpopulation of dendritic cells.* J Exp Med, 1992. **176**(1): p. 47-58.
132. Traver, D., et al., *Development of CD8alpha-positive dendritic cells from a common myeloid progenitor.* Science, 2000. **290**(5499): p. 2152-4.
133. Poulin, L.F., et al., *Characterization of human DNGR-1+ BDCA3+ leukocytes as putative equivalents of mouse CD8alpha+ dendritic cells.* J Exp Med, 2010. **207**(6): p. 1261-71.
134. Perussia, B., V. Fanning, and G. Trinchieri, *A leukocyte subset bearing HLA-DR antigens is responsible for in vitro alpha interferon production in response to viruses.* Nat Immun Cell Growth Regul, 1985. **4**(3): p. 120-37.
135. O'Doherty, U., et al., *Human blood contains two subsets of dendritic cells, one immunologically mature and the other immature.* Immunology, 1994. **82**(3): p. 487-93.
136. McKenna, H.J., et al., *Mice lacking flt3 ligand have deficient hematopoiesis affecting hematopoietic progenitor cells, dendritic cells, and natural killer cells.* Blood, 2000. **95**(11): p. 3489-97.
137. Akashi, K., et al., *A clonogenic common myeloid progenitor that gives rise to all myeloid lineages.* Nature, 2000. **404**(6774): p. 193-7.
138. D'Amico, A. and L. Wu, *The early progenitors of mouse dendritic cells and plasmacytoid predendritic cells are within the bone marrow hemopoietic precursors expressing Flt3.* J Exp Med, 2003. **198**(2): p. 293-303.
139. Bogunovic, M., et al., *Origin of the lamina propria dendritic cell network.* Immunity, 2009. **31**(3): p. 513-25.
140. Fogg, D.K., et al., *A clonogenic bone marrow progenitor specific for macrophages and dendritic cells.* Science, 2006. **311**(5757): p. 83-7.
141. Varol, C., et al., *Monocytes give rise to mucosal, but not splenic, conventional dendritic cells.* J Exp Med, 2007. **204**(1): p. 171-80.
142. Galy, A., et al., *Human T, B, natural killer, and dendritic cells arise from a common bone marrow progenitor cell subset.* Immunity, 1995. **3**(4): p. 459-73.
143. Liu, K., et al., *In vivo analysis of dendritic cell development and homeostasis.* Science, 2009. **324**(5925): p. 392-7.
144. Onai, N., et al., *Identification of clonogenic common Flt3+M-CSFR+ plasmacytoid and conventional dendritic cell progenitors in mouse bone marrow.* Nat Immunol, 2007. **8**(11): p. 1207-16.
145. Naik, S.H., et al., *Development of plasmacytoid and conventional dendritic cell subtypes from single precursor cells derived in vitro and in vivo.* Nat Immunol, 2007. **8**(11): p. 1217-26.
146. Manz, M.G., et al., *Dendritic cell potentials of early lymphoid and myeloid progenitors.* Blood, 2001. **97**(11): p. 3333-41.
147. Becher, B., et al., *High-dimensional analysis of the murine myeloid cell system.* Nat Immunol, 2014. **15**(12): p. 1181-9.
148. Jaitin, D.A., et al., *Massively parallel single-cell RNA-seq for marker-free decomposition of tissues into cell types.* Science, 2014. **343**(6172): p. 776-9.
149. Segura, E., M. Durand, and S. Amigorena, *Similar antigen cross-presentation capacity and phagocytic functions in all freshly isolated human lymphoid organ-resident dendritic cells.* J Exp Med, 2013. **210**(5): p. 1035-47.
150. Robbins, S.H., et al., *Novel insights into the relationships between dendritic cell subsets in human and mouse revealed by genome-wide expression profiling.* Genome Biol, 2008. **9**(1): p. R17.
151. Piccioli, D., et al., *Functional specialization of human circulating CD16 and CD1c myeloid dendritic-cell subsets.* Blood, 2007. **109**(12): p. 5371-9.
152. Guilliams, M., et al., *Unsupervised High-Dimensional Analysis Aligns Dendritic Cells across Tissues and Species.* Immunity, 2016. **45**(3): p. 669-684.

153. Granot, T., et al., *Dendritic Cells Display Subset and Tissue-Specific Maturation Dynamics over Human Life.* Immunity, 2017. **46**(3): p. 504-515.
154. Bachem, A., et al., *Superior antigen cross-presentation and XCR1 expression define human CD11c+CD141+ cells as homologues of mouse CD8+ dendritic cells.* J Exp Med, 2010. **207**(6): p. 1273-81.
155. Villani, A.C., et al., *Single-cell RNA-seq reveals new types of human blood dendritic cells, monocytes, and progenitors.* Science, 2017. **356**(6335).
156. Klechevsky, E., et al., *Functional specializations of human epidermal Langerhans cells and CD14+ dermal dendritic cells.* Immunity, 2008. **29**(3): p. 497-510.
157. McGovern, N., et al., *Human dermal CD14(+) cells are a transient population of monocyte-derived macrophages.* Immunity, 2014. **41**(3): p. 465-477.
158. Sun, C.M., et al., *Small intestine lamina propria dendritic cells promote de novo generation of Foxp3 T reg cells via retinoic acid.* J Exp Med, 2007. **204**(8): p. 1775-85.
159. Coombes, J.L., et al., *A functionally specialized population of mucosal CD103+ DCs induces Foxp3+ regulatory T cells via a TGF-beta and retinoic acid-dependent mechanism.* J Exp Med, 2007. **204**(8): p. 1757-64.
160. Kinnebrew, M.A., et al., *Interleukin 23 production by intestinal CD103(+)CD11b(+) dendritic cells in response to bacterial flagellin enhances mucosal innate immune defense.* Immunity, 2012. **36**(2): p. 276-87.
161. Cerovic, V., et al., *Intestinal CD103(-) dendritic cells migrate in lymph and prime effector T cells.* Mucosal Immunol, 2013. **6**(1): p. 104-13.
162. Fujimoto, K., et al., *A new subset of CD103+CD8alpha+ dendritic cells in the small intestine expresses TLR3, TLR7, and TLR9 and induces Th1 response and CTL activity.* J Immunol, 2011. **186**(11): p. 6287-95.
163. Uematsu, S., et al., *Regulation of humoral and cellular gut immunity by lamina propria dendritic cells expressing Toll-like receptor 5.* Nat Immunol, 2008. **9**(7): p. 769-76.
164. Farache, J., et al., *Luminal bacteria recruit CD103+ dendritic cells into the intestinal epithelium to sample bacterial antigens for presentation.* Immunity, 2013. **38**(3): p. 581-95.
165. Schulz, O., et al., *Intestinal CD103+, but not CX3CR1+, antigen sampling cells migrate in lymph and serve classical dendritic cell functions.* J Exp Med, 2009. **206**(13): p. 3101-14.
166. Netea, M.G., J. Quintin, and J.W. van der Meer, *Trained immunity: a memory for innate host defense.* Cell Host Microbe, 2011. **9**(5): p. 355-61.
167. Kappler, J.W., N. Roehm, and P. Marrack, *T cell tolerance by clonal elimination in the thymus.* Cell, 1987. **49**(2): p. 273-80.
168. Salaun, J., et al., *Thymic epithelium tolerizes for histocompatibility antigens.* Science, 1990. **247**(4949 Pt 1): p. 1471-4.
169. Hardy, R.R., et al., *Resolution and characterization of pro-B and pre-pro-B cell stages in normal mouse bone marrow.* J Exp Med, 1991. **173**(5): p. 1213-25.
170. Sandel, P.C. and J.G. Monroe, *Negative selection of immature B cells by receptor editing or deletion is determined by site of antigen encounter.* Immunity, 1999. **10**(3): p. 289-99.
171. Kappler, J., et al., *The mouse T cell receptor: comparison of MHC-restricted receptors on two T cell hybridomas.* Cell, 1983. **34**(3): p. 727-37.
172. Reinherz, E.L., et al., *Antigen recognition by human T lymphocytes is linked to surface expression of the T3 molecular complex.* Cell, 1982. **30**(3): p. 735-43.
173. Fagraeus, A., *The plasma cellular reaction and its relation to the formation of antibodies in vitro.* J Immunol, 1948. **58**(1): p. 1-13.
174. Brack, C., et al., *A complete immunoglobulin gene is created by somatic recombination.* Cell, 1978. **15**(1): p. 1-14.
175. Max, E.E., J.G. Seidman, and P. Leder, *Sequences of five potential recombination sites encoded close to an immunoglobulin kappa constant region gene.* Proc Natl Acad Sci U S A, 1979. **76**(7): p. 3450-4.

176. Sakano, H., et al., *Sequences at the somatic recombination sites of immunoglobulin light-chain genes.* Nature, 1979. **280**(5720): p. 288-94.
177. Sakano, H., et al., *Two types of somatic recombination are necessary for the generation of complete immunoglobulin heavy-chain genes.* Nature, 1980. **286**(5774): p. 676-83.
178. Early, P., et al., *An immunoglobulin heavy chain variable region gene is generated from three segments of DNA: VH, D and JH.* Cell, 1980. **19**(4): p. 981-92.
179. Tonegawa, S., et al., *Evidence for somatic generation of antibody diversity.* Proc Natl Acad Sci U S A, 1974. **71**(10): p. 4027-31.
180. Shinkai, Y., et al., *RAG-2-deficient mice lack mature lymphocytes owing to inability to initiate V(D)J rearrangement.* Cell, 1992. **68**(5): p. 855-67.
181. Mombaerts, P., et al., *RAG-1-deficient mice have no mature B and T lymphocytes.* Cell, 1992. **68**(5): p. 869-77.
182. Rosenthal, A.S. and E.M. Shevach, *Function of macrophages in antigen recognition by guinea pig T lymphocytes. I. Requirement for histocompatible macrophages and lymphocytes.* J Exp Med, 1973. **138**(5): p. 1194-212.
183. Garboczi, D.N., et al., *Structure of the complex between human T-cell receptor, viral peptide and HLA-A2.* Nature, 1996. **384**(6605): p. 134-41.
184. Zinkernagel, R.M. and P.C. Doherty, *Characteristics of the interaction in vitro between cytotoxic thymus-derived lymphocytes and target monolayers infected with lymphocytic choriomeningitis virus.* Scand J Immunol, 1974. **3**(3): p. 287-94.
185. Grewal, I.S., J. Xu, and R.A. Flavell, *Impairment of antigen-specific T-cell priming in mice lacking CD40 ligand.* Nature, 1995. **378**(6557): p. 617-20.
186. Manickasingham, S.P., et al., *Qualitative and quantitative effects of CD28/B7-mediated costimulation on naive T cells in vitro.* J Immunol, 1998. **161**(8): p. 3827-35.
187. Banchereau, J. and R.M. Steinman, *Dendritic cells and the control of immunity.* Nature, 1998. **392**(6673): p. 245-52.
188. Veldhoen, M., et al., *TGFbeta in the context of an inflammatory cytokine milieu supports de novo differentiation of IL-17-producing T cells.* Immunity, 2006. **24**(2): p. 179-89.
189. Mangan, P.R., et al., *Transforming growth factor-beta induces development of the T(H)17 lineage.* Nature, 2006. **441**(7090): p. 231-4.
190. Chen, Z., et al., *Distinct regulation of interleukin-17 in human T helper lymphocytes.* Arthritis Rheum, 2007. **56**(9): p. 2936-46.
191. Bettelli, E., et al., *Induction and effector functions of T(H)17 cells.* Nature, 2008. **453**(7198): p. 1051-7.
192. Pardoll, D.M., et al., *Differential expression of two distinct T-cell receptors during thymocyte development.* Nature, 1987. **326**(6108): p. 79-81.
193. Groh, V., et al., *Human lymphocytes bearing T cell receptor gamma/delta are phenotypically diverse and evenly distributed throughout the lymphoid system.* J Exp Med, 1989. **169**(4): p. 1277-94.
194. Chien, Y.H., C. Meyer, and M. Bonneville, *gammadelta T cells: first line of defense and beyond.* Annu Rev Immunol, 2014. **32**: p. 121-55.
195. Sandstrom, A., et al., *The intracellular B30.2 domain of butyrophilin 3A1 binds phosphoantigens to mediate activation of human Vgamma9Vdelta2 T cells.* Immunity, 2014. **40**(4): p. 490-500.
196. Hara, T., et al., *Predominant activation and expansion of V gamma 9-bearing gamma delta T cells in vivo as well as in vitro in Salmonella infection.* J Clin Invest, 1992. **90**(1): p. 204-10.
197. Gentek, R., et al., *Epidermal gammadelta T cells originate from yolk sac hematopoiesis and clonally self-renew in the adult.* J Exp Med, 2018. **215**(12): p. 2994-3005.
198. Jensen, K.D., et al., *Thymic selection determines gammadelta T cell effector fate: antigen-naive cells make interleukin-17 and antigen-experienced cells make interferon gamma.* Immunity, 2008. **29**(1): p. 90-100.

199. Roark, C.L., et al., *Exacerbation of collagen-induced arthritis by oligoclonal, IL-17-producing gamma delta T cells.* J Immunol, 2007. **179**(8): p. 5576-83.
200. Cai, Y., et al., *Pivotal role of dermal IL-17-producing gammadelta T cells in skin inflammation.* Immunity, 2011. **35**(4): p. 596-610.
201. Bendelac, A., et al., *A subset of CD4+ thymocytes selected by MHC class I molecules.* Science, 1994. **263**(5154): p. 1774-8.
202. Bendelac, A., et al., *CD1 recognition by mouse NK1+ T lymphocytes.* Science, 1995. **268**(5212): p. 863-5.
203. Beckman, E.M., et al., *Recognition of a lipid antigen by CD1-restricted alpha beta+ T cells.* Nature, 1994. **372**(6507): p. 691-4.
204. Malhotra, N., et al., *SOX4 controls invariant NKT cell differentiation by tuning TCR signaling.* J Exp Med, 2018. **215**(11): p. 2887-2900.
205. Mattner, J., et al., *Exogenous and endogenous glycolipid antigens activate NKT cells during microbial infections.* Nature, 2005. **434**(7032): p. 525-9.
206. Kinjo, Y., et al., *Recognition of bacterial glycosphingolipids by natural killer T cells.* Nature, 2005. **434**(7032): p. 520-5.
207. Kinjo, Y., et al., *Natural killer T cells recognize diacylglycerol antigens from pathogenic bacteria.* Nat Immunol, 2006. **7**(9): p. 978-86.
208. Coquet, J.M., et al., *Diverse cytokine production by NKT cell subsets and identification of an IL-17-producing CD4-NK1.1- NKT cell population.* Proc Natl Acad Sci U S A, 2008. **105**(32): p. 11287-92.
209. Gumperz, J.E., et al., *Functionally distinct subsets of CD1d-restricted natural killer T cells revealed by CD1d tetramer staining.* J Exp Med, 2002. **195**(5): p. 625-36.
210. Lee, Y.J., et al., *Tissue-Specific Distribution of iNKT Cells Impacts Their Cytokine Response.* Immunity, 2015. **43**(3): p. 566-78.
211. Salou, M., et al., *A common transcriptomic program acquired in the thymus defines tissue residency of MAIT and NKT subsets.* J Exp Med, 2019. **216**(1): p. 133-151.
212. Porcelli, S., et al., *Analysis of T cell antigen receptor (TCR) expression by human peripheral blood CD4-8- alpha/beta T cells demonstrates preferential use of several V beta genes and an invariant TCR alpha chain.* J Exp Med, 1993. **178**(1): p. 1-16.
213. Tilloy, F., et al., *An invariant T cell receptor alpha chain defines a novel TAP-independent major histocompatibility complex class Ib-restricted alpha/beta T cell subpopulation in mammals.* J Exp Med, 1999. **189**(12): p. 1907-21.
214. Treiner, E., et al., *Selection of evolutionarily conserved mucosal-associated invariant T cells by MR1.* Nature, 2003. **422**(6928): p. 164-9.
215. Goldfinch, N., et al., *Conservation of mucosal associated invariant T (MAIT) cells and the MR1 restriction element in ruminants, and abundance of MAIT cells in spleen.* Vet Res, 2010. **41**(5): p. 62.
216. Ben Youssef, G., et al., *Ontogeny of human mucosal-associated invariant T cells and related T cell subsets.* J Exp Med, 2018. **215**(2): p. 459-479.
217. Gold, M.C., et al., *Human mucosal associated invariant T cells detect bacterially infected cells.* PLoS Biol, 2010. **8**(6): p. e1000407.
218. Le Bourhis, L., et al., *Antimicrobial activity of mucosal-associated invariant T cells.* Nat Immunol, 2010. **11**(8): p. 701-8.
219. Reantragoon, R., et al., *Antigen-loaded MR1 tetramers define T cell receptor heterogeneity in mucosal-associated invariant T cells.* J Exp Med, 2013. **210**(11): p. 2305-20.
220. Ishimori, A., et al., *Circulating activated innate lymphoid cells and mucosal-associated invariant T cells are associated with airflow limitation in patients with asthma.* Allergol Int, 2016.

221. Gibbs, A., et al., *MAIT cells reside in the female genital mucosa and are biased towards IL-17 and IL-22 production in response to bacterial stimulation.* Mucosal immunology, 2016(October 2015): p. 1-11.
222. Baron, M., et al., *Innate-like and conventional T cell populations from hemodialyzed and kidney transplanted patients are equally compromised.* PloS one, 2014. **9**(8): p. e105422-e105422.
223. Cui, Y., et al., *Mucosal-associated invariant T cell-rich congenic mouse strain allows functional evaluation.* J Clin Invest, 2015. **125**(11): p. 4171-85.
224. Miyazaki, Y., et al., *Mucosal-associated invariant T cells regulate Th1 response in multiple sclerosis.* Int Immunol, 2011. **23**(9): p. 529-35.
225. Haga, K., et al., *MAIT cells are activated and accumulated in the inflamed mucosa of ulcerative colitis.* J Gastroenterol Hepatol, 2016. **31**(5): p. 965-72.
226. Hernandez, P.P., et al., *Single-cell transcriptional analysis reveals ILC-like cells in zebrafish.* Sci Immunol, 2018. **3**(29).
227. Robinette, M.L., et al., *Transcriptional programs define molecular characteristics of innate lymphoid cell classes and subsets.* Nature Immunology, 2015. **16**(3).
228. Seillet, C., et al., *Deciphering the Innate Lymphoid Cell Transcriptional Program.* Cell Rep, 2016. **17**(2): p. 436-447.
229. Simoni, Y., et al., *Human Innate Lymphoid Cell Subsets Possess Tissue-Type Based Heterogeneity in Phenotype and Frequency.* Immunity, 2017. **46**(1): p. 148-161.
230. Björklund, Å.K., et al., *The heterogeneity of human CD127+ innate lymphoid cells revealed by single-cell RNA sequencing.* Nature Immunology, 2016. **17**(4): p. 451-60.
231. Spits, H., et al., *Innate lymphoid cells--a proposal for uniform nomenclature.* Nature reviews. Immunology, 2013. **13**(2): p. 145-9.
232. Kiessling, R., et al., *"Natural" killer cells in the mouse. II. Cytotoxic cells with specificity for mouse Moloney leukemia cells. Characteristics of the killer cell.* Eur J Immunol, 1975. **5**(2): p. 117-21.
233. Mebius, R.E., P. Rennert, and I.L. Weissman, *Developing lymph nodes collect CD4+CD3- LTbeta+ cells that can differentiate to APC, NK cells, and follicular cells but not T or B cells.* Immunity, 1997. **7**(4): p. 493-504.
234. Klose, C.S., et al., *Differentiation of type 1 ILCs from a common progenitor to all helper-like innate lymphoid cell lineages.* Cell, 2014. **157**(2): p. 340-56.
235. Cherrier, M., S. Sawa, and G. Eberl, *Notch, Id2, and RORgammat sequentially orchestrate the fetal development of lymphoid tissue inducer cells.* J Exp Med, 2012. **209**(4): p. 729-40.
236. Possot, C., et al., *Notch signaling is necessary for adult, but not fetal, development of RORγt+ innate lymphoid cells.* Nature Immunology, 2011. **12**(10): p. 949-958.
237. Ishizuka, I.E., et al., *Single-cell analysis defines the divergence between the innate lymphoid cell lineage and lymphoid tissue – inducer cell lineage.* Nature Immunology, 2016. **17**(November 2015): p. 1-9.
238. Villarino, A.V., et al., *Subset- and tissue-defined STAT5 thresholds control homeostasis and function of innate lymphoid cells.* J Exp Med, 2017. **214**(10): p. 2999-3014.
239. Mjösberg, J., et al., *Transcriptional control of innate lymphoid cells.* European Journal of Immunology, 2012. **42**: p. 1916-1923.
240. Satoh-Takayama, N., et al., *IL-7 and IL-15 independently program the differentiation of intestinal CD3-NKp46+ cell subsets from Id2-dependent precursors.* J Exp Med, 2010. **207**(2): p. 273-80.
241. Boos, M.D., et al., *Mature natural killer cell and lymphoid tissue-inducing cell development requires Id2-mediated suppression of E protein activity.* J Exp Med, 2007. **204**(5): p. 1119-30.
242. Geiger, T.L., et al., *Nfil3 is crucial for development of innate lymphoid cells and host protection against intestinal pathogens.* J Exp Med, 2014. **211**(9): p. 1723-31.

243. Yagi, R., et al., *The transcription factor GATA3 is critical for the development of all IL-7Ralpha-expressing innate lymphoid cells.* Immunity, 2014. **40**(3): p. 378-88.
244. Harly, C., et al., *Development and differentiation of early innate lymphoid progenitors.* J Exp Med, 2018. **215**(1): p. 249-262.
245. Diefenbach, A., M. Colonna, and S. Koyasu, *Review Development , Differentiation , and Diversity of Innate Lymphoid Cells.* Immunity, 2014. **41**(3): p. 354-365.
246. Eberl, G., J.P. Di Santo, and E. Vivier, *The brave new world of innate lymphoid cells.* Nature Immunology, 2014. **16**(1): p. 1-5.
247. Hughes, T., et al., *The transcription Factor AHR prevents the differentiation of a stage 3 innate lymphoid cell subset to natural killer cells.* Cell Rep, 2014. **8**(1): p. 150-62.
248. Moro, K., et al., *Innate production of T(H)2 cytokines by adipose tissue-associated c-Kit(+)Sca-1(+) lymphoid cells.* Nature, 2010. **463**(7280): p. 540-4.
249. Spooner, C.J., et al., *Specification of type 2 innate lymphocytes by the transcriptional determinant Gfi1.* Nat Immunol, 2013. **14**(12): p. 1229-36.
250. Wong, S.H., et al., *Transcription factor RORalpha is critical for nuocyte development.* Nat Immunol, 2012. **13**(3): p. 229-36.
251. Fort, M.M., et al., *IL-25 induces IL-4, IL-5, and IL-13 and Th2-associated pathologies in vivo.* Immunity, 2001. **15**(6): p. 985-95.
252. Hurst, S.D., et al., *New IL-17 family members promote Th1 or Th2 responses in the lung: in vivo function of the novel cytokine IL-25.* J Immunol, 2002. **169**(1): p. 443-53.
253. Halim, T.Y., et al., *Lung natural helper cells are a critical source of Th2 cell-type cytokines in protease allergen-induced airway inflammation.* Immunity, 2012. **36**(3): p. 451-63.
254. Liang, H.E., et al., *Divergent expression patterns of IL-4 and IL-13 define unique functions in allergic immunity.* Nat Immunol, 2011. **13**(1): p. 58-66.
255. Salimi, M., et al., *A role for IL-25 and IL-33-driven type-2 innate lymphoid cells in atopic dermatitis.* The Journal of experimental medicine, 2013. **210**(13): p. 2939-2950.
256. Stremska, M.E., et al., *IL233, A Novel IL-2 and IL-33 Hybrid Cytokine, Ameliorates Renal Injury.* J Am Soc Nephrol, 2017. **28**(9): p. 2681-2693.
257. Klose, C.S.N., et al., *A T-bet gradient controls the fate and function of CCR6-RORγt+ innate lymphoid cells.* Nature, 2013. **494**: p. 261-265.
258. Cupedo, T., et al., *Human fetal lymphoid tissue-inducer cells are interleukin 17-producing precursors to RORC+ CD127+ natural killer-like cells.* Nature immunology, 2009.
259. Sciume, G., et al., *Distinct requirements for T-bet in gut innate lymphoid cells.* J Exp Med, 2012. **209**(13): p. 2331-8.
260. Viant, C., et al., *Transforming growth factor-β and Notch ligands act as opposing environmental cues in regulating the plasticity of type 3 innate lymphoid cells.* Science Signaling, 2016. **9**(426): p. ra46-ra46.
261. Verrier, T., et al., *Phenotypic and Functional Plasticity of Murine Intestinal NKp46+ Group 3 Innate Lymphoid Cells.* The Journal of Immunology, 2016. **196**(11): p. 4731-4738.
262. Li, N., et al., *Mass cytometry reveals innate lymphoid cell differentiation pathways in the human fetal intestine.* J Exp Med, 2018. **215**(5): p. 1383-1396.
263. Sonnenberg, G.F., et al., *Snapshot: Innate lymphoid cells.* Immunity, 2013. **39**: p. 622-622.e1.
264. Hazenberg, M.D. and H. Spits, *Review Article Human innate lymphoid cells.* Blood, 2014. **124**(5): p. 700-710.
265. Walker, J.A., J.L. Barlow, and A.N. McKenzie, *Innate Lymphoid cells - how did we miss them?* Nature reviews. Immunology, 2013. **13**: p. 75-87.
266. Eberl, G., et al., *An essential function for the nuclear receptor RORgamma(t) in the generation of fetal lymphoid tissue inducer cells.* Nat Immunol, 2004. **5**(1): p. 64-73.
267. Sanos, S.L., et al., *RORgammat and commensal microflora are required for the differentiation of mucosal interleukin 22-producing NKp46+ cells.* Nat Immunol, 2009. **10**(1): p. 83-91.

268. Luci, C., et al., *Influence of the transcription factor RORgammat on the development of NKp46+ cell populations in gut and skin.* Nat Immunol, 2009. **10**(1): p. 75-82.
269. Chappaz, S., et al., *Kit ligand and Il7 differentially regulate Peyer's patch and lymph node development.* J Immunol, 2010. **185**(6): p. 3514-9.
270. van de Pavert, S.A., et al., *Maternal retinoids control type 3 innate lymphoid cells and set the offspring immunity.* Nature, 2014. **508**(7494): p. 123-7.
271. Goverse, G., et al., *Vitamin A Controls the Presence of ROR γ + Innate Lymphoid Cells and Lymphoid Tissue in the Small Intestine.* The Journal of Immunology, 2016.
272. Li, S., et al., *Ikaros Inhibits Group 3 Innate Lymphoid Cell Development and Function by Suppressing the Aryl Hydrocarbon Receptor Pathway.* Immunity, 2016. **45**(1): p. 185-197.
273. Ahn, Y.O., et al., *Lineage relationships of human interleukin-22-producing CD56+ RORgammat+ innate lymphoid cells and conventional natural killer cells.* Blood, 2013. **121**(12): p. 2234-43.
274. Montaldo, E., et al., *Human RORgammat(+)CD34(+) cells are lineage-specified progenitors of group 3 RORgammat(+) innate lymphoid cells.* Immunity, 2014. **41**(6): p. 988-1000.
275. Spencer, S.P., et al., *Adaptation of innate lymphoid cells to a micronutrient deficiency promotes type 2 barrier immunity.* Science, 2014. **343**(6169): p. 432-7.
276. Bernink, J.H., et al., *Interleukin-12 and -23 Control Plasticity of CD127(+) Group 1 and Group 3 Innate Lymphoid Cells in the Intestinal Lamina Propria.* Immunity, 2015. **43**(1): p. 146-60.
277. Bernink, J.H., et al., *Human type 1 innate lymphoid cells accumulate in inflamed mucosal tissues.* Nature immunology, 2013. **14**(3): p. 221-9.
278. Huang, Y., et al., *IL-25-responsive, lineage-negative KLRG1(hi) cells are multipotential 'inflammatory' type 2 innate lymphoid cells.* Nat Immunol, 2015. **16**(2): p. 161-9.
279. Zhong, C., et al., *Group 3 innate lymphoid cells continuously require the transcription factor GATA-3 after commitment.* Nature Immunology, 2015(November).
280. Serafini, N., et al., *Gata3 drives development of RORγt+ group 3 innate lymphoid cells.* The Journal of experimental medicine, 2014. **211**(2): p. 199-208.
281. Satoh-Takayama, N., et al., *Microbial flora drives interleukin 22 production in intestinal NKp46+ cells that provide innate mucosal immune defense.* Immunity, 2008. **29**(6): p. 958-70.
282. Longman, R.S., et al., *CX3CR1+ mononuclear phagocytes support colitis-associated innate lymphoid cell production of IL-22.* Journal of Experimental Medicine, 2014. **211**(8): p. 1571-83.
283. Pearson, C., et al., *ILC3 GM-CSF production and mobilisation orchestrate acute intestinal inflammation.* eLife, 2016. **5**: p. 1-21.
284. Finke, D., et al., *CD4+CD3- cells induce Peyer's patch development: role of alpha4beta1 integrin activation by CXCR5.* Immunity, 2002. **17**(3): p. 363-73.
285. Fukuyama, S., et al., *Initiation of NALT organogenesis is independent of the IL-7R, LTbetaR, and NIK signaling pathways but requires the Id2 gene and CD3(-)CD4(+)CD45(+) cells.* Immunity, 2002. **17**(1): p. 31-40.
286. Tsuji, M., et al., *Requirement for lymphoid tissue-inducer cells in isolated follicle formation and T cell-independent immunoglobulin A generation in the gut.* Immunity, 2008. **29**(2): p. 261-71.
287. Hepworth, M.R., et al., *Group 3 innate lymphoid cells mediate intestinal selection of commensal bacteria-specific CD4 T cells.* Science, 2015(April): p. 1-11.
288. Abt, Michael C., et al., *Innate Immune Defenses Mediated by Two ILC Subsets Are Critical for Protection against Acute Clostridium difficile Infection.* Cell Host & Microbe, 2015. **18**(1): p. 27-37.
289. Geremia, A., et al., *IL-23-responsive innate lymphoid cells are increased in inflammatory bowel disease.* The Journal of experimental medicine, 2011.

290. Aparicio-Domingo, P., et al., *Type 3 innate lymphoid cells maintain intestinal epithelial stem cells after tissue damage.* J Exp Med, 2015. **212**(11): p. 1783-91.
291. Ahn, Y.-O., et al., *Human group3 innate lymphoid cells express DR3 and respond to TL1A with enhanced IL-22 production and IL-2-dependent proliferation.* European Journal of Immunology, 2015: p. n/a-n/a.
292. Prehn, J.L., et al., *The T cell costimulator TL1A is induced by FcgammaR signaling in human monocytes and dendritic cells.* J Immunol, 2007. **178**(7): p. 4033-8.
293. Glatzer, T., et al., *RORgammat(+) innate lymphoid cells acquire a proinflammatory program upon engagement of the activating receptor NKp44.* Immunity, 2013. **38**(6): p. 1223-35.
294. Scheller, J., et al., *The pro- and anti-inflammatory properties of the cytokine interleukin-6.* Biochim Biophys Acta, 2011. **1813**(5): p. 878-88.
295. Roake, J.A., et al., *Dendritic cell loss from nonlymphoid tissues after systemic administration of lipopolysaccharide, tumor necrosis factor, and interleukin 1.* J Exp Med, 1995. **181**(6): p. 2237-47.
296. Sallusto, F., et al., *Rapid and coordinated switch in chemokine receptor expression during dendritic cell maturation.* Eur J Immunol, 1998. **28**(9): p. 2760-9.
297. Clatworthy, M.R., et al., *Immune complexes stimulate CCR7-dependent dendritic cell migration to lymph nodes.* Nature Medicine, 2014. **20**(12): p. 1458-1465.
298. Fan, X., et al., *Murine CXCR1 is a functional receptor for GCP-2/CXCL6 and interleukin-8/CXCL8.* J Biol Chem, 2007. **282**(16): p. 11658-66.
299. Cacalano, G., et al., *Neutrophil and B cell expansion in mice that lack the murine IL-8 receptor homolog.* Science, 1994. **265**(5172): p. 682-4.
300. Godaly, G., et al., *Transepithelial neutrophil migration is CXCR1 dependent in vitro and is defective in IL-8 receptor knockout mice.* J Immunol, 2000. **165**(9): p. 5287-94.
301. Yamazaki, T., et al., *CCR6 regulates the migration of inflammatory and regulatory T cells.* J Immunol, 2008. **181**(12): p. 8391-401.
302. Gasteiger, G., et al., *Tissue residency of innate lymphoid cells in lymphoid and nonlymphoid organs.* Science, 2015. **350**(6263): p. 981-5.
303. Mackley, E.C., et al., *CCR7-dependent trafficking of RORγ+ ILCs creates a unique microenvironment within mucosal draining lymph nodes.* Nature Communications, 2015. **6**: p. 5862-5862.
304. Ivanov, II, et al., *The orphan nuclear receptor RORgammat directs the differentiation program of proinflammatory IL-17+ T helper cells.* Cell, 2006. **126**(6): p. 1121-33.
305. Yang, X.O., et al., *T helper 17 lineage differentiation is programmed by orphan nuclear receptors ROR alpha and ROR gamma.* Immunity, 2008. **28**(1): p. 29-39.
306. Veldhoen, M., et al., *Natural agonists for aryl hydrocarbon receptor in culture medium are essential for optimal differentiation of Th17 T cells.* J Exp Med, 2009. **206**(1): p. 43-9.
307. Quintana, F.J., et al., *Control of T(reg) and T(H)17 cell differentiation by the aryl hydrocarbon receptor.* Nature, 2008. **453**(7191): p. 65-71.
308. Ghoreschi, K., et al., *Generation of pathogenic T(H)17 cells in the absence of TGF-beta signalling.* Nature, 2010. **467**(7318): p. 967-71.
309. Nurieva, R., et al., *Essential autocrine regulation by IL-21 in the generation of inflammatory T cells.* Nature, 2007. **448**(7152): p. 480-3.
310. Zheng, Y., et al., *Interleukin-22, a T(H)17 cytokine, mediates IL-23-induced dermal inflammation and acanthosis.* Nature, 2007. **445**(7128): p. 648-51.
311. Zhou, L., et al., *IL-6 programs T(H)-17 cell differentiation by promoting sequential engagement of the IL-21 and IL-23 pathways.* Nat Immunol, 2007. **8**(9): p. 967-74.
312. Petermann, F., et al., *gammadelta T cells enhance autoimmunity by restraining regulatory T cell responses via an interleukin-23-dependent mechanism.* Immunity, 2010. **33**(3): p. 351-63.
313. Korn, T., et al., *IL-21 initiates an alternative pathway to induce proinflammatory T(H)17 cells.* Nature, 2007. **448**(7152): p. 484-487.

314. Liang, S.C., et al., *Interleukin (IL)-22 and IL-17 are coexpressed by Th17 cells and cooperatively enhance expression of antimicrobial peptides.* J Exp Med, 2006. **203**(10): p. 2271-9.
315. Langrish, C.L., et al., *IL-23 drives a pathogenic T cell population that induces autoimmune inflammation.* J Exp Med, 2005. **201**(2): p. 233-40.
316. Hirota, K., et al., *Fate mapping of IL-17-producing T cells in inflammatory responses.* Nat Immunol, 2011. **12**(3): p. 255-63.
317. Turner, J.E., et al., *IL-17A production by renal gammadelta T cells promotes kidney injury in crescentic GN.* J Am Soc Nephrol, 2012. **23**(9): p. 1486-95.
318. Mielke, L.A., et al., *Retinoic acid expression associates with enhanced IL-22 production by gammadelta T cells and innate lymphoid cells and attenuation of intestinal inflammation.* J Exp Med, 2013. **210**(6): p. 1117-24.
319. Eken, A., et al., *IL-23R þ innate lymphoid cells induce colitis via interleukin-22-dependent mechanism.* Nature Mucosal Immunology, 2014. **7**(1): p. 143-154.
320. Migone, T.S., et al., *TL1A is a TNF-like ligand for DR3 and TR6/DcR3 and functions as a T cell costimulator.* Immunity, 2002. **16**(3): p. 479-92.
321. Chinnaiyan, A.M., et al., *Signal transduction by DR3, a death domain-containing receptor related to TNFR-1 and CD95.* Science, 1996. **274**(5289): p. 990-2.
322. Bodmer, J.L., et al., *TRAMP, a novel apoptosis-mediating receptor with sequence homology to tumor necrosis factor receptor 1 and Fas(Apo-1/CD95).* Immunity, 1997. **6**(1): p. 79-88.
323. Kitson, J., et al., *A death-domain-containing receptor that mediates apoptosis.* Nature, 1996. **384**(6607): p. 372-5.
324. Meylan, F., et al., *The TNF-family receptor DR3 is essential for diverse T cell-mediated inflammatory diseases.* Immunity, 2008. **29**(1): p. 79-89.
325. Papadakis, K.A., et al., *TL1A synergizes with IL-12 and IL-18 to enhance IFN-gamma production in human T cells and NK cells.* J Immunol, 2004. **172**(11): p. 7002-7.
326. Meylan, F., et al., *The TNF-family cytokine TL1A promotes allergic immunopathology through group 2 innate lymphoid cells.* Mucosal Immunol, 2014. **7**(4): p. 958-68.
327. Yu, X., et al., *TNF superfamily member TL1A elicits type 2 innate lymphoid cells at mucosal barriers.* Mucosal Immunol, 2014. **7**(3): p. 730-40.
328. Price, A.E., et al., *Marking and quantifying IL-17A-producing cells in vivo.* PLoS One, 2012. **7**(6): p. e39750.
329. Toy, D., et al., *Cutting edge: interleukin 17 signals through a heteromeric receptor complex.* J Immunol, 2006. **177**(1): p. 36-9.
330. Acosta-Rodriguez, E.V., et al., *Surface phenotype and antigenic specificity of human interleukin 17-producing T helper memory cells.* Nat Immunol, 2007. **8**(6): p. 639-46.
331. Ishigame, H., et al., *Differential roles of interleukin-17A and -17F in host defense against mucoepithelial bacterial infection and allergic responses.* Immunity, 2009. **30**(1): p. 108-19.
332. Yao, Z., et al., *Herpesvirus Saimiri encodes a new cytokine, IL-17, which binds to a novel cytokine receptor.* Immunity, 1995. **3**(6): p. 811-21.
333. Jovanovic, D.V., et al., *IL-17 stimulates the production and expression of proinflammatory cytokines, IL-beta and TNF-alpha, by human macrophages.* J Immunol, 1998. **160**(7): p. 3513-21.
334. Witowski, J., et al., *IL-17 stimulates intraperitoneal neutrophil infiltration through the release of GRO alpha chemokine from mesothelial cells.* J Immunol, 2000. **165**(10): p. 5814-21.
335. Laan, M., et al., *Neutrophil recruitment by human IL-17 via C-X-C chemokine release in the airways.* J Immunol, 1999. **162**(4): p. 2347-52.
336. Fossiez, F., et al., *T cell interleukin-17 induces stromal cells to produce proinflammatory and hematopoietic cytokines.* J Exp Med, 1996. **183**(6): p. 2593-603.

337. Awane, M., et al., *NF-kappa B-inducing kinase is a common mediator of IL-17-, TNF-alpha-, and IL-1 beta-induced chemokine promoter activation in intestinal epithelial cells.* J Immunol, 1999. **162**(9): p. 5337-44.
338. Hymowitz, S.G., et al., *IL-17s adopt a cystine knot fold: structure and activity of a novel cytokine, IL-17F, and implications for receptor binding.* EMBO J, 2001. **20**(19): p. 5332-41.
339. Lee, H.T., et al., *Critical role of interleukin-17A in murine intestinal ischemia reperfusion injury.* AJP: Gastrointestinal and Liver Physiology, 2012(24): p. 12-25.
340. Dixon, B.R., et al., *IL-17a and IL-22 Induce Expression of Antimicrobials in Gastrointestinal Epithelial Cells and May Contribute to Epithelial Cell Defense against Helicobacter pylori.* PLoS One, 2016. **11**(2): p. e0148514.
341. Besnard, A.G., et al., *Dual Role of IL-22 in allergic airway inflammation and its cross-talk with IL-17A.* Am J Respir Crit Care Med, 2011. **183**(9): p. 1153-63.
342. Sonnenberg, G.F., et al., *Pathological versus protective functions of IL-22 in airway inflammation are regulated by IL-17A.* J Exp Med, 2010. **207**(6): p. 1293-305.
343. Barin, J.G., et al., *Macrophages participate in IL-17-mediated inflammation.* Eur J Immunol, 2012. **42**(3): p. 726-36.
344. Erbel, C., et al., *IL-17A influences essential functions of the monocyte/macrophage lineage and is involved in advanced murine and human atherosclerosis.* J Immunol, 2014. **193**(9): p. 4344-55.
345. Steinbach, S., H.M. Vordermeier, and G.J. Jones, *CD4+ and gammadelta T Cells are the main Producers of IL-22 and IL-17A in Lymphocytes from Mycobacterium bovis-infected Cattle.* Sci Rep, 2016. **6**: p. 29990.
346. Dudakov, J.A., A.M. Hanash, and M.R.M.v.d. Brink, *Interleukin-22: Immunobiology and Pathology.* Annual Review of Immunology, 2015. **33**(1): p. 747-785.
347. Zheng, Y., et al., *Interleukin-22 mediates early host defense against attaching and effacing bacterial pathogens.* Nat Med, 2008. **14**(3): p. 282-9.
348. Lindemans, C.A., et al., *Interleukin-22 promotes intestinal-stem-cell-mediated epithelial regeneration.* Nature, 2015: p. 1-18.
349. Brand, S., et al., *IL-22 is increased in active Crohn's disease and promotes proinflammatory gene expression and intestinal epithelial cell migration.* Am J Physiol Gastrointest Liver Physiol, 2006. **290**(4): p. G827-38.
350. Kulkarni, O.P., et al., *Toll-Like Receptor 4-Induced IL-22 Accelerates Kidney Regeneration.* Journal of the American Society of Nephrology : JASN, 2014: p. 1-12.
351. Nagalakshmi, M.L., et al., *Interleukin-22 activates STAT3 and induces IL-10 by colon epithelial cells.* Int Immunopharmacol, 2004. **4**(5): p. 679-91.
352. Xu, M.-J., et al., *IL-22 ameliorates renal ischemia-reperfusion injury by targeting proximal tubule epithelium.* Journal of the American Society of Nephrology : JASN, 2014. **25**(5): p. 967-77.
353. Sonnenberg, G.F., et al., *CD4(+) lymphoid tissue-inducer cells promote innate immunity in the gut.* Immunity, 2011. **34**(1): p. 122-34.
354. Boniface, K., et al., *A role for T cell-derived interleukin 22 in psoriatic skin inflammation.* Clin Exp Immunol, 2007. **150**(3): p. 407-15.
355. Cochez, P.M., et al., *AhR modulates the IL-22 producing cell proliferation/recruitment in imiquimod-induced psoriasis mouse model.* European journal of immunology, 2016: p. 1449-1459.
356. Helft, J., et al., *GM-CSF Mouse Bone Marrow Cultures Comprise a Heterogeneous Population of CD11c(+)MHCII(+) Macrophages and Dendritic Cells.* Immunity, 2015. **42**(6): p. 1197-211.
357. Chernykh, E.R., et al., *Phenotypic and functional changes of GM-CSF differentiated human macrophages following exposure to apoptotic neutrophils.* Cell Immunol, 2018. **331**: p. 93-99.

358. Fleetwood, A.J., et al., *Granulocyte-macrophage colony-stimulating factor (CSF) and macrophage CSF-dependent macrophage phenotypes display differences in cytokine profiles and transcription factor activities: implications for CSF blockade in inflammation.* J Immunol, 2007. **178**(8): p. 5245-52.
359. Reichwald, K., T.Z. Jorgensen, and S. Skov, *TL1A increases expression of CD25, LFA-1, CD134 and CD154, and induces IL-22 and GM-CSF production from effector CD4 T-cells.* PLoS One, 2014. **9**(8): p. e105627.
360. Sun, L., et al., *GM-CSF Quantity Has a Selective Effect on Granulocytic vs. Monocytic Myeloid Development and Function.* Front Immunol, 2018. **9**: p. 1922.
361. Hui, Z., et al., *Cxxc Finger Protein 1 Positively Regulates GM-CSF-Derived Macrophage Phagocytosis Through Csf2ralpha-Mediated Signaling.* Front Immunol, 2018. **9**: p. 1885.
362. Lemaitre, B., et al., *The dorsoventral regulatory gene cassette spatzle/Toll/cactus controls the potent antifungal response in Drosophila adults.* Cell, 1996. **86**(6): p. 973-83.
363. Medzhitov, R., P. Preston-Hurlburt, and C.A. Janeway, Jr., *A human homologue of the Drosophila Toll protein signals activation of adaptive immunity.* Nature, 1997. **388**(6640): p. 394-7.
364. Xie, Q., et al., *Lipopolysaccharide/adenosine triphosphate induces IL1beta and IL-18 secretion through the NLRP3 inflammasome in RAW264.7 murine macrophage cells.* Int J Mol Med, 2014. **34**(1): p. 341-9.
365. Poltorak, A., et al., *Defective LPS signaling in C3H/HeJ and C57BL/10ScCr mice: mutations in Tlr4 gene.* Science, 1998. **282**(5396): p. 2085-8.
366. Hayashi, F., et al., *The innate immune response to bacterial flagellin is mediated by Toll-like receptor 5.* Nature, 2001. **410**(6832): p. 1099-103.
367. Schilling, J.D., et al., *Toll-like receptor 4 on stromal and hematopoietic cells mediates innate resistance to uropathogenic Escherichia coli.* Proc Natl Acad Sci U S A, 2003. **100**(7): p. 4203-8.
368. Zanoni, I., et al., *CD14 controls the LPS-induced endocytosis of Toll-like receptor 4.* Cell, 2011. **147**(4): p. 868-80.
369. Schiwon, M., et al., *Crosstalk between sentinel and helper macrophages permits neutrophil migration into infected uroepithelium.* Cell, 2014. **156**(3): p. 456-68.
370. Antal-Szalmas, P., et al., *Quantitation of surface CD14 on human monocytes and neutrophils.* J Leukoc Biol, 1997. **61**(6): p. 721-8.
371. Tittel, A.P., et al., *Kidney dendritic cells induce innate immunity against bacterial pyelonephritis.* Journal of the American Society of Nephrology : JASN, 2011. **22**(8): p. 1435-1441.
372. Vincent, P.C., et al., *The intravascular survival of neutrophils labeled in vivo.* Blood, 1974. **43**(3): p. 371-7.
373. Haraoka, M., et al., *Neutrophil recruitment and resistance to urinary tract infection.* J Infect Dis, 1999. **180**(4): p. 1220-9.
374. Isaacson, B., et al., *Stromal Cell-Derived Factor 1 Mediates Immune Cell Attraction upon Urinary Tract Infection.* Cell Rep, 2017. **20**(1): p. 40-47.
375. Agace, W., et al., *Selective cytokine production by epithelial cells following exposure to Escherichia coli.* Infect Immun, 1993. **61**(2): p. 602-9.
376. Agace, W.W., et al., *Escherichia coli induces transuroepithelial neutrophil migration by an intercellular adhesion molecule-1-dependent mechanism.* Infect Immun, 1995. **63**(10): p. 4054-62.
377. Godaly, G., et al., *Role of epithelial interleukin-8 (IL-8) and neutrophil IL-8 receptor A in Escherichia coli-induced transuroepithelial neutrophil migration.* Infect Immun, 1997. **65**(8): p. 3451-6.
378. Svensson, M., et al., *Effects of epithelial and neutrophil CXCR2 on innate immunity and resistance to kidney infection.* Kidney Int, 2008. **74**(1): p. 81-90.

379. Svensson, M., et al., *Acute pyelonephritis and renal scarring are caused by dysfunctional innate immunity in mCxcr2 heterozygous mice.* Kidney Int, 2011. **80**(10): p. 1064-72.
380. Hannan, T.J., et al., *Inhibition of Cyclooxygenase-2 Prevents Chronic and Recurrent Cystitis.* EBioMedicine, 2014. **1**(1): p. 46-57.
381. Gur, C., et al., *Natural killer cell-mediated host defense against uropathogenic E. coli is counteracted by bacterial hemolysinA-dependent killing of NK cells.* Cell Host Microbe, 2013. **14**(6): p. 664-74.
382. Jones-Carson, J., E. Balish, and D.T. Uehling, *Susceptibility of immunodeficient gene-knockout mice to urinary tract infection.* J Urol, 1999. **161**(1): p. 338-41.
383. Sivick, K.E., et al., *The innate immune response to uropathogenic Escherichia coli involves IL-17A in a murine model of urinary tract infection.* Journal of immunology (Baltimore, Md. : 1950), 2010. **184**(4): p. 2065-2075.
384. Chan, A.J., et al., *Innate IL-17AeProducing Leukocytes Promote Acute Kidney Injury via Inflammasome and Toll-Like Receptor Activation.* The American Journal of Pathology, 2014. **184**(5).
385. Odobasic, D., et al., *Interleukin-17A promotes early but attenuates established disease in crescentic glomerulonephritis in mice.* American Journal of Pathology, 2011. **179**(3): p. 1188-1198.
386. Li, L., et al., *IL-17 produced by neutrophils regulates IFN-gamma-mediated neutrophil migration in mouse kidney ischaemia-reperfusion injury.* Journal of Clinical Investigation, 2010. **120**(1).
387. Peng, X., et al., *IL-17A produced by both γδ T and Th17 cells promotes renal fibrosis via RANTES-mediated leukocyte infiltration after renal obstruction.* The Journal of Pathology, 2015. **235**(1): p. 79-89.
388. Dong, X., et al., *Dendritic cells facilitate accumulation of IL-17 T cells in the kidney following acute renal obstruction.* Kidney international, 2008. **74**(10): p. 1294-1309.
389. Kwan, T., et al., *IL-17 Deficiency Attenuates Allograft Injury and Prolongs Survival in a Murine Model of Fully MHC-Mismatched Renal Allograft Transplantation.* American Journal of Transplantation, 2015. **15**(6): p. 1555-1567.
390. Aggarwal, S., et al., *Interleukin-23 promotes a distinct CD4 T cell activation state characterized by the production of interleukin-17.* J Biol Chem, 2003. **278**(3): p. 1910-4.
391. Liu, S.J., et al., *Induction of a distinct CD8 Tnc17 subset by transforming growth factor-beta and interleukin-6.* J Leukoc Biol, 2007. **82**(2): p. 354-60.
392. Ferretti, S., et al., *IL-17, produced by lymphocytes and neutrophils, is necessary for lipopolysaccharide-induced airway neutrophilia: IL-15 as a possible trigger.* J Immunol, 2003. **170**(4): p. 2106-12.
393. Molet, S., et al., *IL-17 is increased in asthmatic airways and induces human bronchial fibroblasts to produce cytokines.* J Allergy Clin Immunol, 2001. **108**(3): p. 430-8.
394. Dube, S., et al., *Endothelial STAT3 Modulates Protective Mechanisms in a Mouse Ischemia-Reperfusion Model of Acute Kidney Injury.* J Immunol Res, 2017. **2017**: p. 4609502.
395. Xu, M.J., et al., *IL-22 ameliorates renal ischemia-reperfusion injury by targeting proximal tubule epithelium.* J Am Soc Nephrol, 2014. **25**(5): p. 967-77.
396. Weidenbusch, M., et al., *Gene expression profiling of the Notch-AhR-IL22 axis at homeostasis and in response to tissue injury.* Biosci Rep, 2017. **37**(6).
397. Xiao, C., et al., *Differentiation and recruitment of IL-22-producing helper T cells in lgA nephropathy.* Am J Transl Res, 2016. **8**(9): p. 3872-3882.
398. Luk, C.C., et al., *Intrarenal and Urinary Th9 and Th22 Cytokine Gene Expression in Lupus Nephritis.* J Rheumatol, 2015. **42**(7): p. 1150-5.
399. Yang, X., et al., *Increased interleukin-22 levels in lupus nephritis and its associated with disease severity: a study in both patients and lupus-like mice model.* Clin Exp Rheumatol, 2018.

400. Weidenbusch, M., et al., *IL-22 sustains epithelial integrity in progressive kidney remodeling and fibrosis.* Physiol Rep, 2018. **6**(16): p. e13817.
401. Wang, S., et al., *Interleukin-22 ameliorated renal injury and fibrosis in diabetic nephropathy through inhibition of NLRP3 inflammasome activation.* Cell Death Dis, 2017. **8**(7): p. e2937.
402. Le, P.T., et al., *IL22 regulates human urothelial cell sensory and innate functions through modulation of the acetylcholine response, immunoregulatory cytokines and antimicrobial peptides: assessment of an in vitro model.* PloS one, 2014. **9**(10): p. e111375-e111375.
403. Zhao, T., X. Wu, and J. Liu, *Association between interleukin-22 genetic polymorphisms and bladder cancer risk.* Clinics (Sao Paulo), 2015. **70**(10): p. 686-90.
404. Sundac, L., et al., *Protein-based profiling of the immune response to uropathogenic Escherichia coli in adult patients immediately following hospital admission for acute cystitis.* Pathog Dis, 2016. **74**(6).
405. Li, Y., et al., *Granulocyte-Macrophage Colony-Stimulating Factor (GM-CSF) Is Released by Female Mouse Bladder Urothelial Cells and Expressed by the Urotheliumas an Early Response to LPS.* Neurourology and urodynamics, 2016.
406. Duell, B.L., et al., *Human bladder uroepithelial cells synergize with monocytes to promote IL-10 synthesis and other cytokine responses to uropathogenic Escherichia coli.* PLoS One, 2013. **8**(10): p. e78013.
407. Juno, J.A., et al., *Mucosal-Associated Invariant T Cells Are Depleted and Exhibit Altered Chemokine Receptor Expression and Elevated Granulocyte Macrophage-Colony Stimulating Factor Production During End-Stage Renal Disease.* Front Immunol, 2018. **9**: p. 1076.
408. Hopkins, W.J., D.T. Uehling, and E. Balish, *Local and systemic antibody responses accompany spontaneous resolution of experimental cystitis in cynomolgus monkeys.* Infect Immun, 1987. **55**(9): p. 1951-6.
409. Svanborg-Eden, C. and A.M. Svennerholm, *Secretory immunoglobulin A and G antibodies prevent adhesion of Escherichia coli to human urinary tract epithelial cells.* Infect Immun, 1978. **22**(3): p. 790-7.
410. Thumbikat, P., et al., *Antigen-specific responses accelerate bacterial clearance in the bladder.* J Immunol, 2006. **176**(5): p. 3080-6.
411. Chan, C.Y., A.L. St John, and S.N. Abraham, *Mast cell interleukin-10 drives localized tolerance in chronic bladder infection.* Immunity, 2013. **38**(2): p. 349-59.
412. Habibi, M., et al., *Intranasal immunization with fusion protein MrpH·FimH and MPL adjuvant confers protection against urinary tract infections caused by uropathogenic Escherichia coli and Proteus mirabilis.* Molecular Immunology, 2015. **64**(2): p. 285-294.
413. Hopkins, W.J., et al., *Vaginal mucosal vaccine for recurrent urinary tract infections in women: results of a phase 2 clinical trial.* J Urol, 2007. **177**(4): p. 1349-53; quiz 1591.
414. Huttner, A., et al., *Safety, immunogenicity, and preliminary clinical efficacy of a vaccine against extraintestinal pathogenic Escherichia coli in women with a history of recurrent urinary tract infection: a randomised, single-blind, placebo-controlled phase 1b trial.* Lancet Infect Dis, 2017. **17**(5): p. 528-537.
415. Hung, C., *A murine model of urinary tract infection.* Nature protocols, 2009. **4**(8): p. 1230-1243.
416. Halim, T.Y. and F. Takei, *Isolation and characterization of mouse innate lymphoid cells.* Curr Protoc Immunol, 2014. **106**: p. 3 25 1-13.
417. Nussbaum, J.C., et al., *Type 2 innate lymphoid cells control eosinophil homeostasis.* Nature, 2013. **502**(7470): p. 245-8.
418. Mjösberg, J.M., et al., *Human IL-25- and IL-33-responsive type 2 innate lymphoid cells are defined by expression of CRTH2 and CD161.* Nature Immunology, 2011. **12**(11): p. 1055-1062.
419. Teunissen, M.B.M., et al., *Composition of Innate Lymphoid Cell Subsets in the Human Skin: Enrichment of NCR(+) ILC3 in Lesional Skin and Blood of Psoriasis Patients.* The Journal of investigative dermatology, 2014. **13**.

420. Lochner, M., et al., *In vivo equilibrium of proinflammatory IL-17+ and regulatory IL-10+ Foxp3+ RORgamma t+ T cells.* J Exp Med, 2008. **205**(6): p. 1381-93.
421. Anderson, K.G., et al., *Intravascular staining for discrimination of vascular and tissue leukocytes.* Nat Protoc, 2014. **9**(1): p. 209-22.
422. Young, M.D., et al., *Single-cell transcriptomes from human kidneys reveal the cellular identity of renal tumors.* Science, 2018. **361**(6402): p. 594-599.
423. Kim, Myung H., Elizabeth J. Taparowsky, and Chang H. Kim, *Retinoic Acid Differentially Regulates the Migration of Innate Lymphoid Cell Subsets to the Gut.* Immunity, 2015: p. 1-13.
424. Dutton, E.E., et al., *Peripheral lymph nodes contain migratory and resident innate lymphoid cell populations.* Sci Immunol, 2019. **4**(35).
425. Manta, C., et al., *CX(3)CR1(+) macrophages support IL-22 production by innate lymphoid cells during infection with Citrobacter rodentium.* Mucosal Immunol, 2013. **6**(1): p. 177-88.
426. Withers, D.R., et al., *Transient inhibition of ROR-γt therapeutically limits intestinal inflammation by reducing TH17 cells and preserving group 3 innate lymphoid cells.* Nature Medicine, 2016(October 2015).
427. Ivanov, II, et al., *Induction of intestinal Th17 cells by segmented filamentous bacteria.* Cell, 2009. **139**(3): p. 485-98.
428. Kim, S.H., et al., *Microbiota-derived butyrate suppresses group 3 innate lymphoid cells in terminal ileal Peyer's patches.* Sci Rep, 2017. **7**(1): p. 3980.
429. Ahn, Y.O., et al., *Human group3 innate lymphoid cells express DR3 and respond to TL1A with enhanced IL-22 production and IL-2-dependent proliferation.* Eur J Immunol, 2015. **45**(8): p. 2335-42.
430. Ferdinand, J.R., et al., *Cleavage of TL1A Differentially Regulates Its Effects on Innate and Adaptive Immune Cells.* J Immunol, 2018. **200**(4): p. 1360-1369.
431. Al-Lamki, R.S., et al., *TL1A both promotes and protects from renal inflammation and injury.* J Am Soc Nephrol, 2008. **19**(5): p. 953-60.
432. Vivier, E., et al., *Innate Lymphoid Cells: 10 Years On.* Cell, 2018. **174**(5): p. 1054-1066.
433. Ferguson, A., *‚Associated bilharziasis and primary malignant disease of the urinary bladder with observations on a series of forty cases.* Journal of Pathology and Bacteriology, 1911. **16**: p. 76-94.
434. Case, R.A. and M.E. Hosker, *Tumour of the urinary bladder as an occupational disease in the rubber industry in England and Wales.* Br J Prev Soc Med, 1954. **8**(2): p. 39-50.
435. Aitken, G. and G. Moon, *Chronic kidney disease prevalence model*, in *National Cardiovascular Network*, P.H. England, Editor. 2014, University of Southampton.